Toru Takebayashi
Robert Landsiedel
Masashi Gamo   *Editors*

In Vivo Inhalation Toxicity Screening Methods for Manufactured Nanomaterials

Springer

Current Topics in Environmental Health and Preventive Medicine

Series editor

Takemi Otsuki
Kawasaki Medical School
Kurashiki
Okayama, Japan

Current Topics in Environmental Health and Preventive Medicine, published in partnership with the Japanese Society of Hygiene, is designed to deliver well written volumes authored by experts from around the globe, covering the prevention and environmental health related to medical, biological, molecular biological, genetic, physical, psychosocial, chemical, and other environmental factors. The series will be a valuable resource to both new and established researchers, as well as students who are seeking comprehensive information on environmental health and health promotion.

More information about this series at http://www.springer.com/series/13556

Toru Takebayashi • Robert Landsiedel
Masashi Gamo

Editors

In Vivo Inhalation Toxicity Screening Methods for Manufactured Nanomaterials

Springer

Editors
Toru Takebayashi
Graduate School of Health Management
Keio University
Fujisawa
Kanagawa
Japan

Robert Landsiedel
Experimental Toxicology and Ecology
BASF SE
Ludwigshafen am Rhein
Germany

Masashi Gamo
National Institute of Advanced Industrial
Science and Technology (AIST)
Tsukuba
Ibaraki
Japan

Contents

Chapter 1
The Role of In Vivo Screening Studies in Assessing Manufactured Nanomaterials

Robert Landsiedel, Masashi Gamo, and Akihiko Hirose

Abstract Information on possible toxic effects of nanomaterials is essential to ensure occupational and consumer safety. As regards human exposure to nanomaterials, inhalation is recognized as an exposure route of potential concern, especially in the occupational context, but also for consumers. Generally, comprehensive regulatory toxicity testing for the hazard and risk assessment of an inhalable chemical encompasses a dose range finding inhalation study using rats followed by a rat 28-day and 90-day inhalation toxicity study (OECD TG 412 and 413). However, performing such inhalation toxicity tests is time-consuming, cost-intensive, and can require up to 160 animals per study. Given the increasing number of products containing nanomaterials entering the market and the multitude of different variants of the same nanomaterial, the fulfillment of all information requirements for every single variant of a given nanomaterial is impractical and undesirable for economic reasons, and it further stands in contradiction to the internationally accepted 3Rs principle to replace, reduce, and refine animal testing. On the other hand, in vivo inhalation toxicity tests cannot yet be replaced by in vitro methods. Taking into account the specific purpose of the investigation, both the short-term inhalation study (STIS) and the intratracheal instillation (IT) study are suitable in vivo screening methods that allow identifying if nanomaterials that reach the lung elicit signs of inflammation. These screening methods allow reducing and refining animal testing as compared to the 28-day and 90-day inhalation toxicity studies. IT studies are useful to obtain initial information on pulmonary effects elicited by nanomaterials, e.g., during product development and as an initial step for hazard identification, but

R. Landsiedel (✉)
Experimental Toxicology and Ecology, BASF SE, Ludwigshafen am Rhein, Germany
e-mail: robert.landsiedel@basf.com

M. Gamo
National Institute of Advanced Industrial Science and Technology (AIST),
Tsukuba, Ibaraki, Japan

A. Hirose
Division of Risk Assessment, Biological Safety Research Center, National Institute of Health Sciences, Kawasaki, Japan

they are less suitable in providing information that is directly relevant for quantitative safety assessments. By comparison, the rat STIS can be used as a range finding study for a subsequent longer-term inhalation toxicity study and can be embedded in a tiered grouping and testing strategy.

Keywords Nanomaterials · Short-term inhalation study (STIS) · Intratracheal instillation (IT) study · Pulmonary inflammation · In vivo screening methods

1.1   Background

Nanotechnology is a key enabling technology that is used to develop materials with particular mechanical, chemical, electrical, or optical characteristics, such as increased strength, chemical reactivity, conductivity, and enhanced optical emission. A broad spectrum of nanomaterials is now commonly used in industrial and technical applications as well as in consumer products (e.g., batteries, coatings, anti-bacterial clothing, and cleaning products) and medical products and devices [1].

Information on possible toxic effects of nanomaterials is essential to ensure occupational and consumer safety. To provide a basis for regulatory provisions for nanomaterial hazard and risk assessment, different jurisdictions have laid down definitions of the term nanomaterial [2]. However, to date there is no unique, internationally accepted definition for the term nanomaterial. ISO [3, 4] drew up technical definitions for nanotechnology-related terms: nanoscale is defined as the size range from approx. 1–100 nm [3], a nanomaterial as a material with any external dimension in the nanoscale or having an internal structure or surface structure in the nanoscale [4], and a nanoparticle as an object with all three external dimensions in the nanoscale [3].

In the European Union (EU), a nanomaterial has been defined as follows [5]:

A natural, incidental or manufactured material containing particles, in an unbound state or as an aggregate or as an agglomerate and where, for 50% or more of the particles in the number size distribution, one or more external dimensions is in the size range 1–100 nm. In specific cases and where warranted by concerns for the environment, health, safety or competitiveness the number size distribution threshold of 50% may be replaced by a threshold between 1 and 50%… fullerenes, graphene flakes and single wall carbon nanotubes with one or more external dimensions below 1 nm should be considered as nanomaterials.

Additionally, the term nanoform is used that the European Chemicals Agency [6] has defined as *a form of a substance that meets the requirements of the Commission Recommendation for the definition of nanomaterial* [5].

No inherently new effects and mechanisms of nanomaterial toxicity have been recorded that had never been observed as such before, and there is no evidence for "nanospecific" toxic effects, which can be attributed to the smallness of the particles alone [7–10]. The potency and localization of effects can, however, be different from the bulk material [11]. Nanomaterials are similar to non-nanosized

substances in that some may be toxic and some may not [12–14]. In the EU, just as in most other jurisdictions, nanomaterials and the potential risks associated with them are covered by existing and updated product-specific legislations as well as by new guidance that specifically addresses nanomaterials and nanomaterial-specific information requirements [15].

As regards human exposure to nanomaterials, inhalation is recognized as an exposure route of potential concern, especially in the occupational context, but also for consumers [8, 16–18]. The systemic availability of inhaled nanomaterials is generally low [11, 19]. The upper and middle respiratory tracts provide a mucus layer barrier preventing most foreign material from gaining access to the airway epithelia. Further, the bronchiolar epithelium contains ciliated cells that are firmly connected by tight junctions and form a mucociliary escalator transporting particles and phagocytic cells from the bronchiolar regions towards the larynx. Notwithstanding, a considerable fraction of respirable materials (with sizes below 1–3 μm for the rat) can reach the non-ciliated lower respiratory tract. In the alveoli, defense mechanisms include the alveolar epithelial type II cells that produce and secrete surfactants and alveolar macrophages that phagocytize particles that reach the alveoli and then migrate to the mucociliary escalator. To a far lesser extent, respirable materials can also be taken up by alveolar epithelial cells [20–22].

Inhaled particles can damage lung cells especially if the volume of inhaled particles exceeds the macrophages' clearance capacity [22–24]. The clearance of particles from the lung can be accelerated when the particles dissolve [25, 26], and it can be hampered when the macrophages are compromised by volumetric overload or by intracellular damage caused by the particles (e.g., when toxic irons are released, lysosomes are damaged, or reactive species are formed catalytically at the cell surfaces) [12, 13]. The rat, the animal species commonly used in inhalation studies, appears particularly sensitive to developing pathological responses under volumetric particle overload conditions [22]. By contrast, the relevance of the "pulmonary overload" concept for humans has been questioned [8, 27, 28].

Generally, comprehensive regulatory toxicity testing for the hazard and risk assessment of an inhalable chemical encompasses a dose range finding inhalation study using rats followed by a rat 28-day and 90-day inhalation toxicity study (Organisation for Economic Cooperation and Development (OECD) Test Guidelines (TGs) 412 and 413 [29, 30]). By contrast, the acute inhalation toxicity of nanomaterials in accordance with OECD TG 403 [31] is scarcely investigated and may indeed provide very little useful information [8, 32]. Performing the 28-day and 90-day inhalation toxicity tests is time-consuming, cost-intensive, and can require up to 160 animals per study. Given the increasing number of products containing nanomaterials entering the market and the multitude of different variants of the same nanomaterial, the fulfillment of all information requirements for every single variant of a given nanomaterial is impractical and undesirable for economic reasons, and it further stands in contradiction to the internationally accepted 3Rs principle to replace, reduce, and refine animal testing [33] that has been imple-

mented in the EU in *Directive 2010/63/EU on the protection of animals used for scientific purposes* [34]. Therefore, alternative methods in accordance with the 3Rs principle are urgently needed for early stage screening of the toxic potential of nanomaterials upon inhalation exposure.

In vitro assays can inform on the specific cellular mechanisms by which nanomaterial effects evolve [8]. To date, only a limited number of such cellular mechanisms have been identified, i.e., (1) membrane damage including cationic phagolysosome damage that may ultimately lead to apoptosis and autophagy; (2) generation of reactive oxygen species, oxidative stress, redox activities, and photo-catalytic effects; (3) inflammasome activation and cytokine and chemokine production; (4) the cytotoxic effects of toxic ions; (5) fiber effects [8, 12, 13, 35–41]; and (6) primary and secondary DNA damage, with primary DNA damage rarely being observed in vitro [42–44]. However, standardized in vitro assays to assess the cellular effects of nanomaterials, let alone guidance on how to incorporate in vitro assays into the regulatory hazard and risk assessment of nanomaterials, continue to be unavailable. To date, quantitative information on nanomaterial effects, and dose-response relationships yielding relevant predictions of their in vivo toxic potential and potency are hardly possible [41]. For these reasons, in vivo inhalation toxicity tests cannot yet be replaced by in vitro methods.

However, two in vivo screening assays are available that allow reducing and refining the use of animals in accordance with the 3Rs principle [33]. These two in vivo screening assays are the rat short-term inhalation study (STIS) and the intratracheal instillation (IT) study. Both assays provide first information on the toxic potential and toxic potency of nanomaterials when entering the organism via the respiratory tract. Further, the rat STIS can be used as a range finding study for a subsequent longer-term inhalation toxicity study.

The following Sects. 1.2 and 1.3 present the concepts of the rat STIS and the IT study, respectively. Section 1.4 describes how the rat STIS can be used within an integrated grouping and testing strategy that provides information relevant for nanomaterial hazard and risk assessment, Sect. 1.5 describes the validity of IT study from the viewpoint of inhalation toxicity assessment, and Sect. 1.6 summarizes the conclusions from this chapter.

1.2 Concept of the Rat STIS

The concept of a rat STIS was first described by Arts et al. [45], and then further elaborated by Landsiedel et al. [46] and Ma-Hock et al. [47] within the projects NanoCare (http://www.ptj.de/nanocare; supported by the German Federal Ministry of Education and Research) and NanoSafe2 (www.nanosafe.org; supported by the EU Sixth Research Framework Programme). The rat STIS was designed to obtain more relevant data as compared to the 28-day inhalation study protocol that was valid at that time (OECD TG 412 as adopted in 2006) and with less burden to the animals. In addition to histopathological evaluations, the rat STIS includes

evaluations of bronchoalveolar lavage fluid (BALF) and organ burdens. Further, it includes a postexposure observation period, or recovery period, that serves to examine the reversibility or progression of the effects as well as the pulmonary clearance of the test material. The recovery period can range from 2 to 13 weeks [18, 45]; generally, a 3-week recovery period is recommended so that the postexposure observation lasts at least 3 times as long as the exposure period.

The rat STIS allows investigating a number of key elements that are essential for the assessment of toxic effects of nanomaterials upon inhalation exposure, i.e., (1) toxic potential/potency in the upper, middle, and lower respiratory tract (mainly: inflammatory effects); (2) deposition and biopersistence of the particles in the lung; (3) systemic uptake of test materials, toxic potential/potency and biopersistence in non-respiratory tract tissues and organs; and (4) reversibility or progression of the (respiratory tract or non-respiratory tract) effects.

Since the rat STIS was first described more than 10 years ago, it has been used by different research teams ((e.g., [46, 48–51]; Kim et al. 2018) and in further publicly funded research projects including NanoGEM (https://nanopartikel. info/en/projects/completed-projects/nanogem), supported by the German Federal Ministry for Education and Research; NanoMILE (http://nanomile.eu-vri.eu) and NanoToxClass (http://www.nanotoxclass.eu/project.htm), both supported by the EU Seventh Research Framework Programme. Numerous test materials have been tested following its general study design that has been updated over the years (cf. Chap. 2 for a comprehensive overview of rat STISs conducted so far).

The rat STIS, as performed in accordance with the most recent protocol, uses between 48 and 64 male rats (Fig. 1.1):

- 32 rats are assigned to the exposure group and a further 32 rats to the recovery group.
- In both the exposure and the recovery groups, 8 male rats each are assigned to the control group and 3 test groups receiving different aerosol concentrations of the test material. All animals are exposed to the respective aerosol concentrations for 5 days, 6 h per day. On day 1 and approx. day 21 after the last exposure (for the exposure and recovery groups, respectively), 5 animals per control group or test group are used for histopathology and bronchoalveolar lavage (BAL), and 3 animals per group for the determination of lung burden.
- Notably, in this most recent STIS study design, only half a lung (preferably the left lobe) is used for BAL and the remaining lung lobes for histopathology. Thereby, 5 rats per concentration and time point are sufficient to cover both BAL and histopathology.
- If the test groups receiving the two lower aerosol concentrations are omitted from the recovery group (which may be possible depending upon the question under investigation), total animal numbers applying the most recent STIS study design can be further reduced from 64 to 48 rats per study.

The originally proposed STIS [47] encompassed a total of 88 rats (11 rats each (5 for BALF analysis, 3 for histopathology, 3 for determination of lung burden) for the control group and 3 test groups × 2 for the exposure and recovery groups). As com-

	Exposure Groups		Recovery Groups	
Number of groups	Control + 3 concentrations		Control + 3 concentrations or Control + 1 high concentration	
Endpoints	Histopathology and lung lavage	Organ burden	Histopathology and lung lavage	Organ burden
Rats/group	5 males	3 males	5 males	3 males
	Exposure: 6 h/day for 5 days		Exposure: 6 h/day for 5 days	
Necropsy / lavage	Day 5 (the day after the last exposure)		Post-exposure observation period 21 days	
Necropsy / lavage			Day 27 (the day after the end of the post-exposure period)	
Total numbers of rats	32 male Wistar rats		32 male Wistar rats or 16 male Wistar rats	

Fig. 1.1 Current study design of the rat STIS

pared to that study design, an increased statistical confidence for histopathology has been achieved in the current protocol since 5 rats are now available for histopathology instead of originally only 3, while total animal numbers were reduced from 88 to 64 or possibly even only 48 animals. By comparison, a 28-day or 90-day inhalation toxicity study can require up to 160 animals.

1.3   Concept of the Intratracheal Instillation (IT) Study

IT implies instillation of a liquid (soluble particles) or a suspension (insoluble particles) via the trachea into the lungs of anesthetized animals (mostly rats or mice), and sacrifice of the animals for BALF evaluation and histopathology after a predetermined period (e.g., 3 days up until several weeks). As compared to inhalation studies, IT studies do not require complex equipment to prepare, characterize, and apply aerosols. A further advantage of IT studies, especially in the context of

substance screening during product development, is that they require lower quantities of the test materials than inhalation studies, which can require up to 1 kg of test material per study [52].

As the technical requirements for IT studies are significantly lower than those for inhalation studies, many screening studies assessing the pulmonary toxicity potential of nanomaterials have been performed as IT studies (e.g., [25, 26, 44, 53–62]).

In IT studies, the lung burden shortly after the exposure is widely concordant with the total applied bolus dose. Therefore, lung burden shortly postexposure does not have to be measured. However, this also implies that the initial dose following IT is much higher than during inhalation exposure of a comparable nominal dose over a longer period of time, because only a limited fraction is retained in the lung upon inhalation, while the remainder of the inhaled dose is exhaled. A comparison of the results from rat STISs and IT studies using the same test materials at comparable lung burden demonstrates that IT, i.e., the administration of a bolus dose, generally causes more pronounced effects than inhalation exposure [41, 63, 64]. At equal lung burden, the dose rate affects the severity of effects, and this is especially pronounced for bolus dose administrations.

Especially the histopathological findings upon IT appear to be more pronounced, and they are already observable 3-days post-administration. By comparison, the morphological changes in the rat STIS are often rather mild. However, even though the rat STIS and the IT study may have different sensitivities, the same spectrum of findings can be expected with both methods [41, 63, 64].

A number of parameters should be considered when planning IT studies including the influence of the selected dispersion medium on nanomaterial toxicity [65]. Further, the period until sacrifice of the animals should be selected with care. If animals are sacrificed very shortly after the IT, vehicle-induced effects can be predominant. Such effects are reversible within the first few days post-administration. By comparison, substance-induced effects, which would also be observed after inhalation, take a few days to evolve and are observable at approx. 3 days postexposure.

While IT is frequently used as a surrogate for inhalation exposure, it has been considered a drawback of IT studies that NOAECs cannot be determined following IT, but only no observed adverse effect levels (NOAELs). NOAECs, and not NOAELs, are relevant for the occupational safety assessment of inhalable compounds. Further, since the administration of bolus doses can affect the severity of observable effects, it is much more difficult to perform an initial occupational safety assessment using data from IT studies. On the other hand, it has been reported that when the same initial lung burden was applied in both studies, the inflammatory response in the IT study was almost equal to that in the inhalation study [66–68]. Hence, if the dose level and observation period are set appropriately, the effective dose of nanomaterials in the lung after IT can approximate the lung burden observed in a repeated exposure inhalation study. Lung tumor formation is thought to be linked to altered particle clearance kinetics and chronic inflammation associated with oxidative stress, secondary genotoxicity, and cell proliferation [28, 69]. A critical lung burden could be achieved by chronic inhalation as well as IT. The IT study is a valuable tool for substance screening for initial hazard identifica-

tion or ranking toxicity during product development. However, IT studies only allow assessing pulmonary effects, whereas the inhalation route of exposure allows assessing a test material's potential to induce effects in the upper and middle airways as well. This reduces the applicability of IT studies as compared to the rat STIS for initial safety assessments.

1.4 Use of the Rat STIS as Screening Tool Within an Integrated Grouping and Testing Strategy

The grouping of substances has been identified as an important means to avoid unnecessary testing when fulfilling the regulatory information requirements for nanomaterials—and non-nanosized materials [70–72]. During grouping, closely related chemicals are considered *as a group, or category, rather than as individual chemicals…* [so that] *not every chemical needs to be tested for every endpoint. Instead, the overall data for that category should prove adequate to support a hazard assessment…* [and] *must enable an estimate of hazard for the untested endpoints* [73]. Applying the grouping concept using read-across techniques, endpoint information for one chemical is used to predict the same endpoint for another chemical, which is considered to be similar, even though regular patterns of properties as a result of structural (or other) similarities are not necessarily apparent [73].

Specific grouping approaches for nanomaterials need to account for the complexity of these materials. Therefore, grouping approaches for nanomaterials should address all relevant aspects of the nanomaterials' life cycle and biological pathway from their release up until (potential) apical effects [74, 75] (Fig. 1.2). Similar to adverse outcome pathways [76], biological pathways may encompass a multitude of interlinked steps. These are not necessarily already fully understood for each and every type of nanomaterial. Nevertheless, nanomaterial grouping does not require that all pieces of knowledge concerning the respective steps are available. While the apical effects of a nanomaterial are eventually directed by its intrinsic material properties, they are the result of several preceding steps, including uptake, distribution, functionalities, and early cellular and apical effects [70, 77–79]. Functionalities include system-dependent material properties (such as dissolution rate in biologically relevant media), biophysical interactions, in vitro effects and release and exposure [70, 75, 80–83]. If the exact correlation between a nanomaterial's intrinsic material properties and its apical effect are not obvious, grouping should take into account the nanomaterial's functionalities rather than relying on intrinsic material properties alone.

Against this background, Arts et al. [80] proposed a *Decision-making framework for the Grouping and testing of nanomaterials (DF4nanoGrouping)* that allows grouping nanomaterials by their specific intrinsic material properties and functionalities. In Tier 1 of the DF4nanoGrouping, intrinsic material properties are assessed (water solubility, particle morphology and chemical composition) and in Tier 2 functionalities (dissolution in biological media, surface reactivity, particle dispersibility and in vitro effects) (cf. Table 1.1 for grouping criteria and thresh-
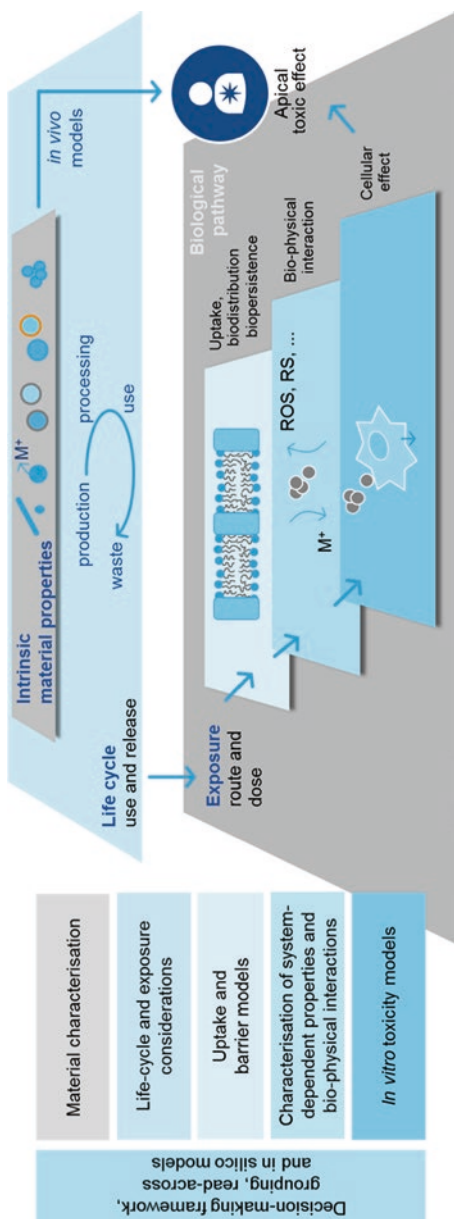
Fig. 1.2 Framework for nanomaterial grouping addressing all relevant aspects of a nanomaterial's life cycle and biological pathway, i.e., intrinsic material properties, use, release and exposure, uptake and biokinetics, functionalities and cellular and apical toxic effects (Figure adapted from that presented at the second International Congress on Safety of Engineered Nanoparticles and Nanotechnologies (SENN) 2015, Helsinki, Finland by R. Landsiedel)

Table 1.1 DF4nanoGrouping: grouping criteria, threshold values, relation to main group assignment (adapted from: [80–81])

DF4nano-Grouping tier	Grouping criterion	Threshold value for grouping	Main group (MG) assignment or indication	Benchmark material; if applicable[a]
Tier 1 Intrinsic material properties	Water solubility	>100 mg/L[b]	Assignment to MG1	ZnO NM-110 and NM-111, 10 nm-CuO: Limited water solubility TiO$_2$ NM-105: Low water solubility
	Particle size and shape	Aspect ratio >3:1,length >5 μm,diameter <3 μm[c]	Indication for MG2	
	Composition including impurities	≥0.1% of component with GHS classification for systemic effects	Indication for MG4	
Tier 2 System-dependent properties In vitro effects	Dissolution in biological fluids[d]	>100 mg/L[b]	Globular nanomaterials: >100 mg/L: indication for MG1 Fibers: <100 mg/L: indication for MG2	10 nm-CuO: High dissolution
	Surface reactivity[e]	≥10% of Mn$_2$O$_3$ reactivity, which is equal to: ≥0.19 μU FRAS/m^2 h	Assignment to MG4	Quartz dust DQ12: High surface reactivity BaSO$_4$ NM-220: Not oxidative
	Dispersibility	AAN <3 or diameter <100 nm	Assignment to MG2 or MG4, as applicable	a-SiO$_2$-susp with acrylate surface functionalization: Dispersible a-SiO$_2$-susp without surface functionalization: Agglomeration
	Cellular effects	Effect at ≤10 μg/cm^{2f}	Assignment to MG4	ZnO NM-110 and NM-111: Activity (shedding of ions) CeO$_2$ NM-211 and NM-212: Activity BaSO$_4$ NM-220: Passivity

Tier 3 In vivo screening	Toxic potency	STIS NOAEC; four ranges: I: <0.5 mg/m^3 and no regression or progression of effects II: <1 mg/m^{3}III: <10 mg/m^3 IV: ≥10 mg/m^3	Ranges I–III: Confirmation of MG2 or MG4; Sub-grouping of MG4; Range IV: Confirmation of MG3	MWCNT NM-400: Range I CeO$_2$ NM-211 and NM-212: Range II TiO$_2$ NM-105; a-SiO$_2$-susp without surface functionalization: Range III BaSO$_4$ NM-220: Range IV
	Biopersistence	t_{50} < 40 days	Confirmation of MG1	CeO$_2$ NM-211 and NM-212: Decelerated clearance TiO$_2$ NM-105: Physiological clearance BaSO$_4$ NM-220: Accelerated clearance
Qualifier	Dustiness	None assigned	Indication of a substance's emission potential	
Supplementary criteria	Surface area	None assigned	Not primary grouping criteria	
	Surface chemistry	None assigned	Not primary grouping criteria	
	Surface charge	Positive: ζ > 10 mV	Joint evaluation with "dispersibility"g Pos. surface charge: Indication for MG4	CeO$_2$ NM-211 and NM-212: Positive surface charge
	Hydrophobicity	None assigned	Joint evaluation with "dispersibility"; cf. also Hofmann et al. [32]g	

Abbreviations: *AAN* average agglomeration number; *a-SiO₂-susp* suspended colloidal amorphous SiO₂, *FRAS* ferric reducing ability of serum, *GHS* globally harmonized system, *MG* main group, *NM* nanomaterial, *NOAEC* no observed adverse effect concentration, *STIS* short-term inhalation study
[a]All NM-x numberings (e.g., ZnO NM-111) relate to the codes of representative nanomaterials of the OECD sponsorship program for the testing of manufactured nanomaterials. Extensive information on the intrinsic material properties of these representative nanomaterials has been collated at the European Commission's Joint Research Centre (cf. https://ec.europa.eu/jrc/en/scientific-tool/jrc-nanomaterials-repository). Due to their comprehensive characterization,
(continued)

Table 1.1 (continued)

the representative nanomaterials are highly suitable benchmark materialsBased upon the outcome of the case studies, Arts et al. [81] laid down and justified the following adaptations to the threshold values that had been established in Arts et al. [80]:

[b]While the threshold values for water solubility and dissolution are adequate for nanomaterials that release ions with the GHS classification for systemic effects, they may have to be reconsidered for substances that dissolve into nontoxic components

[c]Nanomaterials may be assigned to MG2 on account of high aspect ratio, fiber diameter, and insolubility/low dissolution in water or biological media, even though their length does not meet the World Health Organization criterion (>5 μm)

[d]The method originally proposed for the DF4nanogrouping [80] involves static dissolution in a relevant fluid, as implemented specifically for the DF4nanoGrouping by Health Canada-funded research [84]. Even though this method continues to be valid, it has been observed to underestimate the dissolution of borderline materials. Therefore, the nanoGRAVUR project (http://www.nanogravur.info/index.php/kontakt; supported by the German Federal Ministry for Education and Research) proposes to replace the static dissolution setup by a dynamic setup and metrics: Thereby, the dissolution rate in lysosomal fluid is determined in flow through testing using a 5 kDa filter. This method has been applied to colloidal amorphous SiO_2 [41], and it can be generalized for the screening of pulmonary bio-dissolution of borderline materials such as $BaSO_4$ and a wide range of fully (CuO, ZnO) or partially (SiO_2) dissolving nanomaterials with confirmation by rat STIS in vivo clearance [64, 85]. In dynamic metrics, the dissolution rate k is expressed in units of $ng/cm^2/h$, with a cutoff of highly soluble materials of $k > 100 \ ng/cm^2/h$. The benchmark material is also 10-nm-CuO. Interestingly, the method can be adapted to oral bio-dissolution screening [86]

[e]Since the publication of the DF4nanoGrouping [80, 81], a tutorial review [87] for selecting an appropriate assay for surface reactivity testing (especially electron spin resonance or the FRAS assay) and a detailed standard operating procedure for the FRAS assay (Gandon et al. 2017) have been published. These documents include dose-dependent results for the positive control Mn_2O_3, for ZnO NM-110 and NM-111 as well as CeO_2 NM-211 and NM-212. The consortium of the nanoGRAVUR project (cf. footnote d above) proposes to maintain the positive control Mn_2O_3 and the 10% of positive control cutoff but prefers a *surface* dose metrics (i.e., surface-based biological oxidative damage sBOD; expressing results as nM trulox equivalent units per m^2 nanomaterial). First results on the use of this approach have been published for colloidal amorphous SiO_2 [41], and a full comparison to electron spin resonance, in vitro and in vivo studies shows its validity for identifying highly reactive nanomaterials [88]

[f]This threshold value applies for cytotoxicity tests performed with lung epithelial cells. For in vitro assays performed with alveolar macrophages, a particle surface-area based threshold value of 6000 nm^2/mL is laid down [40, 41]

[g]"Joint evaluation'' implies that strong nanoparticle surface charge, and especially strong negative surface charge, leads to low opsonization, which then leads to potentially higher mobility, e.g., quantum dots [89]; SiO_2:acrylate [81]; ZrO_2:acrylate [8]. Since dispersibility is assessed directly as essential grouping criterion, surface charge does not need to be assessed separately

old values of the DF4nanoGrouping). Based upon this Tier 1 and 2 information, all nanomaterials can be grouped into one of four main groups (MGs). Thereby, the DF4nanoGrouping allows sorting out nanomaterials that could undergo hazard assessment without further testing:

- Soluble nanomaterials (MG1) whose further hazard assessment should rely on read-across to the dissolved materials.
- High aspect ratio (HAR) nanomaterials (MG2) which should be assessed according to their potential fiber toxicity.
- Passive nanomaterials (MG3) that only elicit effects under pulmonary overload conditions.

All remaining nanomaterials are assigned as active nanomaterials (MG4) that merit in-depth investigations.

In the final Tier 3 of the DF4nanoGrouping, the Tier 1 and Tier 2 assignment to one of the MGs that is based upon non-animal testing alone is confirmed or corrected using data from in vivo short-term studies. For the inhalation route of exposure, the rat STIS is recommended [80, 81]. Using the rat STIS data, the (MG4) active nanomaterials can further be sub-grouped by range of NOAEC, biopersistence, and the reversibility or progression of effects (Table 1.1). This MG assignment and the sub-grouping of (MG4) active nanomaterials allows refining further information needs.

Arts et al. [81] conducted extensive case studies to allocate 22 nanomaterials and 3 non-nanosized materials into the different DF4nanoGrouping MGs. As compared to the data from the Tier 3 rat STIS, altogether 22 of the 25 test materials fitted into the four MGs based on the non-animal Tiers 1 and 2 alone. For the other three materials, the hazard was over-predicted in the non-animal tiers, i.e., they indicated a concern that was not confirmed in Tier 3 in the rat STIS. Hazard was never under-predicted in the non-animal tiers. While 90-day studies were not available for all test materials, the outcome of the available sub-chronic studies stood in accordance with the DF4nanoGrouping MG assignments [81].

The concept of the DF4nanoGrouping is compliant with guidance from the ECHA on the application of quantitative structure-activity relationships and grouping approaches to identify the hazard and fate of different nanoforms of the same substance [90]. This ECHA guidance presents a stepwise strategy to identify nanoforms ("*what they are*"; corresponding to Tier 1 of the DF4nanoGrouping) and to evaluate their behavior ("*where they go*"; corresponding to Tier 2 of the DF4nanoGrouping) and their reactivity ("*what they do*"; corresponding to Tier 3 of the DF4nanoGrouping) [90].

The EU project GRACIOUS (*Grouping, Read-Across, Characterization and classification framework for regulatory risk assessment of manufactured nanomaterials and safer design of nano-enabled products;* https://www.cordis.europa.eu/project/rcn/212339_en.html) that began in January 2018 and is funded under the EU Research Framework Programme Horizon 2020 has the main goal to generate a science-based framework to enable practical application of the DF4nanoGrouping, leading to read-across and classification of nanomaterials. It is planned to adapt

and expand the DF4nanoGrouping with the specific aim to substantiate the ECHA [90] guidance on the application of grouping approaches for nanoforms. Within the GRACIOUS framework, the rat STIS shall play a pivotal role in assessing the toxic potential and potency of nanomaterials.

1.5   Validity of the IT Study Results from the Viewpoint of Inhalation Toxicity Assessment

In 2011, the Japanese Ministry of Economy, Trade and Industry (METI) initiated the 5-year research project *Development of Innovative Methodology for Safety Assessment of Industrial Nanomaterials* to explore the suitability of the IT test as a screening tool to assess the pulmonary toxicity of nanomaterials. To establish an efficient nanomaterial hazard assessment framework, it is important to develop equivalence criteria for nanomaterials by using the IT screening tool, since they would contribute to reducing the number of inhalation studies. Altogether 7 TiO_2, 4 NiO, and 9 SiO_2 nanomaterials with different physicochemical properties were evaluated in both 28-days inhalation toxicity tests and intratracheal instillation studies in rats. A comparison of the findings from the inhalation and IT studies showed that, at the same lung burden, pulmonary inflammation and related factors (e.g., cell analysis, chemokine, proinflammatory cytokine and oxidative stress parameters in the BALF) were similar. Nevertheless, there is a tendency that the inflammatory response recorded in the well-designed IT study is greater than or equal to that of the inhalation study [55, 67, 91]. The following points should be considered when IT studies are used to screen for the inhalation toxicity of nanomaterials: (1) well-dispersed nanomaterials (up to 2–3 µm in the dispersion); (2) low concentration of dispersant in the dispersion; (3) observation period 3 days to 6 months postexposure; and (4) Instilled dose selected to match lung burden of inhalation study. Regarding the delivery devices and postures in IT study, Morimoto et al. [56] reported that two types of delivery devices (a gavage needle and a microspray aerosolizer) and two types of posture (an angle of approximately 45° and a standing posture on a board) resulted in no difference in the acute pulmonary toxicity findings. A detailed description of the standardized IT study protocol for use as a screening tool is presented in Chap. 7.

Further, the Japanese Ministry of Health, Labour and Welfare (MHLW) has funded the evaluation and/or development of methods to assess the chronic toxicity of nanomaterials, with a focus on carcinogenicity assessments. These studies showed that multiple IT administration of multiwalled carbon nanotubes to rats over 2 weeks induced malignant mesothelioma and lung tumors by the end of the 2-year postexposure period [92]. In this IT study, the total administered lung burden was 1 mg/lung. This level was similar to the lung burden after 1 year of exposure at the highest dose group in the 2-year inhalation study [93], also the incidence of lung tumors (adenoma and/or carcinoma) in both studies was similar [94].

1.6 Conclusions

Taking into account the specific purpose of the investigation, both the STIS and the IT study are suitable in vivo screening methods that allow identifying if nanomaterials that reach the lung elicit signs of inflammation. These screening methods allow reducing and refining animal testing as compared to the 28-day and 90-day inhalation toxicity studies (OECD TG 412 and 413). IT studies are useful to obtain initial information on pulmonary effects elicited by nanomaterials, e.g., during product development and as an initial step for hazard identification, but they are less suitable in providing information that is directly relevant for quantitative safety assessments. By comparison, the rat STIS embedded in a tiered grouping and testing strategy, such as the DF4nanoGrouping [80, 81], allows distinguishing (MG1) soluble nanomaterials and (MG2) HAR nanomaterials from poorly soluble particles. Among the poorly soluble particles, the rat STIS (DF4nanoGrouping Tier 3) serves to substantiate the DF4nanoGrouping Tier 1 and 2 distinction between biologically active (MG4) and passive (MG3) nanomaterials. Further, data from the rat STIS can be used to subgroup the (MG4) active nanomaterials to refine further information needs. Thereby, data from the rat STIS build a solid database for the further testing strategy and facilitate concentration selection and the setting of appropriate study designs for studies with a prolonged exposure period.

The relevance of the rat STIS is also reflected by the fact that the *German Commission for the Investigation of Health Hazards of Chemical Compounds in the Work Area* (acronym: MAK) Report on Nanomaterials includes the rat STIS as important pillar for the screening of occupationally relevant hazards [95]. Finally, an expert Working Group of European regulators, academics and industry scientists led by the *United Kingdom's National Centre for the Replacement, Refinement and Reduction of Animals in Research* (NC3Rs) has identified the rat STIS an essential component of a roadmap for opportunities to align the 3Rs principle with improved approaches for nanomaterial safety assessment [71]. The Working Group experts highlighted that the rat STIS can serve three purposes: (1) as an in vivo screening assay to determine the need for subsequent longer-term toxicity tests; (2) to group nanomaterials for read-across purposes, thereby reducing the number of 90-day inhalation toxicity studies; and (3) to inform dose setting and refine subsequent longer-term in vivo studies by ensuring high doses are only administered where necessary [71].

The following Chap. 2 provides details on the concept of the rat STIS and on its use within the DF4nanoGrouping during initial safety assessments to inform on early nanomaterial effects upon inhalation exposure. Chapter 3 summarizes the Use of short-term inhalation study to obtain initial hazard data and prepare for subacute and sub-chronic inhalation studies, and toxicokinetic studies. Chapter 6 compares the toxicity information obtained in IT and inhalation studies. Chapter 7 provides a standardized protocol for IT studies. Chapter 9 provides case studies regarding carcinogenicity assessment via IT studies.

References

1. Stark WJ, et al. Industrial applications of nanoparticles. Chem Soc Rev. 2015;44(16):5793–805.
2. Boverhof DR, Bramante CM, Butala JH, Clancy SF, Lafranconi M, West J, Gordon SC. Comparative assessment of nanomaterial definitions and safety evaluation considerations. Regul Toxicol Pharmacol. 2015;73:137–50.
3. ISO. International Standardization Organization Technical Standard: Nanotechnologies—Terminology and definitions for nanoobjects—nanoparticle, nanofibre, nanoplate. ISO/TS 27687:2008, 2008. Available at http://www.iso.org/iso/catalogue_detail?csnumber=44278
4. ISO. International Standardization Organization Technical Standard: Nanotechnologies—Vocabulary—Part 1: Core terms. ISO/TS 80004-1:2010, 2010. Available at http://www.iso.org/iso/catalogue_detail.htm?csnumber=51240
5. Commission. Commission recommendation on the definition of nanomaterial. OJ L 275/38, 18 Oct 2011
6. ECHA. European Chemicals Agency. How to prepare registration dossiers that cover nano-forms: best practices. Version 1.0, May 2017, ECHA-17-G-13-EN, 21 pp
7. Donaldson K, Poland CA. Nanotoxicity: challenging the myth of nano-specific toxicity. Curr Opin Biotechnol. 2013;24:724–34.
8. Landsiedel R, Sauer UG, Ma-Hock L, Schnekenburger J, Wiemann M. Pulmonary toxicity of nanomaterials: a critical comparison of published *in vitro* assays with *in vivo* inhalation or instillation studies. Nanomedicine. 2014;9:2557–85.
9. Oberdörster G, Maynard A, Donaldson K, Castranova V, Fitzpatrick J, Ausman K, Carter J, Karn B, Kreyling W, Lai D, Olin S, Monteiro-Riviere N, Warheit D, Yang H, ILSI Research Foundation/Risk Science Institute Nanomaterial Toxicity Screening Working Group. Principles for characterizing the potential human health effects from exposure to nanomaterials: elements of a screening strategy. Part Fibre Toxicol. 2005;2:8.
10. Oberdörster G, Oberdörster E, Oberdörster J. Nanotoxicology: an emerging discipline evolving from studies of ultrafine particles. Environ Health Perspect. 2005;113:823–39.
11. Moreno-Horn M, Gebel T. Granular biodurable nanomaterials: no convincing evidence for systemic toxicity. Crit Rev Toxicol. 2014;44(10):849–75.
12. Nel AE, Xia T, Meng H, Wang X, Lin S, Ji Z, Zhang H. Nanomaterial toxicity testing in the 21st century: use of a predictive toxicological approach and high-throughput screening. Acc Chem Res. 2013;46:607–21.
13. Nel AE, Parak WJ, Chan WC, Xia T, Hersam MC, Brinker CJ, Zink JI, Pinkerton KE, Baer DR, Weiss PS. Where are we heading in nanotechnology environmental health and safety and materials characterization? ACS Nano. 2015;9:5627–30.
14. SCENIHR. The Scientific Committee on Emerging and Newly Identified Health Risks. Opinion on risk assessment of products of nanotechnologies, 19 Jan 2009. Available at: http://ec.europa.eu/health/archive/ph_risk/committees/04_scenihr/docs/scenihr_o_023.pdf
15. Rauscher H, Rasmussen K, Sokull-Klüttgen B. Regulatory aspects of nanomaterials in the EU. Chemie Ingenieur Technik. 2017;89(3):224–31.
16. Aitken RA, Bassan A, Friedrichs S, Hankin SM, Hansen SF, Holmqvist J, Peters SAK, Poland CA, Tran CL. Specific advice on exposure assessment and hazard/risk characterisation for nanomaterials under REACH (RIP-oN 3). Final project report. REACH-NANO consultation. RNC/RIP-oN3/FPR/1/FINAL, 2011
17. Klein CL, Wiench K, Wiemann M, Ma-Hock L, van Ravenzwaay B, Landsiedel R. Hazard identification of inhaled nanomaterials: making use of short-term inhalation studies. Arch Toxicol. 2012;86:1137–51.
18. Landsiedel R, Ma-Hock L, Hofmann T, Wiemann M, Strauss V, Treumann S, Wohlleben W, Groeters S, Wiench K, van Ravenzwaay B. Application of short-term inhalation studies to assess the inhalation toxicity of nanomaterials. Part Fibre Toxicol. 2014;11(1):16.
19. Molina RM, Konduru NV, Jimenez RJ, Pyrgiotakis G, Demokritou P, Wohlleben W, Brain JD. Bioavailability, distribution and clearance of tracheally instilled, gavaged or injected cerium dioxide nanoparticles and ionic cerium. Environ Sci: Nano. 2014;1(6):561–73.

20. Hayes A, Bakand S. Inhalation toxicology. Mol Clin Exp Toxicol Exp. 2010;(Suppl 100):461–88.
21. ICRP (International Commission on Radiological Protection). Human respiratory tract model for radiological protection. ICRP publication 66; Annales of ICRP 24, 1994, p. 231
22. Morrow PE. Possible mechanisms to explain dust overloading of the lungs. Fund Appl Toxicol. 1988;10:369–84.
23. Donaldson K, Tran L. Inflammation caused by particles and fibers. Inhal Toxicol. 2002;14:5–27.
24. Monteiller C, Tran L, MacNee W, Faux S, Jones A, Miller B, Donaldson K. The pro-inflammatory effects of low-toxicity low-solubility particles, nanoparticles and fine particles, on epithelial cells in vitro: The role of surface area. Occup. Environ. Med. 2007;64:609–15.
25. Konduru N, Keller J, Ma-Hock L, Gröters S, Landsiedel R, Donaghey TC, Brain JD, Wohlleben W, Molina RM. Biokinetics and effects of barium sulfate nanoparticles. Part Fibre Toxicol. 2014;11:55.
26. Konduru NV, Murdaugh KM, Sotiriou GA, Donaghey TC, Demokritou P, Brain JD, Molina RM. Bioavailability, distribution and clearance of tracheally-instilled and gavaged uncoated or silica-coated zinc oxide nanoparticles. Part Fibre Toxicol. 2014;11:44.
27. ECETOC. European Centre for Ecotoxicology and Toxicology of Chemicals. Technical Report No. 122. Poorly soluble particles. Lung overload. Brussels, Belgium: ECETOC; 2013. Available at: www.ecetoc.org
28. ILSI (International Life Sciences Institute Risk Science Institute Workshop Participants). The relevance of the rat lung response to particle overload for human risk assessment: a workshop consensus report. Inhal Toxicol. 2000;12(1–2):1–17.
29. OECD. Organisation for economic co-operation and development. Guideline for testing of chemicals no. 412. Subacute inhalation toxicity: 28-day study. Paris: OECD; 2017.
30. OECD. Organisation for economic co-operation and development. Guideline for testing of chemicals no. 413. Subchronic inhalation toxicity: 90-day study. Paris: OECD; 2017.
31. OECD. Organisation for economic co-operation and development. Guideline for testing of chemicals no. 403. Acute inhalation toxicity. Paris: OECD; 2009.
32. Hofmann T, Ma-Hock L, Athas J-C, Neubauer N, Wohlleben W, Veith U, End N, Gröters S, van Ravenzwaay B, Landsiedel R. Reduction of acute inhalation toxicity testing in rats: the contact angle of pigments predicts their suffocation potentials. Appl In Vitro Toxicol. 2018;4:220–8.
33. Russell WMS, Burch RL. The principles of humane experimental technique. London: Methuen; 1959. Reprinted by UFAW, 1992. 238 pp
34. EP and Council. Directive 2010/63/EU of the European Parliament and of the Council of 22 Sept 2010 on the protection of animals used for scientific purposes. OJ L 276/33, 20 Oct 2010
35. Cho WS, Duffin R, Bradley M, Megson IL, MacNee W, Lee JK, Jeong J, Donaldson K. Predictive value of *in vitro* assays depends on the mechanism of toxicity of metal oxide nanoparticles. Part Fibre Toxicol. 2013;10:55.
36. Delaval M, Wohlleben W, Landsiedel R, Baeza-Squiban A, Boland S. Assessment of the oxidative potential of nanoparticles by the cytochrome c assay: assay improvement and development of a high-throughput method to predict the toxicity of nanoparticles. Arch Toxicol. 2017;91(1):163–77.
37. Kroll A, Dierker C, Rommel C, Hahn D, Wohlleben W, Schulze-Isfort C, Göbbert C, Voetz M, Hardinghaus F, Schnekenburger J. Cytotoxicity screening of 23 engineered nanomaterials using a test matrix of ten cell lines and three different assays. Part Fibre Toxicol. 2011;8:9.
38. Park EJ, Lee GH, Han BS, Lee BS, Lee S, Cho MH, Kim JH, Kim DW. Toxic response of graphene nanoplatelets *in vivo* and *in vitro*. Arch Toxicol. 2015;89:1557–68.
39. Stern ST, Adiseshaiah PP, Crist RM. Autophagy and lysosomal dysfunction as emerging mechanisms of nanomaterial toxicity. Part Fibre Toxicol. 2012;9:20.
40. Wiemann M, Vennemann A, Sauer UG, Wiench K, Ma-Hock L, Landsiedel R. An alveolar macrophage assay for predicting the short-term inhalation toxicity of nanomaterials. J Nanobiotechnol. 2016;14:16.
41. Wiemann M, Sauer UG, Vennemann A, Bäcker S, Keller J-G, Ma-Hock L, Wohlleben W, Landsiedel R. *In vitro* and *in vivo* short-term pulmonary toxicity of differently sized colloidal amorphous SiO_2. Nanomaterials. 2018;8:160.

42. Haase A, Dommershausen N, Schulz M, Landsiedel R, Reichardt P, Krause BC, Tentschert J, Luch A. Genotoxicity testing of different surface-functionalized SiO$_2$, ZrO$_2$ and silver nanomaterials in 3D human bronchial models. Arch Toxicol. 2017;91:3991–4007.
43. Landsiedel R, Kapp MD, Schulz M, Wiench K, Oesch F. Genotoxicity investigations on nanomaterials: methods, preparation and characterization of test material, potential artifacts and limitations—many questions, some answers. Mutat Res. 2009;681:241–58.
44. Maser E, Schulz M, Sauer UG, Wiemann M, Ma-Hock M, Wohlleben W, Hartwig A, Landsiedel R. *In vitro* and *in vivo* genotoxicity investigations of differently sized amorphous SiO$_2$ nanomaterials. Mutat Res. 2015;794:57–74.
45. Arts JH, Muijser H, Duistermaat E, Junker K, Kuper C. Five day inhalation toxicity study of three types of synthetic amorphous silicas in Wistar rats and post-exposure evaluations for up to 3 months. Food Chem Toxicol. 2007;45(10):1856–67.
46. Landsiedel R, Wiench K, Wohlleben W. Geeignete Methoden zur Prüfung der Sicherheit von Nanomaterialien. Chemie Ingenieur Technik. 2008;80(11):1641–51.
47. Ma-Hock L, Burkhardt S, Strauss V, Gamer AO, Wiench K, van Ravenzwaay B, Landsiedel R. Development of a short-term inhalation test in the rat using nano-titanium dioxide as a model substance. Inhal Toxicol. 2009;21(2):102–18.
48. Gosens I, Mathijssen LE, Bokkers BG, Muijser H, Cassee FR. Comparative hazard identification of nano- and micro-sized cerium oxide particles based on 28-day inhalation studies in rats. Nanotoxicology. 2014;8(6):643–53.
49. Hahn D, Wiemann M, Haase A, Ossig R, Alessandrini F, M-Hock L, Landsiedel R, Nern M, Vennemann A, Driessen MD, Luch L, Dopp E, Schnekenburger J. Toxicological effects of metal oxide nanomaterials, Chapter 8. In: Wohlleben W, Kuhlbusch TAJ, Lehr CM, Schnekenburger J, editors. Safety of nanomaterials along their lifecycle: release, exposure, human hazards. Boca Raton, FL: CRC Press; 2014. p. 191–211.
50. Robert L, et al. Application of short-term inhalation studies to assess the inhalation toxicity of nanomaterials. Part Fibre Toxicol. 2014;11(1):16.
51. Kim YH, et al. Short-term inhalation study of graphene oxide nanoplates. Nanotoxicology. 2018;12(3):224–38.
52. Landsiedel R, Ma-Hock L, Kroll A, Hahn D, Schnekenburger J, Wiench K, Wohlleben W. Testing metal oxide nanomaterials for human safety. Adv Mater. 2010;22:2601–27.
53. Cho WS, Choi M, Han BS, Cho M, Oh J, Park K, Kim SJ, Kim SH, Jeong J. Inflammatory mediators induced by intratracheal instillation of ultrafine amorphous silica particles. Toxicol Lett. 2007;175(1–3):24–33.
54. Morimoto Y, Hirohashi M, Ogami A, Oyabu T, Myojo T, Todoroki M, Yamamoto M, Hashiba M, Mizuguchi Y, Lee BW, et al. Pulmonary toxicity of well-dispersed multi-wall carbon nanotubes following inhalation and intratracheal instillation. Nanotoxicology. 2012;6:587–99.
55. Morimoto Y, Izumi H, Yoshiura Y, Tomonaga T, Oyabu T, Myojo T, Kawai K, Yatera K, Shimada M, Kubo M, Yamamoto K, Kitajima S, Kuroda E, Kawaguchi K, Sasaki T. Pulmonary toxicity of well-dispersed cerium oxide nanoparticles following intratracheal instillation and inhalation. J Nanopart Res. 2015;17(11):442.
56. Morimoto Y, Izumi H, Yoshiura Y, Fujisawa Y, Yatera K, Fujita K, Maru J, Endoh S, Honda K. Basic study of intratracheal instillation study of nanomaterials for the estimation of the hazards of nanomaterials. Ind Health. 2018;56(1):30–9.
57. Ran L, Lihong Y, Yuepu P, Geyu L, Juan Z, Yaoyao S, Zhiping X, Bing Y. Pulmonary toxicity induced by three forms of titanium dioxide nanoparticles via intra-tracheal instillation in rats. Progr Nat Sci. 2009;19:573–9.
58. Schulz M, Ma-Hock L, Brill S, Strauss V, Treumann S, Gröters S, van Ravenzwaay B, Landsiedel R. Investigation on the genotoxicity of different sizes of gold nanoparticles. Mutat Res. 2012;745:51–7.
59. Stoeger T, Reinhard C, Takenaka S, Schroeppel A, Karg E, Ritter B, Heyder J, Schulz H. Instillation of six different ultrafine carbon particles indicates a surface area threshold dose for acute lung inflammation in mice. Environ Health Perspect. 2006;114(3):328–33.

60. Vennemann A, Alessandrini F, Wiemann M. Differential effects of surface-functionalized zirconium oxide nanoparticles on alveolar macrophages, rat lung, and a mouse allergy model. Nanomaterials. 2017;7:280.
61. Warheit DB, Webb TR, Reed KL. Pulmonary toxicity screening studies in male rats with TiO_2 particulates substantially encapsulated with pyrogenically deposited amorphous silica. Part Fibre Toxicol. 2006;3(3)
62. Yang H, Wu QY, Li MY, Lao CS, Zhang YJ. Pulmonary toxicity in rats caused by exposure to intratracheal instillation of SiO_2 nanoparticles. Biomed Environ Sci. 2017;30(4):264–79.
63. Baisch BL, Corson NM, Wade-Mercer P, Gelein R, Kennell AJ, Oberdörster G, Elder A. Equivalent titanium dioxide nanoparticle deposition by intratracheal instillation and whole body inhalation: the effect of dose rate on acute respiratory tract inflammation. Part Fibre Toxicol. 2014;11:5.
64. Keller JG, Graham U, Koltermann-Jülly J, Gelein R, Ma-Hock L, Landsiedel R, Wiemann M, Oberdörster G, Elder A, Wohlleben W. Predicting dissolution and transformation of inhaled nanoparticles in the lung using abiotic flow cells: the case of barium sulfate. Manuscript under review, 2019
65. Hadrup N, Bengtson S, Jacobsen NR, Jackson P, Nocun M, Saber AT, Jensen KA, Wallin H, Vogel U. Influence of dispersion medium on nanomaterial-induced pulmonary inflammation and DNA strand breaks: investigation of carbon black, carbon nanotubes and three titanium dioxide nanoparticles. Mutagenesis. 2017;32(6):581–97.
66. Horie M, Yoshiura Y, Izumi H, Oyabu T, Tomonaga T, Okada T, Lee BW, Myojo T, Kubo M, Shimada M, Morimoto Y. Comparison of the pulmonary oxidative stress caused by intratracheal instillation and inhalation of NiO nanoparticles when equivalent amounts of NiO are retained in the lung. Antioxidants (Basel). 2016;5(1):4.
67. Morimoto Y, Izumi H, Yoshiura Y, Tomonaga T, Lee BW, Okada T, Oyabu T, Myojo T, Kawai K, Yatera K, Shimada M, Kubo M, Yamamoto K, Kitajima S, Kuroda E, Horie M, Kawaguchi K, Sasaki T. Comparison of pulmonary inflammatory responses following intratracheal instillation and inhalation of nanoparticles. Nanotoxicology. 2016;10(5):607–18.
68. Oyabu T, Myojo T, Lee BW, Okada T, Izumi H, Yoshiura Y, Tomonaga T, Li YS, Kawai K, Shimada M, Kubo M, Yamamoto K, Kawaguchi K, Sasaki T, Morimoto Y. Biopersistence of NiO and TiO2 nanoparticles following intratracheal instillation and inhalation. Int J Mol Sci. 2017;18(12):2757.
69. Greim H, Ziegler-Skylakakis K. Risk assessment for biopersistent granular particles. Inhal Toxicol. 2007;19(Suppl 1):199–204.
70. Arts JH, Hadi M, Keene AM, Kreiling R, Lyon D, Maier M, Michel K, Petry T, Sauer UG, Warheit D, Wiench K, Landsiedel R. A critical appraisal of existing concepts for the grouping of nanomaterials. Regul Toxicol Pharmacol. 2014;70:492–506.
71. Burden N, Aschberger K, Chaudhry Q, Clift MJD, Fowler P, Johnston H, Landsiedel R, Rowland J, Stone V, Doak SH. Aligning nanotoxicology with the 3Rs: What is needed to realise the short, medium and long-term opportunities? Regulate Toxicol Pharmacol. 2017;91:257–66.
72. Godwin H, Nameth C, Avery D, Bergeson LL, Bernard D, Beryt E, Boyes W, Brown S, Clippinger AJ, Cohen Y, Doa M, Hendren CO, Holden P, Houck K, Kane AB, Klaessig F, Kodas T, Landsiedel R, Lynch I, Malloy T, Miller MB, Muller J, Oberdörster G, Petersen EJ, Pleus RC, Sayre P, Stone V, Sullivan KM, Tentschert J, Wallis P, Nel AE. Nanomaterial categorization for assessing risk potential to facilitate regulatory decision-making. ACS Nano. 2015;9(4):3409–17.
73. OECD. Organisation for economic co-operation and development series on testing and assessment no. 194. Guidance on grouping of chemicals. ENV/JM/MONO(2014)4. 2nd ed. Paris: OECD; 2014.
74. Bos PM, Gottardo S, Scott-Fordsmand JJ, van Tongeren M, Semenzin E, Fernandes TF, Hristozov D, Hund-Rinke K, Hunt N, Irfan MA, Landsiedel R, Peijnenburg WJ, Sánchez Jiménez A, van Kesteren PC, Oomen AG. The MARINA Risk Assessment Strategy: A flex-

ible strategy for efficient information collection and risk assessment of nanomaterials. Int J Environ Res Public Health. 2015;12:15007–21.

75. Braakhuis HM, Oomen AG, Cassee FR. Grouping nanomaterials to predict their potential to induce pulmonary inflammation. Toxicol Appl Pharmacol. 2016;299:3–7.

76. Ankley GT, Bennett RS, Erickson RJ, Hoff DJ, Hornung MW, Johnson RD, Mount DR, Nichols JW, Russom CL, Schmieder PK, Serrrano JA, Tietge JE, Villeneuve DL. Adverse outcome pathways: a conceptual framework to support ecotoxicology research and risk assessment. Environ Toxicol Chem. 2010;29:730–41.

77. Oomen AG, Bos PMJ, Fernandes TF, Hund-Rinke K, Boraschi D, Byrne HJ, Aschberger K, Gottardo S, van der Kammer F, Kühnel D, Hristozov D, Marcomini A, Migliore L, Scott-Fordsmand J, Wick P, Landsiedel R. Concern-driven integrated approaches to nanomaterial testing and assessment—Report of the NanoSafety Cluster Working Group 10. Nanotoxicology. 2014;8:334–48.

78. Oomen AG, Bleeker EA, Bos PM, van Broekhuizen F, Gottardo S, Groenewold M, Hristozov D, Hund-Rinke K, Irfan MA, Marcomini A, Peijnenburg WJ, Rasmussen K, Jiménez AS, Scott-Fordsmand JJ, van Tongeren M, Wiench K, Wohlleben W, Landsiedel R. Grouping and read-across approaches for risk assessment of nanomaterials. Int J Environ Res Public Health. 2015;12:13415–1334.

79. Stone V, Pozzi-Mucelli S, Tran L, Aschberger K, Sabella S, Vogel U, Poland C, Balharry D, Fernandes T, Gottardo S, Hankin S, Hartl MG, Hartmann N, Hristozov D, Hund-Rinke K, Johnston H, Marcomini A, Panzer O, Roncato D, Saber AT, Wallin H, Scott-Fordsmand JJ. ITS-NANO—prioritising nanosafety research to develop a stakeholder driven intelligent testing strategy. Part Fibre Toxicol. 2014;11:9.

80. Arts JH, Hadi M, Irfan MA, Keene AM, Kreiling R, Lyon D, Maier M, Michel K, Petry T, Sauer UG, Warheit D, Wiench K, Wohlleben W, Landsiedel R. A decision-making framework for the grouping and testing of nanomaterials (DF4nanoGrouping). Regul Toxicol Pharmacol. 2015;71(2 Suppl):S1–27.

81. Arts JH, Irfan MA, Keene AM, Kreiling R, Lyon D, Maier M, Michel K, Neubauer N, Petry T, Sauer UG, Warheit D, Wiench K, Wohlleben W, Landsiedel R. Case studies putting the decision-making framework for the grouping and testing of nanomaterials (DF4nanoGrouping) into practice. Regul Toxicol Pharmacol. 2016;76:234–61.

82. Landsiedel R, Ma-Hock L, Wiench K, Wohlleben W, Sauer UG. Safety assessment of nanomaterials using an advanced decision-making framework, the DF4nanoGrouping. J Nanopart Res. 2017;19:171.

83. Landsiedel R, Sauer UG, De Jong W. Risk assessment and risk management, Chapter 8. In: Fadeel B, Pietroiusti A, Shvedova AA, editors. Adverse effects of engineered nanomaterials: exposure, toxicology, and impact on human health. 2nd ed. London: Academic Press; 2017. p. 189–222.

84. Avramescu M-L, Rasmussen PE, Chénier M, Gardner HD. Influence of pH, particle size and crystal form on dissolution behaviour of engineered nanomaterials. Environ Sci Pollut Res. 2017;24:1553–64.

85. Koltermann-Jülly J, Keller JG, Vennemann A, Werle K, Ma-Hock L, Landsiedel R, Wiemann M, Wohlleben W. Abiotic dissolution rates of 24 (nano)forms of 6 substances compared to macrophage-assisted dissolution and in vivo pulmonary clearance: grouping by biodissolution and transformation. NanoImpact. 2018;12:29–41.

86. De Jong WH, De Rijk E, Brunelli A, Wohlleben W, Stone V, Bonetto A, Marcomini A, Gosens I, Cassee FR. Toxicity of copper oxide and basic copper carbonate nanoparticles after short term oral exposure in rats. Nanotoxicology. 2019;13(1):50–72.

87. Hellack B, Nickel C, Albrecht C, Kuhlbusch TAJ, Boland S, Baeza-Squiban A, Wohlleben W, Schins RPF. Analytical methods to assess the oxidative potential of nanoparticles: a review. Environ Sci Nano. 2017;4:1920–34.

88. Hellack B, Werle K, Bahl A, Nickel C, Ruggiero E, Haase A, Wohlleben W. Surface reactivity measured by the ESR and FRAS assays substantiates the similarity of nanoforms for several substances, but may not establish hazard groups. Manuscript in preparation, 2019

89. Choi HS, Ashitate Y, Lee JH, Kim SH, Matsui A, Insin N, Bawendi MG, Semmler-Behnke M, Frangioni JV, Tsuda A. Rapid translocation of nanoparticles from the lung airspaces to the body. Nat Biotechnol. 2010;28:1300–3.
90. ECHA. European Chemicals Agency. Guidance on information requirements and chemical safety assessment. Appendix R.6-1 for nanomaterials applicable to the Guidance on QSARs and Grouping of Chemicals. Version 1.0, May 2017, ECHA-17-G-17-EN, 29 pp
91. Morimoto Y, Izumi H, Yoshiura Y, Fujishima K, Yatera K, Yamamoto K. Usefulness of intra-tracheal instillation studies for estimating nanoparticle-induced pulmonary toxicity. Int J Mol Sci. 2016;17(2):165.
92. Suzui M, Futakuchi M, Fukamachi K, Numano T, Abdelgied M, Takahashi S, Ohnishi M, Omori T, Tsuruoka S, Hirose A, Kanno J, Sakamoto Y, Alexander DB, Alexander WT, Jiegou X, Tsuda H. Multiwalled carbon nanotubes intratracheally instilled into the rat lung induce development of pleural malignant mesothelioma and lung tumors. Cancer Sci. 2016;107(7):924–35.
93. Kasai T, Umeda Y, Ohnishi M, Mine T, Kondo H, Takeuchi T, Matsumoto M, Fukushima S. Lung carcinogenicity of inhaled multi-walled carbon nanotube in rats. Part Fibre Toxicol. 2016;13(1):53.
94. Fukushima S, Kasai T, Umeda Y, Ohnishi M, Sasaki T, Matsumoto M. Carcinogenicity of multi-walled carbon nanotubes: challenging issue on hazard assessment. J Occup Health. 2017;60(1):10–30.
95. MAK. Commission for the investigation of health hazards of chemical compounds in the work area. Nanomaterials. Report. Edited by Deutsche Forschungsgemeinschaft (DFG). Germany: Wiley-VCH; 2013, 94 pp., ISBN: 978-3-527-33571-8

Part I
Short-Term Inhalation Study

Chapter 2
The Short-Term Inhalation Study (STIS) as a Range Finder and Screening Tool in a Tiered Grouping Strategy

Karin Wiench and Lan Ma-Hock

Abstract The rat short-term inhalation study (STIS; 5 days exposure, 6 h/day; approx. 3-week postexposure observation) allows assessing test material-induced early respiratory tract effects, the progression or reversibility of effects, pulmonary particle deposition, and potential test material translocation to extra-pulmonary tissues and the evolvement of systemic effects. This chapter provides details on the STIS study design focusing on aerosol characterization, performance of bronchoalveolar lavage in half a lung and preparation of the other half for histopathology. Five case studies (CSs) exemplify how the rat STIS can be used for initial safety assessments, e.g., within the previously published *Decision-making framework for the grouping and testing of nanomaterials*. This tiered framework allows grouping nanomaterials as soluble (CS 1: CuO, ZnO); high aspect ratio nanomaterials (CS 2: multiwall carbon nanotubes); passive (CS 3: BaSO$_4$, ZrO$_2$, graphite nanoplatelets); or active (CS 4: CeO$_2$, TiO$_2$). CS 5 addresses different amorphous SiO$_2$ that are either soluble, passive, or active. In conclusion, the rat STIS and 28-day/90-day inhalation toxicity studies reveal comparable effects, and the rankings of no-observed adverse effect concentrations are very similar. Compared with 28-day and 90-day inhalation toxicity studies (OECD Test Guidelines 412 and 413), the rat STIS requires fewer animals and its duration is considerably shorter. Thereby, this test serves the 3Rs principle to replace, reduce, and refine animal testing. If 28-day and 90-day inhalation toxicity studies are mandatory for regulatory purposes, the rat STIS is a suitable range-finding study to select appropriate concentrations for the longer-term studies.

Keywords Engineered nanoparticles · Short-term inhalation study (STIS) Pulmonary inflammation · Pulmonary particle deposition · Systemic uptake Decision-making framework for the grouping and testing of nanomaterials

K. Wiench (✉)
Product Safety, BASF SE, Ludwigshafen, Germany
e-mail: karin.wiench@basf.com

L. Ma-Hock
Experimental Toxicology and Ecology, BASF SE, Ludwigshafen, Germany

(DF4nanoGrouping) · Initial safety assessment · 3Rs principle (replacement, reduction, refinement of animal testing)

2.1 Introduction

The rat short-term inhalation study (STIS) is an in vivo inhalation screening tool that provides information on early key elements of pulmonary pathogenesis and on the progression or reversibility of effects. Further, it allows measuring pulmonary particle deposition, i.e., lung burden, thereby also yielding limited biokinetic data, and it includes an assessment of potential test material translocation to extrapulmonary tissues and the evolvement of systemic effects [1–4].

Generally, the rat STIS should be performed in compliance with the most recent versions of Organisation for Economic Co-operation and Development (OECD) Test Guidelines (TGs) 412 and 413 [5, 6] with the exception of the shorter exposure period of 5 days and the use of fewer animals in compliance with the 3Rs principle to replace, reduce, and refine animal testing [7]. An overview of the STIS study design has been provided in Chap. 1. In brief, the rat STIS protocol includes 5 days of inhalation exposure (6 h/day); sacrifice of exposure groups on day 1 postexposure and of recovery groups on approx. day 20–22 postexposure. The exposure and recovery groups encompass 8 rats each for the control group and 3 test groups (5 rats/group for BALF analysis and histopathology; 3 rats/group to determine lung burden). Optionally, the two lower test groups can be omitted from the recovery group, thereby allowing to investigate early pulmonary effects of nanomaterials using a total of 48 animals as compared to up to 160 rats/study when OECD TG 412 or 413 is performed.

In the rat STIS, the inflammation potency in the respiratory tract is investigated by analyzing the bronchoalveolar fluid (BALF) and by histopathology of the respiratory tract as two complementary methods to examine the portal of entry toxicity of inhaled particles. The BALF evaluation allows detecting treatment-related early inflammatory reactions that might not yet be observable by histopathology after 5-day inhalation exposure. The histopathological examination allows detecting early morphological changes of the lung.

Generally, inhaled particles that reach the lung attract macrophages that phagocytize the particles. In the alveolar region, alveolar macrophage-mediated mucociliary transport is considered the main mechanism for clearance. As long as inflammatory reactions do not evolve, the attraction of macrophages and particle phagocytosis are not adverse findings. However, if pronounced accumulations of alveolar macrophages coincide with inflammatory reactions (revealed by moderate to severe histiocytosis and mild bronchiolar hypertrophy or hyperplasia), the findings most likely indicate pulmonary particle overload. This mechanism of action is observed when rats are exposed to high concentrations of poorly soluble particles that exceed the pulmonary clearance mechanisms. By contrast, the human health relevance of pulmonary overload has been questioned (cf. Chap. 1, Sect. 1.1).

Lung burden is determined in the rat STIS to assess pulmonary particle deposition, i.e., the inhaled nanomaterial's internal dose. This parameter appears to be more predictive of toxicity than the total applied mass of the aerosolized nanomaterial, i.e., the external dose [8, 9]. Accordingly, the nanomaterials' deposition pattern (i.e., the regions of the respiratory tract in which particles deposit) appears to determine their interaction with the lung and subsequent lung clearance and toxicity [8, 9]. For poorly soluble particles, the lung burden immediately postexposure is consistent with the total deposition because their daily clearance during the exposure period is negligible (for which reason pulmonary overload can evolve). By determining lung burden immediately postexposure and at the end of the recovery period and relating the two values, tendencies for retarded test material clearance, i.e., biopersistence, can be assessed.

This chapter provides further details on the performance of the rat STIS and shows how this test can be used for initial safety assessments:

- Section 2.2 discusses selected key elements of the rat STIS:
    - Section 2.2.1: Characterization of the test material and aerosol particle size distribution.
    - Section 2.2.2: BALF parameters, bronchoalveolar lavage (BAL), and fixation of the lung.
- Section 2.3 presents five case studies exemplifying how the rat STIS can be used as a screening tool within a tiered grouping and testing strategy. Provides an overall comparison of the rat STISs and 28-dazy and 90-day inhalation studies presented in the case studies.
- Section 2.4 draws conclusions from this chapter.

2.2   Selected Key Elements of the Rat STIS

2.2.1   Characterization of the Test Material and Aerosol Particle Size Distribution

Test material characterization and the specific methodological aspects of aerosol generation should always be considered in inhalation studies assessing nanomaterials. The generated nanomaterial-containing aerosols need to be characterized for consistency, homogeneity, and stability with respect to a variety of physicochemical properties including particle size distribution, morphology, chemical composition and impurities, solubility (and leaching), surface area, surface chemistry and surface reactivity (cf. Wohlleben et al. [10–14] and Gandon et al. [15] for details on suitable methodologies for nanomaterial characterization).

When surveying the particle spectra in the test atmosphere, different devices should be used to ensure that large size ranges are covered [16]. The "gold standard" for measuring particle sizes in aerosols during inhalation studies is the *cas-*

cade impactor measurement, which yields the mass median aerodynamic diameter (MMAD). Consideration of the MMAD is crucial when assessing the likely deposition behavior of inhaled particles. However, the cascade impactor measurement does not cover particle sizes in the submicron range that is relevant for nanomaterials, because the movement of particles with diameters below 0.4 μm in the air does not follow aerodynamic rules, but is driven by diffusion.

The *Scanning Mobility Particle Sizer* (SMPS) is considered appropriate for measurements in the submicron range (from a few nm to 1000 nm). It comprises an Electrostatic Classifier separating the particles into known size fractions and a Condensation Particle Counter measuring particle count concentrations. Finally, particle sizes can be measured using a *white light aerosol spectrometer* in which single particles are illuminated with a non-polarized white-light source, and the light scattered by the particles is measured. This device allows determining the size range from a few 100 nm to a maximum of 100 μm. Notably, the SMPS measures the particles' electro-mobility, whereas the white light aerosol spectrometer measures the light scattered by the particles. As different physical properties of the particles are measured, the data obtained with different devices are often not comparable [16].

2.2.2   Best Practice of Bronchoalveolar Lavage and Histological Examination of the Lung in the Same Animal

BALF parameters, i.e., absolute and relative cell counts, total protein, enzyme activities, and the release of pro-inflammatory cytokines and chemokines, provide an indication for acute reactions of the lung, which are not necessarily associated to a specific type of morphological change. BALF parameters are very sensitive, especially during the early phase of exposure to nanomaterials that is covered by the rat STIS, whereas their alterations may attenuate during prolonged exposure periods.

The polymorphonuclear neutrophils (PMNs) in the BALF respond very sensibly to the presence of inhaled particles. Due to their low absolute counts in the BALF of healthy rats, a slight increase already leads to a high relative increase. An increase in the number of PMNs is often accompanied by increased lymphocytes, total protein concentrations, and enzyme activities (especially lactate dehydrogenase (LDH), γ-glutamyltransferase (GGT), alkaline phosphatase (ALP), and *N*-acetyl glucosaminidase (NAG)). Additionally, cytokines and chemokines (e.g., monocyte chemoattractant protein-1 (MCP-1), cytokine-induced neutrophil chemoattractant/interleukin-8 (CINC/IL-8), macrophage colony stimulating factor (M-CSF), and osteopontin, a marker for fibro-proliferative lung disease in rodents and human [17]) can be investigated in the BALF to provide early indications for potential morphological changes after sub-chronic or chronic exposure [2, 3, 18].

The BAL technique using the whole lung for lavage has been described extensively, e.g., by Henderson et al. [19]. Thereby, histopathology is performed using non-manipulated lungs from designated animals. To reduce overall animal numbers,
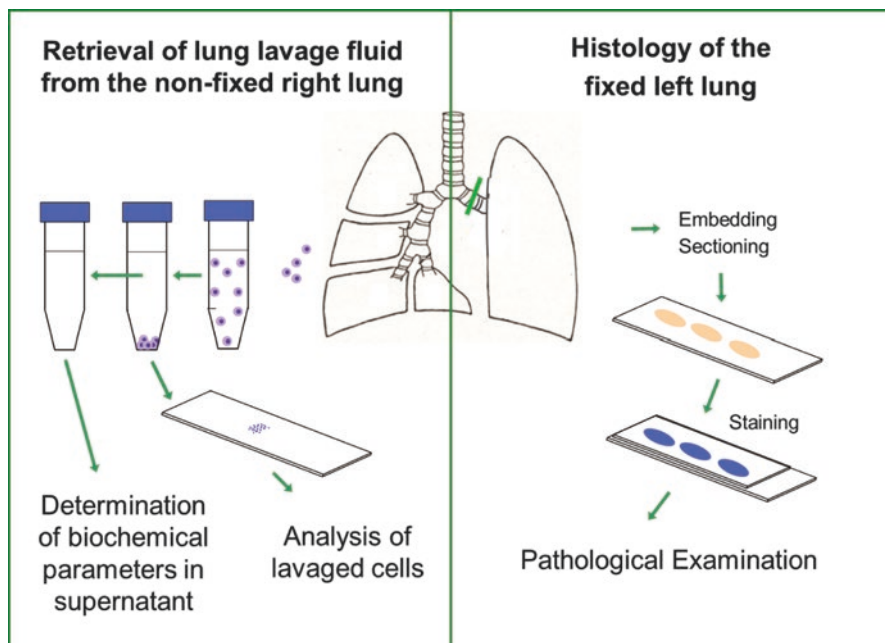
Fig. 2.1 Rat STIS: preparation of the rat lung for subsequent analysis of the bronchoalveolar fluid and histopathology of the lung

the most recent updates of OECD TGs 412 and 413 [5, 6] recommend performing the BAL in half a lung and using the remaining tissue for lung histopathology. The method has been described lately by Wiemann and his colleagues [20, 21]. The best praxis procedure established in the authors' laboratory is described below (Fig. 2.1), which is a modified and standardized version of abovementioned method by Wiemann et al. [21].

Since the BAL is performed to detect an inflammatory response in the bronchoalveolar region after inhalation exposure to a test material, a gentle, standardized procedure is warranted. For this purpose, the lung is lavaged in situ with as little manipulation as possible.

Rats are deeply anesthetized (e.g., using pentobarbiturate) and then euthanized by opening the abdominal aorta. Thereafter, the thorax is opened and the tissues around the trachea are removed. As only the right lung is being lavaged, the left lung is tied shortly after the bifurcation to prevent lavage fluid from entering. A catheter is tied into the trachea, and a syringe is used to administer the lavage fluid. The fluid is instilled by pumping 3 mL (for a 300-g rat) physiological NaCl (6 mL/min) into the right lung. After a 30-s dwell time the fluid is gently withdrawn at a speed of 6 mL/min. The right lung is washed a second time in the same manner. The BALF of these two washes is pooled and examined for the abovementioned cytological and biochemical parameters. Wash volume and number of washes are well in accordance with the method described by Henderson et al. [19] with some modi-

fications for using the same animal for BAL and histopathology. The applicability of the procedure to perform the BAL using half a lung has been tested in positive control animals exposed to quartz DQ 12: Evaluating the relative changes of BALF parameters (to account for the inevitable absolute differences when an entire or half a lung are used), there were no statistically significant differences between whole lung and right lung lavage [22].

After lavaging of the right lung, the ligation is detached. The whole lung is excised and fixed under 20–30 cm water pressure with 4% buffered formalin according to the instructions of OECD TG 413. Histopathology of the so prepared lung showed that the lung was preserved properly and that the alveolar lumen of the right lung was not distorted by the lavage procedure [22]. Further, the examination showed that in situ lavage was superior to ex situ lavage with respect to reproducibility and integrity of the lung tissue.

2.3 Use of the Rat STIS as a Screening Tool Within a Tiered Grouping and Testing Strategy

A broad variety of nanomaterials has been assessed using the rat STIS study protocol either during product development or in the context of research projects addressing nanomaterial safety assessments. Moreover, the rat STIS is an integral component of the *Decision-making framework for the Grouping and testing of nanomaterials* (*DF4nanoGrouping*; Arts et al. [23, 24]). As described in Chap. 1, Sect. 1.4, the DF4nanoGrouping is a tiered grouping and testing strategy that includes information on intrinsic material properties in Tier 1, functionalities in Tier 2, and the rat STIS in the final Tier 3 (cf. Chap. 1, Table 1.1, for an overview of the DG4nanoGrouping grouping criteria and thresholds for nanomaterial grouping). Application of the DF4nanoGrouping provides information on the toxic potential and potency of inhaled nanomaterials and on the mechanisms by which effects are likely to evolve. Embedded in the DF4nanoGrouping, the rat STIS yields information that is both relevant for initial safety assessments and for the identification and refinement of further toxicity testing needs [23, 24].

Below, five case studies show how the rat STIS can be used within the DF4nanoGrouping. In line with the DF4nanoGrouping concept to assign nanomaterials to one of four main groups (MGs), the case studies cover:

1. Soluble metal oxide nanomaterials (MG1): 10 nm-CuO, ZnO NM-111
2. High aspect ratio (HAR) nanomaterials (MG2): Multiwall carbon nanotubes
3. Passive nanomaterials (MG3): $BaSO_4$ NM-220, nano-ZrO_2, graphite nanoplatelets
4. Active nanomaterials (MG4); CeO_2 NM-212, TiO_2 NM-105
5. The special case of amorphous SiO_2: (MG1, MG3, or MG4)

Of note, all NM-x numberings (e.g., ZnO NM-111) relate to the codes of representative nanomaterials of the OECD sponsorship program [25]. Extensive information on the intrinsic material properties of these representative nanomaterials

has been collated at the European Commission's Joint Research Centre (cf. https://ec.europa.eu/jrc/en/scientific-tool/jrc-nanomaterials-repository). Due to their comprehensive characterization, the representative nanomaterials are highly suitable benchmark materials.

Each case study covers three aspects:

1. A summary of those DF4nanoGrouping Tier 1 intrinsic material properties and/or Tier 2 functionalities that are decisive for nanomaterial assignment to the respective MG.
2. A discussion of the outcomes of rat STISs as compared to the DF4nanoGrouping Tier 1 and Tier 2 MG assignments. For the sake of clarity and brevity, the case studies focus on BALF parameters, histopathology, the reversibility or progression of effects, and test material clearance behavior. Nevertheless, in compliance with OECD TG 412 and 413 [5, 6], the studies generally also included assessments of clinical signs, body weight, hematology, and serum biochemistry.
3. A comparison of the outcomes of the rat STISs to the findings from 28-day, 90-day, or 2-year studies for the same (or similar) nanomaterials.

To provide a foundation for further comparisons of rat STISs and longer-term studies, the tables referred to in the case studies present further published rat STISs, 28-day, 90-day, and 2-year inhalation toxicity studies other than those discussed in the 5 case studies.

2.3.1 Soluble Metal Oxide Nanomaterials (MG1): 10 nm-CuO, ZnO NM-111

2.3.1.1 Decisive Intrinsic Material Properties and Functionalities (Data Published by Arts et al. [24])

Water solubility of 10 nm-CuO and ZnO NM-111 was below the DF4nanoGrouping threshold of 100 mg/L. However, high dissolution in different media (>100 mg/L) resulted in assignment of these metal oxide nanomaterials to MG1. This high dissolution also indicated that cytotoxic copper or zinc ions might be released into biological media and fluids.

2.3.1.2 Rat STISs for Soluble Metal and Metal Oxide Nanomaterials (Table 2.1)

In all rat STISs assessing different variants of ZnO or CuO, rapid clearance of the test materials from the lung was recorded [2, 26, 27]. This confirmed the DF4nanoGrouping Tier 2 assignment as (MG1) soluble materials. For such non-biopersistent nanomaterials, the chemical composition is more important for hazard assessment than the as-produced nanostructure. Accordingly, the further hazard assessment of (MG1) soluble nanomaterials should be based upon read-across to

Table 2.1 Soluble metal and metal oxide nanomaterials (DF4nanoGrouping: MG1): rat STISs

Test material	Target conc. (mg/m³)	NOAEC (mg/m³); rat strain	Findings in BALF (significant as compared to control)	Pathological and histological findings	Progression or regression of effects	Clearance or pulmonary t_{50}	Reference
ZnO NM-111[a]	0.5, 2.0, 8.0	2.0; m Wi	Not available	At 8 mg/m³: (multi)focal very slight to slight degeneration of olfactory epithelium in nasal cavities, and alveolar accumulation of particle-laden macrophages in lungs	Fully reversible within 2 weeks	Rapid clearance within 2 weeks	[26]
ZnO NM-111	0.5, 2.5, 12.5	0.5; m Wi	Increased total cell counts and PMNs, lymphocyte, monocyte, total protein, GGT, LDH, ALP and NAG. Many mediators increased; above tenfold at highest concentration as compared to respective control values: CINC-1; clusterin; cystatin C; GCP-2; MCP-1; M-CSF; MDC; MPO; OPN	Nasal cavity: Moderate multifocal necrosis of olfactory epitheliaLung: Pronounced histiocytosis, granulocytic infiltration Mediastinal lymph nodes: lympho-reticulo-cellular hyperplasia	Not fully reversible within 3 weeks: Moderate histiocytosis in the lung and irregularities of olfactory epithelium remaining	Rapid clearance within 3 weeks	[2]
Micron-scale ZnO	12.5	<12.5; m Wi	Increased total cell counts and PMNs, lymphocytes, monocytes, total protein, GGT, LDH, ALP and NAG. Many mediators increased; above tenfold as compared to respective control values: clusterin; CRP; MCP-1; MCP-3; MDC; MPO; OPN	Nasal cavity: severe multifocal necrosis of olfactory epitheliaLung: Increased absolute (+27%) and relative lung (+34%) weight, bronchoalveolar hyperplasia, pronounced histiocytosis, granulocytic infiltration;Mediastinal lymph nodes: lympho-reticulo-cellular hyperplasia	Not fully reversible within 3 weeks: Slight to moderate histiocytosis in the lung and irregularities of olfactory epithelium remaining	Rapid clearance within 3 weeks	[2]

10 nm-CuO	0.6–13.2	0.6; m HsdCpb:WU	Increased total cell counts, macrophages, PMNs, lymphocytes, total protein, LDH, ALP, NAG, GGT	Alveolitis, bronchiolitis, vacuolation of respiratory epithelium and emphysema in the lung starting at 2.4 mg/m³	Not fully reversible within 3 weeks: Inflammation remnants at highest dose	Full clearance within 3 weeks	[27]
15 nm-Ag[b,c]	0.18 (3.8 × 10⁶ particles/cm³)	<0.18; m F-344	Increased total cell counts, PMNs, lymphocytes, monocytes, total protein, LDH, IL–1β and MCP-1, decreased MIP-2	No adverse findings	Increased macrophages at 7 days postexposure	At 24 h and 7 days postexposure: 5.5 and 2.1 µg Ag[d]	[28]
410 nm-Ag[b]	0.17 (2.0 × 10⁴ particles/cm³)	≥0.17; m F-344	Increased total protein	No adverse findings	Fully reversible within 7 days postexposure	At 24 h and 7 days postexposure: 8.5 and 5.9 µg Ag[d]	[28]

Abbreviations: *ALP* alkaline phosphatase, *BALF* bronchoalveolar lavage fluid, *CINC* cytokine-induced neutrophil chemoattractant, *CRP* C-reactive protein, *DPP* diketopyrrolopyrrole, *GCP* granulocyte chemotactic peptide, *GGT* γ-glutamyltransferase, *IL* interleukin, *LDH* lactate dehydrogenase, *LoD* limit of detection, *m* male, *M-CSF* macrophage colony stimulating factor, *MCP* monocyte chemoattractant protein, *MDC* macrophage-derived chemoattractant, *MIP* macrophage inflammatory protein, *NAG* N-acetyl-1-β-glucosaminidase, *NOAEC* no observed adverse effect concentration, *OPN* osteopontin, *PMN* polymorphonuclear neutrophil, *Wi* Wistar, *WU* Wistar Unilever

[a]Creutzenberg [29] performed a 14-day inhalation study using Wistar rats, assessing 0.5, 2, and 8 mg/m³ ZnO NM-111. At the highest dose, BALF parameters and histopathology indicated inflammatory reactions. Effects were fully reversible within 14 days. The 14-day NOAEC was assessed as 2 mg/m³

[b]4-Day exposure, 6 h/day. This study assessing 15 and 410 nm-Ag was added to DF4nanoGrouping MG1 on account of the test material's rapid clearance from the pulmonary tissue

[c]Seiffert et al. [30] exposed S-D rats to 0.67 mg/m³ 15 nm-Ag for 4 days (3 h/day). In the BALF, increased total cell numbers, neutrophils, lymphocytes, total protein, malondialdehyde, and cytokines/chemokines were recorded and by histopathology, mild inflammation with few inflammatory cell infiltrations in bronchial and vascular walls and alveolar septa. Lung inflammatory changes persisted within 7 days postexposure. There was significant clearance within 24 h, and further clearance by day 7 postexposure

[d]Silver in lung tissue determined by high resolution inductively coupled plasma mass spectrometry. Deposited dose (in mass) in alveolar region was 3.5 times higher in rats exposed to 15 nm-Ag than in those exposed to 410 nm-Ag

the bulk counterpart and/or the dissolved ions as well as available data from the nanomaterial itself.

Both by BALF analysis and histopathological evaluation, the available rat STISs for ZnO and CuO nanomaterials [2, 26, 27] as well as a 14-day inhalation toxicity study [29] provided indications for pronounced inflammatory reactions that were mostly not reversible within the 14–21-day recovery periods. For ZnO NM-111, a STIS NOAEC of 0.5 mg/m^3 was set [2] and for 10 nm-CuO, 0.6 mg/m^3 [27]. (Bellmann [26] established a 5-day NOAEC for ZnO NM-111; however this study did not include BALF evaluations.) In accordance with the DF4nanoGrouping thresholds, these NOAECs are graded as STIS NOAEC Range II (between <1 and 0.5 mg/m^3). By comparison, the STIS NOAEC Range I is set at <0.5 mg/m^3; Range III between ≥1 and <10 mg/m^3; and Range IV at ≥10 mg/m^3 (Arts et al. [24]; Chap. 1, Table 1.1).

2.3.1.3 28-Day and 90-Day Inhalation Studies for Soluble Metal Oxide Nanomaterials (Table 2.2)

To the best of the authors' knowledge, 28-day or 90-day studies assessing the inhalation toxicity of CuO nanomaterials have not yet been published (cf. also review by [33]). Consistent with the findings from the rat STIS, a 90-day inhalation study for ZnO NM-111 [32] as well as a 28-day inhalation study for 35-nm ZnO [31] revealed pronounced inflammatory reactions (both by BALF and histopathology) that were fully reversible within the 1–3 months recovery periods. For ZnO NM-111, a 90-day NOAEC of 1.5 mg/m^3 was set, i.e., threefold higher

Table 2.2 Soluble metal oxide nanomaterials (DF4nanoGrouping: MG1): rat 28-day and 90-day inhalation studies

Test material	Target conc. (mg/m^3); duration	NOAEC (mg/m^3); rat strain	Findings in BALF (significant as compared to control)	Pathological and histological findings	Progression or regression of effects	Reference
35 nm-ZnO[a]	2, 10; 28 days	2.0; m F-344	Increased total cell and PMN count and oxidative stress markers	Macrophage infiltration in alveolar space	Fully reversible within 3 months	[31]
ZnO NM-111	0.3, 1.5, 4.5; 90 days	1.5; m Wi	Increased markers for cellular damage and inflammation	Macrophage accumulation, alveolar hyperplasia in nose and lungs	Fully reversible within 1 month	[32]

Abbreviations: *m* male, *NOAEC* no observed adverse effect concentration, *PMN* polymorphonuclear neutrophil, *Wi* Wistar

[a]Source dispersion containing 2 weight% 3-aminopropyltriethoxysilane as a dispersing agent

than the corresponding STIS NOAEC, and for 35-nm ZnO a 28-day NOAEC of 2.0 mg/m^3.

2.3.2   HAR Nanomaterials (MG2): Multiwall Carbon Nanotubes (MWCNTs)

2.3.2.1   Decisive Intrinsic Material Properties and Functionalities (Data Published by [24])

HAR nanomaterials, such as MWCNTs, are nanomaterials that fulfill the fiber criteria of the World Health Organization [34], i.e., that have an aspect ratio of ≥3:1, a length >5 μm, and a diameter <3 μm. Hence, HAR nanomaterials are assigned to MG2 based upon the DF4nanoGrouping Tier 1 intrinsic material properties particle size and shape alone. In addition to the HAR, the rigidity, biopersistence, and residual metal catalyst content of HAR nanomaterials contribute to their hazard potential upon inhalation exposure [35–38]. Nevertheless, the rigidity of HAR nanomaterials was not addressed in the case studies published by Arts et al. [24] since there are currently no established methods for this parameter. Fiber diameter could be used as a proxy for rigidity, if the diameter of the material under investigation is comparable to the diameter of a MWCNT with known fiber toxicity [39]. Generally, rigid, biopersistent HAR nanomaterials, such as long, straight MWCNTs, may be expected to elicit asbestos-like effects [40] including pulmonary fibrosis [38], lung carcinoma [41, 42], and mesothelioma [43].

2.3.2.2   Rat STISs for MWCNTs (Table 2.3)

MWCNT NM-402 (forming fibrils and large spongy agglomerates) was evaluated in a STIS exposing male Wistar rats head-nose only to concentrations of 0.1, 0.5, or 2.5 mg/m^3 [18]. Significant increases of BALF markers indicative for inflammatory processes were recorded at 0.5 mg/m^3 and higher. Consistent with these changes in the BALF, microgranulomas were observed at 2.5 mg/m^3, which progressed in incidence after the 3-week recovery period. Based upon these findings, a STIS NOAEC of 0.1 mg/m^3 was set for MWCNT NM-402 [18]. In accordance with the DF4nanoGrouping thresholds, STIS NOAECs <0.5 mg/m^3 are graded as STIS NOAEC Range I indicating pronounced toxic potential.

2.3.2.3   90-Day and 2-Year Inhalation Studies for MWCNTs (Table 2.4)

Three 90-day inhalation studies have been published in which three different MWCNTs were tested that all form particle-like low-density agglomerates consisting of intertwined and coiled MWCNT fibers.

Table 2.3 High aspect ratio nanomaterials (DF4nanoGrouping MG2): rat STISs

Test material	Target conc. (mg/m³)	NOAEC (mg/m³); rat strain	Findings in BALF (significant as compared to control)	Pathological and histological findings	Progression or regression of effects	Clearance or pulmonary t_{50}	Reference
MWCNT NM-400	2.0, 8.0, 32.0	<2.0; m Wi	Increased total cell counts (due to significantly increased PMNs), total protein content, and enzyme activities	Lung: Minimal to mild diffuse pulmonary histiocytosis and minimal infiltration with neutrophils (granulocytes); irritation of upper respiratory tract at high concentrations	Not fully reversible within 24 days: BALF alterations remaining; diffuse or focal histiocytosis, particle-laden macrophages and bronchoalveolar hypertrophy and hyperplasia remaining	Determination not possible	[44]
MWCNT NM-402	0.1, 0.5, 2.5	0.1; m Wi	All BALF parameters increased among which marked increases in PMNs and lymphocytes, and MPO	Diffuse alveolar histiocytosis; one animal: intraseptally located microgranulomas	Not fully reversible within 3 weeks: BALF parameters still increased	Determination not possible	[18]

Abbreviations: *BALF* bronchoalveolar lavage fluid, *m* male, *MPO* myeloperoxidase, *MWCNT* multi-walled carbon nanotube, *NOAEC* no observed adverse effect concentration, *PMN* polymorphonuclear neutrophil, *Wi* Wistar

Table 2.4 High aspect ratio nanomaterials (DF4nanoGrouping MG2): rat 90-day and 2-year inhalation studies

Test material	Target conc. (mg/m³); duration	NOAEC (mg/m³); rat strain	Findings in BALF (significant as compared to control)	Pathological and histological findings	Progression or regression of effects	Reference
MWCNT NM-400	0.1, 0.5, 2.5; 90 days	<0.1; m Wi	Not determined	Granuloma, alveolar proteinosis, changes in upper respiratory tract	All animals sacrificed on day 1 postexposure	[44]
MWCNT NM-402	0.05, 0.25, 5.0; 90 days	<0.25; m and f Wi	At 5 mg/m³: Inflammatory lung reactions and release of inflammatory factors	Minimal to moderate concentration-related infiltration of alveolar macrophages with alveolar eosinophilic material; minimal infiltration of neutrophils in the alveoli; and minimal to slight interstitial inflammation	Not fully reversible within 3 months: BALF parameters still increased, histological alterations remaining	[45, 46]
MWCNT (Baytubes®)	0.1, 0.4, 1.5, 6.0; 90 days	0.1; m and f Wi	Inflammation (increased PMNs and soluble collagen)	Septal thickening, focal inflammation with granulomatous appearance, focally increased collagen, changes in upper respiratory tract	Not fully reversible within 6 months: Increases in BALF parameters and histological alterations remaining	[47]
MWCNT-7[a]	0.2, 2.0; 2 years	0.02; m F-344	All cell types increased, increased total protein, ALP, LDH	Inflammatory reactions, additionally: bronchiolo-alveolar carcinoma, combined carcinomas and adenomas	Persistence	[48]

Abbreviations: *ALP* alkaline phosphatase, *BALF* bronchoalveolar lavage fluid, *f* female, *LDH* lactate dehydrogenase, *m* male, *MWCNT* multi-walled carbon nanotube, *NOAEC* no observed adverse effect concentration, *PMN* polymorphonuclear neutrophil, *Wi* Wistar

[a]Sargent et al. [49] exposed mice (that had received 10 μg/g body weight of the initiator methylcholanthrene by intraperitoneal injection (i.p.) 1 week prior to the inhalation exposure period) to 5 mg/m³ MWCNT-7 for 15 days (5 h/day; 5 days/week). 91% of the mice developed bronchiolo-alveolar adenomas and adenocarcinomas with an average of 2.9 tumors per mouse 17 months after exposure. By comparison, 27% 52% of mice that either only received MWCNT-7 by inhalation or only the i.p. injection of methylcholanthrene developed such tumors

Assessing aerosol concentrations of 0.1, 0.5, and 2.5 mg/m^3 MWCNT NM-400, Ma-Hock et al. [44] reported increased lung weights, pronounced multifocal granulomatous inflammation, diffuse histiocytic and neutrophilic inflammation, and lipoproteinosis in the lung and the lung-associated lymph nodes. These effects were accompanied by a slight increase in blood neutrophilia at 2.5 mg/m^3. The 90-day NOAEC for MWCNT NM-400 was set at <0.1 mg/m^3 since minimal granulomatous inflammation in the lung and in lung-associated lymph nodes were also recorded at this lowest concentration.

For MWCNT Baytubes® (0.1, 0.4, 1.5, 6.0 mg/m^3), Pauluhn [47] described the same spectrum of histological findings in the respiratory tract as Ma-Hock et al. [18], i.e., septal thickening and focal inflammation with granulomatous appearance. Additionally, focally increased collagen was observed in the lung. The 90-day NOAEC for MWCNT Baytubes® was set at 0.1 mg/m^3 [47].

Pothmann et al. [45] reported increased lung weight and histological changes in the lung only at 5 mg/m^3 MWCNT NM-402 (concentration range: 0.05, 0.25, and 5.0 mg/m^3), which persisted after the 3-month recovery period. Since BALF parameters were increased at 0.25 mg/m^3, the 90-day NOAEC for MWCNT NM-402 is most likely <0.25 mg/m^3.

As compared to these three 90-day inhalation studies, the rat STIS [18] allowed predicting the high inflammation potential of the MWCNTs and the persistence of the effects. The low STIS NOAEC of 0.1 mg/m^3 for MWCNT NM-402 (DF4nanoGrouping STIS NOAEC Range I) was consistent with the three 90-day NOAECs for MWCNT NM-400, Baytubes® and NM-402 (<0.1, 0.1, and 0.25 mg/m^3).

As compared to these findings from studies assessing coiled MWCNTs, in a 2-year carcinogenicity study assessing fibrous straight MWCNT-7 at 0.2 and 2 mg/m^3 in male Fischer 344 rats, similar morphological changes of inflammatory reactions were recorded, but additionally increased incidences of bronchiolo-alveolar carcinoma, combined carcinomas and adenomas were observed [48]. The 2-year NOAEC for the fibrous straight MWCNT-7 was set at 0.02 mg/m^3, i.e., fivefold lower than the STIS or 90-day NOAECs for the coiled MWCNTs.

2.3.3   Passive Nanomaterials (MG3): BaSO$_4$ NM-220, Nano-ZrO$_2$, Graphite Nanoplatelets

2.3.3.1   Decisive Intrinsic Material Properties and Functionalities (Data Published by [24])

Nanomaterials are assigned as (MG3) passive if *all* of the following DF4nano Grouping Tier 1/Tier 2 criteria are fulfilled [23, 24]:

1. Lack of (or no release of) components that have been assigned a category of the Globally Harmonized System (<0.1% of the respective elements or molecules).
2. Low dissolution in biological media (≤100 mg/L).

3. Low surface reactivity (<10% of the reactivity of the reference material Mn_2O_3 in the *ferric reducing ability of serum assay*).
4. Low dispersibility (average agglomeration number ≥3).
5. Low cytotoxic potency (no effects up to 10 μg/cm^2, i.e., over the entire range of in vitro effective dosages that do not reflect in vivo pulmonary overload [50]).

The exemplary (MG3) passive nanomaterials $BaSO_4$ NM-220 and nano-ZrO_2 fulfill all of these DF4nanoGrouping criteria. Graphite nanoplatelets fulfill all of these grouping criteria with the exception of surface reactivity that could not be determined due to the pronounced hydrophobicity of the graphite nanoplatelets. Therefore, high surface reactivity could not be excluded based upon the DF4nanoGrouping Tier 1/Tier 2 criteria alone, and MG4 (activity) was implied by *conservative default*.

2.3.3.2 $BaSO_4$ NM-220

Rat STIS (Table 2.5)

In a STIS, male Wistar rats were exposed to up to 50 mg/m^3 $BaSO_4$ NM-220. Except for a transient and negligible increase in pro-inflammatory IL-1a in the lavaged lung tissue, no adverse effects were observed during clinical observation, body weight assessment, hematology, BALF evaluation, or histopathology [2]. Immediately after the 5-day inhalation exposure to 50 mg/m^3 $BaSO_4$ NM-220, a lung burden of approx. 1 mg was measured, which was cleared very quickly (pulmonary half times (t_{50}): 9.8 days at 50 mg/m^3) within the 3-week recovery period [2]. The STIS NOAEC was set at ≥50 mg/m^3 (STIS NOAEC Range IV indicating negligible toxic potential).

28-Day and 90-Day Inhalation Studies (Table 2.6)

Similar findings as those recorded in the rat STIS [2] were reported in a 28-day inhalation study (exposure 6 h/day, 5 day/week) exposing female Wistar rats to 50 mg/m^3 $BaSO_4$ NM-220 [55]. Also here, a lung burden of approx. 1 mg/lung was recorded, which was also cleared very quickly, i.e., with a t_{50} of about 10 days. These results were again confirmed by Schwotzer et al. [56], who tested the same batch of $BaSO_4$ NM-220 in a 90-day inhalation study with interim sacrificing of a satellite group after 4 weeks of exposure. Schwotzer et al. [56] recorded a lung burden 1.6 mg/lung after 4 weeks of exposure. This was very similar as the burden determined by Konduru et al. [55] although the two studies were performed in different laboratories using different exposure and dust generation systems. As in the rat STIS [2] and in the 28-day study [55], Schwotzer et al. [56] did not report any adverse findings in the animals of the 28-day interim sacrifice group. After 90-day inhalation exposure, slightly increased PMNs, lymphocytes as well

Table 2.5 Passive nanomaterials (DF4nanoGrouping MG3): rat STIS

Test material	Target conc. (mg/m³)	NOAEC (mg/m³); rat strain	Findings in BALF (significant as compared to control)	Pathological and histological findings	Progression or regression of effects	Clearance or pulmonary t_{50}	Reference
DPP pigments: coarse and fine Pigment Red 254	30.0	10; m Wi	No adverse findings	Minimal epithelial hypertrophy and/or hyperplasia; primarily at the level of terminal bronchioles and alveolar ducts; pigment-laden macrophages	Tissue alterations fully reversible within 3 weeks, some pigment-laden macrophages remaining	Not available	[51]
DPP pigments: mixed chlorinated DPP isomers	30.0	10; m Wi	Slightly increased PMNs	Slight epithelial hypertrophy and/or hyperplasia; primarily at the level of terminal bronchioles and alveolar ducts; pigment-laden macrophages	Not fully reversible within 3 weeks: Accumulation of pigment-laden macrophages in lumen of bronchiole-alveolar junction	Not available	[51]
DPP pigments: coarse and fine meta-chloro DPP isomer	3.0, 10.0, 30.0	Coarse: 10; fine: 30; m Wi	Coarse; at 30 mg/ m³. Increased PMNs and total protein, MCP-1, OPN, CINC; Fine: No adverse findings	Coarse; at 30 mg/m³: Minimal to slight hypertrophy of terminal bronchioles; pigment-laden macrophages	Fully reversible within 3 weeks	Not available	[51]
Nanostructured calcium silicate hydrate seeds	2.5, 12.5, 50	12.5; m Wi	No adverse findings	At 50 mg/m³: Minimal to slight diffuse multifocal histiocytosis; adaptive alterations of the larynx	Minimal histiocytosis remaining after three weeks	Not available	[52]
Nano-ZrO₂	0.5, 2.0, 10.0	≥10.0; m Wi	No adverse findings	No adverse findings	Not applicable	15.0 days at 0.5 mg/ m³; 26.9 days at 10.0 mg/m³	[2]
NP-containing acrylic ester-based polymer dispersions	3.0, 10.0	≥10; m Wi	No adverse findings	No adverse findings	Not applicable	Not available	[53]

Low surface area carbon black	0.5, 2.5, 10	≥10; m Wi	No adverse findings	No adverse findings	Not applicable	Determination not possible	[18]
Graphite nanoplatelets	0.5, 2.5, 10	≥10; m Wi	No adverse findings	No adverse findings	Not applicable	Determination not possible	[18]
Graphene oxide nanoplatelets	0.5, 2.5, 10	≥10.0; m S-D	No adverse findings	No tissue alterations; increase in alveolar macrophages	Some alveolar macrophages remaining 3 weeks postexposure	Not available	[54]
Iron oxide pigments: coarse and fine pigment red 101	10.0, 30.0	≥30; m Wi	No adverse findings	Minimal epithelial hypertrophy and/or hyperplasia of bronchioles and alveolar ducts; increased size and number of bronchiolar epithelial cells, accompanied by slight cytoplasmic basophilia; pigment-laden macrophages	Histopathological alterations reversible within 3 weeks, some pigment-laden macrophages remaining	Not available	[51]
BaSO$_4$, NM-220	2.0; 10.0; 50.0	≥50; m Wi	No adverse findings	No adverse findings	Not applicable	9.8 days at 50 mg/m^3	[2]
ZrO$_2$ with acrylate or TODA SF	2.0; 10.0; 50.0	≥50; m Wi	No adverse findings	No adverse findings	Not applicable	40.8 and 14.8 days at 10.0 mg/m^3 ZrO$_2$ with acrylate or TODA SF, respectively	[2]

Abbreviations: *BALF* bronchoalveolar lavage fluid, *CINC* cytokine-induced neutrophil chemoattractant, *DPP* diketopyrrolopyrrole, *m* male, *MCP* monocyte chemoattractant protein, *NOAEC* no observed adverse effect concentration, *NP* nanoparticle, *OPN* osteopontin, *PMN* polymorphonuclear neutrophil, *S-D* Sprague-Dawley, *SF* surface functionalization, *TODA* trioxadecanoic acid, *Wi* Wistar

Table 2.6 Passive nanomaterials (DF4nanoGrouping MG3): rat 28-day, 90-day, and longer-term inhalation studies

Test material	Target conc. (mg/m³); duration	NOAEC (mg/m³); rat strain	Findings in BALF (significant as compared to control)	Pathological and histological findings	Progression or regression of effects	Reference
BaSO₄ NM-220	50.0; 28 days	<50.0; f Wi	Minimal increase in PMNs	No adverse findings	Reversible within one month; rapid clearance	[55]
BaSO₄ NM-220	50.0; 90 days	<50.0; f Wi	Slight increase in PMNs, lymphocytes, LDH	Very slight accumulation of particle-laden macrophages in lung, bronchus-associated lymphoid tissue and lung-associated lymph nodes; eosinophilic globules in epithelium of nasal cavity, changes in expression of genes related to inflammatory mediators[a]	Pulmonary effects reversible within 90-days, rapid clearance; eosinophilic globules in epithelium of nasal cavity remaining	[56, 57]
BaSO₄ (MMAD: 4.3 μm)	37.5; 203 days; 75.0; 119 days	<75.0; m Wi	Slight increase in PMNs at high concentration level	Accumulation of macrophages	Rapid clearance	[58, 59]
Graphene nanoplatelets[b]	0.125, 0.5, 2; 28 days	≥2.0; m S-D	No adverse findings	No adverse findings	Not applicable	[60]

Abbreviations: *BALF* bronchoalveolar lavage fluid, *f* female, *LDH* lactate dehydrogenase, *m* male, *MMAD* mass mean aerodynamic diameter, *NOAEC* no observed adverse effect concentration, *PMN* polymorphonuclear neutrophil, *S-D* Sprague-Dawley, *Wi* Wistar
[a]Gene expression changes lower than those elicited by CeO₂ NM-212, but great overlap in the gene pattern (cf. Table 2.8)
[b]Average thickness: 20–30 layers

as increased LDH activity were detected in the BALF. The main histopathological findings were accumulation of particle-laden macrophages in the lung and associated lymph nodes. All effects were fully reversible during the 90-day post-exposure observation period, and the test materials were cleared from the lungs rapidly [55, 56].

In summary, for $BaSO_4$ NM-220 the rat STIS was predictive of the outcomes of the rat 28-day and 90-day inhalation studies in two aspects: It showed the very low and transient pulmonary toxicity of this test material upon inhalation exposure to the very high aerosol concentration of 50 mg/m^3. The clearance of $BaSO_4$ NM-220 was unusually rapid for this poorly soluble particle.

However, after 12-month inhalation exposure to aerosol concentrations of 50 mg/m^3 $BaSO_4$ NM-220, the findings changed considerably: The lung burden increased from 1.6 mg/lung [56] to around 10 mg/lung, and this high lung burden resulted in significant inflammatory responses indicating particle overload [75]. Clearly, the rat STIS, just as the 28-day and 90-day inhalation toxicity studies, were unable to predict pathological findings that only evolve after chronic exposure.

2.3.3.3 Nano-ZrO_2

Rat STIS (Table 2.5)

In a rat STIS, up to 10 mg/m^3 nano-ZrO_2 did not induce any adverse findings in either the BALF or histopathology [2]. The poorly soluble test material was cleared fairly rapidly from the lung (t_{50}: 15.0 days at 0.5 mg/m^3 and 26.9 days at 10.0 mg/m^3). The STIS NOAEC for nano-ZrO_2 was set at $\geq$10 mg/m^3 (STIS NOAEC Range IV indicating negligible toxic potential).

Human Data

To the best of the authors' knowledge, no 28-day or 90-day inhalation toxicity studies have been published using nano-ZrO_2. Two reports focused on effects of zirconium compounds ($ZrSiO_4$ and ZrO_2) on the lung health of workers. A study on 32 manual finishers of zirconium metal, who were exposed to 5.75–14.7 mg/m^3 of dust (25% zirconium), revealed no exposure-related symptoms [76]. Similarly, a study by Marcus et al. [77] on ZrO_2-exposed workers showed that even under long-term exposure conditions of up to 20 years and peak concentrations up to 30 mg/m^3, zirconium exposure elicited neither abnormal chest radiographs, nor did it impair lung function parameters [78]. Hence, the available data from workers exposed to zirconium metal support the findings from the rat STIS [2] indicating negligible inhalation toxicity of nano-ZrO_2.

2.3.3.4 Graphite Nanoplatelets

Rat STIS (Table 2.5)

In a rat STIS, up to 10 mg/m^3 graphite nanoplatelets did not induce any adverse findings in either the BALF or histopathology [18]. Hence, the precautionary assignment of graphite nanoplatelets as (MG4) active in DF4nanoGrouping Tier 2 (since surface reactivity of this strongly hydrophobic material could not be assessed) was rebutted in the Tier 3 rat STIS. Pulmonary deposition or clearance of the carbon-based graphite nanoplatelets was not assessed since this would have required special isotope-based methodologies. The STIS NOAEC was set at ≥10 mg/m^3 (STIS NOAEC Range IV indicating negligible toxic potential).

28-Day Inhalation Study (Table 2.6)

In a 28-day inhalation toxicity study, aerosol concentrations of (only) 2 mg/m^3 graphene nanoplatelets (similar to the graphite nanoplatelets assessed by Ma-Hock et al. [18]) did not induce any adverse findings in either the BALF or histopathology [60]. Hence, also based upon the outcome of this 28-day study, the precautionary assignment of graphite nanoplatelets as (MG4) active in Tier 2 of the DF4nanoGrouping was rebutted. Therefore, the available in vivo data allow concluding that the tested graphene nanoplatelets are (MG3) passive.

2.3.4 Active Nanomaterials (MG4): CeO$_2$ NM-212, TiO$_2$ NM-105

2.3.4.1 Decisive Intrinsic Material Properties and Functionalities (Data Published by [24])

Briefly, in the DF4nanoGrouping Tiers 1 and 2, nanomaterials are assigned as (MG4) active if they are neither identified as MG1, MG2, or MG3 in Tiers 1 and 2, i.e., these are poorly soluble particles for which any single decisive property listed for MG3 is not met. In the DF4nanoGrouping case studies [24], CeO$_2$ NM-212 and TiO$_2$ NM-105 were assigned as (MG4) active nanomaterials on account of the in vitro cellular effects they elicited in the rat NR8383 alveolar macrophage assay [79].

2.3.4.2 CeO$_2$ NM-212

Rat STIS (Table 2.7)

In a rat STIS [67], aerosol concentrations of 0.5, 5.0, and 25.0 mg/m^3 CeO$_2$ NM-212 elicited concentration-related inflammatory responses. Mainly, BALF parameters were altered, whereas histopathological findings were rather mild

Table 2.7 Active nanomaterials (DF4nanoGrouping MG4): rat STISs

Test material	Target conc. (mg/m³)	NOAEC (mg/m³); rat strain	Findings in BALF (significant as compared to control)	Pathological and histological findings	Progression or regression of effects	Clearance or pulmonary t_{50}	Reference
Quartz dust	25.0	No NOAEC; m and f Wi	Increased neutrophils, NAG, ALP	Immediately postexposure: Very slight to slight granulocytic cell infiltrate	Progressively severe effects over 3-month postexposure period	Lung silicon levels remained high during 3 months postexposure	[1]
Quartz DQ12	100	No NOAEC; m Wi	Increased PMNs, lymphocytes, GGT, NAG, ALP, LDH, total protein	Strong increase in lung weight, diffuse histiocytosis, multifocal granulocytic infiltration; activation of mediastinal lymph nodes	Effects progressive: mild to moderate diffuse inflammation composed of alveolar macrophages, neutrophils and cell detritus	43.8 days	[80]
Nano-CeO$_2$	0.5, 2.5, 10.0	<0.5; m Wi	All cytological and biochemical parameters in BALF increased; increased CINC-1, IFN-γ, IL–1α, MCP-1, M-CSF, in BALF and lung tissue	Lung; Particles in macrophages (recovery group: additionally, mild histiocytosis)	Not fully reversible within 3 weeks: BALF effects and mild diffuse or multifocal alveolar histiocytosis	89.6 and 287.0 days at 0.5 and 2.5 mg/m³ nano-CeO$_2$, respectively	[2]
Al-doped nano-CeO$_2$	0.5, 2.0 10.0	<0.5; m Wi	All cytological and biochemical parameters in BALF increased; increased MCP-1 and CINC-1 in BALF, increased IL1-α in lung tissue	Lung; Single or aggregated particle-loaded macrophages	Not fully reversible within 3 weeks: BALF effects and particle-loaded alveolar macrophages remaining	207.9 days at 10 mg/m³ Al-doped nano-CeO$_2$	[2]

Table 2.7 (continued)

Test material	Target conc. (mg/m³)	NOAEC (mg/m³); rat strain	Findings in BALF (significant as compared to control)	Pathological and histological findings	Progression or regression of effects	Clearance or pulmonary t_{50}	Reference
CeO$_2$, NM-211 and NM-212	0.5, 5.0, 25.0	<0.5; m Wi	Increased PMNs, lymphocytes, monocytes, total protein, GGT, LDH, ALP, MCP-1, CINC-1, M-CSF, OPN	Alveolar histiocytosis and free eosinophilic granular material with particles	Progression to granulomatous inflammation within 4 weeks postexposure; BALF parameters still increased a higher dose groups	196.4 and 51.7 days at 25.0 mg/m³ CeO$_2$ NM-211 and NM-212, respectively	[67]
Coated nano-TiO$_2$	0.5, 2.0, 10.0	0.5; m Wi	Increased total cell counts, and PMNs, monocytes, total protein, GGT, LDH, ALP and NAG (cytokines not measured)	Lung: Numerous pigment-loaded alveolar macrophages and slight diffuse histiocytosis	Not fully reversible within 3 weeks: Slight increases in BALF parameters remaining	No measurable clearance within 3 weeks postexposure	[2]
TiO$_2$ NM-105[a]	2, 10, 50	<2.0; m Wi	Increased total cell and PMNs, total protein content, enzyme activities and levels of a number of cell mediators	Lung: minimal to mild diffuse alveolar infiltration with histiocytes; minimal to mild increase of epithelium thickness	Not fully reversible within 3 weeks: PMN and LDH in BALF still increased; multifocal histiocytosis	53.0, 31.5, and 48.8 days at 2, 10, 50 mg/m³, respectively	[3]
CdS/Cd(OH)$_2$ core shell QDs	4.1 (max. feasible concentration)	<4.1; m Wi	Increased PMNs (25-fold)	Slight local inflammation (infiltration of neutrophils and histiocytes in the lung); increased macrophages in draining lymph nodes	Lung inflammation not fully reversible within 3 weeks; increased macrophages in draining lymph nodes progressed to granulomas	Lung clearance not complete within 3 weeks	[81]

Glutaraldehyde-coated CdS/Cd(OH)$_2$ core shell QDs	2.0 (max. feasible concentration)	≥2.0; m Wi	Slight increase in PMNs (sixfold) without increase in total cell counts	Slight focal adaptation of the larynx epithelium (treatment-related adaptive alteration)	Not fully reversible within 3 weeks: Slight increase in BALF PMNs remaining; additionally, ALP increased	Lung clearance not complete within 3 weeks	[82]
CdCl$_2$	0.4 (equiv. to 0.12 mg/m^3 Cd)	No NOAEC; m Wi	Slight increase in PMNs without increase in total cell counts; increase in PMNs and CINC-1	Slight focal adaptation of the larynx epithelium (treatment-related adaptive alteration)	BALF alterations fully reversible within three weeks; diffuse minimal increase of alveolar macrophages remaining	Lung clearance not complete within 3 weeks	[82]
Graphene	0.5, 2.5, 10	<2.5; m Wi	Increased eosinophils, PMNs, lymphocytes, GGT, ALP, CINC-1, MCP-1, OPN	Single microgranulomas	Not fully reversible within 3 weeks: Single or few microgranulomas remaining	Determination not possible	[18]

Abbreviations: *ALP* alkaline phosphatase, *BALF* bronchoalveolar lavage fluid, *CINC* cytokine-induced neutrophil chemoattractant, *f* female, *GGT* γ-glutamyltransferase, *IFN* interferon, *IL* interleukin, *LDH* lactate dehydrogenase, *m* male, *M-CSF* macrophage colony stimulating factor, *MCP* monocyte chemoattractant protein, *NAG* N-acetyl-β-glucosaminidase, *NOAEC* no observed adverse effect concentration, *OPN* osteopontin, *PMN* polymorphonuclear neutrophil, *QD* quantum dot, *S-D* Sprague-Dawley, *Wi* Wistar

[a]Further, Kwon et al. [83] performed a rat 14-day inhalation study assessing 11 mg/m^3 anatase 53 nm–TiO$_2$ with 5% rutile 61 nm–TiO$_2$. No adverse findings were recorded in the BALF. Histopathological evaluation revealed an increase in lung macrophages and degeneration of nasal olfactory epithelium with inflammatory cell infiltration. These effects were fully reversible, and the 14-day NOAEC was assessed as <11 mg/m^3

(alveolar histiocytosis and free eosinophilic granular material with particles). Strongly retarded clearance was observed from 5 mg/m^3 onward (lung burden 0.53 mg directly after the 5-day exposure period; t_{50}: 51.7 days at 25.0 mg/m^3). During the recovery period, the morphological effects regressed but were still present 21 days after the end of exposure, and the BALF parameters remained increased in the higher dose groups [67]. The STIS NOAEC was set at <0.5 mg/m^3 (STIS NOAEC Range I indicating pronounced toxic potential).

28-Day and 90-Day Inhalation Studies (Table 2.8)

Keller et al. [67] further assessed 5.0 and 25.0 mg/m^3 CeO$_2$ NM-212 in a rat 28-day inhalation study. The BALF findings recorded in the STIS and the 28-day study were similar, but slightly less pronounced in the 28-day study. By comparison, the histopathological evaluation in the 28-day study showed progressive granulomatous inflammation, which was not observed in the STIS. The CeO$_2$ NM-212 lung burden in the rat STIS immediately after the exposure period (0.53 mg/lung at 25.0 mg/m^3) was one quarter of the burden in rats exposed for 4 weeks (2.62 mg/lung at 25.0 mg/m^3), i.e., lung burden increased proportionally with increasing exposure duration. Consistent with the STIS findings, retarded clearance was determined in the 28-day study (t_{50}: 40 and 200 days at 5 and 25 mg/m^3, respectively). Similarly, in a 90-day inhalation study evaluating CeO$_2$ NM-212 [56], comparable histopathological findings were recorded without qualitatively new morphological alterations setting a 90-day NOAEC <1 mg/m^3. The 28-day NOAEC for CeO$_2$ NM-212 was set at <5.0 mg/m^3.

In summary, for CeO$_2$ NM-212, the rat STIS was generally predictive of effects observed in the 28-day and 90-day studies. The BALF parameters in the STIS were more sensitive showing beginning inflammatory responses already at 0.5 mg/m^3, while histopathological changes were not manifested after only 5 days of exposure. In a comprehensive review of different inhalation studies assessing different variants of CeO$_2$ nanomaterials, Dekkers et al. [9] found rats to be more sensitive to developing pulmonary inflammation than mice. Additionally, the different nanoforms of CeO$_2$ showed differences in toxic potency. While primary particle and aggregate/agglomerate size distributions substantially affected the deposited dose and consequently the pulmonary response, size alone could not fully explain the differences observed in the reviewed studies [9].

2.3.4.3   TiO$_2$ NM-105

Rat STIS (Table 2.7)

In a rat STIS [3], aerosol concentrations of 2.0, 10.0, and 50.0 mg/m^3 TiO$_2$ NM-105 elicited minimal to mild diffuse alveolar infiltration with histiocytes and minimal to mild increase of pulmonary epithelium thickness that coincided with an increase

Table 2.8 Active nanomaterials (DF4nanoGrouping MG4): rat 28-day, 90-day and 2-year inhalation studies

Test material	Target conc. (mg/m³); duration	NOAEC (mg/m³); rat strain	Findings in BALF (significant as compared to control)	Pathological and histological findings	Progression or regression of effects	Reference
α-Quartz (median particle size 1.7 mm)	0.1, 1.0, 10; 28-days	0.1; f F-344/N	Increased PMNs	Pulmonary interstitial granuloma, multiple microgranulomas in bronchial-associated lymphoid tissue, mild to moderate, chronic active pneumonia (foamy, hypertrophic and degenerating alveolar macrophages associated with influx of neutrophils, fewer lymphocytes and nuclear and proteinaceous debris in alveolar air spaces	Progressive: 24 weeks postexposure: Increased pulmonary alveolar macrophages, PMNs, total protein, LDH, GGT, acid protease	[19]
Quartz dust	60; 90 days	No NOAEC; m and f Wi	Not determined	Accumulation of alveolar macrophages, inflammation, alveolar bronchiolization, fibrosis, granulomatous lesions	Progression to squamous cell carcinoma, silicotic nodules	[61]
Crystalline SiO₂ (cristoballite)	30; 90 days	No NOAEC; m F-344	Significant changes in all BALF parameters: Increased PMNs and total cells, LDH, total protein, β-glucuronidase, MIP-2	Increased numbers of neutrophils and macrophages; mild proliferative response and fibrosis Increased HPRT mutation frequency	Not reversible: persistence of alterations in BALF and histopathological findings; lung burden at end of exposure: 882.7 µg/lung; relatively unchanged within 8 months postexposure	[62]
TiO₂ NM-105	0.5, 2.0, 10; 90 days	0.5; m F-344/CrlBR	Inflammation, (increased soluble markers (LDH and protein))	Macrophage accumulation, alveolar bronchiolization	Progression	[63]

Table 2.8 (continued)

Test material	Target conc. (mg/m³); duration	NOAEC (mg/m³); rat strain	Findings in BALF (significant as compared to control)	Pathological and histological findings	Progression or regression of effects	Reference
TiO₂ NM-105	10.0; 2 years	<10.0; f Wi	Inflammation	Benign squamous cell tumor, adenocarcinoma, squamous cell carcinoma	Not reversible	[64][a]
TiO₂ NM-105	10.0; 28 days	<10.0; m F-344	Not available	Age-dependent modulation of blood-brain-barrier integrity parameters associated with increase of cytokines in brain; decreased expression of neuronal activity marker; titanium not detectable in brain	Not available	[65]
TiO₂	0.5, 1.84; 28 days	<0.5; m Fischer	Macrophage phagocytosis of test materials	Some alveolar macrophages with pigment-like material deposition in alveoli	Reversible within 3 months; biological half time in high and low exposure groups: 1.8 and 2.0 months	[66]
NiO	0.32, 1.65; 28 days	<0.32; m Fischer	Increased PMNs, macrophage phagocytosis of test materials, death of cells upon phagocytosis	Mild infiltration of alveolar macrophages and neutrophils in alveoli and interstitial area	Not reversible within 3 months; biological half time in high and low exposure groups: 5.2 and 2.9 months	[66]
CeO₂ NM-212	0.5, 5.0 25.0; 28 days	<5.0; m Wi	Increased total cell counts, PMNs, lymphocytes, mediators	Alveolar histiocytosis and eosinophilic granular material with particles	Not fully reversible within 129 days: Some BALF parameters still increased; alveolar histiocytosis and eosinophilic granular material with particles remaining; multifocal granulomatous inflammation; retention halftimes: 40 and 200 days at 5.0 and 25 mg/m³, respectively	[67]

Material	Concentration; duration	Strain/species	BALF effects	Histopathology	Reversibility	Ref
5–10 nm CeO$_2$ NM-211; 40 nm CeO$_2$ NM-212; micron-scale CeO$_2$ NM-213	50 (daily exposure: 40 min, 2 h, 6 h); 28 days	No NOAEC; m and F Crl: [WI] WU BR	Increased total cell counts, especially neutrophils, lymphocytes, increases in ALP, GGT, LDH, NAG and total protein	Dose-dependent pulmonary inflammation and lung cell damage (mass concentration-based exposure levels: CeO$_2$ NM-211 most potent; surface area-based exposure levels: CeO$_2$ NM-213 most potent; particle number-based concentrations: All three equipotent)	Not fully reversible within 4 weeks: BALF parameters still increased (all test materials); increased septal cellularity (CeO$_2$ NM-211 and 212)	[68]
CeO$_2$ NM-212	0.1, 0.3, 1.0, 3.0; 90 days	<1.0; m Wi	Increased PMNs and lymphocytes	Macrophages, inflammation, hyperplasia, fibrosis, nose and lungs affected; in alveolar epithelial type 2 cells: changes in expression of genes related to inflammatory mediators[b]	Not reversible within 90 days	[56]
7.8 nm-CeO$_2$ (irregularly shaped)	2.0, 10.0; 28 days	<2.0; m F-344	Persistent influx of PMNs and expression of oxidative stress markers CINC-1, CINC-2, and HO-1	inflammatory cells, macrophages and neutrophils in alveolar space	Not reversible within 90 days	[69]
104 nm-La$_2$O$_3$	0.5, 2.5, 10; 28 days	<0.5; m S-D	Increased total cell counts including macrophages and PMNs, LDH, albumin, nitric oxide, and TNF-α	Alveolar proteinosis with alveolar macrophage aggregation	Not fully reversible within 4 weeks: Alveolar inflammation remaining; Increase in BALF cells progressed	[70]
210–270 nm-Nd$_2$O$_3$	0.5, 2.5, 10.0; 28 days	<0.5; m S-D	Increased total cell counts, including macrophages and LDH, albumin, IL-6, and TNF-α	Infiltration of inflammatory cells and pulmonary alveolar proteinosis	After 4 weeks: changes generally reversed in 0.5 mg/m^3 group, but exacerbated in 10 mg/m^3 group	[71]

Table 2.8 (continued)

Test material	Target conc. (mg/m³); duration	NOAEC (mg/m³); rat strain	Findings in BALF (significant as compared to control)	Pathological and histological findings	Progression or regression of effects	Reference
High surface carbon black	1, 7, 50; 90 days	1.0; F-344	Increased total cell numbers and PMNs	Macrophage accumulation. Alveolar hypertrophy/hyperplasia, interstitial fibrosis	Not fully reversible within 11 months: Increased BALF parameters, fibrosis	[72]
High surface carbon black	12.0; 2 years	<12.0; f Wi	Inflammation	Benign squamous cell tumor, adenocarcinoma, squamous cell carcinoma	Not reversible within 6 months	[64][c]

Abbreviations: *ALP* alkaline phosphatase, *BALF* bronchoalveolar lavage fluid, *CINC* cytokine-induced neutrophil chemoattractant, *f* female, *GGT* γ-glutamyltransferase, *HO-1* heme oxygenase-1, *IL* interleukin, *LDH* lactate dehydrogenase, *m* male, *MIP* macrophage inflammatory protein, *NAG* N-acetyl-β-glucosaminidase, *NOAEC* no observed adverse effect concentration, *OPN* osteopontin, *PMN* polymorphonuclear neutrophil, *S-D* Sprague-Dawley, *TNF-α* tumor necrosis factor alpha, *Wi* Wistar

[a]Two-year exposure to extremely high 250 mg/m³ non-nanosized TiO_2 in rats elicited bronchiolo-alveolar adenomas and cystic keratinizing squamous cell carcinomas, whereas concentrations of up to 50 mg/m³ of this test substance did not [73]. Lee and co-workers questioned the human health relevance of these observations since the recorded lung tumors were different from common human lung cancers in terms of tumor type, anatomic location, and tumorigenesis and lack of tumor metastasis

[b]Gene expression changes higher than those elicited by $BaSO_4$ NM-220, but great overlap in the gene pattern (cf. Table 2.6)

[c]Similarly: Nikula et al. [74]

of most BALF parameters. These effects were not fully reversible within the recovery period. Pulmonary t_{50} of 53.0, 31.5, and 48.8 days were recorded at 2, 10, and 50 mg/m^3, respectively [3]. Based upon these findings, the STIS NOAEC for TiO$_2$ NM-105 is <2.0 mg/m^3, i.e., presumably STIS NOAEC Range II or I. For coated nano-TiO$_2$, a STIS NOAEC of 0.5 mg/m^3 was reported [2], i.e., STIS NOAEC Range II on the border to Range I.

(Notably, the STIS pulmonary clearance rates (t_{50}) for the (MG4) active poorly soluble substances (CeO$_2$ NM-212: 51.7 days at 25.0 mg/m^3; TiO$_2$ NM-105: 48.8 days at 50 mg/m^3) were much longer than those recorded for the (MG3) passive poorly soluble particles (BaSO$_4$ NM-220: 9.8 days at 50 mg/m^3; nano-ZrO$_2$: 26.9 days at 10.0 mg/m^3).)

90-Day and 2-Year Inhalation Studies (Table 2.8)

Ma-Hock et al. [3] compared the rat STIS data for TiO$_2$ NM-105 with published data from a rat 90-day inhalation toxicity study evaluating a similar nano-TiO$_2$ [63]. The findings were overall comparable between the two studies [3]. Further, 2-year inhalation exposure to high concentrations (10 mg/m^3) of a nano-TiO$_2$ caused tumor effects [64]. Lung tumor formation in rats upon long-term exposure to high levels of biopersistent granular particles is thought to result from reduced particle clearance involving chronic inflammation associated with oxidative stress, secondary genotoxicity, and cell proliferation [84].

2.3.5   *The Special Case of Amorphous SiO$_2$ (MG1, MG3, or MG4)*

2.3.5.1   **Decisive Intrinsic Material Properties and Functionalities (Data Published by [24])**

In the DF4nanoGrouping case studies [24], a precipitated amorphous SiO$_2$ (equivalent to SiO$_2$ NM-200) and a pyrogenic amorphous SiO$_2$ (equivalent to SiO$_2$ NM-203) were assigned as "borderline" (MG1) soluble nanomaterials, since they were partially soluble in water and Dulbecco's Modified Eagle Medium supplemented with 10% fetal calf serum, but highly soluble in Gamble's solution. By contrast, a colloidal 15 nm-SiO$_2$ was not water soluble and did not dissolve in biological media, and it was assigned as (MG4) active nanomaterial on account of its in vitro cellular effects. Further, of four surface-functionalized variants of 15 nm-SiO$_2$, SiO$_2$·amino and SiO$_2$·polyethyleneglycol (SiO$_2$·PEG) were assigned as (MG3) passive since they fulfilled all DF4nanoGrouping Tier 1 and Tier 2 criteria for passivity. By contrast, SiO$_2$·acrylate and SiO$_2$·phosphonate were assigned as (MG4) active on account of their high dispersibility indicating potential for mobility in the body.

2.3.5.2   Rat STISs (Table 2.9)

In the rat STIS, the toxic potency of the different amorphous SiO_2 differed considerably depending on the type of production or surface functionalization. The STIS NOAECs ranged from 1.0 mg/m^3 for precipitated SiO_2 NM-200 and pyrogenic SiO_2 NM-203 and silica gel [1] and 2.5 mg/m^3 for colloidal 15-nm-SiO_2 to ≥50 mg/m^3 for SiO_2·amino, SiO_2·PEG and SiO_2·phosphonate [2]. For SiO_2·acrylate, no pulmonary effects were recorded (pulmonary STIS NOAEC: ≥10 mg/m^3); however, the weight of the spleen increased by 25% as compared to its weight in the control group so that the systemic STIS no observed effect concentration was set at 0.5 mg/m^3 [2].

Accordingly, the DF4nanoGrouping Tier 1 and Tier 2 assignment of colloidal 15 nm-SiO_2 as (MG4) active and of SiO_2·amino and SiO_2·PEG as (MG3) passive was confirmed by the rat STIS data. Also, the potential for mobility in the body indicated by the high dispersibility of SiO_2·acrylate was confirmed by the splenetic findings recorded for this material. By comparison, the high dispersibility of SiO_2·phosphonate was not reflected by rat STIS findings reflecting mobility in the body. Hence, the DF4nanoGrouping Tier 2 assignment of this test material as (MG4) was not confirmed by the Tier 3 STIS data. Finally, for SiO_2 NM-200 and NM-203 and silica gel, full clearance was recorded in the rat STIS [1], which supported DF4nanoGrouping Tier 2 assignment of these test materials as (MG1) soluble, and further a STIS NOAEC of 1 mg/m^3 (STIS NOAEC Range III) was recorded for these three amorphous SiO_2.

2.3.5.3   90-Day Inhalation Studies (Table 2.10)

Consistent with the findings from the rat STISs [1], 90-day NOAECs <1 mg/m^3 were recorded for SiO_2 NM-200 [85] and SiO_2 NM-203 [61]. For SiO_2 NM-200, Creutzenberg et al. [85] reported increased BALF parameters, bronchoalveolar hyperplasia, and granulocyte infiltration that were not fully reversible within 90 days. For SiO_2 NM-203, Reuzel et al. [61] reported accumulation of alveolar macrophages, inflammation, alveolar bronchiolization, and fibrosis that was reversible within 1 year.

2.4   Summary and Conclusions

As the preceding case studies show, the rat STIS allows detecting early signs of lung inflammation, and it allows assessing the progression or regression of effects. Although the histopathological alterations are often not pronounced after 5 days of exposure, BALF parameters are highly responsive within this short time frame. If data from 28-day or 90-day inhalation toxicity studies are available for the same (or very similar) nanomaterials, the qualitative effects are comparable between the rat

Table 2.9 Amorphous SiO$_2$ nanomaterials (DF4nanoGrouping MG1, MG3, or MG4): rat STISs

Test material	Target conc. (mg/m^3)	NOAEC (mg/m^3); rat strain	Findings in BALF (significant as compared to control)	Pathological and histological findings	Progression or regression of effects	Clearance or pulmonary t_{50}	Reference
Precipitated amorphous SiO$_2$; equivalent to NM-200	1, 5, 25	1.0; m and f Wi	Changes of all cytological and biochemical parameters	Intra-alveolar granulocytic infiltrates, accumulation of alveolar macrophages, bronchial/bronchiolar hypertrophy	Fully reversible within 1 month	1 and 5 mg/m^3: below LoD; 25 mg/m^3: Full clearance	[1]
Pyrogenic amorphous SiO$_2$; equivalent to NM-203	1, 5, 25	1.0; m and f Wi	Changes of all cytological and biochemical parameters	Intra-alveolar granulocytic infiltrates, accumulation of alveolar macrophages, bronchial/bronchiolar hypertrophy	Fully reversible within 1 month	1 and 5 mg/m^3: below LoD; 25 mg/m^3: Full clearance	[1]
Silica gel	1, 5, 25	1.0; m and f Wi	Changes of all cytological and biochemical parameters	Accumulation of alveolar macrophages bronchiolar hypertrophy	Fully reversible within 1 month	1 and 5 mg/m^3: below LoD; 25 mg/m^3: Full clearance	[1]
Colloidal amorphous 15 nm-SiO$_2$	0.5, 2.5, 10.0, 50.0	2.5; m Wi	Slightly increased PMNs and lymphocytes	Slightly increased neutrophil counts in blood after the end of exposure; respiratory tract: Multifocal macrophage aggregates	Exacerbation towards slight multifocal pulmonary inflammation within 3 weeks	29.3 days at 50 mg/m^3	[2]

(continued)

Table 2.9 (continued)

| Test material	Target conc. (mg/m³)	NOAEC (mg/m³); rat strain	Findings in BALF (significant as compared to control)	Pathological and histological findings	Progression or regression of effects	Clearance or pulmonary t_{50}	Reference
15 nm-SiO₂ with acrylate SF	2.0, 10.0, 50.0	Local: ≥10; systemic NOEC: 0.5; m Wi	No adverse findings	Respiratory tract: no adverse effects; spleen: increased weight (+25%) without histological correlate; particles and high numbers of thrombocytes (TEM)	No pulmonary effects at any time point; full reversibility of splenetic effects within 2 weeks	85.9, 68.5, and 35.1 days at 2.0, 10.0 and 50.0 mg/m³, respectively	[2]
15 nm-SiO₂ with amino, PEG, or phosphonate SF	2.0, 10.0, 50.0	≥50; m Wi	No adverse findings	No adverse findings	Not applicable	22.4, 32.7, and 23.5 days at 10 mg/m³ 15 nm-SiO₂ with amino, PEG, or phosphonate SF, respectively	[2]

Abbreviations: *BALF* bronchoalveolar lavage fluid, *f* female, *m* male, *NOAEC* no observed adverse effect concentration, *PEG* polyethylene glycol, *PMN* polymorphonuclear neutrophil, *SF* surface functionalization, *Wi* Wistar

Table 2.10 Amorphous SiO$_2$ nanomaterials (DF4nanoGrouping MG1, MG3, or MG4): rat 28-day and 90-day inhalation studies

Test material	Target conc. (mg/m³); duration	NOAEC (mg/m³); rat strain	Findings in BALF (significant as compared to control)	Pathological and histological findings	Progression or regression of effects	Reference
Precipitated amorphous SiO$_2$ NM-200	1.0, 2.5, 5.0; 90 days	<1.0; m Wi	Increased PMNs, lymphocytes, LDH, GGT, total protein	Bronchoalveolar hyperplasia, granulocyte infiltration	Pulmonary t_{50} approx. 30 days; effects not fully reversible within 90 days	[85]
Pyrogenic amorphous SiO$_2$; equiv. to NM-203	50; 90 days	No NOAEC; m F-344	Increased inflammatory markers	Severe inflammation	Fully reversible within 8 months	[62]
Pyrogenic amorphous SiO$_2$; equiv. to NM-203	1, 6, 30; 90 days	<1.0; m Wi	Inflammation	Accumulation of alveolar macrophages, inflammation, alveolar bronchiolization and fibrosis	Reversible within 1 year	[61]
60–70 nm amorphous SiO$_2$[a]	0.5, 1.5, 5.0; 28 days	No NOAEC; S-D	No significant alterations, except for increase malondialdehyde in mid- and high-test groups (Alterations of serum biochemistry parameters)	No adverse findings	Not applicable re. BALF and histopathology; however, serum biochemistry alterations were recorded not fully reversible within 4 weeks	[86]

Abbreviations: *BALF* bronchoalveolar lavage fluid, *GGT* γ-glutamyltransferase, *NOAEC* no observed adverse effect concentration, *PMN* polymorphonuclear neutrophil, *S-D* Sprague-Dawley, *Wi* Wistar
[a]Produced by the method described by Stöber et al. [88]
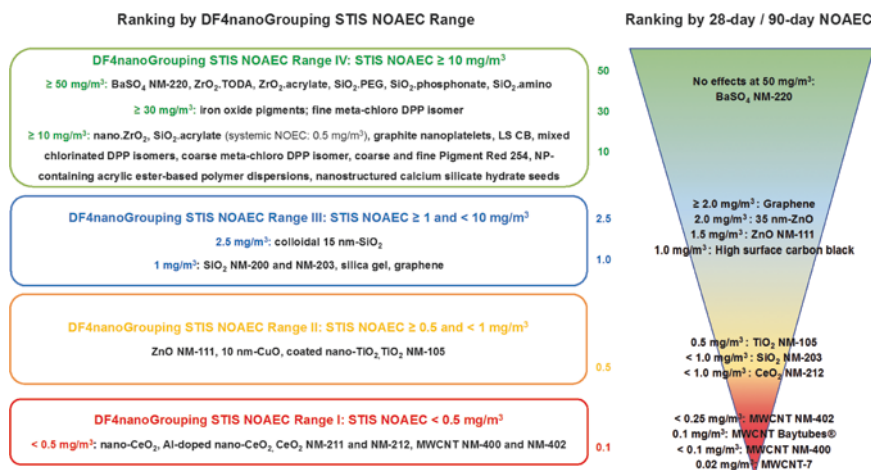
Fig. 2.2 Toxic potency ranking STIS NOAEC versus 28-day/90-day NOAEC. Abbreviations: *DPP* diketopyrrolopyrrole, *LS CB* low surface carbon black, *MWCNT* multiwall carbon nanotube, *NOAEC* no observed adverse effect concentration, *NOEC* no observed effect concentration, *NP* nanoparticle, *PEG* polyethylene glycol, *STIS* short-term inhalation study, *TODA* trioxadecanoic acid

STIS and the longer-term studies. Further, comparing different nanomaterials and non-nanosized materials with different inflammation potency, the rankings regarding STIS NOAECs on the one hand and the corresponding 28-day/90-day NOAECs on the other hand, just as the NOAEC levels as such, are very similar (Fig. 2.2).

As compared to the 28-day and 90-day inhalation toxicity studies (OECD TG 412 and 413; [5, 6]), the rat STIS uses fewer animals and the duration of the STIS is considerably shorter. Consequently, results on the toxic potential and toxic potency of nanomaterials are available on shorter notice (e.g., time for BALF and histopathology in the STIS a minimum of 6 weeks after end of recovery period as compared to a minimum of 3 months in 90-day studies). The findings recorded in the rat STIS can be directly related to a NOAEC and can therefore be used for initial risk assessments. Moreover, the rat STIS not only allows establishing quantitative concentration-response relationships, but it also provides (first) information on the progression or regression of effects, on the test materials' deposition and clearance behavior, as well as on particle translocation to tissues outside the respiratory tract.

Generally, the rat STIS reveals *early* effects that mostly reflect inflammation, and/or beginning morphological alterations. By contrast, reliable predictions of longer-term effects, such as fibrosis and carcinoma, are hardly possible. Nevertheless, sustained inflammation (that can be detected in the rat STIS) is suspected to be a necessary, though not sufficient, prerequisite for enhanced reactive oxygen species formation, fibrosis and even cancer, at least in the rat lung [38, 42]. Therefore, the identification of early inflammatory responses in the rat STIS (recorded shortly postexposure) combined with data on the persistence or even progression of effects (recorded after the postexposure period), and on lung clearance or test material

accumulation can be used as indicators for the severity of toxic effects. Thereby, the rat STIS can provide early indications of effects that only evolve over time and hence only become evident in longer-term studies, possibly even only in 2-year studies as the example of $BaSO_4$ NM-220 shows [75].

In summary, the rat STIS, applying the most recent study design (cf. Sects. 2.1 and 2.2), has the following advantages:

1. Reduction and refinement method in accordance with the 3Rs principle [7].
2. Physiological route of administration (i.e., inhalation exposure versus intratracheal instillation).
3. Timely indication for hazard to the respiratory tract (in a shorter period of time than when performing 28-day and 90-day inhalation studies) and/or non-respiratory tract tissues and organs.
4. Relevant data on deposition and clearance kinetics with relation to atmospheric concentration.
5. Information about progression or regression of effects.
6. Findings applicable for the establishment of NOAECs which can be used, e.g., for occupational safety assessments.

Comprehensive nanomaterial characterization is indispensible for their meaningful hazard and risk assessment. This is ensured when the rat STIS is embedded in an integrated testing strategy such as the DF4nanoGrouping (in Tier 3) which includes intrinsic material properties in Tier 1 and functionalities in Tier 2 [23, 24]. Importantly, even though hazard can be over-predicted in the DF4nanoGrouping Tiers 1 and 2 (cf. case studies for graphite nanoplatelets and SiO_2·phosphonate), it has not yet been under-predicted [24]. By yielding conservative predictions of nanomaterial hazard potential, the DF4nanoGrouping is a suitable tool for initial risk assessments. The evaluation of rat STIS data within the DF4nanoGrouping allows to prioritize nano-materials for further examinations and to decide on appropriate and targeted further investigations including sub-chronic or chronic inhalation toxicity tests.

While the rat STIS covers many aspects of nanomaterial toxicity potential and potency that are relevant for risk assessment, performance of the 28-day and/ or 90-day inhalation toxicity studies is mandatory in many regulatory settings. Further, the rat STIS may reveal specific findings that require further investigations in longer-term studies. In these cases, the rat STIS is a suitable range-finding study to allow selecting appropriate aerosol concentrations (and their spacing) for subsequent 28-day or 90-day inhalation toxicity studies. The range-finding should be based on the dose-response curve of STIS BALF parameters and the incidence and severity of histopathological findings. Specifically, the NOAEC of STIS BALF parameters can serve as a reference for the lowest concentration in the subsequent longer-term study. The pulmonary deposition immediately after the STIS exposure period can be used to assess the daily internal dose. Finally, if the rat STIS indicates nanomaterial biopersistence, an appropriate postexposure observation period can be scheduled accordingly for the longer-term study.

An increasing number of nanomaterials (and non-nanosized test materials) is being assessed in the rat STIS. To provide a foundation for further comparisons

of rat STIS and longer-term inhalation toxicity studies that may eventually allow reducing the need for such longer-term studies, Tables 2.1, 2.3, 2.5, 2.7, and 2.9 present further published rat STISs, just as Tables 2.2, 2.4, 2.6, 2.8, and 2.10 present further published 28-day, 90-day, and 2-year inhalation toxicity studies other than those discussed in the 5 case studies presented in this chapter.

Ultimately, the STIS may be supplemented or even, in a distant future, replaced by appropriate in vitro assays as they become applicable for regulatory purposes [79, 88]. The increasing database on available rat STISs can form a solid basis for the development and validation of such in vitro assays, thereby further serving the 3Rs principle to replace, reduce, and refine animal testing [7].

References

1. Arts JH, Muijser H, Duistermaat E, Junker K, Kuper C. Five day inhalation toxicity study of three types of synthetic amorphous silicas in Wistar rats and post-exposure evaluations for up to 3 months. Food Chem Toxicol. 2007;45(10):1856–67.
2. Landsiedel R, Ma-Hock L, Hofmann T, Wiemann M, Strauss V, Treumann S, Wohlleben W, Gröters S, Wiench K, van Ravenzwaay B. Application of short-term inhalation studies to assess the inhalation toxicity of nanomaterials. Part Fibre Toxicol. 2014;11:16.
3. Ma-Hock L, Burkhardt S, Strauss V, Gamer AO, Wiench K, van Ravenzwaay B, Landsiedel R. Development of a short-term inhalation test in the rat using nano-titanium dioxide as a model substance. Inhal Toxicol. 2009;21(2):102–18.
4. Ma-Hock L, Hofmann T, Landsiedel R, van Ravenzwaay B. A short-term inhalation study protocol: designed for testing of toxicity and fate of nanomaterials. Methods Mol Biol. 2014;1199:207–12.
5. OECD. Organisation for Economic Co-operation and Development. Guideline for testing of chemicals no. 412. Subacute inhalation toxicity: 28-day study. Paris: OECD; 2017.
6. OECD. Organisation for Economic Co-operation and Development. Guideline for testing of chemicals no. 413. Subchronic inhalation toxicity: 90-day study. Paris: OECD; 2017.
7. Russell WMS, Burch RL. The principles of humane experimental technique. London: Methuen; 1959. Reprinted by UFAW, 1992, England, 238 pp.
8. Braakhuis HM, Cassee FR, Fokkens PH, de la Fonteyne LJ, Oomen AG, Krystek P, de Jong WH, van Loveren H, Park MV. Identification of the appropriate dose metric for pulmonary inflammation of silver nanoparticles in an inhalation toxicity study. Nanotoxicology. 2016;10(1):63–73.
9. Dekkers S, Ma-Hock L, Lynch I, Russ M, Miller MR, Schins RPF, Keller J, Römer I, Küttler K, Strauss V, de Jong WH, Landsiedel R, Cassee FR. Differences in the toxicity of nanomaterials after inhalation can be explained by lung deposition, animal species and nanoforms. The case of cerium dioxide. Inhal Toxicol. 2018;30(7-8):273–86.
10. Wohlleben W, Meier MW, Vogel S, Landsiedel R, Cox G, Hirth S, Tomović Ž. Elastic CNT-polyurethane nanocomposite: synthesis, performance and assessment of fragments released during use. Nanoscale. 2013;5(1):369–80.
11. Wohlleben W, Kuhlbusch T, Lehr C-M, Schnekenburger J. Safety of nanomaterials along their lifecycle: release, exposure and human hazards. Hoboken, NJ: Taylor & Francis; 2014. ISBN 978-1-46-656786-3, 472 pp.

12. Wohlleben W, Driessen MD, Raesch S, Schaefer UF, Schulze C, Von Vacano B, Vennemann A, Wiemann M, Ruge CA, Platsch H, Mues S, Ossig R, Tomm JM, Schnekenburger J, Kuhlbusch TAJ, Luch A, Lehr C-M, Haase H. Influence of agglomeration and specific lung lining lipid/protein interaction on short-term inhalation toxicity. Nanotoxicology. 2016;10(7):970–80.

13. Wohlleben W, Mielke J, Bianchin A, Ghanem A, Freiberger H, Rauscher H, Gemeinert M, Hodoroaba VD. Reliable nanomaterial classification of powders using the volume-specific surface area method. J Nanopart Res. 2017;19(2):61.

14. Wohlleben W, Waindok H, Daumann B, Werle K, Drum M, Egenolf H. Composition, respirable fraction and dissolution rate of 24 stone wool MMVF with their binder. Part Fibre Toxicol. 2017;14:29.

15. Gandon A, Werle K, Neubauer N, Wohlleben W. Surface reactivity measurements as required for grouping and read-across: an advanced FRAS protocol. J Phys Conf Ser. 2017;838:012033.

16. Ma-Hock L, Gamer AO, Landsiedel R, Leibold E, Frechen T, Sens B, Linsenbuehler M, van Ravenzwaay B. Generation and characterization of test atmospheres with nanomaterials. Inhal Toxicol. 2007;19:833–48.

17. Mangum J, Bermudez E, Sar M, Everitt J. Osteopontin expression in particle-induced lung disease. Exp Lung Res. 2004;30(7):585–98.

18. Ma-Hock L, Strauss V, Treumann S, Küttler K, Wohlleben W, Hofmann T, Gröters S, Wiench K, van Ravenzwaay B, Landsiedel R. Comparative inhalation toxicity of multi-wall carbon nanotubes, graphene, graphite nanoplatelets and low surface carbon black. Part Fibre Toxicol. 2013;10:23.

19. Henderson RF, Driscoll KE, Harkema JR, Lindenschmidt RC, Chang I-Y, Maples KR, Barr EB. A comparison of the inflammatory response of the lung to inhaled versus instilled particles in F-344 rats. Fundam Appl Toxicol. 1995;24:183–97.

20. Vennemann A, Alessandrini F, Wiemann M. Differential effects of surface functionalized zirconium oxide nanoparticles on alveolar makrophages, rat lung and a mouse model. Nanomaterials. 2017;7:280.

21. Wiemann M, Vennemann A, Blaske F, Sperling M, Karst U. Silver nanoparticle in the lung: toxic effects and focal accumulation of silver in remote organs. Nanomaterials. 2017;7:441.

22. Strauss V, Ma-Hock L, Rey Moreno MC, Groeters S, Landsiedel R, Wiemann M, van Ravenzwaay B. Validation of an appropriate lavage procedure of the left pulmonary lobe and accompanying histopathology in the frame of the draft OECD TG 413. In: The toxicologist: supplement to toxicological sciences, 156 (1), Society of Toxicology, 2017. Abstract no. 2385.

23. Arts JH, Hadi M, Irfan MA, Keene AM, Kreiling R, Lyon D, Maier M, Michel K, Petry T, Sauer UG, Warheit D, Wiench K, Wohlleben W, Landsiedel R. A decision-making framework for the grouping and testing of nanomaterials (DF4nanoGrouping). Regul Toxicol Pharmacol. 2015;71(2 Suppl):S1–27.

24. Arts JH, Irfan MA, Keene AM, Kreiling R, Lyon D, Maier M, Michel K, Neubauer N, Petry T, Sauer UG, Warheit D, Wiench K, Wohlleben W, Landsiedel R. Case studies putting the decision-making framework for the grouping and testing of nanomaterials (DF4nanoGrouping) into practice. Regul Toxicol Pharmacol. 2016;76:234–61.

25. OECD. Organisation for Economic Co-operation and Development list of manufactured nanomaterials and list of endpoints for phase one of the sponsorship programme for the testing of manufactured nanomaterials: revision. Series on the safety of manufactured nanomaterials. ENV/JM/MONO(2010)46. Paris: OECD; 2010.

26. Bellmann B. DRF, 5-day nose-only inhalation toxicity study of Z-COTE® HP1 in Wistar WU rats (DRF study) 02 N 09 515 (Draft report). Hannover: Fraunhofer ITEM; 2009. Study owner: Cefic, Bruxelles.

27. Gosens I, Cassee FR, Zanella M, Manodori L, Brunelli A, Costa AL, Bokkers BG, de Jong WH, Brown D, Hristozov D, Stone V. Organ burden and pulmonary toxicity of nano-sized copper (II) oxide particles after short-term inhalation exposure. Nanotoxicology. 2016;10(8):1084–95.

28. Braakhuis HM, Gosens I, Krystek P, Boere JA, Cassee FR, Fokkens PH, Post JA, van Loveren H, Park MV. Particle size dependent deposition and pulmonary inflammation after short-term inhalation of silver nanoparticles. Part Fibre Toxicol. 2014;11:49.

29. Creutzenberg O. 14-Day nose-only inhalation toxicity study of Z-COTE HP1 in Wistar WU rats. 02 G 09 005. Hannover: Fraunhofer ITEM; 2013. Study owner: Cefic, Bruxelles.

30. Seiffert J, Buckley A, Leo B, Martin NG, Zhu J, Dai R, Hussain F, Guo C, Warren J, Hodgson A, Gong J, Ryan MP, Zhang JJ, Porter A, Tetley TD, Gow A, Smith R, Chung KF. Pulmonary effects of inhalation of spark-generated silver nanoparticles in Brown-Norway and Sprague-Dawley rats. Respir Res. 2016;17(1):85.

31. Morimoto Y, Izumi H, Yoshiura Y, Tomonaga T, Oyabu T, Myojo T, Kawai K, Yatera K, Shimada M, Kubo M, Yamamoto K, Kitajima S, Kuroda E, Kawaguchi K, Sasaki T. Evaluation of pulmonary toxicity of zinc oxide nanoparticles following inhalation and intratracheal instillation. Int J Mol Sci. 2016;17(8):1241.

32. Creutzenberg O. 3-Month nose-only inhalation toxicity study of Z-COTE HP1 in Wister WU rats. 02 G 10 024. Hannover: Fraunhofer ITEM; 2013. Study owner: Cefic, Bruxelles.

33. Ahamed M, Akhtar MJ, Alhadlaq HA, Alrokayan SA. Assessment of the lung toxicity of copper oxide nanoparticles: current status. Nanomedicine (Lond). 2015;10(15):2365–77.

34. WHO. WHO air quality guidelines for Europe. 2nd ed. Geneva: WHO; 2002. Available at http://www.euro.who.int/__data/assets/pdf_file/0005/74732/E71922.

35. Donaldson K, Aitken R, Tran L, Stone V, Duffin R, Forrest G, Alexander A. Carbon nanotubes: a review of their properties in relation to pulmonary toxicology and workplace safety. Toxicol Sci. 2006;92:5–22.

36. Donaldson K, Murphy FA, Duffin R, Poland CA. Asbestos, carbon nanotubes and the pleural mesothelium: a review of the hypothesis regarding the role of long fibre retention in the parietal pleura, inflammation and mesothelioma. Part Fibre Toxicol. 2010;7:5.

37. Donaldson K, Murphy F, Schinwald A, Duffin R, Poland CA. Identifying the pulmonary hazard of high aspect ratio nanoparticles to enable their safety-by-design. Nanomedicine. 2011;6:143–56.

38. Duke KS, Bonner JC. Mechanisms of carbon nanotube-induced pulmonary fibrosis: a physicochemical characteristic perspective. Wiley Interdiscip Rev Nanomed Nanobiotechnol. 2018;10:e1498. https://doi.org/10.1002/wnan.1498.

39. Poulsen SS, Saber AT, Williams A, Andersen O, Købler C, Atluri R, Pozzebon ME, Mucelli SP, Simion M, Rickerby D, Mortensen A, Jackson P, Kyjovska ZO, Mølhave K, Jacobsen NR, Jensen KA, Yauk CL, Wallin H, Halappanavar S, Vogel U. MWCNTs of different physicochemical properties cause similar inflammatory responses, but differences in transcriptional and histological markers of fibrosis in mouse lungs. Toxicol Appl Pharmacol. 2015;284:16–32.

40. Poland CA, Duffin R, Kinloch I, Maynard A, Wallace WA, Seaton A, Stone V, Brown S, Macnee W, Donaldson K. Carbon nanotubes introduced into the abdominal cavity of mice show asbestos-like pathogenicity in a pilot study. Nat Nanotechnol. 2008;3(7):423–8.

41. Fukushima S, Kasai T, Umeda Y, Ohnishi M, Sasaki T, Matsumoto M. Carcinogenicity of multi-walled carbon nanotubes: challenging issue on hazard assessment. J Occup Health. 2018;60(1):10–30.

42. Kobayashi N, Izumi H, Morimoto Y. Review of toxicity studies of carbon nanotubes. J Occup Health. 2017;59(5):394–407.

43. Chernova T, Murphy FA, Galavotti S, Sun XM, Powley IR, Grosso S, Schinwald A, Zacarias-Cabeza J, Dudek KM, Dinsdale D, Le Quesne J, Bennett J, Nakas A, Greaves P, Poland CA, Donaldson K, Bushell M, Willis AE, MacFarlane M. Long-fiber carbon nanotubes replicate asbestos-induced mesothelioma with disruption of the tumor suppressor gene Cdkn2a (Ink4a/Arf). Curr Biol. 2017;27(21):3302–14. e6.

44. Ma-Hock L, Treumann S, Strauss V, Brill S, Luizi F, Mertler M, Wiench K, Gamer AO, van Ravenzwaay B, Landsiedel R. Inhalation toxicity of multi-wall carbon nanotubes in rats exposed for 3 months. Toxicol Sci. 2009;112:468–81.

45. Pothmann D, Simar S, Schuler D, Dony E, Gaering S, Le Net JL, Okazaki Y, Chabagno JM, Bessibes C, Beausoleil J, Nesslany F, Régnier JF. Lung inflammation and lack of genotoxicity in the comet and micronucleus assays of industrial multiwalled carbon nanotubes Graphistrength(©) C100 after a 90-day nose-only inhalation exposure of rats. Part Fibre Toxicol. 2015;12:21.
46. Régnier J-F, Pothmann-Krings D, Simar S, Dony E, Le Net J-L, Beausoleil J. Graphistrength© C100 multiwalled carbon nanotubes (MWCNT): thirteen-week inhalation toxicity study in rats with 13- and 52-week recovery periods combined with comet and micronucleus assays. J Phys Conf Series. 2017;838:012030.
47. Pauluhn J. Subchronic 13-week inhalation exposure of rats to multiwalled carbon nanotubes: toxic effects are determined by density of agglomerate structures, not fibrillar structures. Toxicol Sci. 2010;113:226–42.
48. Kasai T, Umeda Y, Ohnishi M, Mine T, Kondo H, Takeuchi T, Matsumoto M, Fukushima S. Lung carcinogenicity of inhaled multi-walled carbon nanotube in rats. Part Fibre Toxicol. 2016;13(1):53.
49. Sargent LM, Porter DW, Staska LM, Hubbs AF, Lowry DT, Battelli L, Siegrist KJ, Kashon ML, Mercer RR, Bauer AK, Chen BT, Salisbury JL, Frazer D, McKinney W, Andrew M, Tsuruoka S, Endo M, Fluharty KL, Castranova V, Reynolds SH. Promotion of lung adenocarcinoma following inhalation exposure to multi-walled carbon nanotubes. Part Fibre Toxicol. 2014;11:3.
50. Kroll A, Dierker C, Rommel C, Hahn D, Wohlleben W, Schulze-Isfort C, Göbbert C, Voetz M, Hardinghaus F, Schnekenburger J. Cytotoxicity screening of 23 engineered nanomaterials using a test matrix of ten cell lines and three different assays. Part Fibre Toxicol. 2011;8:9.
51. Hofmann T, Ma-Hock L, Strauss V, Treumann S, Rey Moreno M, Neubauer N, Wohlleben W, Gröters S, Wiench K, Veith U, Teubner W, van Ravenzwaay B, Landsiedel R. Comparative short-term inhalation toxicity of five organic diketopyrrolopyrrole pigments and two inorganic iron-oxide-based pigments. Inhal Toxicol. 2016;7:1–17.
52. Bräu M, Ma-Hock L, Hesse C, Nicoleau L, Strauss V, Treumann S, Wiench K, Landsiedel R, Wohlleben W. Nanostructured calcium silicate hydrate seeds accelerate concrete hardening: a combined assessment of benefits and risks. Arch Toxicol. 2012;86(7):1077–87.
53. Ma-Hock L, Landsiedel R, Wiench K, Geiger D, Strauss V, Gröters S, van Ravenzwaay B, Gerst M, Wohlleben W, Scherer G. Short-term rat inhalation study with aerosols of acrylic ester-based polymer dispersions containing a fraction of nanoparticles. Int J Toxicol. 2012;31:46–57.
54. Kim YH, Jo MS, Kim JK, Shin JH, Baek JE, Park HS, An HJ, Lee JS, Kim BW, Kim HP, Ahn KH, Jeon K, Oh SM, Lee JH, Workman T, Faustman EM, Yu IJ. Short-term inhalation study of graphene oxide nanoplates. Nanotoxicology. 2018;1:1–15.
55. Konduru N, Keller J, Ma-Hock L, Gröters S, Landsiedel R, Donaghey TC, Brain JD, Wohlleben W, Molina RM. Biokinetics and effects of barium sulfate nanoparticles. Part Fibre Toxicol. 2014;11:55.
56. Schwotzer D, Ernst H, Schaudien D, Kock H, Pohlmann G, Dasenbrock C, Creutzenberg O. Effects from a 90-day inhalation toxicity study with cerium oxide and barium sulfate nanoparticles in rats. Part Fibre Toxicol. 2017;14:23.
57. Schwotzer D, Niehof M, Schaudien D, Kock H, Hansen T, Dasenbrock C, Creutzenberg O. Cerium oxide and barium sulfate nanoparticle inhalation affects gene expression in alveolar epithelial cells type II. J Nanobiotechnol. 2018;16(1):16.
58. Cullen RT, Tran CL, Buchanan D, Davis JMG, Searl A, Jones AD, Donaldson K. Inhalation of poorly soluble particles. Differences in inflammatory response and clearance during exposure. Inhal Toxicol. 2000;12:1089–111.
59. Tran CL, Buchanan D, Cullen RT, Searl A, Jones AD, Donaldson K. Inhalation of poorly soluble particles. II. Influence of particle surface area on inflammation and clearance. Inhal Toxicol. 2000;12:1113–26.

60. Kim JK, Shin JH, Lee JS, Hwang JH, Lee JH, Baek JE, Kim TG, Kim BW, Kim JS, Lee GH, Ahn K, Han SG, Bello D, Yu IJ. 28-Day inhalation toxicity of graphene nanoplatelets in Sprague-Dawley rats. Nanotoxicology. 2016;10(7):891–901.
61. Reuzel PG, Bruijntjes JP, Feron VJ, Woutersen RA. Subchronic inhalation toxicity of amorphous silicas and quartz dust in rats. Food Chem Toxicol. 1991;29:341–54.
62. Johnston CJ, Driscoll KE, Finkelstein JN, Baggs RF, O'Reilly MA, Carter J, Gelein R, Oberdörster G. Pulmonary chemokine and mutagenic responses in rats after subchronic inhalation of amorphous and crystalline silica. Toxicol Sci. 2000;56(2):405–13.
63. Bermudez E, Mangum JB, Wong BA, Asgharian B, Hex PM, Warhead DB, Everett JI. Pulmonary responses of mice, rats, and hamsters to subchronic inhalation of ultrafine titanium dioxide particles. Toxicol Sci. 2004;77(2):347–57.
64. Heinrich U, Fuhst R, Rittinghausen S, Creutzenberg O, Bellmann B, Koch W, Levsen K. Chronic inhalation exposure of Wistar rats and two different strains of mice to diesel exhaust, carbon black, and titanium dioxide. Inhal Toxicol. 1995;7:533–56.
65. Disdier C, Chalansonnet M, Gagnaire F, Gaté L, Cosnier F, Devoy J, Saba W, Lund AK, Brun E, Mabondzo A. Brain inflammation, blood brain barrier dysfunction and neuronal synaptophysin decrease after inhalation exposure to titanium dioxide nano-aerosol in aging rats. Sci Rep. 2017;7(1):12196.
66. Oyabu T, Myojo T, Lee BW, Okada T, Izumi H, Yoshiura Y, Tomonaga T, Li YS, Kawai K, Shimada M, Kubo M, Yamamoto K, Kawaguchi K, Sasaki T, Morimoto Y. Biopersistence of NiO and TiO_2 nanoparticles following intratracheal instillation and inhalation. Int J Mol Sci. 2017;18(12):2757.
67. Keller J, Wohlleben W, Ma-Hock L, Strauss V, Gröters S, Küttler K, Wiench K, Herden C, Oberdörster G, van Ravenzwaay B, Landsiedel R. Time course of lung retention and toxicity of inhaled particles: short-term exposure to nano-ceria. Arch Toxicol. 2014;88(11):2033–59.
68. Gosens I, Mathijssen LE, Bokkers BG, Muijser H, Cassee FR. Comparative hazard identification of nano- and micro-sized cerium oxide particles based on 28-day inhalation studies in rats. Nanotoxicology. 2014;8(6):643–53.
69. Morimoto Y, Izumi H, Yoshiura Y, Tomonaga T, Oyabu T, Myojo T, Kawai K, Yatera K, Shimada M, Kubo M, Yamamoto K, Kitajima S, Kuroda E, Kawaguchi K, Sasaki T. Pulmonary toxicity of well-dispersed cerium oxide nanoparticles following intratracheal instillation and inhalation. J Nanopart Res. 2015;17(11):442.
70. Shin SH, Lim CH, Kim YS, Lee YH, Kim SH, Kim JC. Twenty-eight-day repeated inhalation toxicity study of nano-sized lanthanum oxide in male sprague-dawley rats. Environ Toxicol. 2017;32(4):1226–40.
71. Kim YS, Lim CH, Shin SH, Kim JC. Twenty-eight-day repeated inhalation toxicity study of nano-sized neodymium oxide in male Sprague-Dawley rats. Toxicol Res. 2017;33(3):239–53.
72. Elder A, Gelein R, Finkelstein JN, Driscoll KE, Harkema J, Oberdörster G. Effects of subchronically inhaled carbon black in three species. Retention kinetics, lung inflammation and histopathology. Toxicol Sci. 2005;88(2):614–29.
73. Lee KP, Trochimowicz HJ, Reinhardt CF. Pulmonary response of rats exposed to titanium dioxide (TiO_2) by inhalation for two years. Toxicol Appl Pharmacol. 1985;79:179–92.
74. Nikula KJ, Snipes MB, Barr EB, Griffith WC, Henderson RF, Mauderly JL. Comparative pulmonary toxicities and carcinogenicities of chronically inhaled diesel exhaust and carbon black in F344 rats. Fundam Appl Toxicol. 1995;25:80–94.
75. Groeters S, Ernst H, Ma-Hock L, Strauss V, Landsiedel R, Wiench K, van Ravenzwaay B. Long-term inhalation study with nano barium sulfate: unexpected morphological findings and lung-burden after 12 months of exposure. In: The Toxicologist: Supplement to Toxicological Sciences, 156(1), Society of Toxicology, 2017. Abstract no. 1328.
76. Hadjimichael OC, Brubaker RE. Evaluation of an occupational respiratory exposure to a zirconium-containing dust. J Occup Med. 1981;23(8):543–7.
77. Marcus RL, Turner S, Cherry NM. A study of lung function and chest radiographs in men exposed to zirconium compounds. Occup Med (Lond). 1996;46(2):109–13.

78. Klein CL, Wiench K, Wiemann M, Ma-Hock L, van Ravenzwaay B, Landsiedel R. Hazard identification of inhaled nanomaterials: making use of short-term inhalation studies. Arch Toxicol. 2012;86(7):1137–51.
79. Wiemann M, Vennemann A, Sauer UG, Wiench K, Ma-Hock L, Landsiedel R. An alveolar macrophage assay for predicting the short-term inhalation toxicity of nanomaterials. J Nanobiotechnol. 2016;14:16.
80. Van Ravenzwaay B, Landsiedel R, Fabian E, Burkhardt S, Strauss V, Ma-Hock L. Comparing fate and effects of three particles of different surface properties: nano-TiO₂, pigmentary TiO₂ and quartz. Toxicol Lett. 2009;186:152–9.
81. Ma-Hock L, Brill S, Wohlleben W, Farias PM, Chaves CR, Tenório DP, Fontes A, Santos BS, Landsiedel R, Strauss V, Treumann S, Ravenzwaay B. Short term inhalation toxicity of a liquid aerosol of CdS/Cd(OH)₂ core shell quantum dots in male Wistar rats. Toxicol Lett. 2012;208(2):115–24.
82. Ma-Hock L, Farias PM, Hofmann T, Andrade AC, Silva JN, Arnaud TM, Wohlleben W, Strauss V, Treumann S, Chaves CR, Gröters S, Landsiedel R, van Ravenzwaay B. Short term inhalation toxicity of a liquid aerosol of glutaraldehyde-coated CdS/Cd(OH)₂ core shell quantum dots in rats. Toxicol Lett. 2014;225(1):20–6.
83. Kwon S, Yang YS, Yang HS, Lee J, Kang MS, Lee B, Lee K, Song CW. Nasal and pulmonary toxicity of titanium dioxide nanoparticles in rats. Toxicol Res. 2012;28(4):217–24.
84. Greim H, Ziegler-Skylakakis K. Risk assessment for biopersistent granular particles. Inhal Toxicol. 2007;19(Suppl 1):199–204.
85. Creutzenberg O, Pohlmann G, Hansen T, Schuchardt S, Ernst H, Tillmann T, Schaudien D. CEFIC-LRI N1 project: inhalation toxicity of a synthetic amorphous silica (SAS) in rats. In: The toxicologist: supplement to toxicological sciences, 138 (1), Society of Toxicology, 2014. Abstract no. 600.
86. Shin JH, Jeon K, Kim JK, Kim Y, Jo MS, Lee JS, Baek JE, Park HS, An HJ, Park JD, Ahn K, Oh SM, Yu IJ. Subacute inhalation toxicity study of synthetic amorphous silica nanoparticles in Sprague-Dawley rats. Inhal Toxicol. 2017;29(12–14):567–76.
87. Stöber W, Fink A, Bohn E. Controlled growth of monodisperse silica spheres in the micron size range. J Colloid Interface Sci. 1968;26:62–9.
88. Wiemann M, Sauer UG, Vennemann A, Bäcker S, Keller J-G, Ma-Hock L, Wohlleben W, Landsiedel R. *In vitro* and *in vivo* short-term pulmonary toxicity of differently sized colloidal amorphous SiO₂. Nanomaterials. 2018;8:160.

Chapter 3
Use of Short-Term Inhalation Study to Obtain Initial Hazard Data and Prepare for Subacute and Subchronic Inhalation Studies, and Toxicokinetic Studies

Ki Soo Jeon, Jae Seong Yi, and Il Je Yu

Abstract A short-term inhalation study (STIS) protocol that has been specifically developed for testing nanomaterials can be used as an alternative testing choice for acute toxicity testing, and a range-finding study for subacute and subchronic studies. The STIS can also be used to characterize the nanoparticle physicochemical properties and determine the type of exposure and particle monitoring methods in the inhalation chamber for subsequent subacute and subchronic inhalation studies. In addition, importantly, the particle generation method and particle concentration stability can be studied before and during the STIS. Furthermore, combining an STIS with a lung burden analysis, which is now a mandatory requirement for OECD 412 (subacute) and 413 (subchronic) test guidelines, can provide toxicokinetic information, including the biodistribution and lung clearance of nanoparticles.

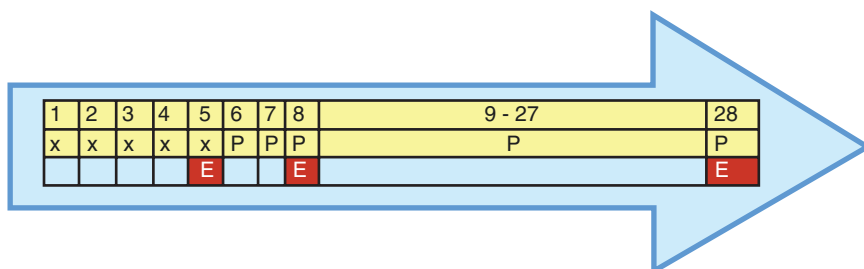**Keywords** Short-term inhalation study · Inhalation toxicity · Toxicokinetics Nanomaterials · Nanoparticles

3.1 Introduction

Human exposure to nanomaterials can occur through multiple routes, including inhalation, ingestion, skin absorption, and injection. However, in the case of aerosolized nanomaterials, nano-objects and their aggregates and agglomerates (NOAAs), the primary route of exposure is inhalation. Specifically, NOAAs are nano-objects with one, two, or three nanoscale external dimensions, ranging from approximately 1 to 100 nm, and can include spheres, fibers, tubes, and other structures. Moreover, NOAAs can comprise of individual primary nanoscale structures or aggregated and

K. S. Jeon · J. S. Yi · I. J. Yu (✉)
HCTm Co. Ltd., Icheon, Republic of Korea
e-mail: ijyu@hctm.co.kr

agglomerated structures with sizes larger than 100 nm [1]. Inhalation toxicity studies using experimental animals are currently a regulatory requirement for chemical risk assessment, and the OECD provides 3 acute inhalation toxicity test guidelines: 403 [2], 433 [3] and 436 [4], one subacute toxicity test guideline: 412 [5], and one subchronic toxicity test guideline: 413 [6]. Guidelines 412 and 413 were recently revised as the original guidelines were not intended for testing nanomaterials [7, 8]. A short-term inhalation study (STIS) protocol has also been specifically developed for testing nanomaterials or NOAAs [9], consisting of 5-day inhalation exposure with a subsequent 3-week postexposure period (Fig. 3.1 and Table 3.1). This protocol was already introduced to the OECD WPMN (Working Party on Manufactured Nanomaterials) as an alternative testing method for nanomaterials along with case-study examples based on an Integrated Testing Strategy, while a case study for hazard identification of inhaled nanomaterials was presented in 2012 [10] and further discussed at the OECD WPMN inhalation toxicity test workshop in Washington, DC in 2015. Unlike the acute inhalation toxicity test guidelines 403 [2], 433 [3] and 436 [4], where animals are exposed to the test article for 4 h, an appropriately designed STIS can facilitate the investigation of both the basic toxicity of the nanomaterial or test article and the toxicokinetics or particokinetics, including particle retention in the lungs and clearance or the extrapulmonary translocation of the

Fig. 3.1 Study design of short-term inhalation study for nanomaterials (x: head/nose-only inhalation exposure for 6 h/day; E: examination; P: postexposure period) [10]

Table 3.1 Study design [10]

Study day	1	2	3	4	5	6	7	8	9–27	28
Study phase	x	x	x	x	x	R	R	R	R	R
Examinations and time points					E + L			L		E + L

x: head/nose exposure for 6 h/day
R: recovery period
E: gross necropsy, organ weights and histopathology (three animals/time point and concentration group); optional lung burden (three animals/time point and concentration group)
L: bronchoalveolar lavage (five animals/time point and concentration group)

nanomaterial to other organs. Moreover, as suggested in the OECD acute inhalation toxicity guidance document GD 39 [11], a high limit concentration for aerosol testing of more than 2 mg/L (2 g/m^3) should be attempted if a respirable size is achievable. However, in actual nanomaterial inhalation testing, the maximum aerosol concentration of nanomaterials is less than 50 mg/m^3, where a higher concentration is indicative of an agglomerated or aggregated state. Furthermore, a high limit concentration is very difficult to achieve for nanomaterials and acute toxicity is rarely found at such concentrations. Therefore, an STIS represents an alternative testing choice for acute toxicity testing. Plus, an STIS can be used as a range-finding study for subacute and subchronic studies. As regards current OECD regulatory inhalation toxicity test guidelines, OECD TG 403 for acute inhalation toxicity testing was not designed to test poorly soluble isometric, fibrous, or manufactured nanomaterials [1]. Similarly, OECD TG 436 is inapplicable due to difficulties in generating aerosolized nanomaterials and NOAA aerosols. Such concentrations were intended to classify or label nanomaterials according to the GHS (UN Globally Harmonized System of classification and labelling of chemicals) [12]. Meanwhile, OECD TG 412 for subacute inhalation toxicity testing and OECD TG 413 for subchronic inhalation toxicity testing do not provide any toxicokinetics or particle kinetics, such as the lung burden, clearance, or extrapulmonary translocation to other tissue. Thus, an STIS can replace OECD TG 403 and 436 for acute toxicity testing, and can be used as a concentration range-finding study for subacute and subchronic inhalation toxicity testing. The recently revised OECD inhalation toxicity test guidelines 412 (subacute) and 413 (subchronic) include toxicokinetics or particokinetics with the requirement of lung burden measurements following exposure and during postexposure observation periods for poorly soluble particles including poorly soluble nanomaterials [7, 8]. Since a properly designed STIS can identify a range of concentrations for subacute and subchronic inhalation studies, an STIS represents a convenient range-finding method for subacute or subchronic studies, and an excellent method for identifying the toxicokinetics of nanomaterials or NOAAs.

3.2   STIS Design Considerations for Nanomaterial Testing

Inhalation toxicity tests are important for evaluating the health risks of workers, consumers, and the general population exposed to aerosolized nanomaterials or NOAAs. When planning inhalation studies of NOAAs or nanomaterials using STIS, subacute, or subchronic studies, the important design considerations include the exposure characteristics, physicochemical properties of the nanomaterial, particle characterization methods, and appropriate selection of the aerosol generator, as described in ISO 19601 [1] and Table 3.2 [13].

Table 3.2 Basic scheme for selecting appropriate generator (summarized form of TR 19601, from [1])

Step	Considerations
Selection of study	Guideline-based study: strictly recommended to follow TG
	Hazard identification research
Characterization of physicochemical properties of NOAA being studied	Size and size distribution
	Aggregation/agglomeration
	Surface characteristics: area and charge
	Crystalline structure
	Electrical properties
	Dustiness
	Composition and purity
Exposure information on possible use or handling and manufacturing	Simulating actual workplace exposure situation
	Depending on particle shape and concentration
Exposure characteristics	Frequency and duration of worker exposure
	NOAA generating operation
	NOAA release procedure and handling information
	Temperature and humidity of workplace
Type of inhalation exposure method	Whole-body chamber: less stress on animals
	Nose-only chamber: less oral or skin exposure
	Secured safety of chamber
Particle characterization methods	Real-time monitoring
	Off-line monitoring
	Stability determination
Selection of generator	Based on type of nanomaterial being considered
	Dry or wet aerosol generation
	Ensuring maintenance of generator
	Considering risk management system: malfunctioning of generator, protection against dust explosion

3.2.1 Exposure Characteristics

Similar to subacute and subchronic inhalation studies, an STIS of nanomaterials or NOAAs should consider and simulate the actual exposure situation in the workplace or a consumer exposure scenario. In particular, the STIS design should consider the exposure characteristics, including the particle mass, concentration, number, size, dispersion (dispersed or aggregated/agglomerated), and shape of the nanomaterials or NOAAs, along with exposure information on the frequency and duration of worker/user exposure and activities, nanomaterial or nanoproduct manufacturing operations, source release scenarios, and handling information.

3.2.2 Characterization of Physicochemical Properties of Nanomaterials

When conducting an STIS, physicochemical characterization of the "as manufactured" or pristine nanomaterial is important before generating a nanomaterial aerosol or NOAA aerosol. Nanomaterials are manufactured and fabricated using diverse synthesis procedures that impose unique properties designed for specific applications, which means they can have complex structures with impurities and different surface properties, including coating, doping, functionalization, or other modifications. As these physicochemical properties affect the toxicological output of nanomaterials, they should be thoroughly characterized [14]. Such physicochemical properties include the particle size, size distribution, shape, aggregation/agglomeration, surface characteristics (such as charge), crystalline structure, dustiness, composition, and purity/impurities. Even trace impurities, such as the presence of endotoxin, a metal catalyst residue, can affect the toxicity outcomes [15–17]. Therefore, before initiating the STIS, physicochemical characterization of the nanomaterial is critical to ensure that its properties match the claims made by the manufacturer. Moreover, for NOAAs, it is essential to predetermine whether the particle size distribution represents the size distribution observed during typical handling and use of the subject NOAAs. Most workplace exposure has been found to include exposure to agglomerated primary particles [18]. Plus, it is also important to determine the particle size distribution as prescribed by regulatory guidelines, such as OECD inhalation test guidelines, which suggest an MMAD <2 μm and GSD <3.

3.2.3 Types of Inhalation Exposure Method

There are currently two types of inhalation chamber: whole-body and nose-only. While the whole-body method is more relevant to human exposure and causes less pain and suffering to the animals, the nose-only method reduces the potential for oral and skin exposure and consumes a lower quantity of the test article when compared with whole-body exposure. Selecting the appropriate inhalation chamber will be according to the study design. Plus, the chamber should also incorporate safety measures, such as a leak proof design and leak testing, safety cabinet, and proper encapsulated ventilation with emissions control and waste treatment. Revised OECD TGs 412 and 413 recommend the primary use of nose-only exposure, with whole-body exposure only used in the case of specific documented justification [7, 8]. Nose-only exposure is also generally preferable for an STIS.

3.3 Particle Characterization Methods

3.3.1 Real-Time Monitoring

Monitoring the particle size and number is included in revised OECD TGs 412 and 413, which recommend the use of real-time monitors to test the stability of the chamber atmosphere and particle size distribution. Monitoring devices, such as DMAS (differential mobility analyzing system), APS (aerodynamic particle sizer), and ELPI (electrical low-pressure impactor), can provide the particle size distribution and particle number concentration in real time to confirm the concentration stability of the test article in the chamber.

3.3.2 Off-Line Monitoring

Off-line filter sampling can be used to determine the mass concentration of a nanomaterial or NOAA in the inhalation chamber. For example, MOUDI (micro-orifice uniform deposit impactor) can be used to determine the time-resaved particle size exposure concentration by mass for fiber materials such as CNTs and CNFs. Plus, off-line filter on TEM/SEM grid sampling can be processed using TEM/SEM observation to determine the size and morphology of nanomaterials and NOAAs and using EDX (energy dispersive X-ray analyzer) to analyze the composition. Such filter samples can also be further analyzed to determine the chemical composition and concentration.

3.3.3 Maintenance of Stability

Regulatory test guidelines require regular testing to monitor the stability of the nanomaterial or NOAA concentration in the inhalation chamber during the exposure period, preferably in real time. If the concentration deviates more than 20% during the test period, the stability needs to be improved [7, 8].

3.3.4 Selecting Aerosol Generator for STIS

When selecting an aerosol generator for an STIS, the main considerations include simulating a real exposure situation with a neutralized electrical charge and minimal production of undesirable by-products during the generation process that require dilution

or removal. Moreover, a generator maintenance and risk management plan should be secured to prevent malfunctions, dust explosions, etc. For a description of the types and characteristics of aerosol generators refer to ISO TR 19601 (ISO 2017) [1].

3.3.5 Particle Size Distribution

In the revised OECD inhalation toxicity test guidelines for nanomaterials, the particle size or MMAD (mass median aerodynamic diameter) is up to 2 μm with a geometric standard deviation (GSD) up to 3.

3.4 Applications of STIS

3.4.1 Initial Hazard Evaluation Study to Establish Subacute and Subchronic Inhalation Studies

3.4.1.1 STIS to 28-Day Subacute Inhalation Study of Graphene

A graphene nanoplate STIS was conducted to evaluate the toxicity of graphene nanoplates and as a range-finding study for a subacute inhalation study. The STIS results indicated the minimum toxicity of graphene at a maximum of 3.86 mg/m^3 [19]. Rats were exposed to graphene nanoplates in three concentration groups: control, low (0.68 ± 0.14 mg/m^3), and high (3.86 ± 0.94 mg/m^3) concentrations for 6 h/day for 5 days, followed by recovery for 1, 3, 7, or 28 days. No changes in body or organ weights were observed following the 5-day graphene exposure or during the recovery period. Also, no statistically significant difference was observed in the levels of lactate dehydrogenase, protein, and albumin between the exposed and control groups. However, graphene ingestion by alveolar macrophages was observed in the exposed groups. Thus, the STIS concluded that 5 days of repeated exposure to graphene only had a minimal toxic effect at the concentrations and time points used in the study [19]. A subsequent 28-day subacute inhalation toxicity study of graphene nanoplates was then conducted based on the results of the STIS. Rats were exposed to graphene nanoplates in four concentration groups: fresh air control, low (0.12 mg/m^3), moderate (0.47 mg/m^3), and high (1.88 mg/m^3) concentrations for 28 days (6 h/day, 5 days/week), and then allowed to recover for 1, 28, or 90 days [20]. As a result, no dose-dependent effects were recorded for the body weights, organ weights, bronchoalveolar lavage fluid inflammatory markers, and blood biochemical parameters at 1 day postexposure and 28 days postexposure. The inhaled

graphene was mostly ingested by macrophages. No distinct lung pathology was observed at 1, 28, and 90 days postexposure. The inhaled graphene was translocated to lung lymph nodes. Therefore, the results of the 28-day graphene inhalation study suggested low toxicity and a NOAEL of no less than 1.88 mg/m^3. Therefore, the STIS predicted a similar toxicity evaluation to the subacute inhalation test.

3.4.1.2   STIS to 90-Day Subchronic Inhalation Study of Graphene Oxide

In the graphene oxide STIS, the rats were exposed to a graphene oxide control (fresh air), low (0.76 ± 0.16 mg/m^3), moderate (2.60 ± 0.19 mg/m^3), or high (9.78 ± 0.29 mg/m^3) concentration for 6 h/day for 5 days, followed by recovery for 1, 3, or 21 days. No significant body or organ weight changes were noted after the short-term exposure or during the recovery period. Similarly, no significant systemic effects of toxicological importance were noted in the hematological assays, bronchoalveolar lavage fluid (BAL) inflammatory markers, BAL fluid cytokines, or blood biochemical assays following the graphene oxide exposure or during the postexposure observation period. Moreover, no significant differences were observed in the BAL cell differentials, such as lymphocytes, macrophages, or polymorphonuclear cells. Macrophage-ingested graphene oxide as a spontaneous clearance reaction was observed in the lungs of all the concentration groups from post 1 day to post 21 days. Histopathological examination of the liver and kidneys did not reveal any significant test-article-relevant histopathological lesions. Importantly, similar to previously reported graphene inhalation data, this short-term nose-only inhalation study found only minimal or unnoticeable graphene oxide toxicity in the lungs and other organs [21].

Based on the STIS, a 90-day subchronic inhalation study was conducted using 0 (control), 0.34 ± 0.002 (low), 1.01 ± 0.099 (moderate), and 3.02 ± 0.176 mg/m^3 (high) concentrations. The rats were exposed to the test substance via nose-only inhalation for 6 h a day, 5 days a week for a total of 90 days. Although significant differences were observed in some tests, such as the urinalysis (ketone body and pH), hematology (MPV, RBC, and HCT), and biochemistry (ALP, Cl, IP, and TG), no dose dependency was observed with normal range values. In the histopathological examination, macrophage-ingested graphene oxide was detected in the lungs of the moderate and high concentration groups. This was regarded as a spontaneous and adaptive reaction for pulmonary clearance, and no abnormalities related with pulmonary functions were found. The NOAEL for the subchronic inhalation toxicity study of graphene oxide powder was 3.02 mg/m^3 and no target organs were identified under the present conditions. Thus, both studies showed negative toxicity results for graphene nanomaterials [22]. Consequently, an appropriately conducted STIS can provide valuable initial toxicity evaluation information, as well as concentration ranges for subacute and subchronic studies.

3.4.1.3   STIS as Toxicokinetic Study

The revised OECD TGs 412 (subacute) and 413 (subchronic) require lung bur-
den measurements following exposure and postexposure periods [7, 8] for poorly
soluble particles including nanomaterials. Such lung burden measurements, which
inform on pulmonary deposition and retention of particles in the lungs, need to be
conducted when a range-finding study or other relevant information suggests that
the inhaled test particles are poorly soluble and likely to be retained in the lungs.
Thus, an STIS can be used as a range-finding study for subacute and subchronic
inhalation studies, providing both a concentration setting and initial particle toxico-
kinetic information.

In an STIS, rats were exposed to two sizes of gold nanoparticles (13 and
105 nm), followed by a recovery period of 1, 3, or 28 days. The biodistribution
from the lungs to extrapulmonary organs and the toxicokinetics were investi-
gated. The biodistribution of gold nanoparticles from the lungs to secondary target
organs was significantly higher with the small gold nanoparticles than with the
large gold nanoparticles. While the large gold nanoparticles were only found in
the blood, the small gold nanoparticles were detected in the liver, spleen, brain,
testes, and blood. In addition, the elimination half-life of the small gold nanopar-
ticles ($t_{1/2}$ = 44.5 days) from the lungs was significantly shorter than that of the
large gold nanoparticles ($t_{1/2}$ = 179.5 days), as shown in Table 3.3 [17]. Since the
STIS included three postexposure observation time points, this facilitated a toxi-
cokinetic analysis followed by lung burden measurements. An STIS can also be
used to study the extrapulmonary translocation of nanoparticles to other organs.
While a sufficient number of male and female animals is preferable, an appro-
priately designed STIS with fewer animals can be used as a range-finding study
and provide valuable information for designing further subacute and subchronic
inhalation studies. Finally, the tissue distribution of gold nanoparticles in the STIS
corresponded with the results of a previous 90-day subchronic inhalation toxicity
study of gold nanoparticles based on OECD TG 413 [24]. Therefore, this confirms
that an STIS can be effective for providing toxicokinetics to predict the outcomes
of subchronic exposure.

Table 3.3 Non-compartmental pharmacokinetic parameters of gold nanoparticle clearance during
28-day recovery period in lungs of rats (Table 3 of [23])

Particle size	$t_{1/2}$ (day)	C_{max} (ng/g)	AUC_{all} (ng day/g)	AUC_{inf} (ng day/g)	MRT_{all} (day)	MRT_{inf} (day)
13 nm	44.5	830.1	19416.5	55539.4	11.9	64.2
105 nm	179.5	430.4	10523.1	105678.5	13.7	259.7

AUC area under curve, *AUC_{inf}* infinite area under curve, *MRT* mean residence time, *MRT_{inf}* infinite
mean residence time

3.5   Conclusions

A short-term inhalation study (STIS) can substitute for acute inhalation toxicity testing, which sometimes use unrealistic nanomaterial concentrations that can affect the appropriate nanoparticle size distribution as required by regulatory testing guidelines. Essentially, an STIS can lay the foundation for designing inhalation studies from short-term to subacute and subchronic, including such design considerations as the particle dosimetry reflecting the exposure characteristics, frequency, and concentrations experienced by consumers and workers. The STIS can be used to characterize the nanoparticle physicochemical properties and determine the type of exposure and particle monitoring methods in the inhalation chamber. Plus, importantly, the particle generation method and particle concentration stability can be studied before and during the STIS. Thus, an STIS provides an initial hazard evaluation for subsequent subacute and subchronic inhalation studies, as seen in the example studies of graphene and graphene oxide. Furthermore, combining an STIS with a lung burden analysis can provide toxicokinetic information, including the biodistribution and lung clearance of nanoparticles.

References

1. ISO/TR 19601. Nanotechnologies—Aerosol generation for Nano-objects and their aggregates and agglomerates (NOAA) air exposure studies. Geneva: ISO; 2017.
2. OECD. OECD guidelines for testing of chemicals, Test Guideline (TG) 403. Acute Inhalation Toxicity. Paris: OECD; 2009.
3. OECD. OECD guidelines for testing of chemicals, Test Guideline (TG) 433. Acute inhalation toxicity: Fixed concentration procedure. Paris: OECD; 2017.
4. OECD. OECD guidelines for testing of chemicals, Test Guideline (TG) 436. Acute Inhalation Toxicity—Acute Toxic Class Method. Paris: OECD; 2009.
5. OECD. OECD guidelines for testing of chemicals, Test Guideline (TG) 412. Subacute Inhalation Toxicity: 28-Day Study. Paris: OECD; 2009.
6. OECD. OECD guidelines for testing of chemicals, Test Guideline (TG) 413. Subchronic Inhalation Toxicity: 90-day Study. Paris: OECD; 2009.
7. OECD. OECD guidelines for testing of chemicals, Test Guideline (TG) 412. Subacute Inhalation Toxicity: 28-Day Study, vol. 201. Paris: OECD.
8. OECD. OECD guidelines for testing of chemicals, Test Guideline (TG) 413. Subchronic Inhalation Toxicity: 90-day Study. Paris: OECD; 2018.
9. Ma-Hock L, Burkhardt S, Strauss V, Gamer AO, Wiench K, van Ravenzwaay B, Landsiedel R. Development of a short-term inhalation test in the rat using nano-titanium dioxide as a model substance. Inhal Toxicol. 2009;21:102–18.

10. OECD. A steering group 7 case-study for hazard identification of inhaled nanomaterials: An integrated approach with short-term inhalation studies. ENV/CHEM/NANO(2011)6/REV1. Paris: OECD; 2013.
11. OECD. Guidance document on acute inhalation toxicity testing, series on testing and assessment No. 39, ENV/JM/MONO(2009)28/REV1. 2nd ed. Paris: OECD; 2018.
12. UN. United Nations Globally Harmonized System of Classification and Labelling of Chemicals (GHS), ST/SG/AC.10/30, New York: UN; 2017. Available: https://www.unece.org/trans/danger/publi/ghs/ghs_rev07/07files_e0.html
13. Ahn K, Ensor D, Shama M, Ostraat M, Ramsden J, Kanno J, Ghazi-Khansari M, Lazos R, Gulumian M, Cassee FR, De Jong WH, Jeon K, Yu IJ. Development of International Standard on Nano Aerosol Generation for Inhalation Toxicology Study. Toxicol Open Access. 2017;3(2) https://doi.org/10.4172/2476-2067.10.
14. ISO/TR 13014. Nanotechnologies—Guidance on physico-chemical characterization of engineered nanoscale materials for toxicologic assessment. Geneva: ISO; 2012.
15. ISO 29701. Nanotechnologies—endotoxin test on nanomaterial samples for in vitro systems—Limulus amebocyte lysate (LAL) test. Geneva: ISO; 2010.
16. Ech RK, Han L, Ensor DS, Foarde KK. Endotoxin contamination of engineered nanomaterials. Nanotoxicology. 2009;4(1):73–83.
17. Schindler S, von Aulock S, Daneshian M, Hartung T. Development, validation and applications of the monocyte activation test for pyrogens based on human whole blood. ALTEX. 2009;26(4):265–77.
18. Lee JH, Kwan M, Ji JH, Kang CS, Ahn KH, Han JH, Yu IJ. Exposure assessment of workplace manufacturing nanosized TiO2 and silver. Inhal Toxicol. 2011;23(4):226–36.
19. Shin JH, Han SG, Kim JK, Kim BW, Hwang JH, Lee JS, Lee JH, Baek JE, Kim TG, Kim KS, Lee HS, Song NW, Ahn K, Yu IJ. 5-Day repeated inhalation of 28-day post-exposure study of graphene. Nanotoxicology. 2015;9(8):1023–31. https://doi.org/10.3109/17435390.2014.998306.
20. Kim JK, Shin JH, Lee JS, Hwang JH, Lee JH, Baek JE, Kim TG, Kim BW, Kim JS, Lee GH, Ahn K, Han SG, Bello D, Yu IJ. 28-Day inhalation toxicity of graphene nanoplates in sprague-dawley rats. Nanotoxicology. 2016;10(7):891–901. https://doi.org/10.3109/17435390.2015.1133865.
21. Kim YH, Jo MS, Kim JK, Shin JH, Baek JE, Park HS, An HJ, Lee JS, Kim BW, Kim HP, Ahn KH, Jeon K, Oh SM, Lee JH, Workman T, Faustman EM, Yu IJ. Short-term inhalation study of graphene oxide nanoplates. Nanotoxicology. 2018;12(3):224–38. https://doi.org/10.1080/17435390.2018.1431318.
22. An K, Lee S, Sung J, Kim H, Lee J, Song K. A 90-day subchronic inhalation toxicity study of graphene oxide powder in F344 rats. Toxicologist. 2017;150(1):2727.
23. Han SG, Lee JS, Ahn K, Kim YS, Kim JK, Lee JH, Shin JH, Jeon KS, Cho WS. Size-dependent clearance of gold nanoparticles from lungs of Sprague-Dawley rats after short-term inhalation exposure. Arch Toxicol. 2015;89(7):1083–94. https://doi.org/10.1007/s00204-014-1292-9.
24. Sung JH, Ji JH, Park JD, Song MY, Song KS, Ryu HR, Yoon JU, Jeon KS, Jeong J, Han BS, Chung YH, Chang HK, Lee JH, Kim DW, Kelman BJ, Yu IJ. Subchronic inhalation toxicity of gold nanoparticles. Part Fibre Toxicol. 2011;8:16.

Chapter 4
Subchronic Inhalation Toxicity Study with a Vapor-Grown Carbon Nanofiber in Male and Female Rats (OECD 413): Does Nanofiber Exposure Have Adverse Impacts on the Cardiovascular System?

David B. Warheit

Abstract The objective of this 90-day inhalation toxicity study in male/female rats exposed to vapor-grown carbon nanofibers (CNF) was to assess both the lung toxicity and systemic (cardiovascular) effects following exposures to 0, 0.54, 2.5, or 25 mg/m^3. From a respiratory tract standpoint, there was some minor histopathological, cell proliferative, and inflammatory effects at the highest concentration—25 mg/m^3. In addition, there was some evidence that aerosol exposures at the highest concentration (25 mg/m^3) resulted in a minimal translocation of the inhaled nanofibers from the respiratory tract to systemic extrapulmonary sites in the body. This finding led to the hypothesis that the movement of inhaled fibers into the systemic bloodstream could facilitate a cross-talk relationship between the respiratory tract and cardiovascular effects, thus impacting blood coagulation effects. Accordingly, common cardiovascular/coagulation indices were measured—including cardiomyocyte proliferation parameters; systemic inflammation indices—such as C-reactive protein and four different coagulation parameters: (1) fibrinogen levels; (2) platelet counts; (3) PT; and (4) aPTT bleeding times. The results demonstrated no significant differences were measured between air and high dose, CNF-exposed rats. It was concluded that no apparent cross-talk was demonstrated between local respiratory and systemic/cardiovascular endpoints. Based upon the data generated in this 90-day, subchronic inhalation study, it seems likely that the pulmonary toxicity endpoints of this study would be useful in accurately predicting lung inflammatory outcomes in a shorter-term inhalation study. However, the pulmonary histopathology and cardiovascular endpoints described in this study likely require the subchronic inhalation testing exposure protocol.

D. B. Warheit (✉)
Warheit Scientific LLC, Wilmington, Delaware, USA

4.1   Introduction

Carbon nanofibers are commercial products which are known to enhance thermal properties of high performance materials. They are utilized in filter applications and enhance performances of fuel cells and batteries. Although these materials arise from the same chemical family of carbon allotropes or other nanostructured materials, they are fundamentally different from other carbon-based nanomaterials, such as single-walled and multiwalled carbon nanotubes. These physicochemical differences are evident as carbon nanofibers have measured specific surface area metrics of ~14 m^2/g—while single-walled and multiwalled carbon nanotubes have substantially greater surface areas, which are known to exceed 200 m^2/g. In addition, multiwalled and single-walled carbon nanotubes have significantly greater aspect ratios—(length to diameter) ratios when compared to carbon nanofibers. Finally, single-walled and multiwalled carbon nanotubes are known to contain much greater metal catalyst residues (as part of their syntheses) when compared to carbon nanofibers. The addition of metal catalysts is likely to increase the in vivo generation of reactive oxygen species (ROS) leading to pulmonary inflammatory effects following deposition in the distal lung.

The aim of this subchronic inhalation toxicity study was to (1) evaluate the toxicity of aerosols of carbon nanofibers in male and female rats following subchronic, 90-day exposures. These procedures included sensitive investigations of bronchoalveolar endpoints (i.e., cell numbers, inflammation, cell injury) 1 day following 90-day exposures. Additional investigations were comprised of standardized toxicological parameters, cell proliferation methodologies, and standard histopathological/morphological assessments of the respiratory tract and the major systemic organs. In addition, after determining that some fibers had translocated from the respiratory tract compartment to the systemic circulation (at the highest exposure concentration—25 mg/m^3), it was postulated that the inhaled fibers might adversely impact selected cardiovascular and vascular parameters—such as systemic inflammation (as measured by C-reactive protein); coagulation parameters utilized in routine diagnostic procedures—such as fibrinogen levels platelet counts, PT and aPTT bleeding times; and cardiomyocyte cell proliferation. Thus, these cardiovascular parameters were investigated.

4.2   Methods

For the experimental protocol, four groups per sex of rats were exposed by nose-only inhalation exposure for 6 h/day; 5 days/week to target concentrations of 0, 0.50, 2.5, or 25 mg/m^3 vapor-grown carbon nanofibers over a 90-day exposure

period and pulmonary endpoints assessed 24 h after the end of exposures. An additional postexposure period of 3 months was added to the protocol in order to gauge any potential reversibility effects measured in the high dose exposed vs. control animals. Lung evaluations included traditional toxicological/clinical and histopathological investigations, as well as bronchoalveolar lavage fluid (BALF) analysis, and cell proliferation (CP) indices of various pulmonary anatomical subcompartments including the airway—terminal bronchiole (TB), lung parenchymal—alveolar duct (AD) and distal lung—subpleural regions of the respiratory tract. An additional postexposure period of 3 months in the experimental protocol for the high dose and control animals was also implemented to determine whether any measured effects were sustained or reversible.

4.3   Results

Aerosol concentrations of 0.54 (4.9 f/cc), 2.5 (56 f/cc), or 25 (252 f/cc) mg/m^3 of VGCF-H carbon nanofibers (see Figs. 4.1 and 4.2) resulted in concentrated-related small, detectable accumulation of extrapulmonary fibers with no adverse tissue
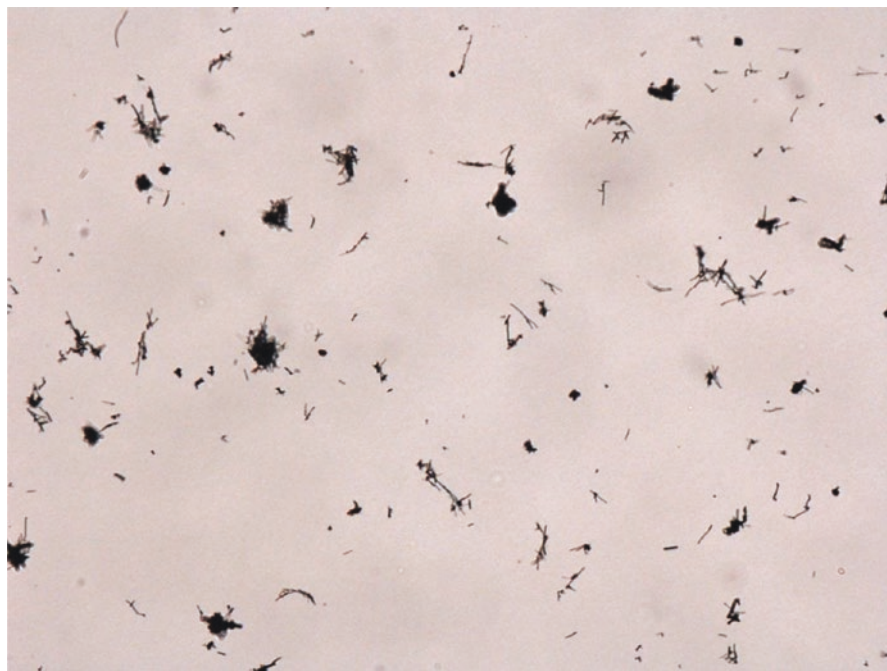
Fig. 4.1 Low magnification light micrograph of a filter used for counting aerosolized CNFs. Note that some of the carbon nanofibers are agglomerated following aerosolization

Fig. 4.2 Transmission electron micrograph of aerosolized carbon nanofibers caught on a filter
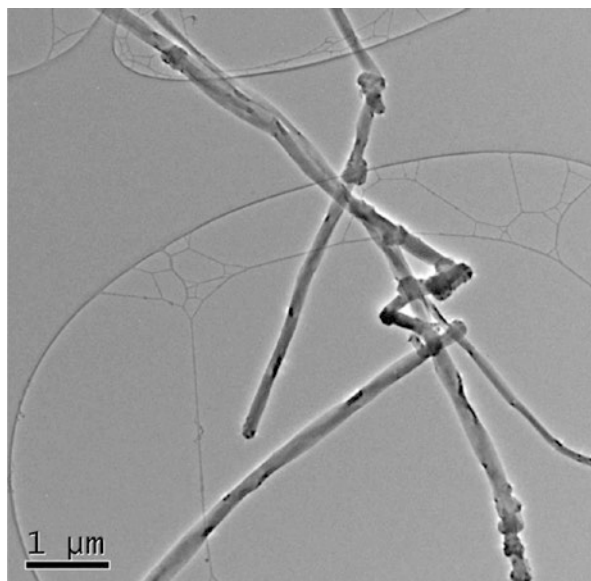
### Incidences of Extrapulmonary Fiber Deposition (Preliminary Findings)

	Male		Female	
Dose (mg/m^3)	0	25	0	25
No. examined	10	10	10	10
Brain (choroid plexus)	0	2	0	2
Heart	0	2	0	1
Kidneys	0	10	0	10
Liver	0	9	0	10
Nose	0	1	0	0
Spleen	0	10	0	7

Fibers also noted in some mediastinal lymph nodes (a non-protocol tissue)

Fig. 4.3 Incidences of extrapulmonary fiber deposition following a 4 week exposure period to carbon nanofibers at 25 mg/m^3

effects (see Fig. 4.3). At the two highest concentrations, some inflammation of the terminal bronchiole and alveolar duct regions of the respiratory tract was described in anatomical locations wherein fiber-laden alveolar macrophages had migrated and accumulated.

These observations were characterized morphologically by minimal pulmonary inflammation concomitant with some minor interstitial thickening, and
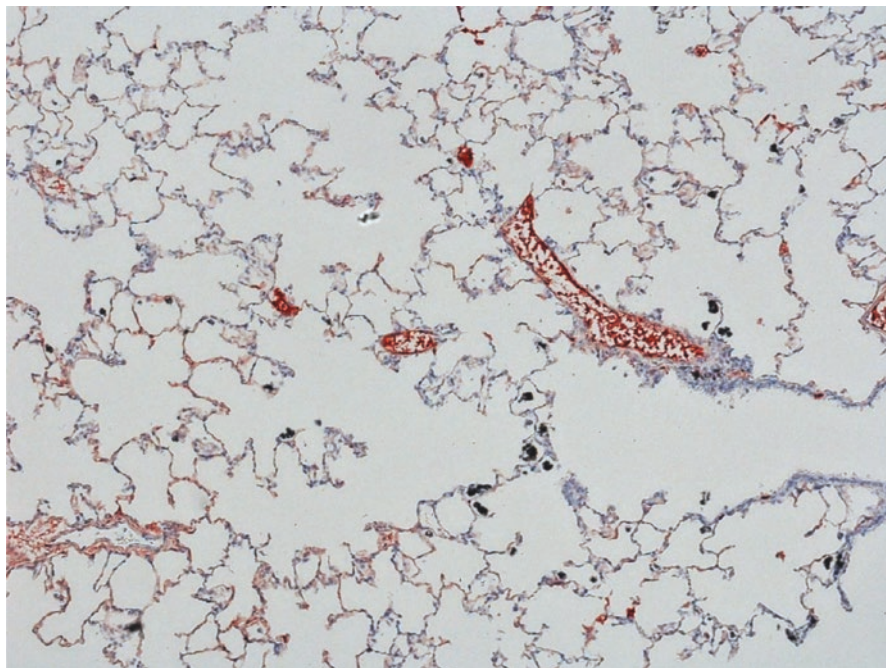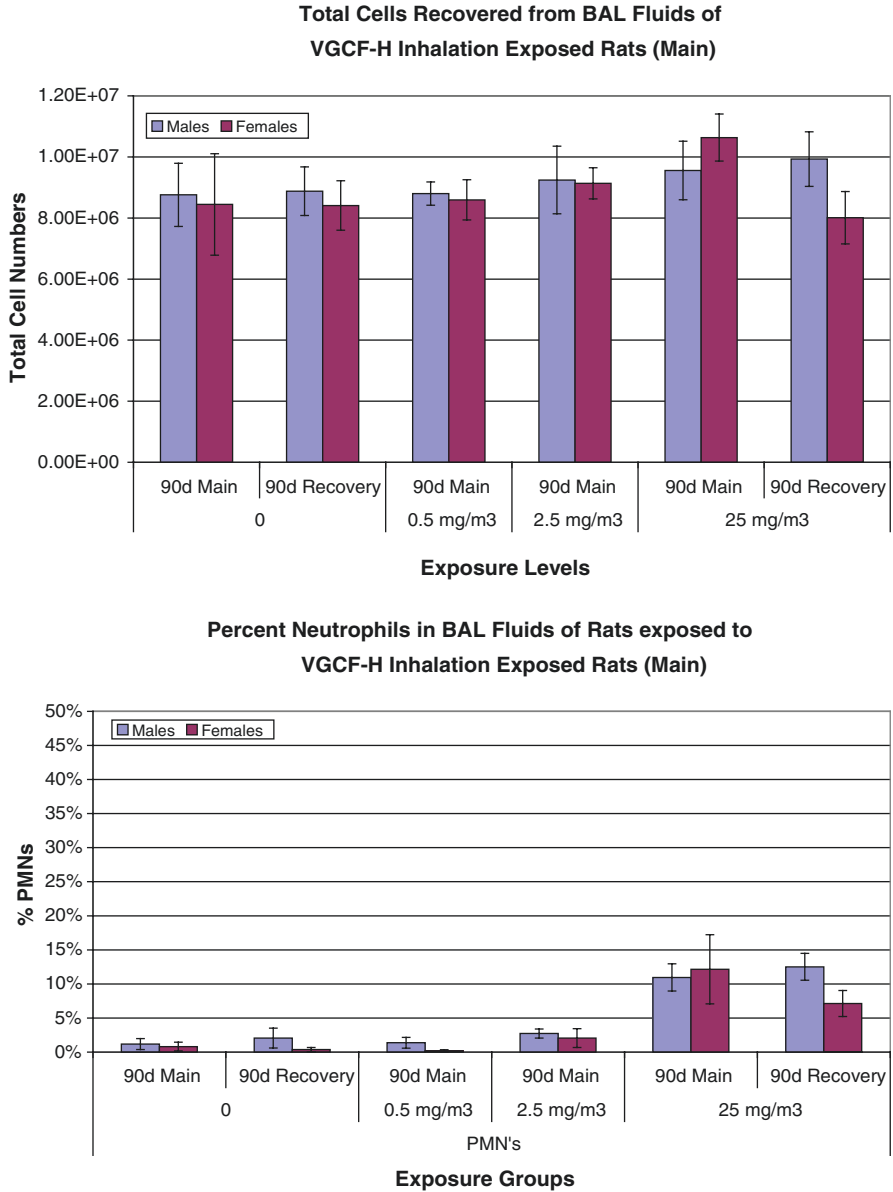
Fig. 4.4 A lung tissue section from a male rat exposed to 25 mg/m^3 CNF for 90 days. Note the sporadic areas of macrophage accumulation and the slight tissue thickening in distal lung—alveolar regions

corresponding slight hypertrophy/hyperplasia of type II alveolar epithelial cells—at the highest tested aerosol concentration, i.e., 25 mg/m^3 (Fig. 4.4). At 90 days post-exposure, the lung inflammatory response at 25 mg/m^3 was decreased (Figs. 4.5 and 4.6). It was noteworthy that no adverse pulmonary effects were measured or observed at the lowest exposure concentration, 0.54 mg/m^3. Increases in bronchoalveolar lavage and cell proliferation endpoint increases vs. unexposed controls were evident at the highest exposure concentration, i.e., 25 mg/m^3 of carbon nanofibers when compared to air-exposed control values; however, it was noteworthy that the low and medium exposure levels of carbon nanofibers did not produce significant differences from control values at either 0.54 or 2.5 mg/m^3 (Figs. 4.6 and 4.7). After 90 days PE, bronchoalveolar lavage biomarkers were still increased at 25 mg/m^3 carbon nanofibers but had somewhat recovered (Figs. 4.6 and 4.7).

Based upon histopathology/morphological observations of minor effects measured at 2.5 mg/m^3, the no adverse effect level (NOAEL) was set at the lowest exposure concentration, 0.54 mg/m^3, due to the finding of minimal cellular inflammation in the small airways terminal bronchiole and alveolar parenchyma—as noted by the pathologist on the study. Moreover, the highest exposure level of inhaled carbon nanofibers (i.e., 25 mg/m^3) produced "slight" pulmonary inflammation and occasional interstitial thickening. However, it is meaningful that none of the biochemical
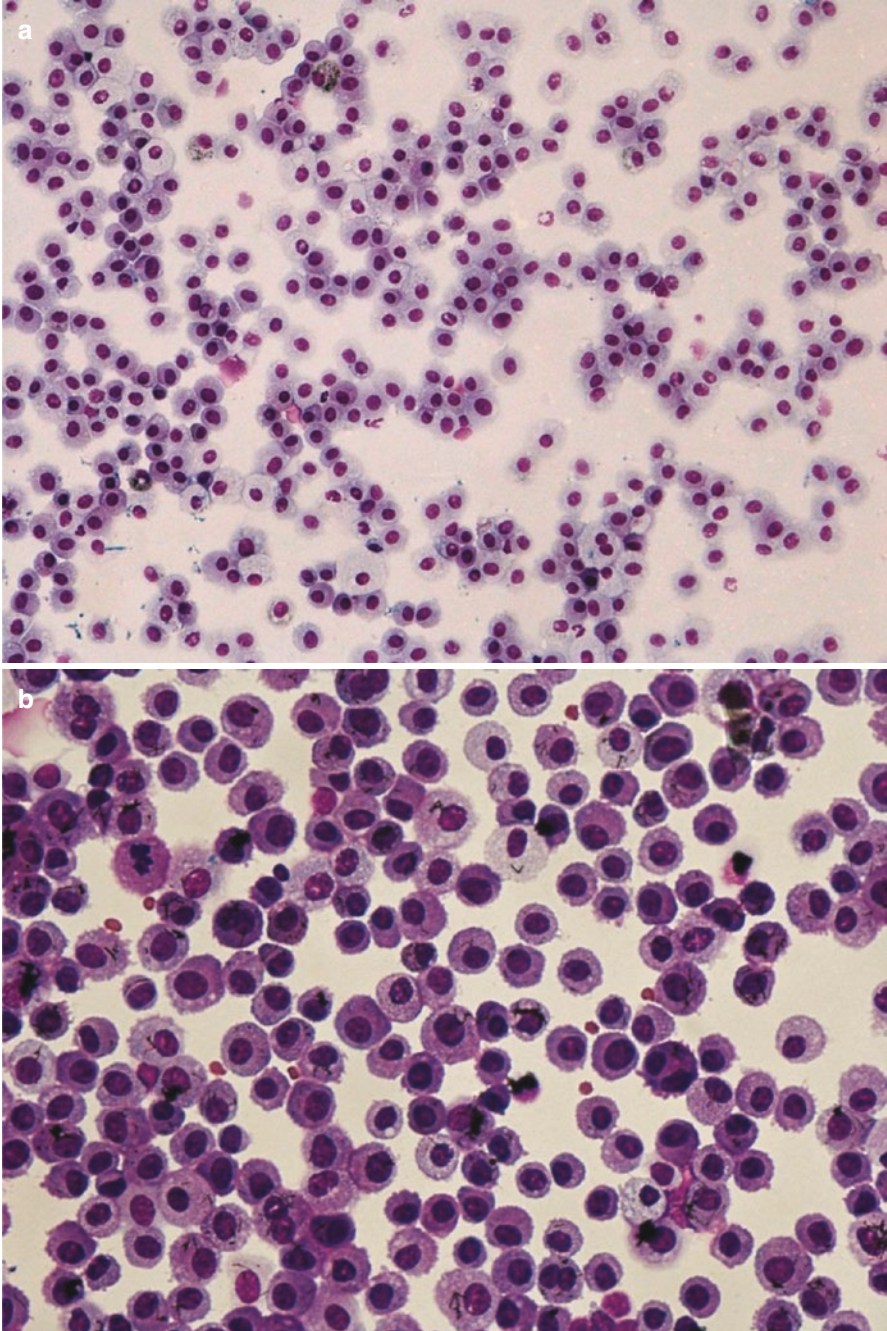
Fig. 4.5 (**a**, **b**) Cytocentrifuge preparations of lung cells recovered by bronchoalveolar lavage. (**a**) Represents a lower magnification micrograph of cells recovered from an air-exposed control rat (20× magnification). (**b**) Demonstrates a high magnification of a micrograph recovered from a rat exposed to 0.5 mg/m³ CNF. Note the lack of neutrophilic inflammation following 90 days of inhalation exposure

Total Cells Recovered from BAL Fluids of
VGCF-H Inhalation Exposed Rats (Main)

Percent Neutrophils in BAL Fluids of Rats exposed to
VGCF-H Inhalation Exposed Rats (Main)

Fig. 4.6 Pulmonary inflammation in CNF-exposed rats and controls as evidenced by the percentages of neutrophils in BAL fluids following 90 days of exposure. Only exposures to 25 mg/m³ produced sustained pulmonary inflammatory responses of 11–12% neutrophils. $^*p < 0.05$
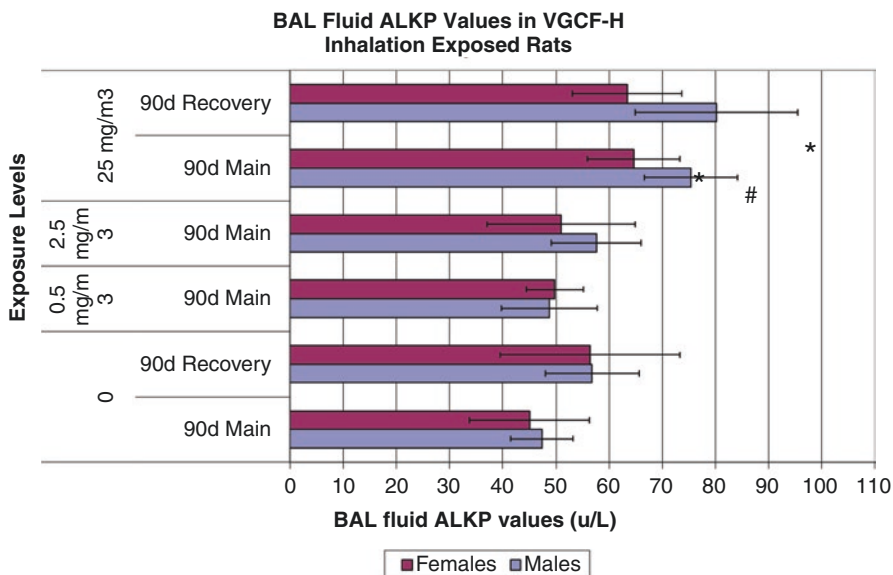
Fig. 4.7 BAL fluid alkaline phosphatase values for CNF-exposed rats and corresponding controls following 90-day inhalation exposures to particulates. BAL fluid alkaline phosphatase was an indicator of Type II cell cytotoxicity. Only exposures to 25 mg/m³ produced sustained pulmonary cytotoxicity responses. $^*p < 0.05$

findings of the more sensitive lung bronchoalveolar or cell proliferative biomarkers/ indices at the exposure level of 2.5 mg/m³ were significantly different from air-exposed control rats (i.e., 0 mg/m³). It has been previously suggested that more comprehensive criteria and guidance measure be formulated to achieve more consistent methodologies for setting no adverse effect level (NOAEL) criteria. Indeed, it has been advocated that a weight of evidence (WOE) approach would represent an advanced procedure for developing no adverse effect levels. This is in part due, on the one hand, to the sensitivity of some of the measured parameters; vs. the alternative—as the traditional approach of simply noting a single statistically different effect from controls in setting a NOAEL (without determining physiological relevance)—and recognizing that some findings may be interpreted as normal physiological adaptations to longer term particle exposures (an example would be normal macrophage phagocytic responses and minimal pulmonary inflammation responses).

Evaluations of cardiovascular endpoints such as cardiomyocytes cell proliferation and histopathology (not presented), C-reactive protein levels (Fig. 4.8); and four different diagnostic coagulation parameters—including—activated partial thromboplastin time (aPTT—Fig. 4.9); Blood fibrinogen levels (Fig. 4.10) and prothrombin time (PT) values (Fig. 4.11) were investigated. No significant differences were measured when comparing air-exposed vs. carbon nanofiber-exposed rats. It was concluded that no apparent cross-talk was evident between local respiratory and systemic/cardiovascular compartments.

**Blood C-reactive protein (CRP) Levels
in VGCF-H Exposed Rats**
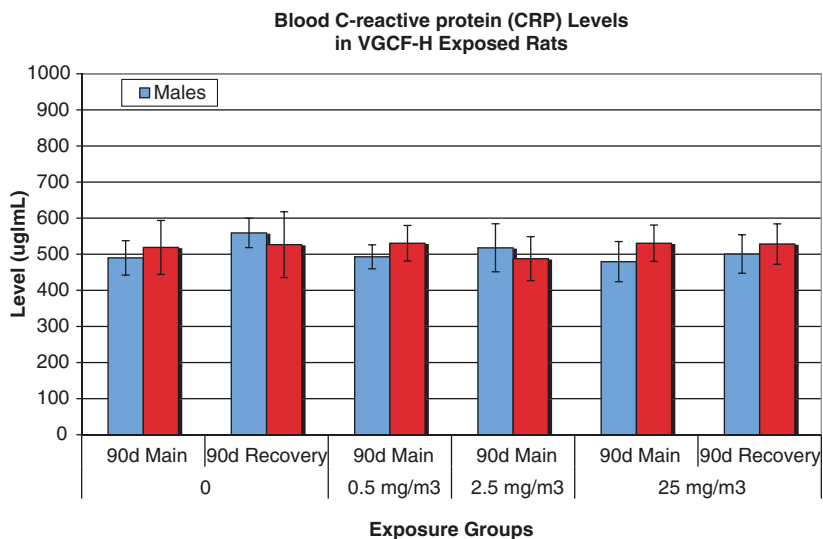
Fig. 4.8 Blood C-reactive protein (CRP) levels in carbon nanofiber-exposed rats. Blood C-reactive protein levels for rats exposed for 90 days to 0.54, 2.5, or 25 mg/m^3 carbon nanofibers. In addition, rats exposed to 25 mg/m^3 and air-exposed control CRP values were also measured after 3 months of recovery. Values given are means ± S.D. No significant increases in CRP values, as indicators of systemic inflammation, were measured among the groups at any time point

**Activated Partial Thromboplastin
Time (aPTT)
Values in VGCF-H Exposed Rats**
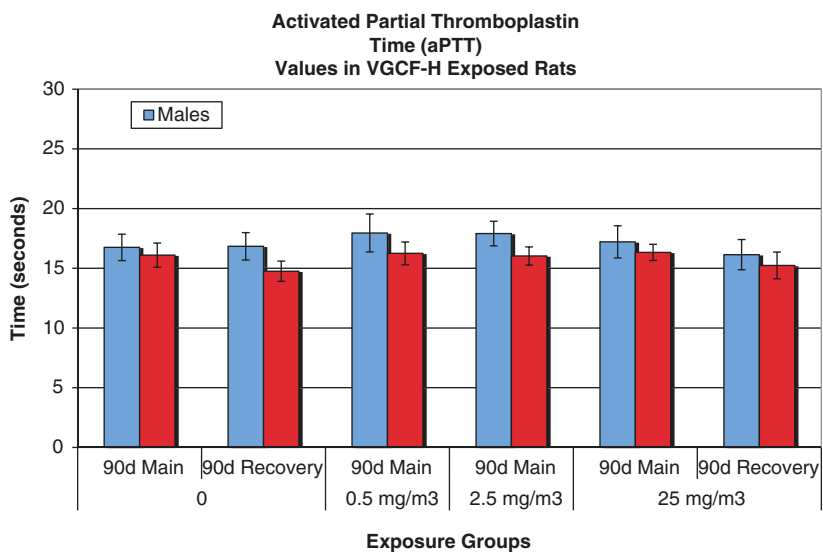
Fig. 4.9 Vascular activated partial thromboplastin time (aPTT) values in carbon nanofiber-exposed rats. Activated partial thromboplastin times (aPTTs) for rats exposed for 90 days to 0.54, 2.5, or 25 mg/m^3 carbon nanofibers. In addition, rats exposed to 25 mg/m^3 and air-exposed control aPTT values were also measured after 3 months of recovery. Values given are means ± S.D. No significant effects, i.e., no shortening, in aPTT were measured among the groups at any time point

**Blood Fibrinogen Levels
in VGCF-H Exposed Rats**
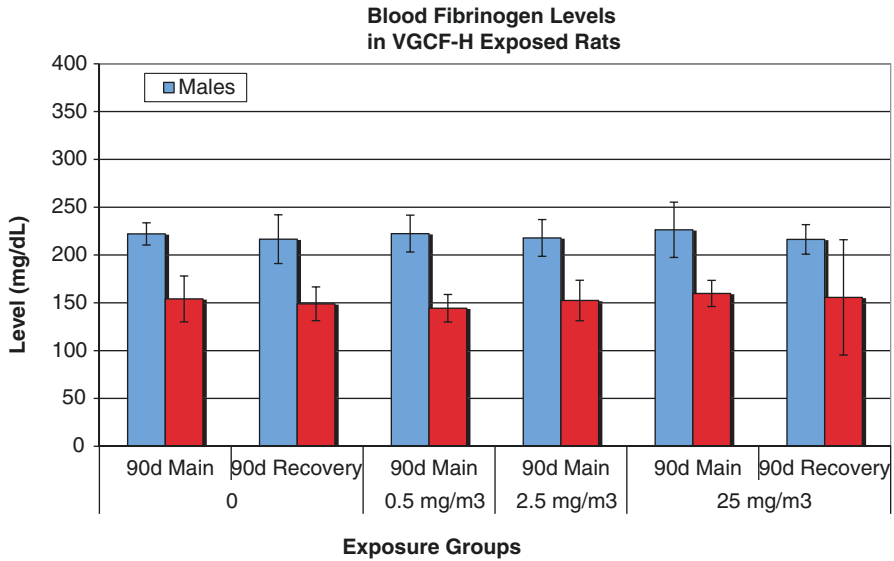
Fig. 4.10 Blood fibrinogen levels in carbon nanofiber-exposed rats. Blood fibrinogen levels for rats exposed for 90 days to 0.54, 2.5, or 25 mg/m^3 carbon nanofibers. In addition, rats exposed to 25 mg/m^3 and air-exposed control fibrinogen values were also measured after 3 months of recovery. Values given are means ± S.D. No significant alterations in fibrinogen values, i.e., whether increased or reduced, were measured among the groups at any time point

**Prothrombin Time (PT) Values
in VGCF-H Exposed Rats**
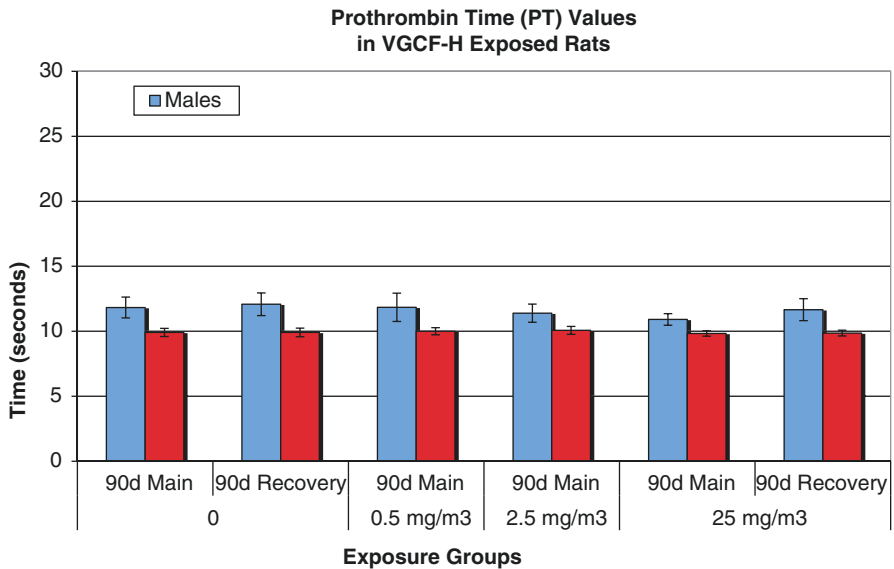
Fig. 4.11 Vascular prothrombin time (PT) values in carbon nanofiber-exposed rats. Blood prothrombin times (PTs) for rats exposed for 90 days to 0.54, 2.5, or 25 mg/m^3 carbon nanofibers. In addition, rats exposed to 25 mg/m^3 and air-exposed control PT values were also measured after 3 months of recovery. Values given are means ± S.D. No significant effects, i.e., no shortening, in prothrombin time values were measured among the groups at any time point

4.4   Discussion and Conclusions

The findings of previously conducted inhalation studies with multiwall carbon nanotubes reported that subchronic, 90-day MWCNT exposures produced significant toxicity in the lungs of rodents at relatively low exposure concentrations. Ma-Hock et al. [1] published the findings of a subchronic inhalation study in rats with Nanocyl® NC 7000 MWCNT containing 10% metal oxide catalysts. The dimensions of the multiwall carbon nanotubes ranged from 5 to 15 nm in diameter and 0.1 to 10 μm in lengths, with BET surface area metrics of 250–300 m^2/g. Similarly, exposures to 0, 0.1, 0.5, or 2.5 mg/m^3 MWCNT in rats produced no extrapulmonary systemic toxicity, yet adverse effects in the respiratory tract included enhanced lung weights in exposed groups versus the controls, consistent with moderate granulomatous and neutrophilic inflammation, alveolar lipoproteinosis in lungs and lymph nodes at 0.5 and 2.5 mg/m^3 MWCNT. Moreover, minimal granulomatous lung inflammation was measured at exposure concentrations as low as 0.1 mg/m^3. As a result, no adverse effect level could be established by these investigators. Pauluhn published a 90-day inhalation toxicity study in rats with a different form of multiwall carbon nanotube test material, i.e., MWCNT-Baytubes® at exposure concentrations of 0, 0.1, 0.4, 1.5, or 6.0 mg/m^3. The physicochemical characteristics of the Baytube/MWCNT composition was reported to be ~99% C, 1% O_2, and 0.46% Co. The mean tube lengths were reported to be 200–300 nm (by TEM), and the BET (Brunauer–Emmett–Teller method) surface area was ~255 m^2/g. Lower respiratory tract lesions were characterized morphologically as cellular inflammation and interstitial collagen staining at the 0.4, 1.5, and 6.0 mg/m^3 exposure levels. The NOAEL was determined to be 0.1 mg/m^3 [2]. Morimoto et al. [3] conducted a 4-week inhalation exposure to assess the pulmonary toxicity of well-dispersed Nikkiso Co. MWCNT in rats after 4-week inhalation (single exposure concentration of 0.37 mg/m^3), also employing intratracheal instillation exposures. The MWCNT test samples were dispersed in a solution and then generated as aerosols, or alternatively intratracheally instilled into the lungs of rats (at doses of 0.1 or 0.2 mg). Physicochemical characteristics of the MWCNT were reported as mean diameter = 44 nm; length = 1.1 μm; BET surface area = 69 m^2/g. Intratracheal instillation exposures of MWCNT resulted in lung inflammatory responses (persistent in the high dose group) concomitant with small granulomatous lesions. Morimoto and colleagues concluded that intratracheal instillation exposures produced *greater* pulmonary inflammatory effects when compared with inhalation exposures. In summary, it seems clear that the results of the three subchronic multiwall carbon nanotubes inhalation studies clearly demonstrated the greater hazard potency of the various MWCNT samples tested, when compared with the subchronic inhalation toxicity studies with carbon nanofibers.

When compared with MWCNT, subchronic 90-day CNF inhalation exposures in male and female rats generally resulted in relatively mild adverse responses in the respiratory tracts of rats. Indeed, these effects appeared to be more benign when compared with inhalation exposures to the aforementioned MWCNT test substances [1, 2, 4, 5]. Exposures to the highest aerosol concentration, 25 mg/m^3 CNF produced low level, but sustained lung inflammatory and cytotoxic responses, as measured by

bronchoalveolar lavage methods—and consistent with enhanced cell proliferation indices in the terminal airways, lung parenchymal and subpleural regions of the distal respiratory tract. These findings were supported by the histopathological observations indicating slight levels of lung inflammatory responses, concomitant with (slight) occasional thickening of interstitial compartments. However, it should be noted that there was a lack of concurrence between the morphological observation of minimal pulmonary inflammation at 2.5 mg/m³ CNF and the other biochemical lung fluid data inputs generated in this study including the lung weight, BALF inflammation and cytotoxicity and cell proliferation findings. In establishing a no adverse effect level for this study, the convention often utilized is to ascribe the lowest effect level to a single endpoint value. Accordingly, it seemed likely that the histopathology morphological observations of "minimal inflammation" served to outweigh all of the other quantitative, more sensitive measurements, for assessing the adverse exposure effect level of the study. However, the morphological findings at the 2.5 mg/m³ concentration were rather subjective in nature, and was not consistent with the other objective biochemical and cell turnover data associated lung inflammation, cytotoxic effects, and cell proliferation indices for that exposure concentration groups of animals. Accordingly, for future studies, we have recommended that there should be a wide-ranging discussion and reconsideration of guidance criteria for determining NOAELs. This should include an assessment of all of the data components generated in a particular study. To be sure, a morphological determination of "minimal lung inflammation" should not outweigh the bronchoalveolar lavage endpoints of inflammation and cytotoxicity, or the cell turnover endpoints in selected compartments of the respiratory tract.

Thus, the following criteria should be considered for interpreting the findings of study results and setting NOAELs in subchronic particulate studies:

(a) Better assessments and comprehension of the adaptive, physiologically relevant responses in the lung following particulate exposures in longer-term studies.
(b) More focused attention to the integrated evaluation of all study endpoints in determining no adverse effect levels—with equivalent weight placed on functional/mechanistic, and objective criterial—in addition to morphological endpoints.

When considering the utility of conducting shorter-term inhalation tests, it seems likely that 2-week inhalation exposure testing might reasonably predict similar profiles of CNF-induced lung inflammatory responses—as evidenced in the 90-day study. This could serve as a useful screen for the subchronic inhalation toxicity study with carbon nanofibers. The lung histopathological endpoints would likely require a longer-term study. Moreover, the cardiovascular endpoints measured in this study are better suited to a subchronic inhalation exposure.

References

1. Ma-Hock L, Treumann S, Strauss V, Brill S, Luizi F, Mertler M, Wiench K, Gamer AO, van Ravenzwaay B, Landsiedel R. Inhalation toxicity of multiwall carbon nanotubes in rats exposed for 3 months. Toxicol Sci. 2009;112:468–81.
2. Pauluhn J. Subchronic 13-week inhalation exposure of rats to multiwalled carbon nanotubes: toxic effects are determined by density of agglomerate structures, not fibrillar structures. Toxicol Sci. 2010;113:226–42.
3. Morimoto Y, Hirohashi M, Ogami A, Oyabu T, Myojo T, Todoroki M, Yamamoto M, Hashiba M, Mizuguchi Y, Lee BW, Kuroda E, Shimada M, Wang WN, Yamamoto K, Fujita K, Endoh S, Uchida K, Kobayashi N, Mizuno K, Inada M, Tao H, Nakazato T, Nakanishi J, Tanaka I. Pulmonary toxicity of well-dispersed multi-wall carbon nanotubes following inhalation and intratracheal instillation. Nanotoxicology. 2012;6:587–99.
4. DeLorme MP, Muro Y, Arai T, Banas DA, Frame SR, Reed KL, Warheit DB. Ninety-day inhalation toxicity study with a vapor grown carbon nanofiber in rats. Toxicol Sci. 2012;128(2):449–60.
5. Warheit DB, DeLorme MP. CNT biopersistence and the fibre paradigm. In: Donaldson K, Poland C, Duffin R, Bonner J, editors. The toxicology of carbon nanotubes. New York: Cambridge University Press; 2012.

Part II
Intratracheal Administration Study

Chapter 5
Comparison of Responses in Rat Lung Following Inhalation and Intratracheal Administration of Nanoparticles

Yukiko Yoshiura, Yuri Fujisawa, Taisuke Tomonaga, Hiroto Izumi, Takako Oyabu, Toshihiko Myojo, Masaru Kubo, Manabu Shimada, and Yasuo Morimoto

Abstract We compared the concentration of total protein in bronchoalveolar lavage fluid (BALF) exposed to four types of nanomaterials in an inhalation study and in an intratracheal instillation study in order to examine whether the ranking of the harmful effect of nanomaterials following intratracheal instillation accorded with the ranking following inhalation. We used nickel oxide (NiO) nanoparticles and cerium dioxide (CeO_2) nanoparticles as high toxicity nanomaterials, and titanium dioxide (TiO_2) and zinc oxide (ZnO) nanoparticles as low toxicity nanomaterials. In the inhalation study, rats were exposed to approximately 2 mg/m^3 of four nanomaterials for 4 weeks, and the total protein concentrations in the bronchoalveolar lavage fluid (BALF) were examined from 3 days to 3 months after the end of exposure as the endpoint of pulmonary toxicity. In the intratracheal instillation study, rats were exposed to 0.2 or 1 mg of four nanomaterials, and, with the same endpoint, the BALF was analyzed from 3 days to 6 months after the exposure. The inhalation of NiO and CeO_2, the high toxicity nanomaterials, induced a significant amount of total protein in the BALF, while the inhalation of ZnO and TiO_2, the low toxicity nanomaterials, did not. The intratracheal instillation of NiO and CeO_2 resulted in a persistently elevated concentration of total protein in the BALF, while the same result with the intratracheal instillation of ZnO and TiO_2 was transient. Taken together, a difference in concentration of total protein in BALF was observed between the high and low toxicity nanomaterials following intratracheal instillation as well as inhalation, suggesting that the ranking of the harmful effects of nanoparticles in intratracheal instillation studies may reflect the ranking in inhalation studies.

Y. Yoshiura · Y. Fujisawa · T. Tomonaga · H. Izumi · T. Oyabu · T. Myojo · Y. Morimoto (✉)
Institute of Industrial Ecological Sciences, University of Occupational
and Environmental Health, Japan, Kitakyushu, Fukuoka, Japan
e-mail: yasuom@med.uoeh-u.ac.jp

M. Kubo · M. Shimada
Department of Chemical Engineering, Hiroshima University, Higashi-Hiroshima, Japan

Abbreviations

ANOVA   Analysis of variance
BALF   Brohchoalveolar lavage fluid
CeO_2 Cerium dioxide
LDH   Lactate dehydrogenase
NiO   Nickel oxide
TiO_2 Titanium dioxide
ZnO   Zinc oxide

5.1   Background

The use of nanomaterials has advanced in a variety of fields, such as electric appliances, cosmetics, and pharmaceutical products, due to the progress of nanotechnology. Titanium dioxide (TiO_2) nanoparticles, for example, are used in cosmetics, sunscreen and photocatalysts [1], and zinc oxide (ZnO) nanoparticles, white powders, are widely used in cosmetics, paint pigment, rubber additives, pharmaceutical products, and electronic materials [2]. The harmful effects of nanomaterials on the human body have become a matter of concern, but their safety has not evaluated sufficiently.

Many in vitro and in vivo studies have reported that nanomaterials induce toxicity in cells and organs [3–12]. In vitro studies have found that nickel oxide (NiO) nanoparticles and ZnO [3, 4] induce the release of lactate dehydrogenase (LDH) as cell damage, and in vivo studies have found apoptosis and acute pulmonary inflammation [5]. Carbon nanotubes have been reported to produce irreversible legion in in vivo studies [6, 7], and continuous inflammation and fibrosis containing mainly neutrophils were observed in an examination of inhalation exposure of rats to carbon nanotubes [8–11], and a 2-year inhalation study induced pulmonary tumor in rat lung [12]. Due to their expanded usage, there will be an increased need in the future for the evaluation of the harmful effects of nanomaterials.

The inhalation study is the gold standard for studying the harmful effects of nanomaterials because they can be performed with high reliability and can reflect the kinetics and dynamics of nanomaterials in the body. However, it is difficult to perform inhalation studies for all nanomaterials because of the expensive costs and the necessity of large-scale exposure equipment and operation by experts. Intratracheal instillation studies, on the other hand, in which materials are directly inserted into the lung, are not so difficult or expensive to perform, and can clarify the relationship between dose and response [13]. Intratracheal instillation studies are expected to be useful in the examination of the harmful effects of nanomaterials, but they have not yet been sufficiently evaluated.

We previously performed inhalation studies and intratracheal instillation studies of four nanomaterials with known toxicity and compared the results between both

studies of cell inflammation and concentration of cytokines in bronchoalveolar lavage fluid (BALF) [14–17]. In the present experiment, we measured the concentration of total protein in BALF following inhalation and intratracheal instillation of four nanomaterials with known toxicity, and examined whether or not the ranking of harmful effect in the intratracheal instillation study was compatible with the ranking in the inhalation study.

5.2 Materials and Methods

5.2.1 Nanoparticles

The four nanomaterials used in this experiment were commercially available. NiO nanoparticles (US3355, USResearch Nanomaterials, Houston, TX) and cerium dioxide (CeO_2) nanoparticles (Wako Pure Chemical Industries, Ltd., Osaka, Japan) were used as materials with high toxicity, and TiO_2 nanoparticles (MT-150AW, TAYCA CORPORATION, Osaka, Japan) and ZnO nanoparticles (Zinc oxide, dispersion ALDRICH 721077-100G) were used as materials with low toxicity. These nanoparticles were dispersed in deionized endotoxin-free water. Table 5.1 shows the physicochemical properties of the four materials.

5.2.2 Animals

Three hundred and thirty-four male Fischer rats (9–11 weeks old) were purchased from Charles River Laboratories International, Inc. (Japan). The animals were kept in the Laboratory Animal Research Center of the University of Occupational and Environmental Health for 2 weeks with free access to a commercial diet and water.

Table 5.1 Manufactured nanomaterials used in the present study

Nanomaterials	TiO_2	ZnO	CeO_2	NiO
Toxicity	Low	Low	High	High
Primary diameter	Short 12 nm Long 55 nm	35 nm	7.8 nm	19 nm
Specific surface area	111 m^2/g	31 m^2/g	101 m^2/g	57 m^2/g
Shape	Spindle-shaped	Sphere like	Irregular shape	Sphere
Secondary diameter in suspension (measured by DLS)	20-80 nm	17-37 nm	2.6-9.3 nm	39.8-47.1 nm
Purity	99.5%		99.9%	More than 99.5%
Bulk density	4.17 g/cm^3	5.6 g/cm^3	7.216 g/cm^3	6.72 g/cm^3
Solubility	Low	High	Low	Low (> CeO_2)

All procedures and animal handling were done in accordance with the guidelines described in the Japanese Guide for the Care and Use of Laboratory Animals as approved by the Animal Care and Use Committee, University of Occupational and Environmental Health, Japan.

5.2.3 Intratracheal Instillation of Nanomaterials

The NiO and TiO$_2$ nanoparticles were suspended in 0.4 mL distilled water. 0.2 mg (0.8 mg/kg) or 1 mg (4 mg/kg) of NiO, CeO$_2$, ZnO, and TiO$_2$ nanoparticles was administered to rats (12 weeks old) by a single intratracheal instillation. Negative control groups received distilled water. The animals were dissected at 3 days, 1 week, 1, 3, and 6 months after the instillation.

5.2.4 Inhalation of Nanomaterials

The experimental setup was partly similar to that used in our previous study [18]. The system primarily comprises a pressurized nebulizer (Nanomaster, JSR Corp., Tokyo, Japan), a spray chamber, a drying section, a stainless steel whole-body exposure chamber with rat cages, an electrostatic precipitator to collect aerosol particles for off-line analysis, and a particle size spectrometer (model 1000XP WPS, MSP Corp., Shoreview, MN, USA) that consists of a differential mobility analyzer (DMA) and a condensation particle counter (CPC) system for in-line monitoring.

Nanoparticle suspensions were diluted and sprayed by the pressurized nebulizer that was supplied with pressurized clean air at a typical airflow rate of 40 L/min and with the suspension at a rate of 0.8 mL/min. The sprayed droplets were transmitted into the spray chamber and subsequently transmitted into a drying section heated to 150 °C to evaporate the water from the droplets. After the drying process, air containing bipolar ions supplied by an ionizer (SJ-M, Keyence Corp., Tokyo, Japan) was introduced at a flow rate of 10 L/min, concurrently with the aerosol flow, to neutralize the aerosol particles and to reduce particle wall loss in the tubing caused by electrostatic forces. The aerosol was diluted with clean air to ensure the necessary total airflow rate of 100 L/min and fed through the exposure chamber for 6 h on each day of the inhalation test (spanning 4 weeks).

The size and number concentration of the aerosol particles inside and outside the exposure chamber were analyzed using a particle size spectrometer built for in-line monitoring. For comparison, the aerosol particles were sampled by an electrostatic precipitator for off-line analysis using field emission scanning electron microscopy (FE-SEM; S-5200, Hitachi High Technologies Corp., Tokyo, Japan). In addition, the mass concentration of the aerosol in the chamber was determined using a gravimetric method wherein the aerosol was filtered over fibrous filters and the collected

particles were weighed. To avoid artifacts in the measurements, pre-weighing, sampling, and post-weighing were conducted under a fixed humidity of 50%.

All the aerosol samples exhibited very stable particle size distributions over 6 h on each day of the entire period of the inhalation test. The particle size distributions showed two peaks at approximately 30 and 100 nm for the NiO aerosols and approximately 30 and 200 nm for the TiO_2 aerosols, which was due to Coulomb explosion [18]. The particle size distributions of the CeO_2 and ZnO aerosols displayed peaks at 90 and 120 nm, respectively. The average mass concentrations of the aerosols measured daily over the 4 weeks were 1.65 ± 0.20 mg/m^3 for NiO, 2.09 ± 0.34 mg/m^3 for CeO_2, 1.84 ± 0.74 mg/m^3 for TiO_2, and 2.11 ± 0.54 mg/m^3 for ZnO.

The animals were dissected at 3 days, 1 and 3 months after the end of the exposure.

5.3 Animals Following Inhalation and Intratracheal Instillation

There were five animals in each group at each time course. The lungs were inflated with 20 mL physiological saline under a pressure of 20 cm water, and BALF was collected from whole lung divided into two to three times. Between 15 and 18 mL of BALF was collected in collection tubes by free fall. The BALF was centrifuged at $400 \times g$ at 4 °C for 15 min, and the supernatant was transferred to a new tube and frozen. The concentration of protein in the supernatant of the BALF was determined by Bio-Rad Protein Assay (500-0006, Bio-Rad Laboratories, Inc., Hercules, CA, USA).
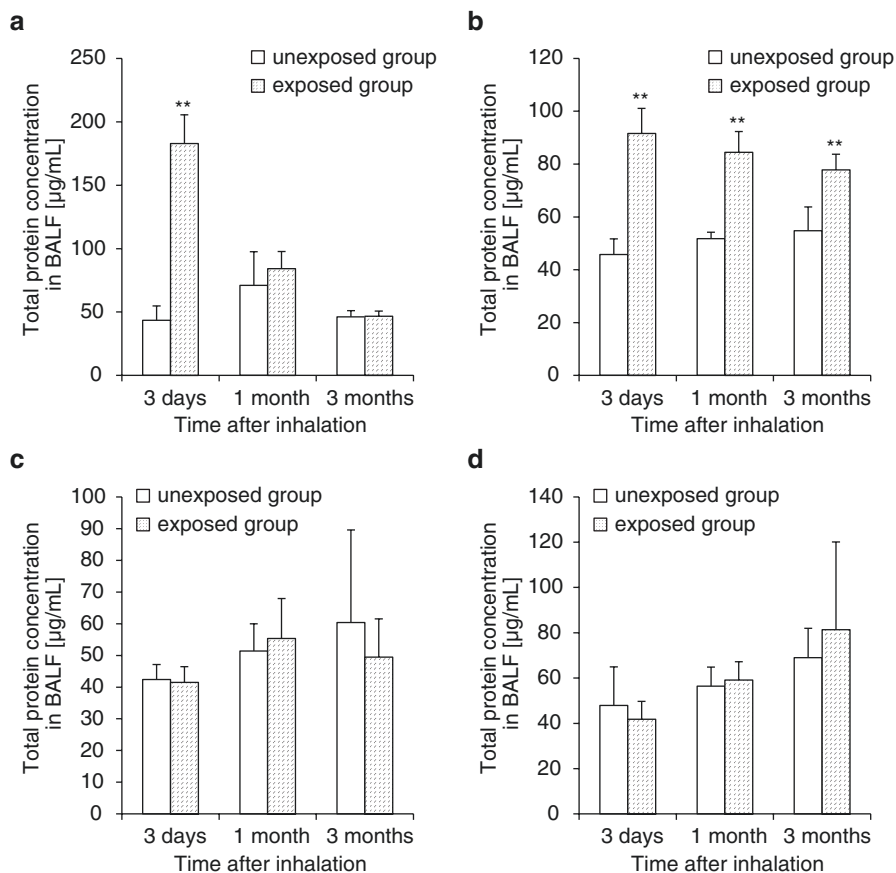
5.4 Statistical Analysis

Analysis of variance (ANOVA) and Dunnett's test were applied where appropriate to determine individual differences using a computer statistical package (SPSS, SPSS Inc., Chicago, IL, USA).

5.5 Results

5.5.1 Inhalation Study

Figure 5.1 shows the total protein concentration in BALF following the inhalation of the four nanomaterials.
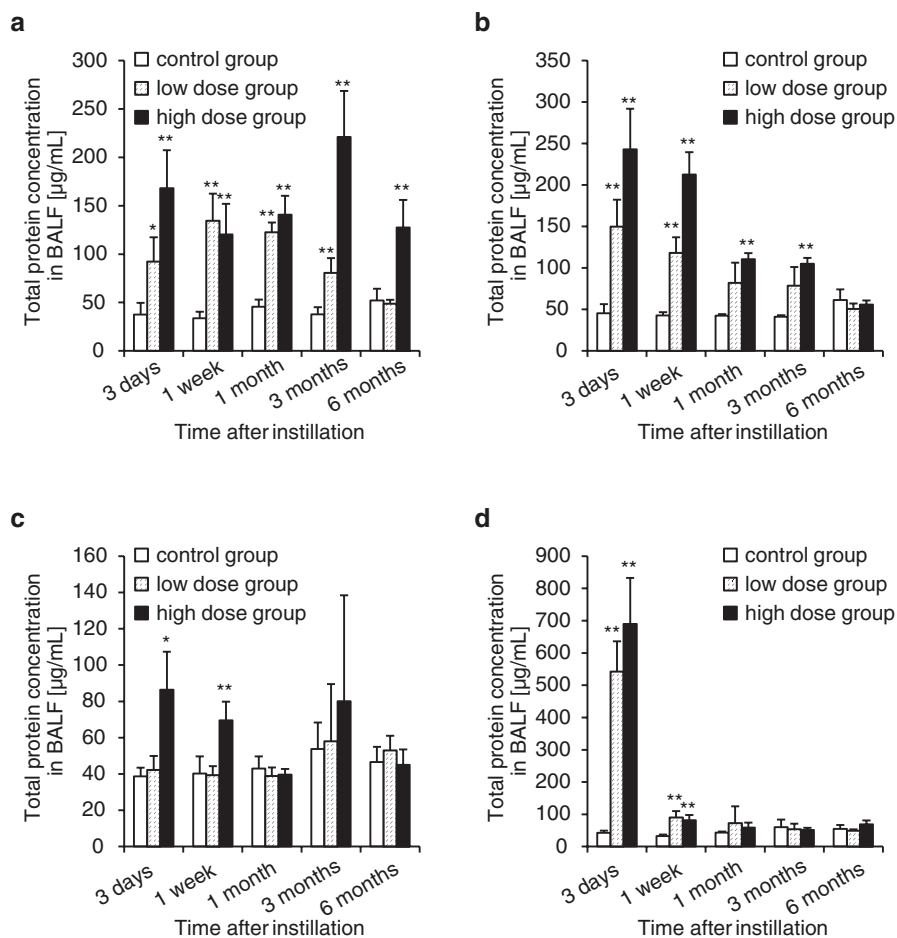
Fig. 5.1 Concentration of total protein in BALF following inhalation of four nanomaterials with different toxicities. (**a**) Protein concentration in BALF following inhalation of NiO, (**b**) protein concentration in BALF following inhalation of CeO_2, (**c**) protein concentration in BALF following inhalation of TiO_2, (**d**) protein concentration in BALF following inhalation of ZnO. Inhalation of NiO and CeO_2 induced an increase in the concentration of total protein, whereas TiO_2 and ZnO nanoparticles did not. Asterisks indicate significant differences compared with each control (ANOVA, Dunnett T3) (*$p < 0.05$, **$p < 0.01$)

The protein concentration in the BALF was significantly higher in the NiO and CeO_2 exposure groups compared to the unexposed group. Especially, the concentration of protein in the CeO_2 exposure group was persistently higher than that in the unexposed group during the observation time. On the other hand, the protein concentration in the BALF in the TiO_2 and ZnO groups after recovery was not significantly high.

5.5.2   Intratracheal Instillation Study

Figure 5.2 shows the total protein concentration in BALF following intratracheal instillation of four nanomaterials.

Fig. 5.2 Concentration of total protein in BALF following intratracheal instillation of four nano-materials of different toxicities. (**a**) Protein concentration in BALF following intratracheal instillation of NiO, (**b**) protein concentration in BALF following intratracheal instillation of CeO_2, (**c**) protein concentration in BALF following intratracheal instillation of TiO_2, (**d**) protein concentration in BALF following intratracheal instillation of ZnO. Intratracheal instillation of NiO and CeO_2 induced a sustained concentration of total protein, whereas TiO_2 and ZnO nanoparticles induced transient expression. Asterisks indicate significant differences compared with each control (ANOVA, Dunnett T3) (*$p < 0.05$, **$p < 0.01$)

The concentration of protein in the BALF was persistently and significantly high over a period of 3 days to 6 months and at 3 months in the high dose NiO and CeO_2 exposure groups, respectively; the low dose NiO exposure group also revealed a persistently high protein concentration from 3 days to 3 months. The low dose of CeO_2 induced a high protein concentration from 3 days to 1 week, and tendency of a high protein concentration was observed at 1 and 3 months after instillation. On the other hand, a transient and significant increase in total protein in the BALF was found at 3 days and 1 week after instillation in the group exposed to a high dose of

TiO_2 and ZnO. There was no significant increase in protein concentration in the group of low dose TiO_2 exposure except at 1 month. A transient increase in protein concentration in the low dose ZnO exposure group was observed at 3 days after instillation.

5.6   Discussion

We used the protein concentration in BALF as the endpoint of pulmonary toxicity in order to compare the difference between an intratracheal instillation and an inhalation (the gold standard) in the ranking of the harmful effects of nanomaterials. Although the total protein concentration in BALF is known as an index of vascular permeability, it is also related to inflammation and injury in the lung. In a study of pulmonary inflammation, the intratracheal instillation of cobalt nanoparticles induced total protein in the BALF of mice as well as infiltration of inflammatory cells, while intratracheal instillation of TiO_2 nanoparticles did not induce either total protein or inflammation [19]. Seiffert et al. found that an increased concentration of total protein linked up with an increase in neutrophils in the BALF of two strains of rats at a high dose following intratracheal instillation of silver nanoparticles [20]. Exposure to cobalt nanoparticles induced LDH activity as a representative marker of lung injury, accompanied by an elevation of total protein in the BALF of mice, while exposure to TiO_2 nanoparticles induced neither LDH activity nor total protein [19]. In a mice model intratracheally exposed to ZnO nanoparticles, there was desquamation of epithelial cells with concomitantly increased barrier permeability of the alveolar/blood [21]. Because total protein is linked not only to inflammation in the lung but also to lung injury, we think that total protein in BALF is a suitable endpoint for pulmonary toxicity.

The intratracheal instillation of NiO and CeO_2 persistently upregulated total protein concentration in the BALF, but TiO_2 and ZnO did so only transiently. We previously reported that inflammatory cell infiltration centering on neutrophils and alveolar macrophages persisted in NiO and CeO_2 exposure groups throughout the observation time as a pathological feature, and that transient inflammation in the acute phase was observed in TiO_2 and ZnO exposure groups [15–17, 22]. We also reported that exposure to NiO and CeO_2 induced persistent LDH activity in BALF, and that exposure to TiO_2 and ZnO did so only transiently [15–17, 22]. Considering that permeability is related to inflammation and injury in lung, the result of total protein concentration was in accordance with the pathological features and LDH activity. Both of these increase in total protein and LDH in BALF from exposure to NiO and CeO_2 suggested that such exposure may induce persistent vascular permeability through persistent lung injury. The protein in the BALF included some cytokines and chemokines, and we also reported a persistent increase in the expression of the cytokine-induced neutrophil chemoattractant (CINC) family, a representative

chemokine for neutrophils in BALF exposed to NiO and CeO_2, and a transient increase in exposure to TiO_2 and ZnO. These changes in chemokine expression suggest neutrophil influx into the rat lung.

On the other hand, there are some reports that the regulation of inflammation and permeability can be controlled by different molecular mechanisms. In infected mice, the downregulation of NADPH-oxidase 4 (NOX4) reduced lung permeability without affecting inflammation in the lung [23]. Although they used mice in a combined exposure of SiO_2 nanoparticles and *Pseudomonas aeruginosa*, Delaval et al. reported that lung permeability measured by IgM in BALF was upregulated without neutrophil influx or proinflammatory cytokines and chemokines in BALF [24]. Future studies on the mechanism of lung permeability are expected.

In the present experiment, the exposure to nanomaterials with high toxicity such as NiO and CeO_2 induced a persistent elevation of total protein, and the exposure to nanomaterials with low toxicity such as TiO_2 and ZnO did transiently, suggesting that ranking of harmful effects following intratracheal instillation through total protein may reflect the ranking of the harmful effect of nanomaterials.

Inhalation of NiO and CeO_2 in the present experiment induced an increase in the total protein concentration in the BALF, and inhalation of TiO_2 and ZnO did not. In our previous study [15–17, 22], the results of LDH activity in BALF had a similar tendency to the increase in LDH activity by inhalation of NiO and CeO_2 and no increase by inhalation of TiO_2 and ZnO. Pathological features revealed a similar tendency that inhalation of NiO and CeO_2 induced pulmonary inflammation, and that inhalation of TiO_2 and ZnO did not. As in the intratracheal instillation study, these data in the inhalation study suggest that the ranking of the harmful effects following inhalation through total protein may reflect the ranking of the harmful effect of nanomaterials. As for the similarities in lung burden of nanomaterials between the inhalation and the intratracheal instillation studies, the initial lung burden at 3 days following the intratracheal instillation of a low dose of NiO and the inhalation of NiO was the same as in the present study [25]. We examined the quantitative difference of total protein concentration in a low dose instillation group and in an inhalation group in the present study. Comparing the concentrations of four nanomaterials in the inhalation study, the total protein concentrations in the BALF in the low doses of NiO, TiO_2, and CeO_2 in the intratracheal instillation study were the same or at a higher qualitative level. As for ZnO, the total protein concentration in the low dose was much higher than that in inhalation. This acute additional effect following intratracheal instillation may have been stimulated by a large amount of released Zn ions due to the high solubility of ZnO. Taken together, the not so large difference in lung burden between both studies may lead to similar rankings of harmful effect of nanomaterials.

Correspondence of pranking of harmful effect of nanomaterials between both approaches through protein level of BALF was consistent with that through neutrophil influx and pathological change [15–17].

5.7 Conclusion

We measured the total protein in BALF exposed to nanomaterials of different toxicities in both inhalation and intratracheal instillation studies. Both studies revealed that the nanomaterials with high toxicity induced significant or persistent concentration of total protein in BALF compared with nanomaterials with low toxicity. Therefore, the ranking of harmful effects of nanomaterials in intratracheal instillation studies through the assessment of total protein in BALF may reflect the ranking in inhalation studies.

References

1. Kaida T, Kobayashi K, Adachi M, Suzuki F. Optical characteristics of titanium oxide interference film and the film laminated with oxides and their applications for cosmetics. J Cosmet Sci. 2004;55:219–20.
2. Reshma VG, Syama S, Sruthi S, Reshma SC, Remya NS, Mohahan PV. Engineered nanoparticles with antimicrobial property. Curr Drug Metab. 2017;18:1040–54.
3. Kim YH, Fazlollahi F, Kennedy IM, Yakobi NR, Hamm-Alvarez SFH, Borok Z, et al. Alveolar epithelial cell injury due to zinc oxide nanoparticle exposure. Am J Respir Crit Care Med. 2010;182:1398–409.
4. Kim IS, Baek M, Choi SJ. Comparative cytotoxicity of Al_2O_3, CeO_2, TiO_2 and ZnO nanoparticles to human lung cells. J Nanosci Nanotechnol. 2010;10:3453–8.
5. Ho M, Wu KY, Chein HM, Chen LC, Cheng TJ. Pulmonary toxicity of inhaled nanoscale and fine zinc oxide particles: mass and surface area as an exposure metric. Inhal Toxicol. 2011;23:947–56.
6. Shvedova AA, Kisin ER, Mercer R, Murray AR, Johnson VJ, Potapovich AI, et al. Unusual inflammatory and fibrogenic pulmonary responses to single-walled carbon nanotubes in mice. Am J Physiol Lung Cell Mol Physiol. 2005;289:L698–708.
7. Pauluhn J. Subchronic 13-week inhalation exposure of rats to multiwalled carbon nanotubes: toxic effects are determined by density of agglomerate structures, not fibrillar structures. Toxicol Sci. 2010;113:226–42.

8. Morimoto Y, Hirohashi M, Ogami A, Oyabu T, Myojo T, Todoroki M, et al. Pulmonary toxicity of well-dispersed multi-wall carbon nanotubes following inhalation and intratracheal instillation. Nanotoxicology. 2012;6:587–99.
9. Morimoto Y, Horie M, Kobayashi N, Shinohara N, Shimada M. Inhalation toxicity assessment of carbon-based nanoparticles. Acc Chem Res. 2013;46:770–81.
10. Kobayashi N, Naya M, Ema M, Endoh S, Maru J, Mizuno K, et al. Biological response and morphological assessment of individually dispersed multi-wall carbon nanotubes in the lung after intratracheal instillation in rats. Toxicology. 2010;276:143–53.
11. Kobayashi N, Naya M, Mizuno K, Yamamoto K, Ema M, Nakanishi J. Pulmonary and systemic responses of highly pure and well-dispersed single-wall carbon nanotubes after intratracheal instillation in rats. Inhal Toxicol. 2011;23:814–28.
12. Kasai T, Umeda Y, Ohnishi M, Mine T, Kondo H, Takeuchi T, et al. Lung carcinogenicity of inhaled multi-walled carbon nanotube in rats. Part Fibre Toxicol. 2016;13:53.
13. Morimoto Y, Izumi H, Yoshiura Y, Fujisawa Y, Fujita K. Significance of intratracheal instillation tests for the screening of harmful effects of nanomaterials. J UOEH. 2017;39:123–32.
14. Morimoto Y, Izumi H, Kuroda E. Significance of persistent inflammation in respiratory disorders induced by nanoparticles. J Immunol Res. 2014;2014:962871.
15. Morimoto Y, Izumi H, Yoshiura Y, Tomonaga T, Oyabu T, Myojo T, et al. Pulmonary toxicity of well-dispersed cerium oxide nanoparticles following intratracheal instillation and inhalation. J Nanopart Res. 2015;17:442.
16. Morimoto Y, Izumi H, Yoshiura Y, Tomonaga T, Oyabu T, Myojo T, et al. Evaluation of pulmonary toxicity of zinc oxide nanoparticles following inhalation and intratracheal instillation. Int J Mol Sci. 2016;17:E1241.
17. Morimoto Y, Izumi H, Yoshiura Y, Tomonaga T, Lee BW, Okada T, et al. Comparison of pulmonary inflammatory responses following intratracheal instillation and inhalation of nanoparticles. Nanotoxicology. 2016;10:607–18.
18. Kubo M, Nakaoka A, Morimoto K, Shimada M, Horie M, Morimoto Y, et al. Aerosol generation by a spray-drying technique under Coulomb explosion and rapid evaporation for the preparation of aerosol particles for inhalation tests. Aerosol Sci Technol. 2014;48:698–705.
19. Wan R, Mo Y, Zhang Z, Jiang M, Tang S, Zhang Q. Cobalt nanoparticles induce lung injury, DNA damage and mutations in mice. Part Fibre Toxicol. 2017;14:38.
20. Seiffert J, Buckley A, Leo B, Martin NG, Zhu J, Dai R, et al. Pulmonary effects of inhalation of spark-generated silver nanoparticles in Brown-Norway and Sprague-Dawley rats. Respir Res. 2016;17:85.
21. Jacobsen NR, Stoeger T, van den Brule S, Saber AT, Beyerle A, Vietti G, et al. Acute and subacute pulmonary toxicity and mortality in mice after intratracheal instillation of ZnO nanoparticles in three laboratories. Food Chem Toxicol. 2015;85:84–95.
22. Yoshiura Y, Izumi H, Oyabu T, Hashiba M, Kambara T, Mizuguchi Y, et al. Pulmonary toxicity of well-dispersed titanium dioxide nanoparticles following intratracheal instillation. J Nanopart Res. 2015;17:241.
23. Fu P, Mohan V, Mansoor S, Tiruppathi C, Sadikot RT, Natarajan V. Role of nicotinamide adenine dinucleotide phosphate-reduced oxidase proteins in Pseudomonas aeruginosa-induced lung inflammation and permeability. Am J Respir Cell Mol Biol. 2013;48:477–88.
24. Delaval M, Boland S, Solhonne B, Nicola M-A, Mornet S, Basza-Squiban A, et al. Acute exposure to silica nanoparticles enhances mortality and increases lung permeability in a mouse model of Pseudomonas aeruginosa pneumonia. Part Fibre Toxicol. 2015;12:1.
25. Oyabu T, Myojo T, Lee BW, Okada T, Izumi H, Yoshiura Y, et al. Biopersistence of NiO and TiO2 nanoparticles following intratracheal instillation and inhalation. Int J Mol Sci. 2017;18:pii: E2757.

Chapter 6
Standardization of Intratracheal Instillation Study of Manufactured Nanomaterials

Toshio Kobayashi, Yutaka Oshima, Yasuhiro Tsubokura, Takakazu Kayashima, Makoto Nakai, Nobuya Imatanaka, Hirokazu Kano, Hideki Senoh, Masaaki Suzuki, Hitomi Kondo, and Shoji Fukushima

Abstract Intratracheal (IT) instillation is a useful method for screening and hazard identification of inhaled materials, including manufactured nanomaterials. However, many variables regarding sample preparation, experimental equipment, and technical procedures influence results from studies involving IT instillation, and a standard procedure has not yet been validated internationally. These drawbacks prevent accurate comparison of hazard information obtained from different test facilities. In this chapter, we summarize representative IT instillation procedure and present acceptable ranges at which various procedural components do not affect the results. Issues requiring consideration prior to experimentation include the preparation of the dose suspension, appropriate vehicle, and delivery device. In addition, practical aspects of the testing procedure including appropriate forms of anesthesia, animal positioning during IT instillation, intubation methodology, and dosing volume, rate, and frequency are addressed, and recommended endpoints for hazard identification are described. Furthermore, an example recommended procedure for reproducible IT instillation is provided. Technical guidance for reproducible procedures, e.g., a Standard Operating Procedure, is pivotal for the standardization of IT instillation studies, and this chapter contributes validated technical information. In conclusion, IT instillation is poised to occupy an important position regarding hazard screening of manufactured nanomaterials.

Keywords Intratracheal instillation · Manufactured nanomaterial · Standard procedure · Hazard screening

T. Kobayashi (✉) · Y. Oshima · Y. Tsubokura · T. Kayashima · M. Nakai · N. Imatanaka
Chemicals Evaluation and Research Institute, Japan, CERI Hita, Hita-shi, Oita, Japan
e-mail: kobayashi-toshio@ceri.jp

H. Kano · H. Senoh · M. Suzuki · H. Kondo · S. Fukushima
Japan Bioassay Research Center, Japan Organization of Occupational Health and Safety, Hadano, Kanagawa, Japan

6.1   Introduction

Intratracheal (IT) instillation is a technique through which test materials are delivered directly into the respiratory tract. Because this method is simpler than inhalation exposure and is useful and cost-effective for pulmonary bioassays, numerous researchers have applied IT instillation for various purposes including hazard assessment, the creation of pulmonary disease models, and immunologic and kinetics investigations [1–4].

In general, to perform IT instillation, test material is dispersed in a liquid and is then directly instilled into the trachea of an anesthetized laboratory rodent. General endpoints for hazard evaluation are in-life examination; clinical examinations including hematology, blood biochemistry, and bronchoalveolar lavage (BAL) evaluation; pathological evaluation; and sometimes lung burden analysis. Many technical variables can affect the results of studies involving IT instillation, and authorized procedural guidelines for IT instillation are not yet established, thus preventing accurate comparison of results between test facilities. This chapter focuses on published articles that have investigated the effects of different experimental conditions and presents a reproducible procedure for IT instillation studies for hazard evaluation of inhaled materials, including manufactured nanomaterials. The aims of this chapter are to illustrate various technical aspects of conducting IT instillation and to contribute toward standardization of the IT instillation procedure.

This work was conducted under the "Development of Innovative Methodology for Safety Assessment of Industrial Nanomaterials" project, supported by the Ministry of Economy, Trade, and Industry (METI) of Japan. The contents are partially available on the project's website (https://metinanojp.aist-riss.jp/) (in Japanese).

6.2   Initial Considerations

IT instillation bypasses the upper respiratory tract, such that the deposition rate of test materials in lung is far higher than that of inhalation and therefore never reproduces the real-life situation of inhalation exposure. In addition, IT instillation is likely to be applied in unrealistic conditions such as excessively high dose levels. Therefore IT instillation cannot be considered an alternative method to inhalation exposure, and the results cannot be used directly for human risk assessment. However, IT instillation is widely recognized to be useful for relative pulmonary toxicity evaluation and hazard screening [1, 5–7].

6.2.1   Animal Selection

In this chapter, techniques are described by using rats as an example; for mice, pharyngeal aspiration is appropriate but is not addressed here. The strain, sex, and age of animals should be determined in light of the purpose of each study; juvenile rats

should be avoided, however, because their tiny body size makes the IT instillation procedure difficult. Preferably rats weighing 250 g or more should be used.

6.2.2   Preparation of Dose Suspension

IT instillation is performed by using the test material powder directly or dispersed in a liquid. This chapter addresses only the liquid form of treatment.

Guidance Document 36 from the Organisation for Economic Co-operation and Development (OECD) describes sample preparation for hazard evaluation testing of manufactured nanomaterials [8]. At least three major study contexts should be considered for assessment of potential health-related effects: human exposure characterization; characterization of administered material; and characterization of as-produced or supplied material [2]. Furthermore, particle size, particle size distribution, and the nanoscale of the particle should all be confirmed through multiple techniques. These contexts should be addressed through IT instillation studies, as well as factors that arise due to the IT instillation technique itself.

IT instillation bypasses the size-dependent filtering function of the upper respiratory tract. Therefore, excessively large components or highly aggregated particles, which otherwise would have been filtered out by the upper respiratory tract, can reach the peripheral part of the lung, which is inaccessible in inhalation studies [9]. The results obtained under such study conditions may lead to incorrect interpretations regarding the hazards associated with the tested material. For example, IT instillation of excessively agglomerated fibrous materials, such as carbon nanotubes, mechanically obstructs the airways, resulting in mortality [10]; the authors of the cited study indicated that death was not due to inherent toxicity. Likewise, unexpected reactions may occur due to IT instillation of unrespirable materials into lower respiratory tract; therefore, suspensions of test materials for which, owing to their dispersion state, exposure to the lower respiratory tract is unrealistic should not be used. The Guidance Document 39 regarding inhalation toxicity studies, which has revised currently, recommends a mass median aerodynamic diameter (MMAD) of ≤2 μm [11]. Therefore, the maximum particle diameter in the dosing suspension for IT instillation should be no larger than its respirable size; otherwise, the reason for disregarding this recommendation should be clarified.

6.2.3   Dispersion Media

Dispersion media vary depending on the material. A survey of the published literature revealed that the vehicles used most often for the dispersion of nanomaterials were physiologic saline, including PBS (used in 68.0% [166 of 244] of published articles for which free full texts were available); saline or PBS supplemented with surfactant (11.1% [27 of 244]); and water (described as distilled, deionized, MilliQ, ultrapure, etc.; 9.0% [22 of 244]). The remaining articles indicated the use of a

specific vehicle for the purpose of the study (10.2% [25 of 244]) or did not describe the medium used (1.6% [4 of 244]).

Regarding specific vehicles, media known to be suitable for dispersion of particles are applied in IT instillation studies. For example, disodium phosphate (DSP) solution, which is an effective dispersion media for TiO_2 particles, has been used as a vehicle in several studies [3, 12, 13]. The results indicated that DSP solution did not induce a pulmonary reaction and therefore is considered to be an appropriate medium for instillation of test materials. When considering the use of a novel vehicle, researchers should clarify in advance any vehicle-associated effects in evaluation assays and on the animal model involved. These effects can be distinguished by using appropriate control groups, such as untreated animals and sham control groups.

6.2.4 Dose Metrics and Dose Levels

The most suitable dosage unit for hazard assessment using IT instillation has not yet been defined. Previously proposed metrics include mass, the number of particles, and surface area. Dosage according to mass is the most common unit for general toxicity studies. Regarding particle toxicity, other dosage contexts such as particle number and specific surface area are often discussed and likely are suitable for some inflammatory parameters [14, 15]. However, given that a definitive conclusion has not yet been reached, the mass basis unit of mg/kg body weight (B.W.) is used in this chapter.

As with general toxicity studies, multiple dose groups should be included to evaluate dose dependency in IT instillation. Dose levels should be determined on the basis of toxicity information regarding the test materials or related materials or in light of the results of a dose-finding study, which is conducted as needed. The highest dose used should induce overt signs of toxicity but should not lead to death or serious toxic symptoms or cause excessive bolus reactions or overload conditions. Optimally the dose level should be set at <1–2.5 mg per rat ([6, 16]: see following paragraph).

In IT instillation studies, bolus delivery of the dose suspension causes a local acute inflammatory reaction [2, 17]. Unlike with other administration methods (e.g., inhalation), this reaction in an IT instillation study is not due to the inherent toxicity of the test material. However, this local reaction can be minimized in IT instillation studies by improving the dispersion state of test materials in the dosing suspension and by avoiding the instillation of excessive amounts of test materials [17].
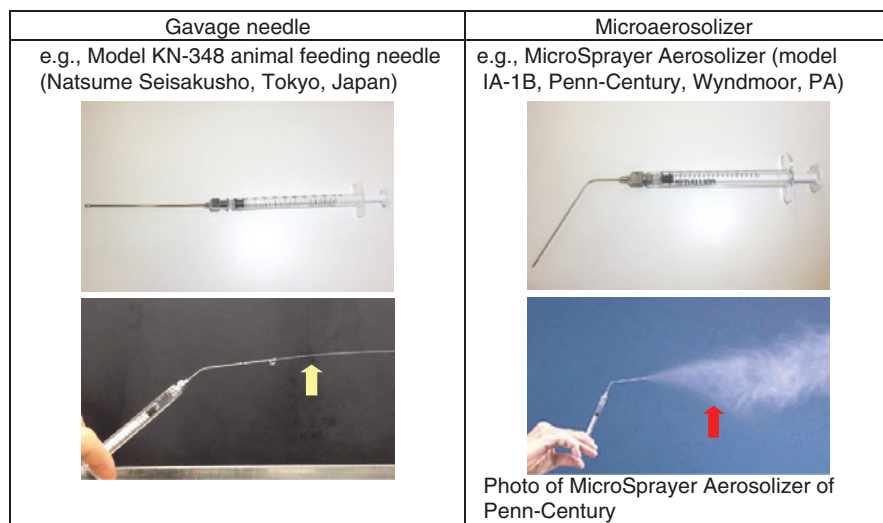
On the other hand, the overload phenomenon [18] may occur in respiratory toxicity studies of insoluble materials. This situation arises owing to impairment of alveolar macrophage clearance correlates with the volumetric loading of the macrophages. Consequently, rats exposed to excessively high concentrations or dose levels of insoluble particles develop chronic inflammation, fibrosis, and tumor [19–21]. An overload threshold may exist, and some studies clearly define this threshold—

e.g., ≥2.5 mg per rat (or lung) [16]; 1 mg per rat [6]. However, whether the overload phenomenon is associated with a surface area metric or volume metric—or both— remains under discussion [22].

6.2.5   Selection of Delivery Device

IT instillation can be accomplished by using a gavage needle or a microaerosolizer (Fig. 6.1). Gavage needles are used to directly expel the dosing solution as a liquid. In contrast, the microaerosolizer (e.g., MicroSprayer Aerosolizer [model IA-1B, Penn-Century, Wyndmoor, PA]) pressurizes and thus aerosolizes the dosing solution (e.g., the droplet size achieved by using a MicroSprayer is 25–30 μm). However, when a dosing solution contains coarse particles, the fine tip of the microaerosolizer may clog, thus altering the particle size distribution or decreasing the dose level. Such clogging of gavage needles is unlikely. Therefore, it is essential to confirm that using a microaerosolizer neither alters the particle size distribution nor dosing solution concentration compared with those of the original test material suspension.

Using India ink, Hasegawa-Baba et al. [23] showed that the India ink distribution is superior with a microaerosolizer compared with a gavage needle. However, the specific state in which the dosing solution is expelled is not considered to affect hazard potential parameters. For example, the acute pulmonary inflammation induced by nano-sized TiO_2 particles did not differ quantitatively between various delivery devices for IT instillation [13]. Therefore, whatever device is available at a facility can be used.

| Gavage needle	Microaerosolizer
e.g., Model KN-348 animal feeding needle (Natsume Seisakusho, Tokyo, Japan)	e.g., MicroSprayer Aerosolizer (model IA-1B, Penn-Century, Wyndmoor, PA)
	Photo of MicroSprayer Aerosolizer of Penn-Century

Fig. 6.1 Delivery devices used for IT instillation. Arrow: appearance of expelled solution

6.3   Experimental Procedure

Several experimental steps during an IT instillation study can affect the results. To obtain reproducible results, the following factors should be considered: (1) anesthesia of animals during IT instillation; (2) animal positioning during IT instillation; (3) intubation methods and orientation of the delivery device; (4) dosing volume; (5) dosing rate; and (6) dosing frequency.

6.3.1   Anesthesia of Animals During IT Instillation

For IT instillation, anesthesia is essential in terms of safety, practicability, and reproducibility. Figure 6.2 summarizes varieties of anesthetic methods applied in IT instillation as reported in articles published during the past two decades. In 1996–2000, halothane or ketamine derivatives (or their combinations) predominated; barbiturate and ether derivatives were used also. A similar trend was also seen in 2001–2005. In 2006–2010, ketamine derivatives predominated, with lesser use of ether and barbiturates; halothane anesthesia decreased, but the use of isoflurane derivatives increased. After 2011, isoflurane application became the predominant mode of anesthesia for IT instillation, whereas the uses of halothane and ether decreased remarkably. As these patterns suggest, choosing the most appropriate type of anesthesia for IT instillation includes consideration of animal welfare, and isoflurane and its derivatives are the most popular and preferable currently.
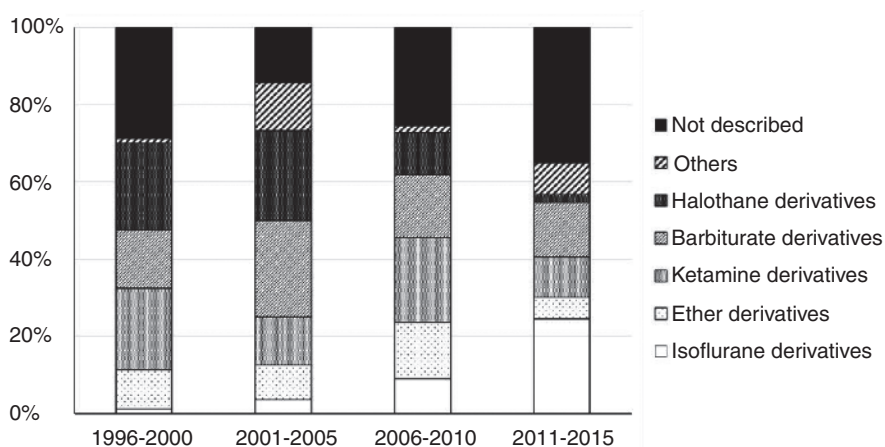
Fig. 6.2 Overview of anesthetic agents applied in IT instillation from 1996 through 2015. A total of 244 free, full-text articles were assessed

6.3.2   Animal Positioning During IT Instillation

To increase the reproducibility of IT instillation, animal positioning during instillation must be consistent. Various types of animal restrainers suitable for use during IT instillation are commercially available; most of these fix the rat in a spine-up position by using a rubber loop or other device around the upper incisors. Because an IT-instilled suspension distributes and moves into the lungs by gravity [23, 24], the position angle of the rat is an important factor. Evaluation of the effects of animal position (vertical, 45° supine, or horizontal) at IT instillation on the pulmonary distribution of India ink revealed that the rat with spine position at a 45° angle yielded the best distribution of ink particles [23]. In addition, the authors reported that some rats dosed in the horizontal position died due to asphyxiation; therefore, instillation into horizontally positioned animals must be avoided. Accordingly, for effective and safe instillation, animals should be placed with supine position at a 45° angle or greater.

In IT instillation, partial loss of the test material is likely due to the animal's natural posture (i.e., quadruped gait). However, this loss can be minimized by adjusting the dose volume range (2 mL/kg B.W. and less, see Sect. 6.3.4). In addition, restraining the animals briefly after dosing prevents backflow of the dose suspension [13].

6.3.3   Intubation Methods and Orientation of the Delivery Device

Several important precautions regarding insertion of the delivery device into the trachea should be followed. First, prior to experiments, the technician must be trained well. Second, using a laryngoscope to visualize the larynx is strongly recommended, so that the technician can successfully accomplish the procedure easily (Fig. 6.3). The glottis opens widely at inspiration, so it is a suitable time for intubation. In addition, incorrect intubation (e.g., insertion into the esophagus) and backflow of the dose suspension can be distinguished visually. In particular, when the device is inserted too deeply, the tip reaches the bronchus, resulting in delivery of the dosing suspension localized to one lung; conversely when the insertion is too shallow, the dosed suspension can backflow into the gastrointestinal tract, leading to loss of test material. Therefore, prior to experiments, the appropriate insertion depth should be determined at each test facility. For example, the measured length (mean ± 1 S.D.) of the airway (the distance between the mouth and carina) of representative animals (12-week-old male F344/DuCrlCrlj rats; approximate B.W., 250 g; n = 20) in the spine-up restrained position was approximately 6 cm (6.41 ± 0.19 cm) [13]. Finally, the delivery device and laryngoscope should be handled carefully to prevent mechanical injury of the surrounding mucosa. Attention to these details will increase the reproducibility of IT instillation.

At inspiration   At expiration

Intubation into trachea   Incorrect intubation into esophagus
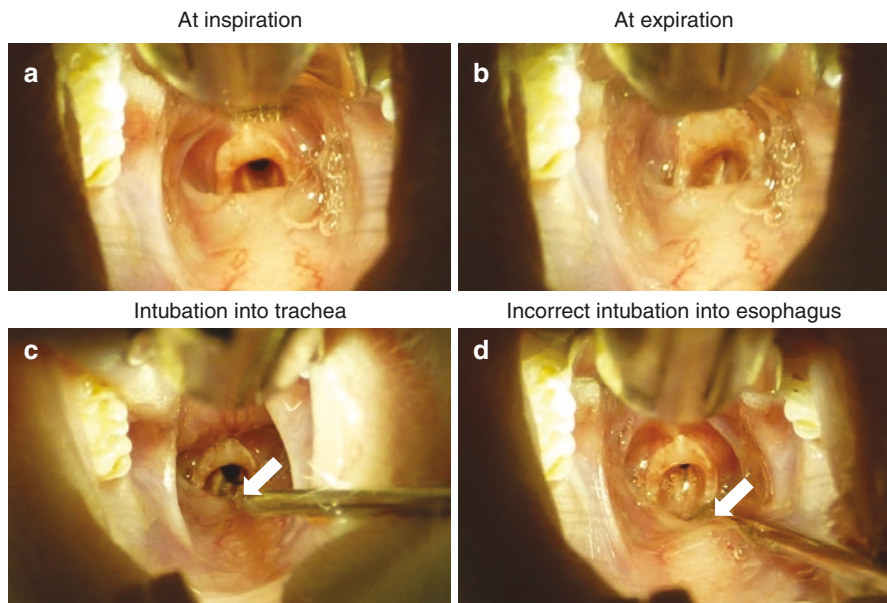
Fig. 6.3 Rat larynx visualized by laryngoscope. (**a**) Appearance at inspiration. (**b**) Appearance at expiration. (**c**) Appearance during appropriate introduction of the delivery device into the trachea. (**d**) Incorrect placement into the esophagus. Arrow: tip of delivery device (gavage needle)

6.3.4 Dosing Volume

Generally the dosing volume used for IT instillation ranges from 1.0 to 2.0 mL/kg B.W. [1]. Increased dosing volumes are considered to improve intrapulmonary distribution, although excessive volume might cause death immediately after IT instillation due to asphyxiation. In fact, the most appropriate volume may differ depending on the type of delivery device: several rats died just after dosing of vehicle only (i.e., purified water and DSP solution) at the dosing volumes of 3.5 mL/kg B.W. for a gavage needle and 2.5 mL/kg B.W. for a microaerosolizer (unpublished information).

In terms of hazard potentials, differences in dosing volume in the range of 0.5–2.0 mL/kg B.W. do not appear to alter various biomarkers. In particular, the acute inflammation (3 days after instillation) induced by IT instillation of 3.0 mg/kg B.W. nano-sized TiO_2 did not differ significantly among dosing volumes of 0.5, 1.0, and 2.0 mL/kg B.W., according to BAL inflammatory parameters; however, excessively high volumes such as 3.0 mL/kg B.W. induced less inflammation [13].

6.3.5 Dosing Rate

Dosing rate is known to influence the intrapulmonary distribution of a dosing solution. For example, intrapulmonary distribution of India ink was more

homogenous at 40 mL/min, regardless of the delivery device, than at 4 mL/min [23]. However, the effect of dosing rate on hazard potential parameters such as BAL values is unclear. Regardless, the dosing technician should determine the dosing rate that optimally expels the dosing suspension. For the MicroSprayer, a pressure ≥700 psi is required to sufficiently atomize a dosing suspension, due to the fine structure in the device (manufacturer's instructions). Sufficient aerosolization of purified water required a dosing rate of approximately 16 mL/min [13].

6.3.6   Dosing Frequency

Although a single instillation is sufficient for hazard screening, multiple instillations might be necessary to achieve the target dosage of nanomaterials [25]. To reveal the frequency-associated effects of dosing, the same total dose of nano-sized NiO was administered by using dose frequencies ranging from once only (i.e., a single instillation) to a total of four doses, one every other day. The results of BAL fluid analysis and histopathologic examinations did not differ between dosing frequencies, thus indicating that the hazard potential of nano-sized NiO can be estimated sufficiently by using single instillation.

6.4   Endpoints for Hazard Evaluation

6.4.1   Observation Period

The observation period is determined according to the objective of each experiment. In previous reports, the observation period was often set as 24 h; 3, 7, or 28 days; or 3 months after IT instillation [2, 26, 27]. However, some authors suggested that assessment at 24 h after instillation might lead to conflicting results, because the treatment procedure itself induces slight response according to BAL examination; that is, this response is not due to the inherent toxicity of test substances [28]. In the context of hazard potential evaluation, the observation period should incorporate at least three sampling points (e.g., 3, 7, and 28 days), to accommodate assessment of change over time [1, 6].

6.4.2   In-life Examination

Observation parameters performed in OECD Test Guidelines (TGs) for general toxicity studies include general clinical condition (Sect. 6.4.2.1) and body weight measurement (Sect. 6.4.2.2).

6.4.2.1   General Clinical Condition

In the IT instillation study, it is important to closely monitor the animals' general clinical conditions, especially respiratory parameters: animals should be observed several times on the day of instillation at least. Because animals that undergo IT instillation are likely to show irregular respiratory features, such as moist rales, just after instillation, care should be taken to distinguish these reaction to the dosing regimen from toxic signs due to the effects of test materials. Moribund animals and those with severe or persistent pain should be euthanized promptly for welfare reasons, according to the principles and criteria summarized in guidance documents on humane endpoints.

6.4.2.2   Body Weight

Body weight is an important index of toxicity. For all animals, body weight should be measured immediately before instillation, at least once weekly, and at the time of death or euthanasia or end of study.

6.4.3   Clinical Pathology

The OECD TGs for inhalation toxicity studies include endpoints of blood examinations and gross necropsy; these same parameters should be recorded for IT instillation studies. Specifically for pulmonary reactions, OECD TGs 412 and 413 require BAL fluid analysis as mandatory [29, 30]. Table 6.1 shows the mandatory parameters for inhalation studies, and these should be measured in IT instillation studies as well. In addition, the Guidance Document on inhalation toxicity studies [11] describes optional parameters including indicators of lysosomal injury, phospholipidosis, fibrosis, and irritant or allergenic inflammation, which may include the determination of pro-inflammatory cytokines and chemokines.

Potential confounders for BAL analysis include anesthesia at the time of euthanasia (Sect. 6.4.3.1) and BAL collection method (Sect. 6.4.3.2). In addition, a reasonable method for preparing samples for histopathologic examination is described (Sect. 6.4.3.3).

Table 6.1 Mandatory BAL fluid parameters

Test parameter	Relevant index
Cell counts and differentials for macrophages, lymphocytes, neutrophils, and eosinophils	Infiltration of inflammatory cells
Total protein or albumin	Enhanced permeability of pulmonary capillaries
Lactate dehydrogenase (LDH)	Cytotoxicity of lung constituent cells

6.4.3.1 Anesthesia at Euthanasia

Traditionally, barbiturate derivatives have been selected predominantly for euthanasia of rats in various experiments; however, this trend is changing. Regardless, selection of the optimal euthanasia method after IT instillation incorporates several factors including animal welfare, experimental validity, equipment availability, and institutional experience and practice. In particular, some anesthetic agents are known to affect BAL fluid evaluation. For example, comparison of the effects of three different anesthesia methods (inhalation of isoflurane; intraperitoneal pentobarbital; and intraperitoneal administration of combined medetomidine—midazolam—butorphanol) on BAL parameters at euthanasia by bleeding from the abdominal aorta revealed that neither isoflurane nor pentobarbital altered BAL fluid parameters whereas triple anesthesia significantly increased the values of vascular permeability markers (total protein and albumin) [31]. Therefore, isoflurane anesthesia is compatible with BAL analysis, but increased caution is advised when triple anesthesia is used.

6.4.3.2 BAL Fluid Collection and Examination

As addressed in OECD TGs 412 and 413, partial lavage (e.g., right lung) is recommended, and the remaining tissue should be used for organ weight and histopathologic examination. Partial lavage is ideal in terms of minimizing animal numbers, and it should be considered for IT instillation studies. However, caution is advised regarding partial lavage when the distribution of the test material after IT instillation is incompletely homogenous [13, 23, 24]. During lavage, the lung should be inflated sufficiently to collect the fluid from the entire sample. To promote reproducibility, lavage fluid should be instilled by using constant pressure, such as 20–30 cm of water, the pressure generally used for inflation of lung prior to fixing.

6.4.3.3 Histopathologic Examination

Methods for trimming the respiratory tract prior to histopathologic examination have been published [32] or can be determined by each test facility. OECD TGs 412 and 413 recommend the use of half of the lungs for histopathologic examination. This is ideal for IT instillation studies although the feasibility of this practice for IT instillation studies is unclear given that test materials do not always distribute homogenously to all lobes [13, 24]. Therefore, caution is advised when the partial tissues is examined histopathologically. In addition, because histopathologic lesions due to IT-instilled test material frequently are located along terminal bronchioles [6], sections containing terminal bronchioles should be prepared from all lobes for appropriate diagnosis.

6.4.4 Lung Burden

The OECD TGs for inhalation studies advocate the inclusion of a lung burden measurement for poorly soluble materials that are likely to be retained in the lungs [29, 30]. This measurement should be done according to the results of a range-finding study or other relevant information. Typically, male rats are preferable for this evaluation because their minute volume is greater than females'; thus, males are likely to have higher lung burdens [11]. On the other hand, IT instillation can achieve precise lung loading, which is likely to be much higher than that after inhalation. Consequently, lung burden analysis can be applied to female rats or even half of the lungs. In addition, lung burden can be measured in post-lavaged lungs by combining the amounts of test material in the BAL and tissue samples [33]. This means that the three analyses of histologic examination, BAL evaluation, and lung burden determination can all be conducted in the same animal. Therefore, IT instillation supports the acquisition of precise toxicological information and promotes animal welfare.

6.5   Summary and Recommended Procedure

Requirements regarding hazard evaluation of inhaled materials, especially manufactured nanomaterials, have been changing recently. During the preparation of this chapter, OECD TGs 412, 413 and related Guidance Document on inhalation toxicity testing were revised. Given that the revised Guidance Document describes the applicability of IT instillation techniques for hazard identification and screening, IT instillation studies will become more prevalent. The current chapter summarizes published findings as well as personal experience. In addition, recommended procedures for conducting reproducible IT instillations follow. The most important points are for (1) a well-trained dosing technician to (2) perform this standardized procedure (3) within acceptable ranges for procedural factors. Consequently, each test facility should establish criteria to assure the technical skill of dosing technicians. Hopefully, this chapter helps researchers, technicians, and other personnel to perform IT instillation effectively, safely, and consistently and to prepare Standard Operating Procedures for their specific testing facility.

6.5.1 Recommended Procedures for IT Instillation Study

Sample preparation
– Select appropriate dispersion media according to the physicochemical properties of the test material.
– Determine dispersibility by using several analytic techniques.

– Clarify whether the vehicle itself has any effects on animals.
– Avoid suspensions that would not be inhalable under actual conditions; the average particle diameter of a suspension should be less than its respirable size (e.g., MMAD ≤2 μm).

Dose selection
– Set multiple dose levels to evaluate dose dependency.
– The maximal dose should induce neither severe toxicity nor an overload condition.
– Consider existing information regarding the toxicity of the test material, and conduct a dose-finding study when indicated.

Selection of delivery device
– Use whatever delivery device (i.e., gavage needles or microaerosolizer) that is available.
– When using a microaerosolizer, confirm that it alters neither the size distribution nor concentration of the instilled dosing suspension.

IT instillation
– Apply appropriate anesthesia (e.g., isoflurane).
– Use an appropriate animal restrainer; rat should be at a 45° angle or greater.
– Visualize the larynx by using a laryngoscope—highly recommended.
– Position the tip of the delivery device near the carina; do not enter the bronchus.
– When using a microaerosolizer, confirm in advance that the dosing suspension is aerosolized sufficiently at the target dose rate.
– Select a dosing volume of 0.5–2.0 mL/kg B.W.
– To prevent backflow of test material, restrain the animal for a while after IT instillation. A laryngoscope can be used for visual confirmation.

Dosing frequency
– Typically a single IT instillation is sufficient for hazard evaluation.
– Consider multiple instillations of a low-concentration dosing suspension when a single, high-concentration instillation is unlikely to achieve effective dispersion.

Clinical examination
– Monitor rats' general clinical condition frequently and thoroughly, particularly soon after IT instillation, to distinguish effects due to the procedure itself from test material toxicity.

Clinical pathological examination
– Provide appropriate anesthesia (e.g., isoflurane).
– Take care when using triple anesthesia with medetomidine, midazolam, and butorphanol. These anesthetics affect vascular permeability parameters in BAL analysis.

– When using partial lavage, consider incompletely homogenous distribution of the test material after IT instillation.
– Infuse lavage buffer under constant pressure (e.g., 20–30 cm of water).
– Measurements of cell counts, cell differentials, total protein or albumin, and LDH are mandatory for BAL analysis.
– When possible, prepare lung sections to include terminal bronchioles.

Lung burden analysis
– Measure lung burden for poorly soluble materials that are likely to be retained in the lungs.
– Use post-lavaged tissues. The amounts of test materials can be estimated by combining those in the BAL and tissue.

References

1. Driscoll KE, Costa DL, Hatch G, Henderson R, Oberdorster G, Salem H. Intratracheal instillation as an exposure technique for the evaluation of respiratory tract toxicity: uses and limitations. Toxicol Sci. 2000;55:24–35.
2. Oberdörster G, Oberdörster E, Oberdörster J. Nanotoxicology: an emerging discipline evolving from studies of ultrafine particles. Environ Health Perspect. 2005;113(7):823–39.
3. Shinohara N, Oshima Y, Kobayashi T, Imatanaka N, Nakai M, Ichinose T, Sasaki T, Kawaguchi K, Zhang G, Gamo M. Pulmonary clearance kinetics and extrapulmonary translocation of seven titanium dioxide nano- and submicron materials following intratracheal administration in rats. Nanotoxicology. 2015;9(8):1050–8.
4. van den Boogaard FE, Hofstra JJ, van't Veer C, Levi MM, Roelofs JJTH, van der Poll TS, Marcus J. Feasibility and safety of local treatment with recombinant human tissue factor pathway inhibitor in a rat model of *Streptococcus pneumoniae* pneumonia. PLoS One. 2015;10(5):e0127261.
5. Cho WS, Duffin R, Bradley M, Megson IL, MacNee W, Lee J, Jeong J, Donaldson K. Predictive value of in vitro assays depends on the mechanism of toxicity of metal oxide nanoparticles. Part Fibre Toxicol. 2013;10:55.
6. Morimoto Y, Izumi H, Yoshiura Y, Fujishima K, Yatera K, Yamamoto K. Usefulness of intratracheal instillation studies for estimating nanoparticle-induced pulmonary toxicity. Int J Mol Sci. 2016;17:165.
7. Nakanishi J, Morimoto Y, Ogura I, Kobayashi N, Naya M, Ema M, Endoh S, Shimada M, Ogami A, Myojyo T, Oyabu T, Gamo M, Kishimoto A, Igarashi T, Hanai S. Risk assessment of the carbon nanotube group. Risk Anal. 2015;35:1940–56.
8. OECD. Guidance on Sample Preparation and Dosimetry for Safety Testing of Manufactured Nanomaterials Series on the Safety of Manufactured Nanomaterials No. 36. ENV/JM/MONO(2012)40. 2012.
9. Dusinska M, Rundéen-Pran E, Schnekenburger J, Kanno J. Toxicity tests: in vitro and in vivo. In: Fadeel B, Pietroiusti A, Shvedova AA, editors. Adverse effects of engineered nanomaterials exposure, toxicology, and impact on human health. 2nd ed. London: Academic Press; 2017. https://doi.org/10.1016/B978-0-12-809199-9.00003-3.

10. Warheit DB, Laurence BR, Reed KL, Roach DH, Reynolds GM, Webb TR. Comparative pulmonary toxicity assessment of single-wall carbon nanotubes in rats. Toxicol Sci. 2004;77:117–25.
11. OECD. 2018. Guidance Document on Acute Inhalation Toxicity Testing. Series on testing and assessment no. 39. 2nd ed.
12. Hashizume N, Oshima Y, Nakai M, Kobayashi T, Sasaki T, Kawaguchi K, Honda K, Gamo M, Yamamoto K, Tsubokura Y, Ajimi S, Inoue Y, Imatanaka N. Categorization of nano-structured titanium dioxide according to physicochemical characteristics and pulmonary toxicity. Toxicol Rep. 2016;3:490–500.
13. Kobayashi T, Oshima Y, Tsubokura Y, Hashizume N, Ajimi S, Kayashima T, Nakai M, Sasaki T, Kawaguchi K, Imatanaka N. Effects of dose volume and delivery device on bronchoalveolar lavage parameters of intratracheally administered nano-sized TiO_2 in rats. Regul Toxicol Pharmacol. 2016;81:233–41.
14. Höhr D, Steinfartz Y, Schins RP, Knaapen AM, Martra G, Fubini B, Borm PJ. The surface area rather than the surface coating determines the acute inflammatory response after instillation of fine and ultrafine TiO_2 in the rat. Int J Hyg Environ Health. 2002;3:239–44.
15. Sager TM, Kommineni C, Castranova V. Pulmonary response to intratracheal instillation of ultrafine versus fine titanium dioxide: role of particle surface area. Part Fibre Toxicol. 2008;5:17.
16. Krug HF. Nanosafety research—are we on the right track? Angew Chem Int Ed. 2014;53:12304–19.
17. Morimoto Y, Horie Y, Kitajima S, Fukushima S, Takebayashi T. Comparison of data between intratracheal instillation and inhalation studies for estimation of harmful effects of manufactured nanomaterials. Nippon Eiseigaku Zasshi. 2013;68:161–7 (in Japanese). https://doi.org/10.1265/jjh.68.161.
18. Morrow PE. Possible mechanism to explain dust overloading of the lungs. Fundam Appl Toxicol. 1988;10(3):369–84.
19. Borm PJ, Schins RP, Albrecht C. Inhaled particles and lung cancer, part B: paradigms and risk assessment. Int J Cancer. 2004;110:3–14.
20. Greim H, Borm P, Schins JA, Donaldson K, Driscoll KE, Hartwig A, Kuempel E, Oberdörster G, Speit G. Toxicity of fibers and particles—report of the workshop held in Munich, Germany, 26–27 October, 2000. Inhal Toxicol. 2001;13:737–54.
21. Pott F, Dungworth DL, Heinrich U, Muhle H, Kamino K, Germann PG, Roller M, Rippe RM, Mohr U. Lung tumours in rats after intratracheal instillation of dusts. Ann Occup Hyg. 1994;38(inhaled particles VII):357–63.
22. Borm P, Cassee FR, Oberdörster G. Lung particle overload: old school—new insights? Part Fibre Toxicol. 2015;12:10.
23. Hasegawa-Baba Y, Kubota H, Takata A, Miyagawa M. Intratracheal instillation methods and the distribution of administered material in the lung of the rat. J Toxicol Pathol. 2014;3(4):197–204.
24. Brain JD, Knudson DE, Sorokin SP, Davis MA. Pulmonary distribution of particles given by intratracheal instillation or by aerosol inhalation. Environ Res. 1976;11:13–33.
25. Senoh H, Kano H, Suzuki M, Ohnishi M, Kondo H, Takanobu K, Umeda Y, Aiso S, Fukushima S. Comparison of single or multiple intratracheal administration for pulmonary toxic responses of nickel oxide nanoparticles in rats. J Occup Health. 2017;59:112–21.
26. Bergmann JD, Metker LW, McCain WC, Beall PA, Michie MW, Lee RB. Intratracheal instillation of zinc-cadmium sulfide (ZnCdS) in Fisher 344 rats. Inhal Toxicol. 2000;12:331–46.
27. Warheit DB, Webb TR, Sayes CM, Colvin VL, Reed KL. Pulmonary instillation studies with nanoscale TiO_2 rods and dots in rats: toxicity is not dependent upon particle size and surface area. Toxicol Sci. 2006;91(1):227–36.
28. Kobayashi N, Naya M, Endoh S, Maru J, Yamamoto K, Nakanishi J. Comparative pulmonary toxicity study of nano-TiO_2 particles of different sizes and agglomerations in rats: different short- and long-term post-instillation results. Toxicology. 2009;264:110–8.

29. OECD. Test Guideline 412. OECD Guideline for Testing of Chemicals. Subacute inhalation toxicity: 28-day study. 2017.
30. OECD. Test Guideline 413. OECD Guideline for Testing of Chemicals. Sub-chronic inhalation toxicity: 90-day study. 2017.
31. Tsubokura Y, Kobayashi T, Oshima Y, Hashizume N, Nakai M, Ajimi S, Imatanaka N. Effects of pentobarbital, isoflurane, or medetomidine– midazolam–butorphanol anesthesia on bronchoalveolar lavage fluid and blood chemistry in rats. J Toxicol Sci. 2016;41:595–604.
32. Kittel B, Ruehl-Fehlert C, Morawietz G, Klapwijk J, Elwell MR, Lenz B, O'Sullivan MG, Roth DR, Wadsworth PF. Revised guides for organ sampling and trimming in rats and mice—part 2. Exp Toxicol Pathol. 2004;55:413–31.
33. Shinohara N, Zhang G, Oshima Y, Kobayashi T, Imatanaka N, Nakai M, Sasaki T, Kawaguchi K, Gamo M. Kinetics and dissolution of intratracheally administered nickel oxide nanomaterials in rats. Part Fibre Toxicol. 2017;14:48.

Chapter 7
Sample Preparation and the Characterization for Intratracheal Administration

Kenji Kawaguchi, Kenji Koga, and Takeshi Sasaki

Abstract This chapter explains how to prepare stable nanomaterial dispersion samples and the characterization techniques. The explanation is focused on practical techniques rather than scientific studies. Several technical terms and definitions are explained and effective lab apparatuses are introduced for the better understanding. First, a standard sample preparation method with the typical experimental conditions is described and several actual nanomaterial examples (TiO_2, NiO, SiO_2, CeO_2, and ZnO) are introduced.

Keywords Nanomaterial · Intratracheal administration · Dispersion · Dynamic light scattering · Characterization · Secondary particle size

7.1 Introduction

This chapter provides a summary of the dispersion sample preparation methods used in intratracheal administration and the characterization techniques therefore, so that researchers and engineers engaged in related research and development can easily understand and learn the techniques and skills. Therefore, priority is given to explanations of practical techniques over detailed descriptions of scientific principles and fundamentals.

While a wide variety of nanomaterials have been developed and used in recent years, attention is being focused on nanomaterial toxicity assessment. As viewed internationally, however, there is yet no sufficiently efficient and rational framework established for the methods and criteria for nanomaterial assessment. In particular, animal tests by the inhalation exposure method so far used as the representative technique for toxicity assessment are impractical for application to each and every nanomaterial production lot from the perspectives of cost, time, and

K. Kawaguchi (✉) · K. Koga · T. Sasaki
Nanomaterials Research Institute, National Institute of Advanced Industrial Science and Technology (AIST), Tsukuba, Ibaraki, Japan
e-mail: k-kawaguchi@aist.go.jp; k.koga@aist.go.jp; takeshi.sasaki@aist.go.jp

technical difficulty among other factors. This study focuses on the intratracheal instillation method as an efficient test method complementary to the inhalation exposure method, and intends to investigate the technical development and effectiveness of the former method and to identify the criteria for (equivalence) ranges in which various nanomaterials are not rated differently in terms of toxicity regardless of their physicochemical differences, in order to develop an efficient and rational toxicity assessment technique.

This document is described on the basis of the results using some commercial apparatuses and materials. This, however, does not mean that we recommend these products or that they are the best products available.

7.2 Terms and Definitions

Some terms used in this chapter need explanation and definition. What follows provides a list of such terms along with explanations and definitions. For other general technical terms, etc., refer to relevant references or literature.

- Primary particles: Particles considered to be single particles showing no clear grain boundary as observed under an electron microscope, etc. Precise definition is difficult, and for some particles it may be difficult to tell whether they are primary particles or secondary particles. Do not confuse this term with "crystallite," which is a grain unit of single crystal grains in crystallographic analysis.
- Endotoxin: Also known as lipopolysaccharide and is a cell wall constituent of Gram negative bacteria. This causes adverse effects such as fever in animal tests. Prevent endotoxin contamination of test samples.
- Zeta (ζ) potential: Also known as "electrokinetic potential." This is the surface potential of an electric double layer that is formed on a solid particle-liquid solvent interface and moves along with particles in solvent. In a colloidal solution, this potential may be positive or negative. As a zeta potential has a greater absolute value, particles tend to be more stably dispersed due to electrostatic repulsive force.
- Dynamic light scattering method (DLS method): A technique reliably usable for measuring nanoparticle sizes in dispersion liquid. A laser beam is applied to a sample to measure the temporal fluctuation of the interference intensity of the scattered light from the sample particles. These intensity fluctuation depend on the Brownian motions of particles, and their Brownian motions are particle size-dependent. Such dynamic fluctuation are model-analyzed to determine particle sizes. Effective for approximately 1–1000 nm particle size measurement.
- Isoelectric point: When used in the context of particle dispersion, this term means the pH value for a zero zeta potential. A zeta potential is variable in response to the pH of the dispersion liquid (colloidal liquid). Generally speaking, with a pH value near the isoelectric point, dispersed particles tend to be destabilized due to the loss of zeta potential-induced electrostatic repulsion.

- Secondary particles: Aggregated particles consisting of agglomerated primary particles. Generally speaking, particles behave as such in this unit of secondary particles in environments including dispersion liquid. Note, however, that the bonding strength between primary particles may not always be strong and hence the size and form of secondary particles may easily be variable.

7.3 Main Lab Apparatuses and Techniques to Be Used

- Water purifying apparatus
    Bio type.
    Used to process tap water into endotoxin-free deionized water.
- Planetary ball mill
    Used for milling down to an appropriate particle size when there is no nanoparticle product commercially available in that size.
    Used in this experiment mainly to prepare crystalline silicon dioxide nanoparticles.
- Autoclave
    Used for high-temperature, high-pressure steam sterilization.
    Used to expose instruments and containers to 20 min of high-pressure saturated steam at 121 °C (boiling point of water under a pressure of 2 atm) for sterilization and endotoxin inactivation.
    In this experiment, endotoxin-free water purified using a water purifying apparatus is also autoclaved to double-ensure safety.
- Ultrasonic cleaner
    Desk top type with 42 kHz 180 W shall mainly be used.
    This apparatus is intended to generate ultrasonic vibration in a water tank to clean glass lab ware, etc., but is used in this experiment for sample-liquid dispersion.
- Ultrasonic homogenizer
    A dispersion apparatus with a throw-in type (20 kHz, 50 or 400 W) vibration probe directly dipped in the sample liquid.
    Provides a higher dispersion capacity than water tank-type ultrasonic cleaners and may cut fibrous/acicular primary particles lengthwise.
    Long-time use may cause the vibration probe to be chipped, resulting in impurity contamination of the sample liquid.
- Centrifuge
    Used for sample particle size classification or for solid-liquid separation during rinsing.
    100–$20,000 \times g$ is mostly employed.
- Precision balance
    Used for gravimetric analysis and weighing of raw samples.
    Minimum resolution of 0.01 mg.

- Dryer
  Used for drying and sterilizing instruments.
  With 15 W germicidal lamp, hot-air blow drying (room temperature + 40 °C).
- Scanning electron microscope (SEM)
  Field emission (FE) SEM with a high resolution of 1.0 nm (catalog value).
  Used for particle shape observation or for particle size distribution measurement of primary particles of large particle size.
- Energy dispersive X-ray spectrometer (EDX)
  Use in combination with the above-described SEM for quantitative analysis and surface analysis of elements bearing an atomic number greater than that of boron and contained in microportions (minimum dia. 10 nm) of samples.
  Used for sample composition analysis and impurity evaluation.
- Transmission electron microscope (TEM)
  Used for particle size distribution measurement of primary particles of samples.
  An accelerating voltage of 200 kV, a resolution of approx. 0.2 nm, equipped with EDX.
- X-ray diffractometer (XRD apparatus: X-Ray Diffraction)
  A powder X-ray diffractometer with a Cu tube source, equipped with a graphite monochromator. Thin film measurement capability with surface sensitivity enhancement by means of a glancing incident angle.
  Used for sample crystal structure identification and crystallinity evaluation.
- Specific surface area measuring apparatus
  BET specific surface area measuring apparatus for powder samples. Equipped with a sample pre-drying apparatus.
  Used for specific surface area measurement of a raw material powder or a sample obtained by drying dispersion liquid. The BET formula shall be used to calculate the total surface area of the sample from the nitrogen gas adsorption volume and determine the surface area per sample weight = specific surface area.
- Dynamic light scattering particle size analyzer (DLS method)
  Used to measure the particle size distribution and zeta potential of 1–1000 nm particles in dispersion liquid (secondary particle size distribution). Used in connection with an optional device for automatic isoelectric point determination.
- X-ray photoelectron spectroscopy (XPS)
  A surface sensitive spectrometer with a monochromatic X-ray (Al-Kα) source. Equipped with a high-efficiency positive and negative neutralizing mechanism for charge-up phenomenon using both electron shower and soft Ar-ion irradiation.
  Used for qualitative elemental analysis, semiquantitative elemental analysis, and chemical state information on the sample surface to the depth of several atomic layers, giving information of the surface modification and contamination properties of the sample particles.
- SEM/TEM sample preparation apparatus
  An apparatus used to spray dispersion liquid for dispersed fixation of relatively small agglomerations of sample particles on substrates (SEM) or on sample grids (TEM).

7.4   Standard Sample Preparation Method

7.4.1   Introduction

This section explains the standard sample preparation method in this study, based on the sample preparation procedure for titanium dioxide nanoparticles to be discussed in the next section. The standard sample preparation method presented in this section was used with partial modifications made to match the material properties of the various nanoparticles to be discussed in the next and subsequent sections.

7.4.2   Sample Preparation Procedure

7.4.2.1   Preparation of Solvent, Containers, and Other Materials

Normally, deionized water was used as a solvent. In principle, endotoxin-free aseptic deionized water is available from the bioproof water purifying apparatus used in this study. Still, this water was autoclaved for use as test solution solvent, to overcome the possibility of insufficient maintenance of the water purifying apparatus.

As for consumables such as micropipette tips and plastic containers for sample liquid preservation, γ-ray sterilized, disposable items were purchased and used as much as possible.

Before using the ultrasonic cleaner, its water tank shall be wiped using rubbing alcohol and filled with an appropriate amount of the above-described autoclaved deionized water.

In addition, as for instruments and containers for use in contact with the sample liquid, heat-resistant items were autoclaved, and non-heat-resistant items rubbed with alcohol, before use. Cleaned and dried instruments and containers were stored in dryers or UV-irradiated sterilization dryers.

Moreover, when the sample preparation procedure was established, the prepared test dispersion liquid was verified as endotoxin-free, using a technique known as the Limulus Amebocyte Lysate (LAL) test. In this study, a reagent called Pyrotell was used which has a sensitivity of 0.03 EU/mL (endotoxin unit).

If any change is made to the verified procedure, this test shall be performed again to ensure that the prepared sample is endotoxin-free.

In addition, when use was made of new glass sample bottles for ultrasonic dispersion or for temporary storage of sample liquid, boron impurities were detected which were probably derived from the glass residue generated during the bottle forming process. Accordingly, these bottles were ultrasonically cleaned and autoclaved before use, and were cleaned before reuse for a series of sample liquids prepared of the same raw material.

7.4.2.2 Dispersion Treatment

For an ultrasonic cleaner to produce an effective dispersion effect, a sample container must have a wall made of a hard material through which ultrasonic waves can pass with a low energy loss. Therefore, glass bottles shall normally be used as sample containers if they require ultrasonic dispersion treatment.

In addition, 50 mL glass sample bottles were used in 2- or 4-bottle sets for dispersion treatment because a liquid amount of 200 mL or less will suffice for ordinary intratracheal instillation studies, because the centrifuge initially used had a maximum capacity of 50 mL × 4 bottles, and because 50 mL glass sample bottles are commercially available at reasonable prices.

The required number of 50 mL glass sample bottles shall be manually shaken well, each filled with deionized water solvent and a sample weighed to meet the prescribed charge concentration. Before preparing a series of dispersion liquids of the same material, a trial preparation shall be performed to determine the ratio of the charge concentration and the final-product dispersion liquid concentration and estimate the charge concentration to obtain the target-concentration dispersion liquid.

Sample bottles well shaken until the content appears homogeneously mixed to the eye shall be set in the water tank of the ultrasonic cleaner for ultrasonic dispersion. If unfixed, sample bottles may jump around and fall down in the water tank during ultrasonic vibration. Test tube stands or any other means of fixation shall be used. The ultrasonic vibration in the water tank turns into a standing wave, whose vibration intensity varies depending on the location inside the water tank. A location with high dispersion efficiency shall be selected.

A large concentration gradient of nanoparticles in sample bottles will reduce the effect of ultrasonic dispersion. Accordingly, sample bottles shall be taken out and manually shaken at the intervals of 30 min during 2 h of ultrasonic dispersion treatment. After dispersion treatment, the dispersion liquid shall be centrifuged at $1000 \times g$ for 30 min to remove poorly dispersible coarse aggregated particles and subject the collected supernatant to DLS particle size analysis.

When an animal test requires intratracheal instillation, the test liquid shall be administered through a thin feeding tube. As for particle-size components DLS-measured to be 2 μm or more in diameter, the particle size distribution was observed to change after the passage of particles through the probe. In addition, it is empirically known that a dispersion liquid revealed by DLS measurement to have a clear particle size distribution of particles 1 μm or more in diameter is poor in long-term stability and prone to agglomeration.

Therefore, when DLS measurement results clearly reveal that the sample liquid centrifuged as described above contains particle-size components 1 μm or more in diameter, the sample liquid shall be ultrasonically dispersed again and centrifuged for coarse particle removal.

In this study, dispersion liquid samples shall be delivered to a testing agency within 1–2 days after preparation and shall be administered to test animals accord-

ing to a planned schedule. The testing agency shall be consulted with to ensure that samples are prepared in such a way as to minimize the number of days preceding the planned date of administration. Still, samples may be left unused for about 2–4 days. Hence, immediately before sample administration, each testing body subjected samples to redispersion treatment using an ultrasonic cleaner or to a combination of agitation using a magnetic stirrer and redispersion treatment using an ultrasonic cleaner.

7.4.2.3   Gravimetric Analysis

Sample dispersion preparation requires centrifugation and other treatments involving changes in concentration. Accordingly, the actual concentration of the final-product sample dispersion shall be measured by gravimetric analysis. The typical steps of the gravimetric analysis procedure used in this preparation procedure are as follows:

(a) Prepare three disposable 6 mL glass sample bottles, each without a cap fitted on, and measure their weights. For weight measurement, use a precision balance that reads down to 0.01 mg. To ensure measurement stability, read measurements to a precision of 0.1 mg. While determined to be approximately 6 g, empty 6 mL glass sample bottles showed a weight change of 0.1 mg or less after being dried as follows:

(b) Using micropipettes, take samples of 1–3 mL of well-dispersed sample liquid and inject them into the three glass sample bottles. Transfer the three sample bottles from the stainless steel vat into the drying oven for 2 or more hours of heated drying at 200 °C. To prevent sample liquid weight losses due to sudden boiling, the heating up to 200 °C shall be set and performed programmatically at the rate of approximately 5 °C/min. Alternatively, first set the drying oven to 80 °C, heat the samples for approximately 20 min, and set the heat-drying temperature to 200 °C.

(c) After heat-drying, leave the sample bottles to cool for approximately 30 min and measure their weights. The differences from the bottle weights taken in advance in Step (a) above are the sample weights. From the volumes of the sample liquid samples taken in Step (b), determine their mass concentrations by gravimetric analysis.

7.4.3   Sample Characterization

The following characterization measurements were performed for the sample dispersion prepared for animal testing and for the raw material powder as necessary.

7.4.3.1   Secondary Particle Size Measurement

For the measurement of the agglomerated particle size in dispersion liquid = "secondary particle size," a dynamic light scattering (DLS) particle size analyzer was used. In DLS particle size measurement, scattered light analysis is performed for the direct determination of the "Z-average particle size." In addition, the "number-based average particle size" and "volume-based average particle size" are calculated based on the scattering data obtained by the analyzer, as well as on the refractive index and viscosity of the dispersion medium and the optical extinction coefficient of the particles.

The Z-average particle size is a value directly determined from measurement data not dependent on material constants, but it is difficult to interpret the physical meaning and cannot be compared with other measurements. Hence, the corresponding number-based or volume-based value shall normally be adopted.

While the DLS method allows easy and quick measurement using small amounts of samples (~1 mL) and a commercially available apparatus, it has problems with high-concentration samples, such as the adverse effects of multiple scattering, and also has problems with a wide particle size distribution, such as a reduced validity of the analysis model. Therefore, use care with the reliability of measurement data.

7.4.3.2   Primary Particle Size Measurement

While the primary particle size of sample particles is difficult to define and measure precisely, the particle images obtained by electron microscopic observation were visually analyzed in this study. Depending on the particle size, the ease of analysis of the obtained images, and other factors, a SEM and a TEM were selectively used for particle size analysis.

Although there are commercially available image analysis software products equipped with automatic particle size determination, none was found capable of effective particle size determination when an image contains many particles overlapping each other, as in those obtained in this study. A conventional image editing software product (Adobe Photoshop) was used to visually determine particle boundaries and fit circles or ellipses to the images as shown in Fig. 7.1. Then, the images thus fitted with circles/ellipses were digitized, using scientific image processing freeware (Image-J), to take particle counts. The number of sampling particles is 500 and large enough for statistical accuracy.

7.4.3.3   Specific Surface Area Measurement

Generally speaking, a material surface has a high chemical activity and provides a starting point of reactions, such as adsorption or dissolution into the solvent. Therefore, the surface area per unit weight = "specific surface area" of a powder material provides important information for the comparison of material properties.
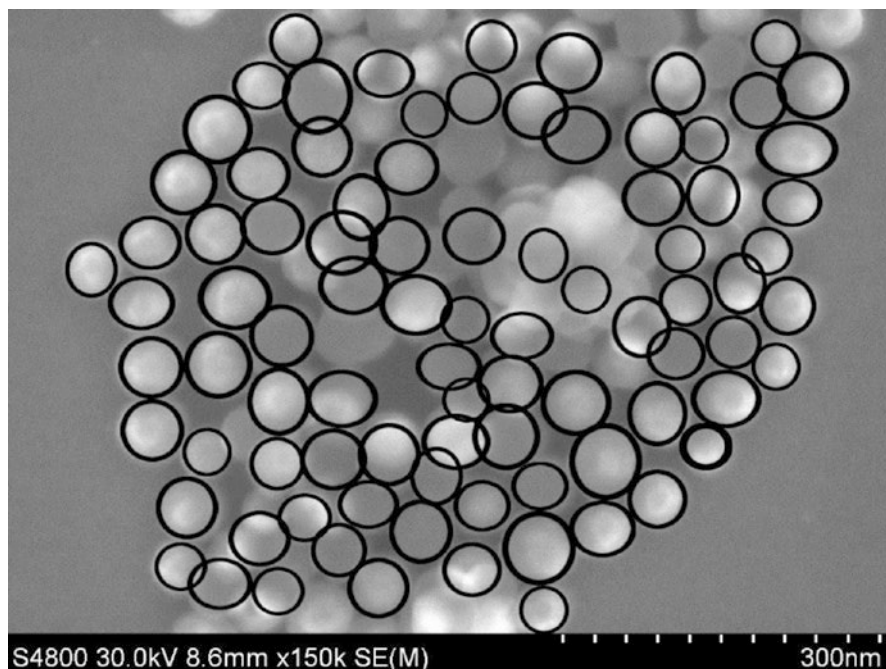
Fig. 7.1 An example of fitting ellipses to SEM image of silica nanoparticles

The measured results can be converted by a simple equation into a particle size using bulk density, assuming that particles are spherical. As for a sample revealed by electron microscopic observation not to contain particles of an extremely anisotropic shape, such as an acicular or a fibrous shape, the converted particle size determined from the specific surface area measurement matches well with the observation results of the primary particle size explained before, confirming that both measurement results are highly reliable values.

7.4.3.4 Impurity Analysis

While raw-material nanoparticles commercially available for use in reagents are normally supplied complete with a manufacturer-issued impurity analysis certificate, raw-material nanoparticles sold for uses such as industrial materials may not be clear about the type and added amount of impurity elements, such as a dispersant or flocculant added during the manufacturing process or a catalyst used for particle growth.

In addition, the unexpected ingress of impurities such as boron derived from glass sample bottles may occur during the sample preparation process as explained in Sect. 7.4.2.1.

Accordingly, the raw materials used for the first time in this study were subjected to an SEM apparatus for particle shape observation, as well as to an EDX apparatus connected to the SEM apparatus for quantitative fluorescent X-ray elemental analysis. Moreover, samples requiring high-sensitive or high-precision quantitative impurity analysis were analyzed by commercial services using an inductively coupled plasma atomic emission spectrometry (ICP-AES) or an inductively coupled plasma mass spectrometry (ICP-MS).

When particles needed to be checked for surface modification or contamination, an XPS apparatus was used as explained below.

7.4.3.5 Zeta Potential and Isoelectric Point Measurements

In this Project, deionized water solvent was often used for dispersion liquid preparation. Hence, zeta potentials provided a good indicator for dispersion liquid stability. Measurements were taken using the laser Doppler electrophoresis function equipped in the DLS measuring apparatus used for secondary particle size measurement described before.

In general, nanoparticles have a longer average interparticle distance at lower particle concentrations and tend to show higher dispersion stability. The zeta potential significantly contributory to stable dispersion is, however, variable depending on pH. Contrarily, therefore, a lower dispersion stability may result when a zeta potential has an extremely small absolute value near the pH 7 of deionized water solvent.

To observe these phenomena, the necessary samples were subjected to isoelectric point measurement for measuring the zeta potential while changing the pH of the dispersion liquid. This measurement can be automated by connecting an optional device to the above-described zeta potential measuring apparatus.

7.4.3.6 Surface Analysis

Samples requiring the information about surface-modification or surface contamination were subjected to XPS measurement. XPS is a measurement method that uses low kinetic energy photoelectrons with a short escape depth to perform qualitative and semiquantitative composition analysis, and valence state analysis to the depth of several atomic layers from the material surface. This method has a relatively long history, and there are reliable measuring apparatuses and analysis software available for XPS measurement. Moreover, an XPS method is capable to some extent of quantitative analysis of C, N, O, and other light elements that are difficult to quantitatively analyze by EDX or ICP-AES.

7.5   Titanium Dioxide Nanoparticles

In this study, titanium dioxide (TiO_2) was selected for the first test sample because it is expected to have a relatively low toxicity and because it is commercially available as nanoparticle products in different particle shapes and sizes. This section provides explanation, using as an example titanium dioxide nanoparticles including several ten nanometer-sized, spherical primary particles assumed for the standard sample preparation method explained in Sect. 7.4.

7.5.1   Selection of Dispersant

As explained above in Sect. 7.4.2, samples were basically prepared without adding additives other than the relevant nanomaterials and deionized water solvent from the perspective of minimizing the number of items to be considered for sample analysis and animal tests.

From a preliminary experiment, etc., titanium dioxide is, however, known to have an isoelectric point near pH 7. Its stable dispersion is difficult because it approaches the isoelectric point at a dilute concentration in deionized water solvent. Therefore, a dispersant was used.

As for the dispersant for the dispersion of titanium dioxide nanoparticles, it is necessary to select a dispersant as a chemical relatively low in impact on animals because the dispersant itself is contained in the solution administered to animals. Accordingly, disodium phosphate (DSP) ($Na_2HPO_4 \cdot 12H_2O$) was selected this time as the candidate dispersant for the stable dispersion of titanium oxide particles, based on the achievements made so far by collaborative research institutes conducting animal tests. Note that all DSP concentrations in this study were calculated based on the solid DSP weight including water of crystallization.

Three different types of solutions, namely, dispersant-free solution (deionized water), 1 mg/mL DSP solution, and 10 mg/mL DSP solution, were prepared and filled up to the liquid level of approximately 10 mL in each screw-capped glass tube bottle (capacity: 13.5 mL), so that the titanium dioxide nanoparticles to be tested would be suspended at a concentration of 1–10 mg/mL. Then, the screw-capped glass tube bottles containing the suspension were subjected to an ultrasonic cleaner for 3-h dispersion treatment for nanoparticle dispersion. Every 30 min in this period, the bottles with some particles settled on the bottom were manually shaken to keep the dispersion liquid homogeneous and improve the effect of ultrasonic dispersion. Immediately after the elapse of 3 h, the bottles containing the dispersion liquid were left to stand to observe the particle settlement status over time. This observation was repeated every

few hours until the elapse of 72 h, revealing that the 1 mg/mL DSP solution-based suspension was superior in dispersion stability. This result is similar to that of the DSP 2 mg/mL solution used in the procedural manual for the TiO_2 dispersion solutions obtained from the NEDO Project on "Research and Development of Nanoparticle Characteristics Evaluation Techniques." Moreover, a preliminary test was conducted at the Japan Bioassay Research Center, a collaborative research institute, to confirm that the DSP solution was low in impact on animals. Finally, the DSP 2 mg/mL solution was selected as the standard solvent for titanium dioxide samples.

7.5.2 Particle Size Distribution in Dispersion Liquid

A dispersion liquid with a titanium dioxide particle concentration of 10 mg/mL using DSP was prepared to the specifications by 3 h of ultrasonic dispersion treatment. In addition, this dispersion liquid was centrifuged at $2000 \times g$ for 3 min to remove supernatant. These dispersion liquids before and after centrifugation were evaluated for the particle size distribution therein, using a DLS particle size analyzer. The results are as shown in Fig. 7.2. The evaluation results of each are shown
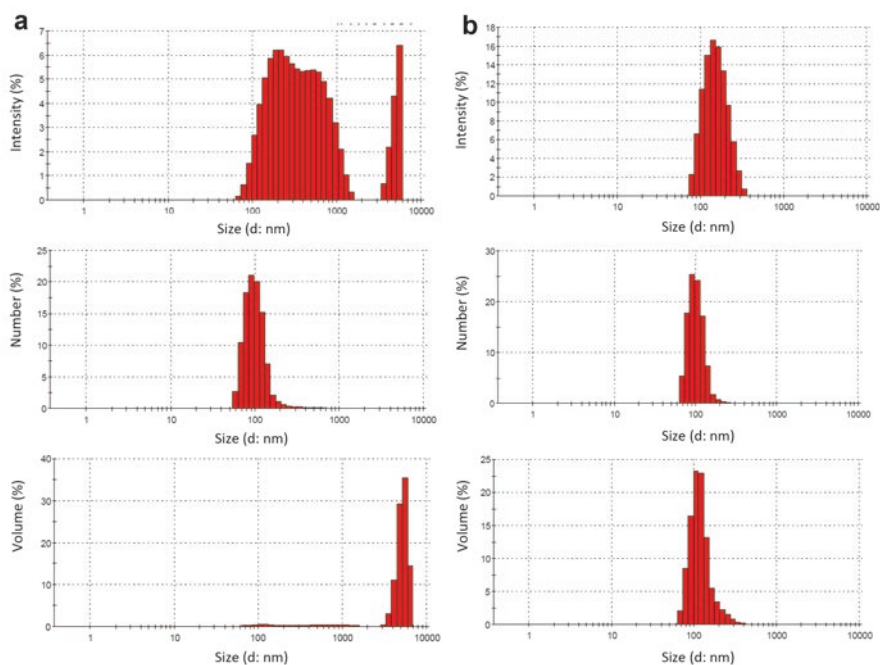
Fig. 7.2 Particle size distribution of TiO_2 dispersion before (**a**) and after (**b**) centrifugation from DLS

as three different types of distributions, i.e., scattering intensity-based distribution, number-based distribution, and volume-based distribution.

It turned out that when not subjected to centrifugation, the dispersion liquids contained 3 μm or larger huge agglomerated particles, although few in number. Meanwhile, it turned out that after 3 min of centrifugation at 2000 × g, 1 μm or larger huge agglomerated particles were removed.

From the perspective of comparing inhalation exposure and intratracheal instillation studies, it is considered desirable that titanium dioxide nanoparticles contained in the dispersion solutions for use in animal tests in this study have an aerodynamic diameter of 2 or 3 μm or less, at which peaks occur for particle deposition in rat lungs. In fact, however, the centrifuged dispersion solution (b) contained only agglomerated particles falling within this size range. In addition, an uncentrifuged dispersion liquid shows extremely poor dispersion stability because huge agglomerated particles settle out easily despite the existence of a dispersant/DSP. Meanwhile, a centrifuged dispersion solution remains stable for approximately a month. It turned out that even if some agglomerated particles settle out, the dispersed condition after centrifugation will be almost fully restored by approximately 10 min of sonication.

7.5.3   Method of Preparing the Dispersion Solution for Use in Animal Tests

As explained in the preceding section, centrifugation turned out to be useful for preparing high-stability dispersion liquids free from 3 μm or larger huge agglomerated particles. For a dispersion liquid to be usable in animal tests, it is important that the dispersion liquid should have high dispersion stability and should be prepared endotoxin-free to an expected concentration. Then, the titanium dioxide nanoparticle dispersion solutions actually used in animal tests were prepared according to the following steps:

1. DSP solution preparation

    Using the endotoxin-free ultrapure water described in section
    Prepare 2 mg/mL of DSP solution in a volumetric flask.

    The container used for DSP solution preparation does not necessarily need to be sterilized but must be rinsed with water to remove any contaminants from inside in advance. The same applies to the aforementioned volumetric flask.

    Sterilize the DSP solution by filtration through a filter. Use a filter unit such as a Nalgene Bottle Top Filter (pore size = 0.45 μm; compatible bottle mouth diameter = 45 mm; and filter container capacity = 500 mL).

    The DSP solution sterilized by filtration shall be autoclaved for additional sterilization.

2. Ultrasonic dispersion and centrifugation

    The dispersion liquid shall be subjected to dispersion treatment and centrifugation for coarse particle removal according to the standard procedure explained in Sect. 7.4.2.

3. Concentration check

The procedure explained in Sect. 7.4.2 shall be used to obtain the actual concentration of the sample, with the solid component weight excluded from that of DSP.

7.5.4 Dispersion Solution Stability

In some animal tests including multiple administration, titanium oxide nanoparticle dispersion solutions of different dilute concentrations may be administered at intervals over a certain period of time. Therefore, the long-term stability of the dispersion liquid for administration with various concentrations becomes extremely important. Then, a high-concentration titanium oxide nanoparticle dispersion liquid was prepared according to the procedure described in the preceding section and then diluted in DSP solutions to prepare five types of dispersion liquids, each different in TiO_2 concentration from the others. The dispersion liquids were subjected to a DLS particle size analyzer to determine the average particle size of agglomerated particles and monitor its change over time. Before measurement, the dispersion liquids were shaken well and then subjected to an ultrasonic cleaner for 10 min of dispersion. In addition, the dispersion liquids were left stored at room temperature.

Figure 7.3 shows the obtained results. It is shown that the dispersion liquids other than the one with the lowest concentration remained very stable and unchanged in particle size, although with small ups and downs, for nearly 2 months. Meanwhile, the lowest-concentration dispersion liquid (0.38 mg/mL) exhibited a tendency of gradual increase in particle size and showed a 15% increase from the initial particle size about 2 months later.

The foregoing reveals that long-term stable TiO_2 dispersion liquids of various concentrations can be prepared, using a DSP dispersant, to the requirements of animal tests, based on the standard sample preparation procedure explained in Sect. 7.4. Note that titanium dioxide particles with a spindle-shaped, needle-like, or otherwise highly anisotropic shape or with a primary particle size of several hundred nanometer or more are difficult to disperse and impossible to sufficiently disperse using a typical water tank-type ultrasonic cleaner and may require some modification, such as the use of an ultrasonic homogenizer, to the preparation procedure for each individual sample.

7.6 Nickel Oxide Nanoparticles

Nickel oxide (NiO) was considered as a material whose administration will produce a long-term persistent effect contrary to titanium dioxide explained in the preceding section. Nickel oxide nanoparticle reagents are, however, limited in the variety of commercially available products including those for industrial use. Accordingly, the following three different types of samples were prepared: fine nanoparticles 18 nm in size, relatively large nanoparticles 300 nm in size, and nanowire 20 nm dia. × 20 μm long (all values are catalog values).
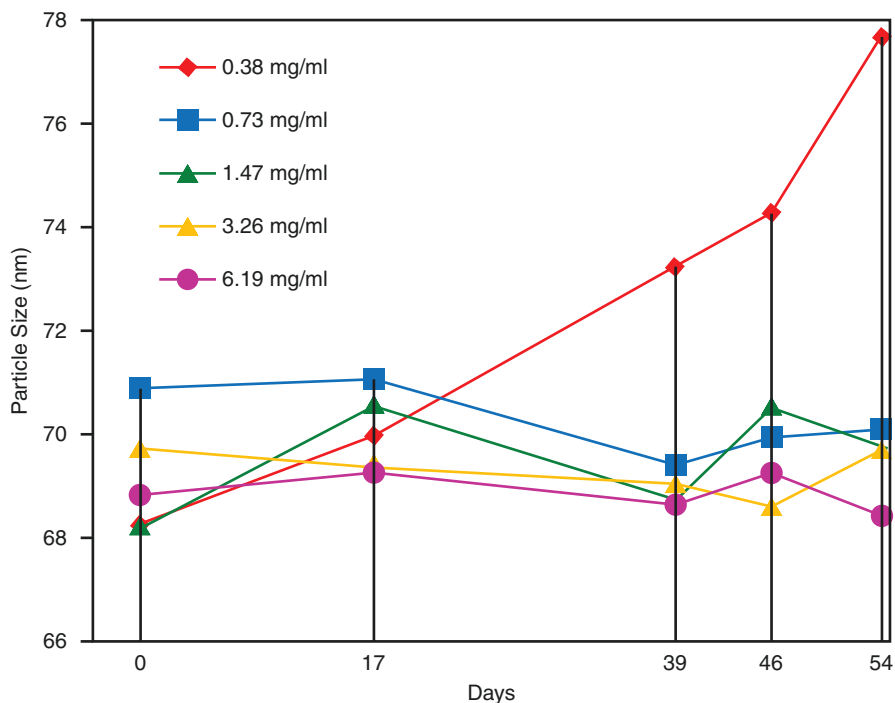
Fig. 7.3 Aging effect for particle size of TiO$_2$ dispersion

7.6.1   18-nm Fine NiO Nanoparticles

The standard sample preparation procedure explained in Sect. 7.4 was used with no substantial changes.

Prepared liquids contained no visible coarse particles with a particle size of 1 μm or more and experienced no particle agglomeration after being left to stand for about a week.

7.6.2   NiO Nanoparticles with a Particle Size of 300 nm

This type of sample is intended for industrial use and hence a polyacrylic acid-based polymer dispersant was added to prevent the agglomeration of particles during use. This dispersant is a water-soluble polymer and hence was subjected to deionized water cleaning to prevent unwanted effects on the animal tests in this study.

The procedure is specifically as follows:

1. The sample liquid with an approximate concentration of 6 mg/mL shall be subjected to an hour of ultrasonic dispersion treatment, followed by 10 min of centrifugation at $10,000 \times g$ for solid-liquid separation.
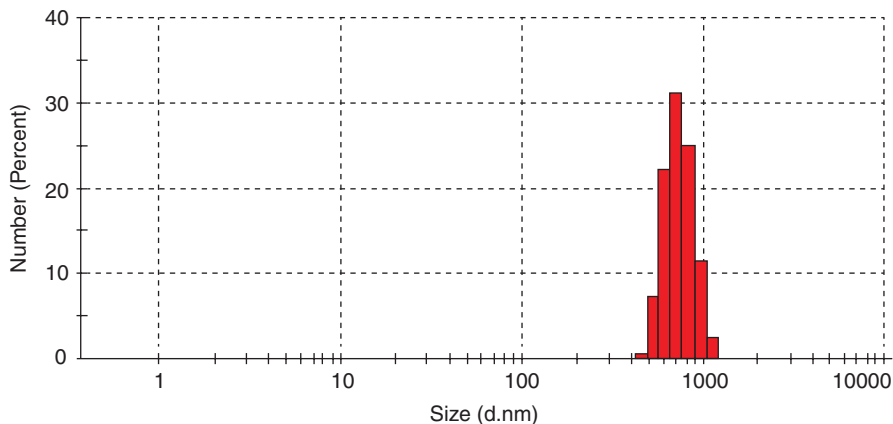
Fig. 7.4 Particle size distribution (number based) of cleaned NiO nanoparticles

2. The collected solid powder component shall have ultrapure water added until the original concentration is reached, then shall be subjected to 10–20 min of ultrasonic dispersion treatment, and shall finally be checked for sufficient redispersion.
3. Repeat the operations in Steps (1) and (2) above three times.

The cleaning effect of the dispersant was confirmed by the absence of organic components as observed by SEM and other methods.

While the raw material powder is also poor in long-term dispersion stability, the cleaned dispersion liquids, which removed the dispersant, are highly poor in long-term stability. Because a concentration gradient occurs in the liquid within several tens of minutes, the liquid should be subjected to ultrasonic dispersion immediately followed by quick administration.

There are no coarse particles in Fig. 7.4 obtained by a DLS particle size analyzer immediately after the liquid preparation. This confirms the absence of coarse agglomerated particles in a freshly prepared dispersion liquid.

7.6.3   NiO Nanowires

Generally speaking, wiry particles are very cohesive and their stable dispersion is difficult. This sample is no exception. Moreover, an EDX measurement revealed that this sample contains impurity elements, such as S and Na, which probably derive from the catalyst used in the production process.

Accordingly, although similar to the cleaning operation performed in Sect. 7.6.2 immediately above, the procedure used here consisted of an initial 10–20-min-long intensive dispersion treatment by a homogenizer and six cycles of cleaning oper-

ation. Consequently, the nanowires were partly broken and reduced into lengths approximately 1/10 of the catalog value, but were improved in dispersion stability to a degree sufficient for practical use, with the S impurity concentration reduced to the acceptable value of 5 wt% or less and the Na impurity concentration reduced to 1/10.

7.7 Silicon Dioxide (Silica) Nanoparticles

Silicon dioxide (SiO_2, silica) is known to have a crystallinity-dependent toxicity and provides an effective model samples checking nanomaterials for equivalence in size, shape, and crystallinity to compare their toxicities.

Amorphous silica nanoparticles are commercially available in different sizes and with various surface modifications. Meanwhile, crystalline silica nanoparticles are limited in the variety of commercially available products. Hence, samples were prepared of small-sized particles for this study.

7.7.1 Amorphous Silica Nanoparticles

Amorphous silica (a-silica) nanoparticle products are commercially available in different sizes and with various surface modifications. In this study, endotoxin-free deionized water-based dispersion liquids usable for animal tests were diluted to match the concentration appropriate for the intended test. Sample preparation involves only the dispersion treatment step of the standard sample preparation method, without the need for any additional complicated operation.

7.7.2 Crystalline Silica, and the Fine Particles Preparation and Crystallinity Evaluation

While crystalline silica (quartz) is known to exist in various crystal structures, α-quartz (crystal: quartz) was selected for this study because it is more widely used in society than any other alternative and because its particulates are easily available.

This α-quartz is, however, not commercially available as nanosized powder products. Therefore, as shown in Table 7.1, nanoparticle samples were prepared of two different types of crystalline silica, one being the natural mineral raw material powder (catalog average particle size: 1400 nm) used as the standard sample in the field of toxicity assessment and the other being particulate powder of synthetic crystal (catalog average particle size: 800 nm).

Table 7.1 Six crystalline silica (α-quartz) prepared for animal tests

Material	Process	Primary-D	Specific surface area-D	Secondary-D (number based)	Secondary-D (volume based)	Crystallinity (%)
A	Raw powder (catalog size, 800 nm)	–	163	–	–	82
A	Classification	218	120	222	1083	78
A	Milling and Classification	–	87	228	299	59
A	Milling, classification and alkali dissolution	–	15	60	86	61
B	Raw powder (catalog size, 1400 nm)	264	371	–	–	89
B	Classification	170	97	193	318	70

D means diameter in nm

The term "classification" in this table refers to the process of centrifugally separating and selecting nanoparticles equal to or smaller than a certain particle size. The term "milling" refers to the process in which a mixture of raw material powder and zirconia balls with ethanol added is wet-milled by a planetary ball mill, followed by sieving and separating the raw material powder, then by drying and removing the ethanol content, and finally dispersed in deionized water solvent using an ultrasonic homogenizer. The term "alkali dissolution" refers to the process in which a sample with some of its crystalline component amorphized due to the mechanical damage induced by the milling process is immersed in a 1 N-sodium hydroxide solution at 80 °C for approximately 20 h to reduce the amorphous component which is more alkali-soluble than the crystalline component. Note that these processes will result in a very poor yield.

Samples were evaluated for crystallinity, using the X-ray diffraction method. A typical method of crystallinity evaluation consists of a comparative calculation of the broad amorphous-derived peak intensity near $2\theta = 20$–$30°$ and the sharp crystalline peak intensity. The samples prepared in this study are very small in particle size, thereby making it difficult to estimate the amorphous peak intensity.

Then, using two different types of standard samples of known crystallinities (alumina and silica), internal standard measurement was performed twice, once on a combination of the standard alumina and the standard silica and the second time on a combination of the standard alumina and the sample, to compare the intensities of crystalline diffraction peaks alone for the purpose of crystallinity evaluation. When performing internal standard measurement of X-ray diffraction, it is important to

ensure that a test sample and a standard sample different in crystal particle size from each other are homogeneously mixed together without preferred orientation. It requires care to prepare measurement samples.

7.8 Cerium Dioxide/Zinc Oxide Nanoparticles

In this study, an intratracheal instillation method was developed and examined as a rapid screening test technique. At the same time, inhalation exposure studies used as the standard toxicity assessment technique were also conducted for comparative examination.

In an inhalation exposure study performed by spraying in air, the test animal shows lower nanoparticle uptake efficiency than in an intratracheal instillation study. Hence, long-term stable, large quantity, and high-concentration dispersion liquids are necessary for inhalation exposure studies. Samples were prepared of cerium dioxide (CeO_2) expected to be low in in vivo dissolution rate and zinc oxide (ZnO) expected to be high in in vivo dissolution rate; CeO_2 and ZnO, both expected to be high in toxicity, were selected as substances usable for comparison with the first-tested, supposedly low-toxicity titanium dioxide and likely to meet the required dispersion liquid characteristics.

7.8.1 Cerium Dioxide Nanoparticles

Cerium dioxide particulates are intended for abrasive powders for optic parts and similar applications. This type of nanoparticle is commercially and readily available in a wide variety of products. In our study, a commercial reagent with a catalog value of 10 nm in diameter (actually measured primary particle size: 8 nm) was used. Cerium dioxide nanoparticles disperse well in deionized water solvent. Stable dispersion liquids can be prepared for the cerium dioxide nanoparticles, without the need for any substantial change to the standard preparation procedure in Sect. 7.4. Because it was necessary to prepare large volumes of dispersion liquids for inhalation exposure studies at an approximate rate of 1 L/week, a small part of the standard procedure was modified for the work efficiency enhancement. Instead of repeating the manual shaking of 50 mL bottles after every 30 min of ultrasonic dispersion, 1 L of dispersion liquid was subjected to the stirrer shown in Fig. 7.5 for ultrasonic dispersion and agitation at the same time.

Dispersion liquids were centrifuged at $20,000 \times g$ for 30 min to remove supernatant and obtain a pale yellow clear stable dispersion liquid with a concentration of approximately 10 mg/mL. Figure 7.6 shows the results of typical particle size distribution measurement. DLS measurements gave secondary particle sizes, resulting

Fig. 7.5 A combination of mechanical stirrer and ultrasonic cleaner

in a certain degree of variations in average value between the prepared dispersion liquids. On the whole, however, the obtained results showed a narrow particle size distribution.

Moreover, centrifugally separated precipitate components were agitated and ultrasonically dispersed again at a charge concentration equal to that of the initial preparation, resulting in dispersion liquids equivalent in concentration and dispersion quality to the originals. It seems probable that settled particles were no different in primary particle size from dispersed particles but just happened not to be dispersed well during the dispersion treatment.

Cerium dioxide seems to adhere strongly to glass instruments used for sample preparation. Use care to avoid leaving hard-to-remove deposits on these glass instruments.
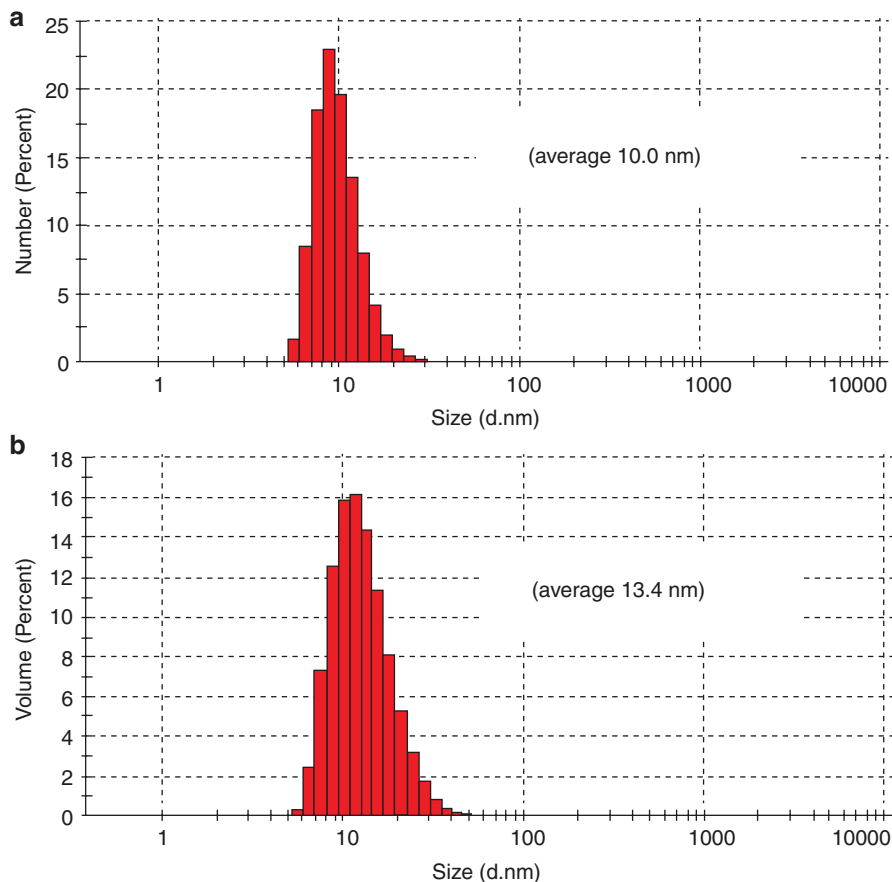
Fig. 7.6 Number-based (**a**) and volume-based (**b**) particle size distribution of CeO$_2$ dispersion from DLS measurements

7.8.2 Zinc Oxide Nanoparticles

Zinc oxide is also commercially and readily available in a wide variety of products for use as a wide-gap semiconductor for device applications. In this study, a commercially available slurry reagent with a particle size of 35 nm or less (catalog value) and dispersed at 50 wt% in deionized water solvent was used.

Just by diluting this dispersion liquid reagent to the required concentration without the need for any special process for removing coarse particles, sample liquids were obtained with a desirable particle size distribution shown in Fig. 7.7.
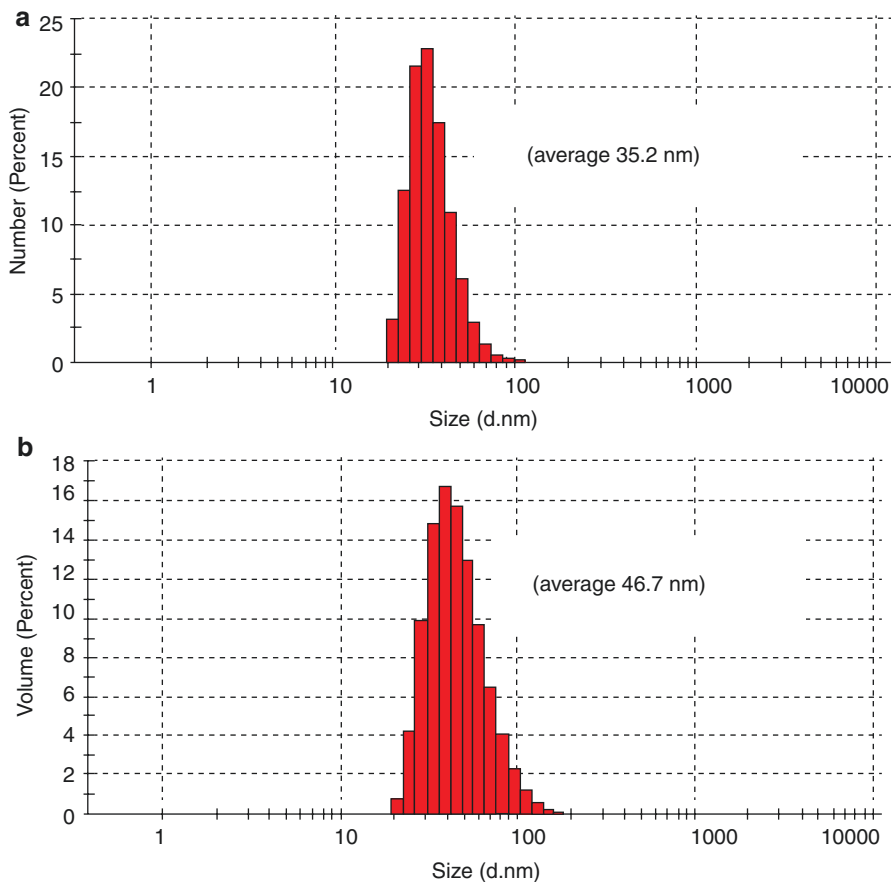
Fig. 7.7 Number-based (**a**) and volume-based (**b**) particle size distribution of ZnO dispersion from DLS measurements

Chapter 8
Development of Intratracheal Intrapulmonary Spraying (TIPS) Administration as a Feasible Assay Method for Testing the Toxicity and Carcinogenic Potential of Multiwall Carbon Nanotubes

Hiroyuki Tsuda and David B. Alexander

Abstract Multiwall carbon nanotubes (MWCNTs) are composed of multiple concentric one-atom thick graphene cylinders. The carbon-carbon bonds of graphene are exclusively sp^2, which gives MWCNT fibers their extraordinary properties. Production of MWCNTs is rapidly increasing because of their superiority over other materials. However, similarly to asbestos, MWCNTs are highly biopersistent in human tissues when inhaled and deposition in tissues causes sustained inflammatory reactions with the potential of inducing carcinogenesis. Several species of MWCNTs, including MWCNT-7, were shown to induce malignant peritoneal mesotheliomas after intraperitoneal administration in rats and mice; inhalation exposure to MWCNT-7 also induces bronchiolo-alveolar tumors in rats; and MWCNT-N, another type of MWCNT, was shown to induce both bronchiolo-alveolar tumor and pleural malignant mesothelioma in rats after administration by intratracheal intrapulmonary spraying (TIPS). Using the TIPS method, we recently found that another MWCNT, MWCNT-B, was carcinogenic to the lung, and that MWCNT-7 induced malignant pleural mesotheliomas as well as bronchiolo-alveolar tumors. Notably, despite the fact that the intraperitoneal injection studies that established the potential carcinogenicity of MWCNTs were published in 2008–2009, at the time of this writing only a single whole-body inhalation study of the toxicity of respirable MWCNTs has been reported. The lack of testing of these economically important, widely used, and potentially dangerous materials is due to the enormous expense of whole-body inhalation administration and to the very few facilities that are equipped to perform such studies. In contrast to whole-body inhalation testing that requires specialized inhalation facilities, the TIPS method uses commonly available equipment and techniques.

H. Tsuda (✉) · D. B. Alexander
Nanotoxicology Project, Nagoya City University, Mizuho-ku, Nagoya, Japan
e-mail: htsuda@phar.nagoya-cu.ac.jp; http://www.med.nagoya-cu.ac.jp/moltox.dir/nanotoxlab/

Consequently, TIPS administration can be widely used to test the carcinogenicity of respirable materials, promoting evaluation of the toxicity and carcinogenic potential of the numerous types of MWCNTs now being produced. For example, we are currently conducting further testing of MWCNTs using the TIPS method to assess the effect of the shape and physical properties of MWCNTs on their toxicity in the lung and pleura.

Keywords Intratracheal intrapulmonary spraying (TIPS) · Carbon nanotubes Chronic toxicity · Malignant mesothelioma · Lung tumors

8.1 Introduction

Multi-walled carbon nanotubes (MWCNTs) are composed of multiple coaxially arranged graphene cylinders and have diameters in the range of 2–100 nm (about 1/100,000 the diameter of a human hair). The carbon-carbon bonds of graphene are exclusively sp^2, which gives MWCNTs remarkable physical and chemical properties. MWCNTs have been produced that have 100 times the tensile strength of stainless steel and more than ten times the tensile strength of the strongest maraging steels. MWCNTs are chemically stabile and have greater thermal stability than diamonds. The delocalized π *electrons* of the sp^2 bonded carbons also give MWCNTs excellent electrical conductivity. At the same time, because of their hollow nature, MWCNTs are exceptionally light. These properties make MWCNTs ideal for use in a large number of commercial applications, including the manufacture of reinforced resins, semiconductors, lithium batteries, fuel cells, display screens, and a vast number of other products. Their use in electrical wiring, automobiles, boats, and commercial and military aircraft is also being planned.

The extent of MWCNT production raises concerns about the potential toxicological risks to workers, the public, and the environment [1–3]. The carcinogenic potential of MWCNTs was first reported in 2008 and 2009 when intraperitoneal and intrascrotal injection of MWCNT-7 (MITSUI [now Hodogaya]) in p53 heterozygous mice and Fisher 344 rats was shown to induce mesotheliomas [4, 5]. Further intraperitoneal injection studies and a later nose-only inhalation study supported the initial findings that MWCNT-7 is a potential carcinogen [6–8]. Based in part on these results, the International Agency for Research on Cancer (IARC) classified MWCNT-7 as a Group 2B agent, sufficient evidence of carcinogenicity in animals and possibly carcinogenic to humans, however, the working group concluded that single wall CNTs (SWCNTs) and MWCNTs excluding MWCNT-7 were not classifiable as to their carcinogenicity to humans [9, 10]. Yet, as can be seen in Table 8.1, at least some other types of MWCNTs are likely to be possibly carcinogenic to humans.

Intraperitoneal injection of a test material for initial testing of its potential carcinogenicity is sensitive and also relatively simple and inexpensive. However, although intraperitoneal injection has been extensively used for the assessment of potential

Table 8.1 Carcinogenesis studies of MWCNTs

Route	MWCNT	Induced tumor		
		Animal	Histology	References
i.p.	MWCNT-7	Mouse[a]	Perit-MM[b]	Takagi et al. [5, 8]
i.p.	MWCNT[c]	Rat	No tumor	Muller et al. [12]
i.p.	MWCNT-7	Rat	Perit-MM	Sakamoto et al. [4]
i.p.	MWCNT-7 NT50a[d], NT50b[d], NT145[d]	Rat	Perit-MM	Nagai et al. [6]
i.p.	MWCNT(A–D)[e]	Rat	Perit-MM	Rittinghausen et al. [13]
Inhalation	MWCNT-7	Mouse	BAT[f,g]	Sargent et al. [7]
Inhalation	MWCNT-7	Rat	BAT[f,h]	Kasai et al. [11]
TIPS[i]	MWCNT-N	Rat	BAT[f] and Pleu-MM[j]	Suzui et al. [14]
TIPS[i]	MWCNT-7	Rat	Pleu-MM[j]	Manuscript submitted
TIPS[i]	MWCNT-B	Rat	BAT[f]	Manuscript submitted
TIPS[i]	MWCNT-A	Rat	Inconclusive	Manuscript submitted

[a]p53^{+/−} mouse
[b]Peritoneal malignant mesothelioma
[c]Shorter than MWCNT-7 (0.7 μm in length)
[d]NT50a: 50 nm diameter, 5.3 μm length; NT50b: 50 nm diameter, 4.6 μm length; NT145: 145 nm diameter, 4.3 μm length
[e]Four different MWCNTs. Fiber characteristics are shown in Table 2 in Rittinghausen et al. [13]
[f]Bronchiolo-alveolar tumors (adenoma and/or carcinoma)
[g]Nose-only administration: MWCNT-7 is given after treatment with benzo(a)pyrene (Promotion of lung carcinogenesis)
[h]Whole-body administration
[i]Intratracheal intrapulmonary spraying
[j]Pleural malignant mesothelioma

carcinogenicity of fibers, metals, and other dusts [15–17], the carcinogenicity of materials that test positive needs to be confirmed using administration by routes that are relevant to humans. For respirable materials, the administration route must be via the airway. Notably, at the time of this writing, which is 10 years after the first published report of the potential carcinogenicity of MWCNTs, only a single carcinogenicity study of MWCNTs using whole-body inhalation has been reported: MWCNT-7 was found to induce bronchiolo-alveolar tumors [11]. The lack of testing of these widely used potential carcinogens by whole-body inhalation is due to the enormous expense of whole-body inhalation administration and to the very few facilities that are equipped to perform such studies. Given the extensive commercial use of MWCNTs and their potential risk to workers, the general population, and the environment, it is clear that risk assessment of MWCNTs by whole-body inhalation testing is inadequate.

Because of differences in the physical properties of the various MWCNTs being produced, the toxicities of different MWCNTs in the lung and pleura can differ. Consequently, it is important to carry out risk assessment studies for each type of MWCNT being produced. However, as pointed out above, whole-body inhalation

is unequal to the task of testing the extensive number of MWCNTs (and other respirable, potentially carcinogenic materials) in commercial production and use. Consequently, MWCNTs are being introduced into the environment without any assessment of their potential toxicities. Therefore, another method is needed for toxicity and carcinogenicity testing of respirable materials. Accordingly, to enable widespread testing of the toxicity and carcinogenic potential of MWCNTs and other respirable materials, we are establishing intratracheal intrapulmonary spraying (TIPS) as an alternative to whole-body inhalation testing. Using TIPS, we have shown that MWCNT-N (Nikkiso) induces bronchiolo-alveolar tumors and malignant pleural mesothelioma in rats [14], and more recently we have shown that in rats MWCNT-7 induces malignant pleural mesotheliomas as well as bronchiolo-alveolar tumors [manuscript submitted] and that a third type of MWCNT is also carcinogenic in rats [manuscript submitted]. Available data from in vivo carcinogenicity studies of MWCNTs are summarized in Table 8.1.

8.2   Development of the TIPS Method for Carcinogenicity Testing of MWCNT Fibers

8.2.1   Determination of a Vehicle Suitable for MWCNTs

We compared the amount of inflammatory cell infiltration, toxicity to lung alveolar cells, and dispersion efficiency of three different vehicles: 0.1% Tween-20, 1% sucrose +1% hydrogenated castor oil, and 0.5% Pluronic F68 (PF68). PF68 showed the best performance among the three vehicles tested (Table 8.2). We then conducted dosing regimen trials, including administration once every other day for 2 weeks (8 doses) and once every other week for 24 weeks (13 doses). We found that short-term and extended administration periods were comparable.

Table 8.2 Comparison of dispersant

| Dispersant added to saline	Inflammatory cell infiltration	Toxicity to alveolar cells	Dispersion efficiency
0.1% Tween 20	+++	±	+
1% Sucrose + 1% HC-40[a]	+	++	+++
0.5% Pluronic F68 (PF68)[b]	+	±	+++

[a]HC-40: hydrogenated castor oil 40
[b]PF68: polyoxyethylene-polyoxypropylene block copolymer (a non-ionic and non-toxic surfactant) [18]

8.2.2   Administration of MWCNTs Using TIPS

MWCNTs can be delivered deep into the lung using a microsprayer (Fig. 8.1a) ([19]: microsprayers are available from DIMS, Institute of Medical Sciences, Ichinomiya, Aichi, Japan). Anesthetized rats are placed on an intubation platform held at an angle of 60°. The mouth is held open by fixing the two cranial incisor teeth with a rubber band and pulling the tongue lightly with tweezers (Fig. 8.1b). A light beam placed on the chest wall brightens the pleural cavity, enabling the administrator to see the vocal cords and trachea (Fig. 8.1c). During inspiration the microsprayer is inserted through the vocal cords into the trachea and the suspension fluid is sprayed into the lungs. After administration, the rat is held gently with the head up for about 1 min to prevent regurgitation of the administered suspension. Using this method, administration once every other day for 2 weeks delivers the test material throughout each of the five lobes of the rat lung (Fig. 8.2). Microscopically, administered MWCNT fibers are evenly distributed in the lung (Fig. 8.3).
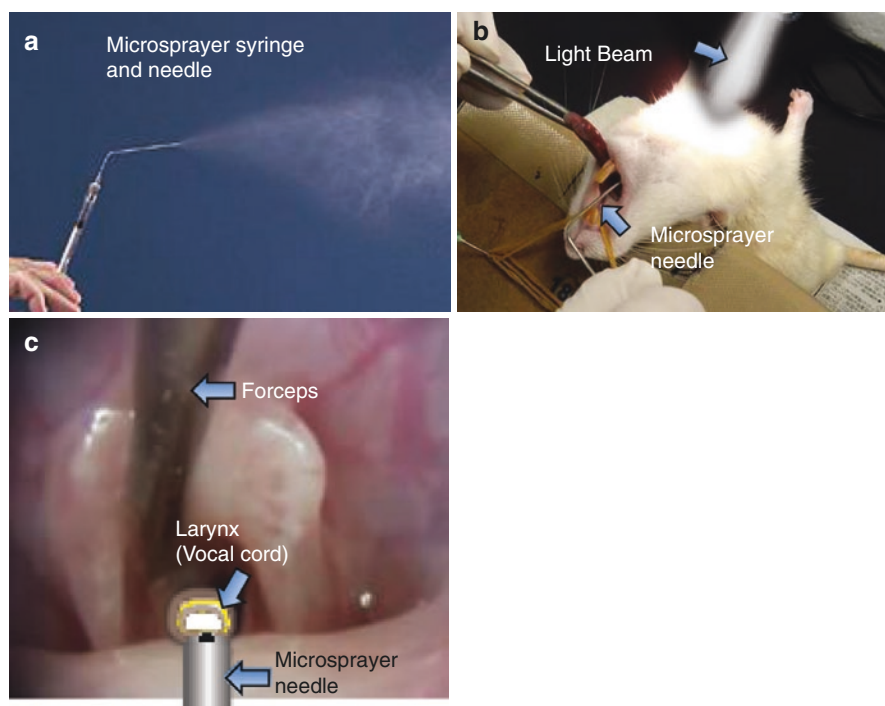
Fig. 8.1 The TIPS method. (**a**) Intratracheal aerosolizer. (**b**) Method for inserting the aerosolizer into the trachea (see the text). (**c**) A view of the trachea through the opened mouth. During inspiration the glottis opens and the aerosolizer is inserted into the trachea through the beam-lightened vocal cords (arrow)
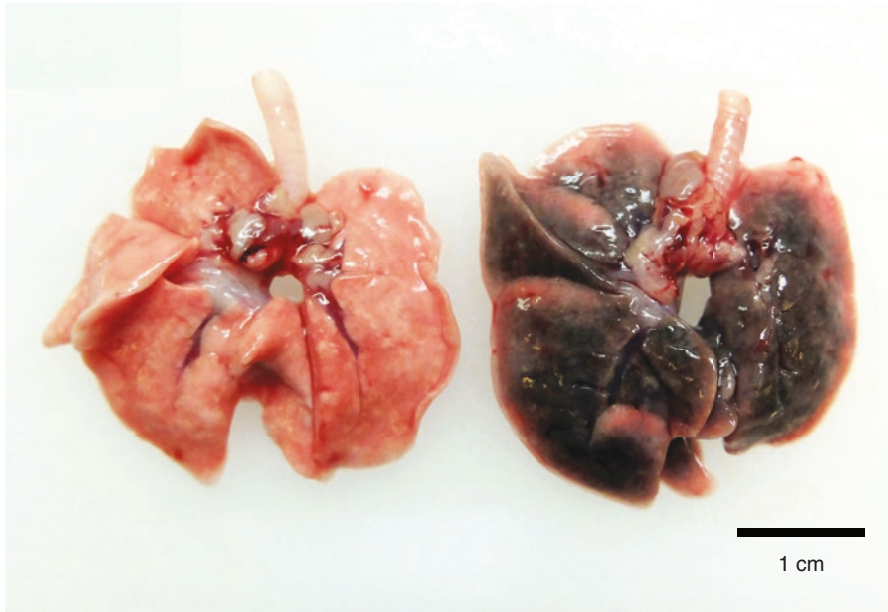
Fig. 8.2 Macroscopic view of a lung administered MWCNT by the TIPS method. Left: A lung treated with the vehicle. Right: The lung of a rat that received 8 doses of MWCNT-N by TIPS administration at 1 mg/rat. The MWCNT fibers are distributed throughout the entire lung
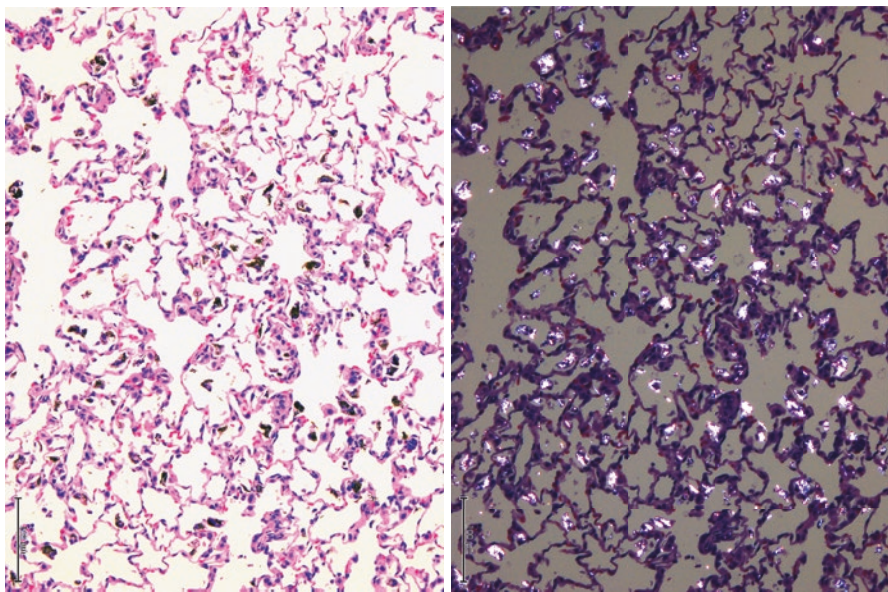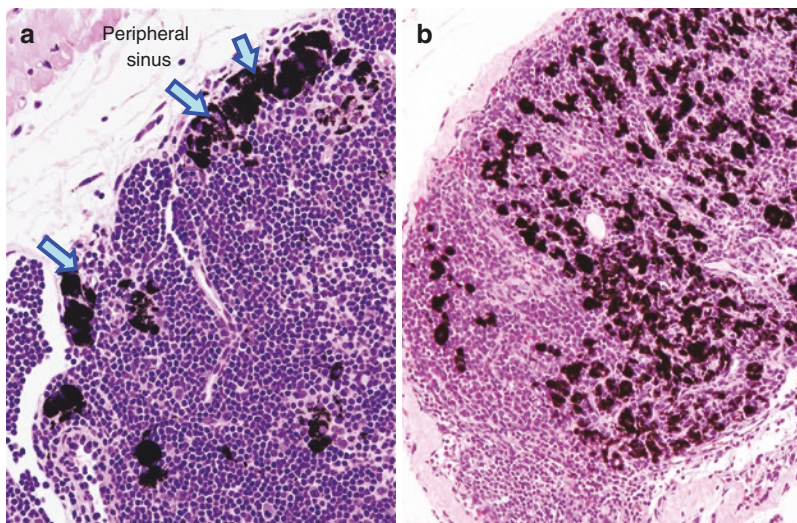

Fig. 8.3 Microscopic view of a lung administered MWCNT by the TIPS method. Left: The lung of a rat administered MWCNT-A by TIPS and killed 12 weeks after the final TIPS administration. Right: Polarized lens view. MWCNT fibers are spread throughout the entire field; fibers can be clearly recognized using polarized light microscopy

8.2.3 Acute Changes

MWCNT-7 (40 layers, 50–60 nm in diameter, 5–20 μm in length), MWCNT-N (30 layers, 20 nm in diameter, 2–20 μm in length), and crocidolite asbestos were suspended in saline containing 0.5% Pluronic F68 and administered to rats using TIPS at a dose of 250 μg/rat every other day over 9 days (5 doses, total 1.25 mg/rat) [20]. Rats were killed 6 h after the last TIPS administration. At the time of sacrifice, pleural lavage fluid (PLF) was collected by injecting 10 mL of RPMI 1640 into the pleural cavity through the left side of the diaphragm, gently massaging the thoracic wall, and collecting the fluid through the right side of the diaphragm. The PLF was centrifuged and the supernatant was stored at −80°, and the pellet was processed for histopathological examination (Fig. 8.4a). The PLF cell pellet was used to analyze the inflammatory cell population of the pleural cavity and fiber translocation into the pleural cavity. Crocidolite asbestos, MWNCT-7, and MWCNT-N caused inflammation in the lung and pleural cavity. In the lung, the majority of MWCNT fibers were observed in alveolar macrophages (see Fig. 8.3). Spotty foci of alveolar epithelial cell proliferation were observed. A considerable amount of MWCNT fibers were found in the peripheral sinuses of the parabronchial and mediastinal lymph nodes (Fig. 8.5a). A small amount of MWCNT fibers was also found in the PLF cell pellet (Fig. 8.6). These results clearly indicate that the administered materials: (1) reached deep into the terminal alveoli and were distributed throughout all five lobes of the lung; (2) were mostly phagocytosed by macrophages; and (3) translocated to the lymphatic system and pleural cavity.
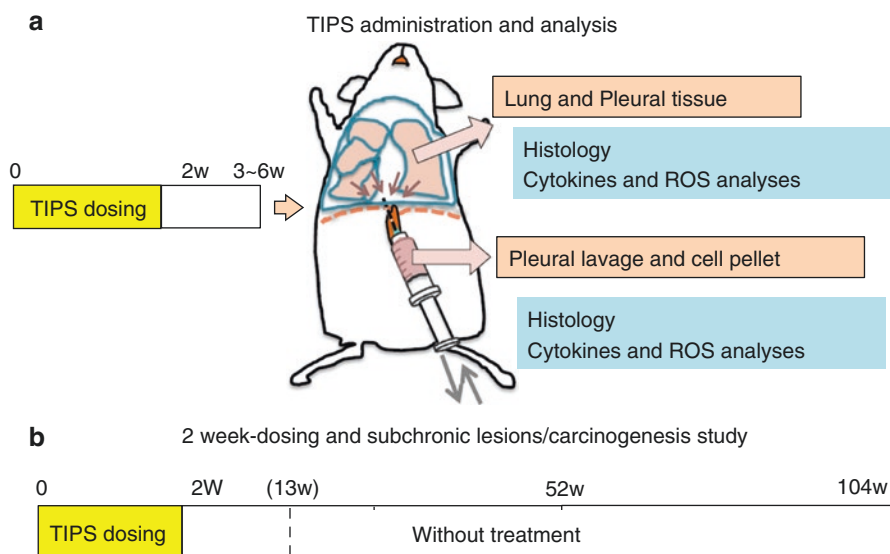
Fig. 8.4 Experimental protocol. (a) Animals used for toxicity and carcinogenicity testing are administered the test material by TIPS. The excised lung and pleural lavage fluid (PLF) are histopathologically and biochemically analyzed. (b) An example of the administration and observation periods. In this panel, animals are administered materials by TIPS once every 2 days for 2 weeks (8 doses) and observed for 2 years without further treatment. Interim sacrifices can be made at suitable times, for example, at 11 and 50 weeks after the final TIPS administration

Fig. 8.5 Microscopic view of a mediastinal lymph node. The mediastinal lymph node of a rat administered MWCNT-N using TIPS and killed 6 h after the final TIPS administration (**a**) or 107 weeks after the final TIPS administration (**b**). The MWCNT-N fibers enter the peripheral sinus through lymphatic vessels and afterwards move into the lymphatic medulla
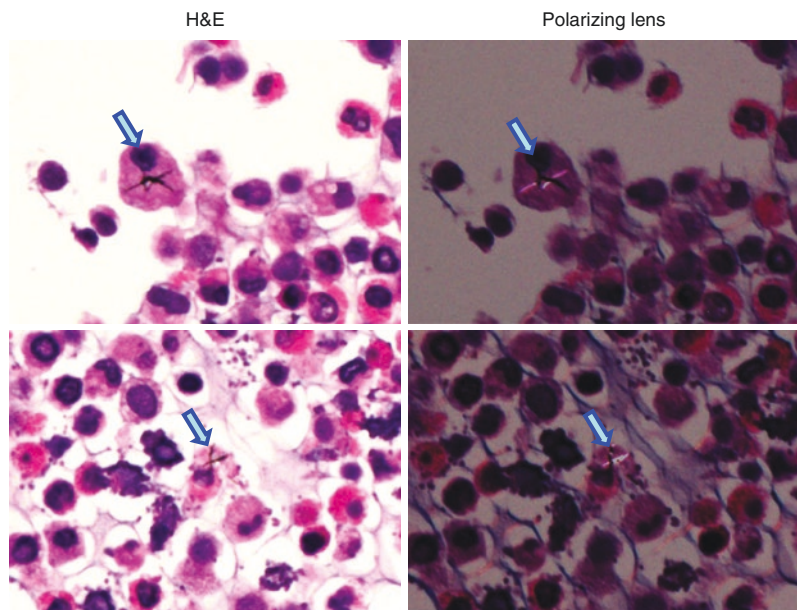
Fig. 8.6 Microscopic view of a pleural lavage fluid cell pellet. The cell pellet obtained from the pleural lavage fluid of rats killed at 6 h after the final TIPS administration of MWCNT-N. The cells are a mixture of inflammatory cells such as macrophages, neutrophilic cells, acidphilic cells, and lymphocytes (left). Some macrophages contain MWCNT fibers in the cytoplasm, as shown in the polarized lens view (right, arrows)

8.2.4   Subchronic Changes

We extended the administration period to once every 2 weeks over a 24-week period to determine whether administration of MWCNT over a longer period of time would cause lesions similar to those that developed after short-term administration. In order to acquire more information about different types of MWCNTs we used two different MWCNTs (provided by company C): MWCNT-A was composed of 213 layers and was 150 nm in diameter and 8 μm in length; MWCNT-B was composed of 15–18 layers and was 15 nm in diameter and 3 μm in length. MWCNT-A forms aggregates of rigid needle-like structures and MWCNT-B is thin and flexible and forms tangled masses. The MWCNTs were administered by TIPS at a dose of 125 μg/rat once every 2 weeks for 24 weeks (13 doses; total 1.625 mg/rat) and the rats were killed 24 h after the last TIPS administration [21]. Both types of MWCNT caused inflammation in the lung comparable to the lesions caused by the 2 weeks administration of MWCNT-N and MWCNT-7. MWCNT-A, but not MWCNT-B, translocated into the pleural cavity and was found deposited in both the parietal (primary site of deposition) and visceral mesothelium. Fibrosis and mesothelial proliferation was associated with MWCNT-A deposition in the mesothelium. In addition, levels of IL-18 were elevated in the PLF of MWCNT-A-treated rats. In the lung tissue, both MWCNT-A- and MWCNT-B-treated rats had elevated levels of inflammatory cytokines: CCL2, CCL3, CXCL1, CXCL2, CXCL10, IL-1α, and IL-1α. Induction of these cytokines was higher in MWCNT-B-treated rats than in MWCNT-A-treated rats. The lung tissue of MWCNT-B-treated rats also had elevated levels of IL-18. In addition, MWCNT-B-treated rats had higher levels of 8-hydroxydeoxyguanosine adducts in the lung tissue. Overall, the lesions induced after short term and extended administration of MWCNTs by TIPS were comparable.

### 8.2.5   Administration of Vehicle and Noncarcinogenic Material

In a study comparing the short-term toxicity of potassium octatitanate fibers, titanium dioxide nanoparticles, and MWCNT-7 [22], two types of vehicles were used, saline and saline containing 0.5% PF68. Rats were administered material by TIPS once every other day for 2 weeks (8 doses). Four weeks after the final TIPS administration, there were no differences between either of the vehicle control groups and the untreated control group in any of the measured parameters in the lung and pleural cavity. In another study comparing the short-term toxicity of DWCNTs with MWCNT-7 [23], the vehicle was saline containing 0.5% PF68. Again, rats were administered material by TIPS once every other day for 2 weeks (8 doses). Six weeks after the final TIPS administration, there were no differences between the vehicle control group and the untreated control group in any of the measured parameters in the lung and pleural cavity. In a third study, transgenic Hras rats (tumor prone) were given no treatment or 0.2% N-nitrosobis(2-hydroxypropyl)

amine (DHPN) in the drinking water for 2 weeks, to initiate lung tumors, and then administered zinc oxide nanoparticles (nZnO) by TIPS at doses of 125 and 250 μg/rat once every 2 weeks for 12 weeks (7 doses; total 0.875 and 1.75 mg/rat) [24]. Three days after the final TIPS administration the Hras rats were sacrificed. There was no evidence of tumor promotion in either the vehicle or nZnO-treated rats. In this experiment, epithelial hyperplasia of the terminal bronchioles was found in the nZnO-treated rats. In a second experiment, wild-type rats were given no treatment or 0.2% *N*-nitrosobis(2-hydroxypropyl)amine (DHPN) in the drinking water for 2 weeks followed by TIPS administration of nZnO at a dose of 250 μg/rat once every 2 weeks for 12 weeks (7 doses; total 1.75 mg/rat) [24]. As with the Hras rats, nZnO-treated rats developed epithelial hyperplasia of the terminal bronchioles. These lesions completely disappeared by 12 weeks after the final TIPS administration. Again, there was no tumor promotion in the vehicle or nZnO-treated groups. Finally, in a 2-year study comparing the toxicity of potassium octatitanate fibers with anatase titanium dioxide nanoparticles (a-nTiO$_2$) and MWCNT-7, rats were administered material at doses of 31.25 and 62.5 μg/rat by TIPS once every other day for 2 weeks (8 doses; total doses of 0.25 and 0.5 mg/rat), and then followed for 2 years without further treatment [manuscript submitted]. There was no indication of carcinogenesis in either the vehicle control or a-nTiO$_2$ groups. These studies demonstrate that TIPS is not toxic to rats and does not promote carcinogenesis.

8.3 Use of the TIPS Method to Assay the Toxicity of MWCNTs

Based on the findings that TIPS administration of MWCNT-7 and MWCNT-N, which is similar in size and physical properties to MWCNT-7, resulted in acute inflammatory lesions in the lung and pleural cavity, MWCNT-N was administered to male rats by TIPS at a dose of 125 μg/rat every other day for 2 weeks (8 doses; total 1.0 mg/rat) [14]. The rats were then observed without further treatment for 107 weeks (Fig. 8.4b). At the end of the experiment, the lung tissue showed extensive chronic inflammation with irregular thickening of the alveolar wall, with tumors developing in approximately half of the treated rats. The large majority of the MWCNTs still present in the lung were phagocytosed by alveolar macrophages in granulation tissue; however, even 2 years after administration of the MWCNT, free macrophages containing phagocytosed MWCNT fibers were found in the alveoli (Fig. 8.7). MWCNT-N fibers were also found in the parenchyma tissue and lymph nodes of the mediastinum (Fig. 8.5b).

The combined incidence of bronchiolo-alveolar adenoma and adenocarcinoma (Fig. 8.8a, b) was 14/38 ($p < 0.01$). The incidence of malignant mesothelioma of the pericardium and visceral pleura (Fig. 8.9a, b) was 6/38 ($p < 0.05$). The combined incidence of pulmonary and pleural tumors was 20/38 ($p < 0.01$). Neither pleural mesothelioma nor pulmonary tumors were observed in the control groups (untreated group and vehicle-administered group) (0/28) [16].
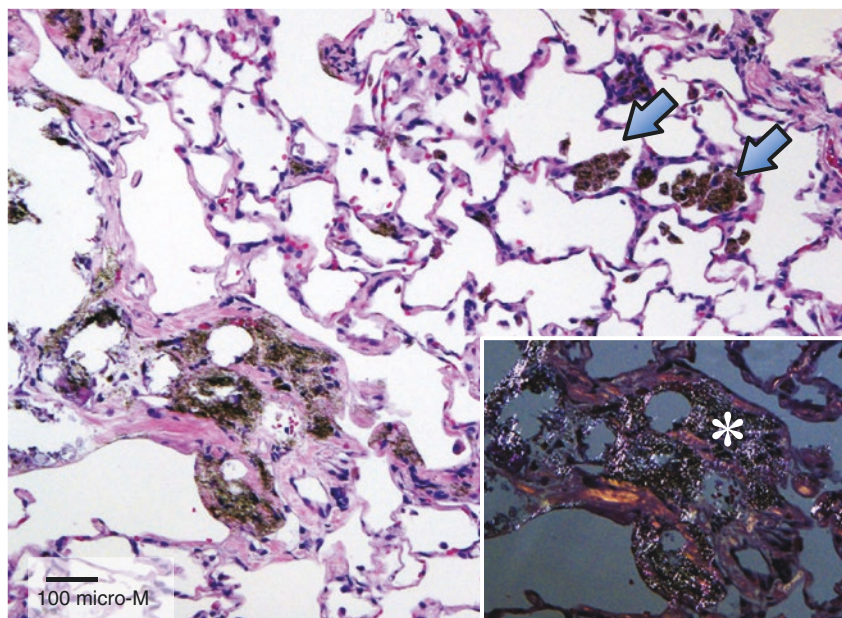
Fig. 8.7 Microscopic view of a lung administered MWCNT-N. A large amount of the MWCNT fibers in the lung are confined in fibrotic granulation tissue (see area marked by the asterisk in the polarized lens view). Free alveolar macrophages with phagocytosed MWCNT-N can also be seen (arrows)
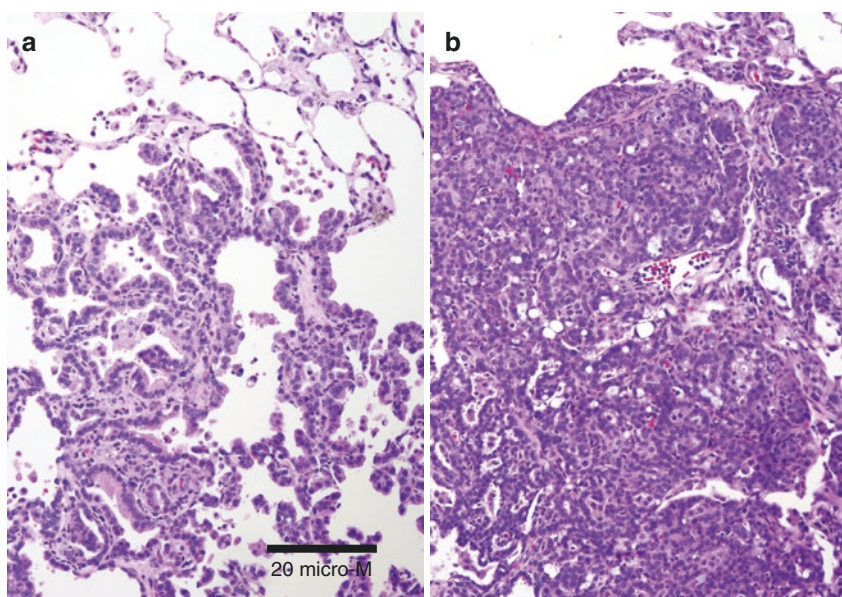
Fig. 8.8 Microscopic view of lung tumors in rats administered MWCNT-N. (**a**) Bronchiolo-alveolar adenoma and (**b**) bronchiolo-alveolar carcinoma in a rat administered MWCNT-N and killed at week 109
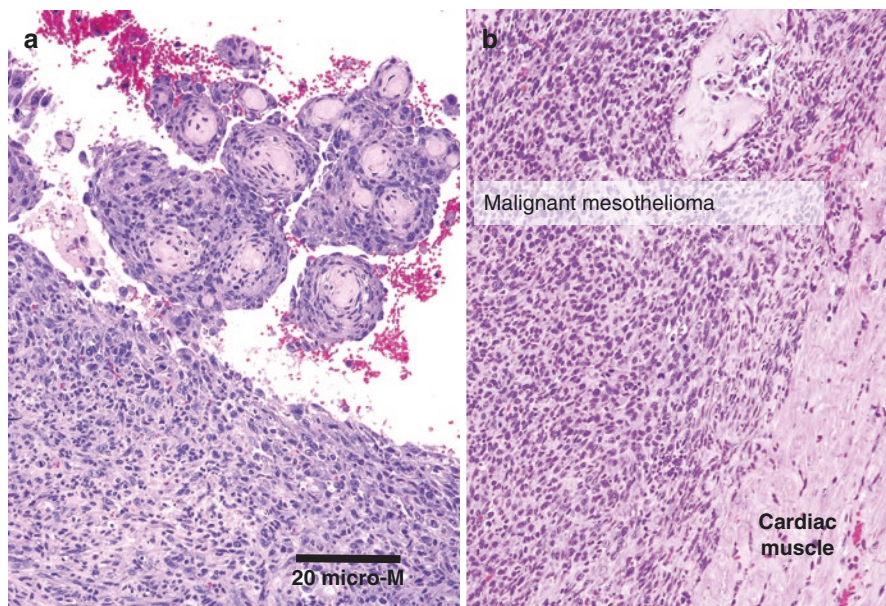
Fig. 8.9 Microscopic view of pleural tumors in rats administered MWCNT-N. (**a**) Malignant mesothelioma in the mediastinal space in a rat administered MWCNT-N and killed at week 109. (**b**) Malignant mesothelioma showing invasion of the cardiac muscle in another rat administered MWCNT-N and killed at week 109

These results clearly show that the MWCNT-N administered during the initial 2 weeks of the study period remained in the lung and caused sustained inflammatory lesions resulting in neoplastic development. This was the first study to show that an MWCNT administered to the lung was a complete carcinogen.

We then assessed the carcinogenicity of MWCNT-7 and two other MWCNTs (provided by company C) with different lengths and wall layers (Table 8.3). MWCNT-7 was administered to male rats by TIPS at a dose of 125 µg/rat once a week for 12 weeks (total 1.5 mg/rat) [manuscript submitted]. 18 of 19 MWCNT-7-treated rats and 0 of 15 rats administered vehicle alone developed malignant mesothelioma ($p < 0.001$). In the second study, MWCNT-A and MWCNT-B (described in Sect. 8.2.4) were administered to male rats at doses of 62.5 µg/rat and 125 µg/rat once a week for 8 weeks (total 0.5 and 1.0 mg/rat) [manuscript submitted]. Rats treated with MWCNT-B, but not MWCNT-A, had a significantly higher incidence of lung tumors (12/40) compared to control rats (1/19) ($p < 0.05$).

Beyond the fact that MWCNT-B is carcinogenic to rats when administered via the airway, the results from the MWCNT-A/B study are important for two other reasons. First, it shows that a thin MWCNT can be more toxic than a thick, needle-like MWCNT. Second, it shows that different MWCNTs of the same shape can have markedly different toxicities: MWCNT-N (20 nm diameter; approximately 3–6 µm length in the lung) and MWCNT-7 (50–60 nm diameter; 5–6 µm length in the lung)

Table 8.3 Tumor site and type induced by three different MWCNTs

MWCNTs	Administration method	Original size			Length in the lung (µm)	Iron content (weight %)[a]	Tumor site	References
		Wall layers	Average diameter (nm)	Average length (µm)				
MWCNT-7	Inhalation	N.S.[b,c]	93–98[c]	5–6[c]	6	0.344	Lung[d]	Kasai et al. [11]
MWCNT-N	TIPS	30	20	3–9	3–6	0.046	Lung[d] Pleura[e]	Suzui et al. [14]
MWCNT-7	TIPS	40	50–60	7	5–6	0.344	Pleura[e]	Manuscript submitted
MWCNT-A	TIPS	213	150	8	5	0.002	Inconclusive	Manuscript submitted
MWCNT-B	TIPS	15–18	15	3	2	1.1	Lung[d]	Manuscript submitted

[a]Dr. Sakamoto, Y. Tokyo Metropolitan Institute of Public Health
[b]Not specified
[c]Values from fibers collected from the inhalation chamber
[d]Bronchiolo-alveolar adenoma and/or carcinoma
[e]Pleural malignant mesothelioma

are carcinogenic to the rat lung and pleura, while the results of carcinogenicity testing of MWCNT-A (150 nm diameter: 5 µm length in the lung) were inconclusive. For these reasons, testing the toxicity/carcinogenicity of MWCNTs needs to be carried out for each type of MWCNT that is produced. Another important point is that testing the toxicity/carcinogenicity of MWCNTs will generate data that will allow manufactures of MWCNTs to produce safer, less toxic MWCNTs with low carcinogenic potential.

8.4   Mechanism of Inflammation and Carcinogenesis

Like crocidolite asbestos, MWCNT-N and MWCNT-7 fibers caused inflammation in the lung and pleura after TIPS administration. The increase in lung and mesothelial cell proliferation in MWCNT-7-treated rats 4 weeks, 6 weeks, and 1 year after the final TIPS administration [22, 23, manuscript submitted] was indicative of tissue repair in response to MWCNT-associated tissue damage: MWCNT-associated tissue damage is caused by (1) the inflammatory response to MWCNT fibers and (2) to the tissue damage caused by the fibers themselves [10]. The increase in 8-OHdG levels seen at 6 weeks and 1 year after the final TIPS administration [23, manuscript submitted] was due to DNA damage caused by reactive oxidants generated upon MWCNT-N interaction with tissue cells and phagocytes.

Since MWCNT fibers cause both generation of reactive oxidants and tissue damage followed by cell proliferation and tissue repair, MWCNT-associated oxidants can damage the DNA of cells replicating in response to MWCNT-associated

tissue damage. This enables damaged DNA to be replicated before it is repaired by the cell's highly efficient DNA monitoring and repair systems, thereby generating mutations in daughter cells. Since normal, checkpoint-intact cells are constrained by numerous tissue and intracellular checkpoints that maintain tissue architecture, multiple cycles of tissue damage and tissue repair in the presence of DNA damaging agents must occur before a cell acquires the mutations that allow it to bypass these checkpoints and undergo aberrant proliferation. An important observation is that macrophages phagocytosing MWCNT fibers can undergo degenerative changes (Fig. 8.10). This will both impair clearance of the fibers from the tissue in which they are deposited, increasing their biopersistence, and expand release of inflammatory mediators, increasing the strength of fiber-induced inflammatory responses. This process helps promote multiple cycles of tissue damage and repair in the presence of DNA damaging agents.

In contrast, if a fiber (or other material) is not biopersistent, the cycles of tissue damage and repair that it causes will cease and mutation of tissue cells will arrest. For example, MWCNT-A caused pleural inflammation and proliferation of mesothelial cells [25]; however, the hyperplasias induced by MWCNT-A did not progress into carcinogenic lesions [manuscript submitted].
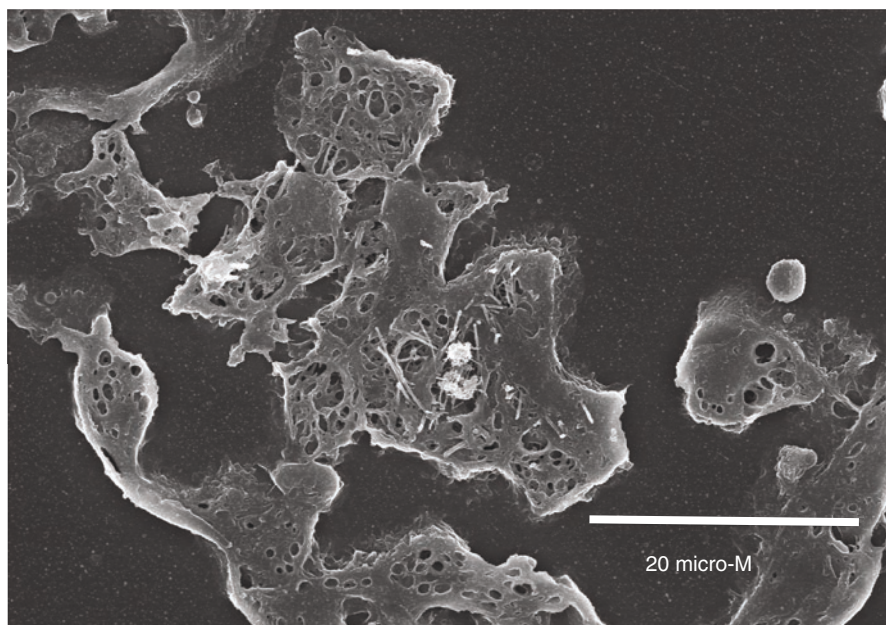
Fig. 8.10 Scanning electron microscopic view of an alveolar macrophage phagocytosing MWCNT fibers. Several individual needle-like MWCNT fibers can be seen in the cytoplasm of this macrophage. The macrophage is undergoing degenerative change, likely as a result of sustained production of reactive oxidants in an attempt to "kill" the MWCNT fibers it has phagocytosed

Therefore, if MWCNT fibers (and other respirable materials) are biopersistent and cause both tissue damage and generation of DNA damaging oxidants, it becomes possible for target cells to acquire the requisite mutations that bring about neoplastic transformation, making these fibers potential carcinogens. Because TIPS is relatively inexpensive and uses commonly available equipment and techniques, interim sacrifices can be set up to monitor tissue damage and repair and the generation of damaged DNA.

8.5 Comparison of TIPS to Whole-Body Inhalation Testing

One notable difference between the whole-body inhalation study with MWCNT-7 and our TIPS administration studies is that whole-body exposure to MWCNT-7 resulted in the development of bronchiolo-alveolar tumors but not malignant pleural mesotheliomas [11], while both bronchiolo-alveolar tumors and malignant pleural mesotheliomas were induced after TIPS administration of MWCNT-N [14] and malignant pleural mesotheliomas developed in rats administered MWCNT-7 [manuscript submitted]. The most likely reason for the different results obtained by whole-body inhalation and TIPS administration is the cumulative dose over time of the MWCNTs. The amount of MWCNT-7 in the lung increased from 0 to up to 1.8 mg/rat in male rats during the 2 years of exposure to air containing 2 mg/m^3. During this time, fibers also accumulated in the pleural cavity. Since neoplastic transformation requires that a single cell acquires all of the mutations required for transformation, the probability of transformation increases only as fibers accumulate in the region in which that cell resides. The lifespan of a short-lived test animal such as a rat may not be long enough for accumulation of fibers in the pleural mesothelium and the subsequent neoplastic process, which is driven by random mutation, to take place [3]. In contrast, administration of MWCNTs by TIPS results in the highest concentration of the MWCNTs in the lung at the beginning of the study, allowing processes involved in carcinogenesis to proceed for the entire length of the experimental period. Notably, in the whole-body inhalation study, rats exposed to MWCNT-7 accumulated fibers in the pleural cavity and developed mesothelial hyperplasia, and it is possible that if exposure to MWCNT-7 could have continued for a further 1 or 2 years these rats may have developed mesotheliomas.

Importantly, after TIPS administration of MWCNT-N, all malignant mesotheliomas were induced in the mediastinal and pericardial space, and high concentrations of MWCNT fibers were exclusively found in the mediastinal stromal tissue and lymph nodes [14]. It is likely that induction of malignant mesothelioma is related to the concentration of MWCNTs in high incidence loci, as is the case in humans exposed to asbestos [26].

Another notable difference between TIPS administration, using MWCNT-7, and the whole-body inhalation study was that when 1.5 mg MWCNT-7 was administered by TIPS only malignant pleural mesotheliomas developed and lung tumors were not induced (Table 8.1). This surprising result is likely due to the fact that once

initiated, malignant mesothelioma is a rapidly developing tumor [27]. Thus, initial administration of 1.5 mg MWCNT-7 allowed the early development of malignant mesothelioma, which may have killed the rat before lung tumors could develop: the average survival time of MWCNT-7-treated rats was only 79 weeks.

It has been suggested that intratracheal instillation can result in poor distribution of the administered material in the lung and that the process of instillation is stressful to the test animals [28]. However, as can be seen in Figs. 8.2 and 8.3, TIPS administration as described in this chapter results in satisfactory distribution of the test material throughout all five lobes of the rat lung. In addition, by 4–6 weeks after the final TIPS administration, there is no evidence that the process of TIPS is harmful to rats. In addition, unlike whole-body inhalation, TIPS administered material is not filtered out in the nasal cavity of the treated rats and the exact dose instilled into the lungs is known.

Perhaps the most important difference between TIPS administration and whole-body exposure is cost and the equipment and animal facilities required by these two methods of exposure to test materials. As noted above, the enormous cost of whole-body exposure has resulted in a very limited number of facilities equipped to carry out whole-body exposure studies. This is amply evidenced by the fact that since the first reports of the possible carcinogenicity of MWCNTs 10 years ago, only a single whole-body exposure study has been carried out with MWCNTs. As we have argued here, each different type of MWCNT needs to be tested, to both identify the carcinogenic potential of the MWCNT and to acquire data that will help manufacturers develop safer, less toxic MWCNTs. It is clear that whole-body inhalation is inadequate for this work. In contrast, TIPS is relatively inexpensive and uses commonly available equipment and techniques, making TIPS administration widely available, thereby allowing the testing required to assess the numerous types of MWCNTs (and other respirable materials) now being produced.

8.6   Conclusion

MWCNT products vary in the number of wall layers, diameter, and surface properties, depending on their purpose of use and manufacturing method. Therefore, it is necessary to establish a standard, reliable risk assessment protocol that can be widely used with which to test the various MWCNTs (and other respirable materials) being produced. Using intratracheal intrapulmonary instillation (TIPS) administration, we have shown that MWCNT-N is carcinogenic to the lung and pleural mesothelium, MWCNT-7 is carcinogenic to the pleural mesothelium as well as to the lung, and MWCNT-B is carcinogenic to the lung. Test materials are administered at the beginning of the study and the animals are then observed for 2 years (Fig. 8.4b). During the observation period, persistent inflammation and generation of reactive oxidants subject the tissue to repeated damage and repair cycles, which is widely accepted as a process that can result in carcinogenesis [29–32]. Carcinogenesis subsequent

to TIPS administration requires that the material being tested (1) causes tissue damage, (2) causes the generation of DNA damaging agents, and (3) is biopersistent, characteristics are accepted properties of foreign body carcinogens. Consequently, TIPS is specific for materials with carcinogenic properties. TIPS is inexpensive and easy to implement, and can be widely used for pulmonary toxicity evaluation and hazard screening of MWCNTs and other respirable materials. TIPS can be used to test the toxicity of low, medium, and high levels of respirable materials, and this data can be used to generate information relevant to risk assessment.

References

1. Donaldson K, Murphy FA, Duffin R, Poland CA. Asbestos, carbon nanotubes and the pleural mesothelium: a review of the hypothesis regarding the role of long fibre retention in the parietal pleura, inflammation and mesothelioma. Part Fibre Toxicol. 2010;7:5. https://doi.org/10.1186/1743-8977-7-5.
2. Donaldson K, Poland CA, Murphy FA, MacFarlane M, Chernova T, Schinwald A. Pulmonary toxicity of carbon nanotubes and asbestos—similarities and differences. Adv Drug Deliv Rev. 2013;65(15):2078–86. https://doi.org/10.1016/j.addr.2013.07.014.
3. Fukushima S, Kasai T, Umeda Y, Ohnishi M, Sasaki T, Matsumoto M. Carcinogenicity of multi-walled carbon nanotubes: challenging issue on hazard assessment. J Occup Health. 2018;60(1):10–30. https://doi.org/10.1539/joh.17-0102-RA.
4. Sakamoto Y, Nakae D, Fukumori N, Tayama K, Maekawa A, Imai K, et al. Induction of mesothelioma by a single intrascrotal administration of multi-wall carbon nanotube in intact male Fischer 344 rats. J Toxicol Sci. 2009;34(1):65–76.
5. Takagi A, Hirose A, Nishimura T, Fukumori N, Ogata A, Ohashi N, et al. Induction of mesothelioma in p53+/− mouse by intraperitoneal application of multi-wall carbon nanotube. J Toxicol Sci. 2008;33(1):105–16.
6. Nagai H, Okazaki Y, Chew SH, Misawa N, Yamashita Y, Akatsuka S, et al. Diameter and rigidity of multiwalled carbon nanotubes are critical factors in mesothelial injury and carcinogenesis. Proc Natl Acad Sci U S A. 2011;108(49):E1330–8. https://doi.org/10.1073/pnas.1110013108.
7. Sargent LM, Porter DW, Staska LM, Hubbs AF, Lowry DT, Battelli L, et al. Promotion of lung adenocarcinoma following inhalation exposure to multi-walled carbon nanotubes. Part Fibre Toxicol. 2014;11:3. https://doi.org/10.1186/1743-8977-11-3.
8. Takagi A, Hirose A, Futakuchi M, Tsuda H, Kanno J. Dose-dependent mesothelioma induction by intraperitoneal administration of multi-wall carbon nanotubes in p53 heterozygous mice. Cancer Sci. 2012;103(8):1440–4. https://doi.org/10.1111/j.1349-7006.2012.02318.x.
9. Grosse Y, Loomis D, Guyton KZ, Lauby-Secretan B, El Ghissassi F, Bouvard V, et al. Carcinogenicity of fluoro-edenite, silicon carbide fibres and whiskers, and carbon nanotubes. Lancet Oncol. 2014;15(13):1427–8. https://doi.org/10.1016/S1470-2045(14)71109-X.
10. IARC. Some nanomaterials and some fibres, vol 111. 2017. http://monographs.iarc.fr/ENG/Monographs/vol111/mono111.pdf. Accessed 30 Nov 2018.
11. Kasai T, Umeda Y, Ohnishi M, Mine T, Kondo H, Takeuchi T, et al. Lung carcinogenicity of inhaled multi-walled carbon nanotube in rats. Part Fibre Toxicol. 2016;13(1):53. https://doi.org/10.1186/s12989-016-0164-2.
12. Muller J, Delos M, Panin N, Rabolli V, Huaux F, Lison D. Absence of carcinogenic response to multiwall carbon nanotubes in a 2-year bioassay in the peritoneal cavity of the rat. Toxicol Sci. 2009;110(2):442–8. https://doi.org/10.1093/toxsci/kfp100.

13. Rittinghausen S, Hackbarth A, Creutzenberg O, Ernst H, Heinrich U, Leonhardt A, et al. The carcinogenic effect of various multi-walled carbon nanotubes (MWCNTs) after intraperitoneal injection in rats. Part Fibre Toxicol. 2014;11:59. https://doi.org/10.1186/s12989-014-0059-z.

14. Suzui M, Futakuchi M, Fukamachi K, Numano T, Abdelgied M, Takahashi S, et al. Multiwalled carbon nanotubes intratracheally instilled into the rat lung induce development of pleural malignant mesothelioma and lung tumors. Cancer Sci. 2016;107(7):924–35. https://doi.org/10.1111/cas.12954.

15. Pott F. Detection of mineral fibre carcinogenicity with the intraperitoneal test—recent results and their validity. Ann Occup Hyg. 1995;39(5):771–9.

16. Pott F, Roller M, Ziem U, Reiffer FJ, Bellmann B, Rosenbruch M, et al. Carcinogenicity studies on natural and man-made fibres with the intraperitoneal test in rats. IARC Sci Publ. 1989;90:173–9.

17. Roller M, Pott F, Kamino K, Althoff GH, Bellmann B. Results of current intraperitoneal carcinogenicity studies with mineral and vitreous fibres. Exp Toxicol Pathol. 1996;48(1):3–12. https://doi.org/10.1016/S0940-2993(96)80084-4.

18. Ryman-Rasmussen JP, Cesta MF, Brody AR, Shipley-Phillips JK, Everitt JI, Tewksbury EW, et al. Inhaled carbon nanotubes reach the subpleural tissue in mice. Nat Nanotechnol. 2009;4(11):747–51. https://doi.org/10.1038/nnano.2009.305.

19. PennCentuury. Information archive. 2018. http://penncentury.com/products/liquid-aerosol-devices/microsprayer-ia-1b/. Accessed 30 Nov 2018.

20. Xu J, Futakuchi M, Shimizu H, Alexander DB, Yanagihara K, Fukamachi K, et al. Multiwalled carbon nanotubes translocate into the pleural cavity and induce visceral mesothelial proliferation in rats. Cancer Sci. 2012;103(12):2045–50. https://doi.org/10.1111/cas.12005.

21. Xu J, Alexander DB, Futakuchi M, Numano T, Fukamachi K, Suzui M, et al. Size- and shape-dependent pleural translocation, deposition, fibrogenesis, and mesothelial proliferation by multiwalled carbon nanotubes. Cancer Sci. 2014;105(7):763–9. https://doi.org/10.1111/cas.12437.

22. Abdelgied M, El-Gazzar AM, Alexander DB, Alexander WT, Numano T, Iigou M, et al. Potassium octatitanate fibers induce persistent lung and pleural injury and are possibly carcinogenic in male Fischer 344 rats. Cancer Sci. 2018;109(7):2164–77. https://doi.org/10.1111/cas.13643.

23. El-Gazzar AM, Abdelgied M, Alexander DB, Alexander WT, Numano T, Iigo M, et al. Comparative pulmonary toxicity of a DWCNT and MWCNT-7 in rats. Arch Toxicol. 2019;93:49–59.

24. Xu J, Futakuchi M, Alexander DB, Fukamachi K, Numano T, Suzui M, et al. Nanosized zinc oxide particles do not promote DHPN-induced lung carcinogenesis but cause reversible epithelial hyperplasia of terminal bronchioles. Arch Toxicol. 2014;88(1):65–75. https://doi.org/10.1007/s00204-013-1086-5.

25. Liao D, Wang Q, He J, Alexander DB, Abdelgied M, El-Gazzar AM, et al. Persistent pleural lesions and inflammation by pulmonary exposure of multiwalled carbon nanotubes. Chem Res Toxicol. 2018;31(10):1025–31. https://doi.org/10.1021/acs.chemrestox.8b00067.

26. Boutin C, Dumortier P, Rey F, Viallat JR, De Vuyst P. Black spots concentrate oncogenic asbestos fibers in the parietal pleura. Thoracoscopic and mineralogic study. Am J Respir Crit Care Med. 1996;153(1):444–9. https://doi.org/10.1164/ajrccm.153.1.8542156.

27. Carbone M, Ly BH, Dodson RF, Pagano I, Morris PT, Dogan UA, et al. Malignant mesothelioma: facts, myths, and hypotheses. J Cell Physiol. 2012;227(1):44–58. https://doi.org/10.1002/jcp.22724.

28. Oberdorster G, Castranova V, Asgharian B, Sayre P. Inhalation exposure to carbon nanotubes (CNT) and carbon nanofibers (CNF): methodology and dosimetry. J Toxicol Environ Health B Crit Rev. 2015;18(3–4):121–212. https://doi.org/10.1080/10937404.2015.1051611.

29. Coussens LM, Werb Z. Inflammation and cancer. Nature. 2002;420(6917):860–7. https://doi.org/10.1038/nature01322.

30. Okada F, Fujii J. Molecular mechanisms of inflammation-induced carcinogenesis. J Clin Biochem Nutr. 2006;39(3):103–13.
31. Topinka J, Loli P, Georgiadis P, Dusinska M, Hurbankova M, Kovacikova Z, et al. Mutagenesis by asbestos in the lung of lambda-lacI transgenic rats. Mutat Res. 2004;553(1–2):67–78. https://doi.org/10.1016/j.mrfmmm.2004.06.023.
32. Yang H, Testa JR, Carbone M. Mesothelioma epidemiology, carcinogenesis, and pathogenesis. Curr Treat Options Oncol. 2008;9(2–3):147–57. https://doi.org/10.1007/s11864-008-0067-z.

Chapter 9
Equivalence Criteria for Nanomaterials Developed from Results of a Comparative Study Using Intratracheal Administration

Yutaka Oshima, Toshio Kobayashi, Takakazu Kayashima, Makoto Nakai, and Nobuya Imatanaka

Abstract The toxicity of nanomaterials is complex and multifactorial and likely depends on their diverse physicochemical properties. Further development and application of nanomaterials requires a systematic, effective, and efficient method for evaluating their toxicity. One approach in this regard is to ascertain the variability in the physicochemical properties of nanomaterials that exhibit the same toxicity—that is, to establish "equivalence criteria" for nanomaterials. However, this approach requires the acquisition and comparison of toxicity data for various nanomaterials. In this chapter, we summarize our efforts to establish equivalence criteria for nanomaterials in regard to their toxicity after intratracheal instillation. To achieve this objective, we focused on intratracheal administration studies for evaluating nanomaterial toxicity simply and efficiently. Intratracheal instillation offers various advantages and disadvantages compared with inhalation exposure, which is widely used as a screening tool. In this study, we used intratracheal instillation to deliver a total of 20 nanomaterials representing three types (TiO_2, NiO, and SiO_2) to rats. We then compared the physicochemical properties and pulmonary toxicities of the tested nanomaterials and thus were able to detect characteristic features of their pulmonary toxic effects according to their physicochemical properties. We here demonstrated the effectiveness of using intratracheal administration studies to screen for pulmonary toxicity of nanomaterials. In addition, we anticipate that our proposed equivalence criteria will facilitate toxicity evaluation of nanomaterials.

Y. Oshima (✉) · T. Kobayashi · M. Nakai
Chemicals Evaluation and Research Institute, Japan, CERI Hita, Hita-shi, Oita, Japan
e-mail: oshima-yutaka@ceri.jp

T. Kayashima · N. Imatanaka
Chemicals Evaluation and Research Institute, Japan, Headquarters, Tokyo, Japan

9.1   Introduction

In general, nanomaterials are defined as materials with at least one dimension of 100 nm or less. Furthermore, for the European Union, the regulatory definition of a nanomaterial is "a natural, incidental or manufactured material containing particles, in an unbound state or as an aggregates or as an agglomerate and where, for 50% or more of the particles in the number size distribution, one or more external dimensions is in the size range 1–100 nm" [1]. The unique physical properties of nanoscale materials likely will convey new functions and thus novel applications of products that contain these compounds. Therefore, nanomaterials have great potential for advancing technology in many fields, including the microelectronics, materials, textiles, energy, healthcare, and cosmetics industries [2]. However, these new nanoscale-associated functions are highly likely to cause new biological reactions. The safety of nanomaterials has garnered concern worldwide because of their potential health risks to consumers, workers, and the environment [3].

Nanomaterial toxicity is complex and multifactorial and likely depends on diverse physicochemical attributes, including size, shape, and surface properties (charge, area, and reactivity) [4]. According to traditional practice, this complexity would prompt impractical approaches to ensuring consumer safety, such as toxicity testing of every manufacturing lot of a particular material, thus bringing the development and application of nanomaterials to a standstill. To efficiently and effectively ensure the safety of nanomaterials, an approach that evaluates their toxicity systematically is necessary. To this end, it could be useful to establish the range in the variability in the physicochemical properties of nanomaterials that exhibit similar toxicities (i.e., equivalence criteria for nanomaterials). However, toxicity data currently available are insufficient for this application, and additional information is necessary. Furthermore, hazard assessment of nanomaterials focuses on their respiratory toxicity, and inhalation exposure studies typically are performed. However, using inhalation studies to investigate the effects of physicochemical properties on the toxicity of nanomaterials is impractical due to the associated cost and technical difficulties [5].

Therefore, we focused on intratracheal administration studies as a means to evaluate nanomaterial toxicity simply and efficiently. Intratracheal administration is widely used to deliver substances to the lungs; consequently it is useful for screening panels of test materials for their relative potential to produce toxicity in the lower respiratory tract or to compare the effects of a new material with similar materials for which inhalation data are available. In addition, we can obtain information regarding the constituents that are most toxicologically relevant by comparing the toxicity of the mixture with those of its components [5].

In this chapter, we summarize our efforts to establish equivalence criteria for nanomaterials through a comparative study involving intratracheal instillation of nanomaterials with different physicochemical properties (specifically nanomaterials containing TiO_2, NiO, and SiO_2) into rats.

9.2 Physicochemical Properties Presumed to Affect the Toxicity of Nanomaterials

9.2.1 Particle Size and Specific Surface Area

The size of nanomaterials is one of the main contributors to their potential biological effects. Decreasing a particle's size increases its surface area-to-mass ratio. Because the part of a particle that is reactive to organisms typically is on its surface, increasing the relative surface area is expected to increase the effect of a given amount of material [4]. In addition, because of their small size, particles of nanomaterials can move throughout the body and cause reactions in various organs [6].

Several research studies have reported that, regardless of the chemical or animal model, a compound yields a single dose–response curve when the dose is expressed as particle surface area [6, 7] but not when determined in terms of mass [6]. Currently the Brunauer–Emmett–Teller (BET) method, which involves adsorbing nitrogen gas onto a dry-state sample, is the method used most often to measure surface area. The BET specific surface area is determined by the primary particle size and scarcely changes even when primary particles are aggregates or agglomerates [7]. In fact, the National Institute for Occupational Safety and Health defines particles with a primary particle size of less than 100 nm and its aggregates and agglomerates as ultrafine particles and states that the recommended work environment standard is applicable even when the diameter of an aggregate of ultrafine particles exceeds 100 nm [8].

9.2.2 Shape

The shape of nanoparticles is another key feature related to their toxicity. Shape is often considered in terms of a particle's aspect ratio, and a high aspect ratio infers a fibrous morphology [9]. The World Health Organization defines a fiber as a structure with a diameter of 3 μm or less [10]. Several fiber-shaped nanomaterials are estimated to have high biopersistence and thus are likely to exert similar harmful effects as asbestos. The fiber pathogenicity paradigm is the most robust structure–activity relationship for any particle and applies to asbestos, glass fibers, ceramic fibers, and p-aramid [11]. This characteristic is not due to the chemical nature of a

fiber but to its shape and persistence in the lungs, and a simple theory is that only long, thin, or bio-persistent fibers are associated with high toxicity [11]. Although large or high-aspect particles typically are unable to access the distal lung, some nanoparticles with an aspect greater than 5 μm penetrate deep into lungs, likely because the aerodynamic diameter of a fiber is not proportional to its length but to its diameter [9]. Although many engineered nanomaterials with potential for human exposure are unlikely to induce significant adverse effects, some could cause an asbestos-type event if their dispersal is not controlled [12].

In addition, shape influences the specific surface area of particles. In calculating the specific surface area of rod-shaped particles, typically the surface area of both ends is ignored such that the specific surface area primarily hinges on the particle's diameter rather than its length [7]. In this way, the BET specific surface area of carbon nanotubes (CNTs) is calculated under the hypothesis that both ends of CNTs are closed. If one end is open, as in single-walled CNTs, the specific surface area is considered to be twice the closed-end value. Consequently, both shape and specific surface area differ significantly between single-walled and multi-walled CNTs [13].

9.2.3   Surface Charge

The surface charge (zeta potential) of particles influences various measures of toxicity. For example, particles larger than 2 μm stimulated the release of IL-6 due to their increased zeta potential [14]. In addition, the toxicity of micron-sized polymers depends on particle charge [15], and the inflammatory potential of several metal-oxide nanoparticles is associated with their zeta potential under acidic conditions [16]. The zeta potential of a material is pH-dependent and thus is relevant to events in phagolysosomes after the particles' uptake into macrophages [9]. Furthermore, both polymer nanoparticles [17] and silica nanoparticles [18] have charge-related toxicity.

9.2.4   Chemical Properties

The toxicity of nanomaterials may be mediated by the specific chemical properties of their component. Surface properties of nanomaterials are known to affect toxicity. As occurs with crystalline silicas, the surfaces of nanomaterials may carry chemically reactive groups that cause toxicity [19]. Furthermore, the surface of nanomaterials might have catalytic properties that could lead to specific toxic effects. Therefore, nanomaterials that release toxic chemical constituents need to be evaluated on a case-by-case basis [20]. It is also known that the solubility of

nanomaterials contributes to toxicity. Nanoparticles with high solubility may cause toxic effects because they release toxic ions, but the toxicity of "poorly soluble, low-toxicity" (PSLT) particles does not depend on specific substances, functional chemical surface groups, or specific surface-related toxicity [20]. Carbon black and TiO_2 are considered to be PSLT particles; however, nano-sized carbon black and nano-sized TiO_2 showed lung carcinogenicity in rats at levels considered to be relevant for extrapolation to humans [21].

9.3 Intratracheal Instillation

Intratracheal administration (instillation) has traditionally been used as a screening tool for inhalation studies because of its technical simplicity. Intratracheal instillation conveys nearly the entire dose of particles to the lungs of an animal. In addition, intratracheal instillation can be used to deliver to the lungs various substances, such as long fibers and reactive or water-soluble compounds, that otherwise would be retained in the nasal passages [5]. However, intratracheal instillation may not ever completely replace inhalation exposure, due to concerns regarding differences in the pulmonary distribution of materials between the two routes of exposure. In addition, instillation is invasive and nonphysiologic, bypassing the upper respiratory tract and thus precluding evaluation of the effects of the delivered materials on that region. Furthermore, the influence of the medium in which the test material is suspended or dissolved and the potential effects of any anesthesia used need to be considered as well. However, when these caveats are addressed, intratracheal instillation is a very useful tool [5, 22].

9.4 Comparing the Pulmonary Toxicity of Nanomaterials by Using Intratracheal Instillation: Project Outline

In 2011, the Ministry of Economy, Trade and Industry (METI) of Japan launched a 5-year project for the "Development of Innovative Methodology for Safety Assessment of Industrial Nanomaterials." In this project, we were challenged to develop a method for evaluating the toxicity of nanomaterials that would serve as the framework for rationally and efficiently evaluating and managing the risks of various nanomaterials. Using several nanomaterials of similar composition but different physicochemical properties, we conducted a systematic intratracheal instillation study. Then we compared the results to establish, for each of several physicochemical properties, the range of values for which nanomaterials in that range showed similar toxicities.

9.4.1 Study Design

The nanomaterials we selected to study had known hazard information, were comparatively easy to obtain, and likely would be used at the tested doses. In total, we tested 20 types of nanomaterials (7 TiO_2, 4 NiO, and 9 SiO_2) that differed in terms of their physicochemical properties (e.g., size, shape).

Each material was instilled into four groups ($n = 30$ each) of 12-week-old, male F344/DuCrlCrlj rats comprising one vehicle control group and three dosage groups. Rats were anesthetized by isoflurane inhalation and received a single instillation of each test material at a dose volume of 1–2 mL/kg body weight through a gavage needle. Bronchoalveolar lavage fluid (BALF) analysis ($n = 5$) and pathologic examination ($n = 5$) were conducted during the acute (day 3), subacute (day 28), and subchronic (day 91) phases after instillation. On each examination day, 10 rats per dose were anesthetized by using pentobarbital and terminally bled from the abdominal aorta. The BALF procedure has been described in detail previously [23]. Briefly, whole lungs were lavaged twice by using two 7-mL aliquots of saline, which were pooled for the following analyses: total cell counts and leukocyte differential (ratio of neutrophil, eosinophil, lymphocyte, macrophage,), total protein content, albumin content, lactate dehydrogenase (LDH) activity, and alkaline phosphatase (ALP) activity. For pathologic examination, the lungs, trachea, parathymic lymph nodes, posterior mediastinal lymph node, liver, kidneys, and spleen were removed from the rats. The lungs, liver, kidneys, and spleen were weighed to calculate relative organ weights per body weight (g/100 g). The organs were fixed with 10% (v/v) neutral phosphate-buffered formalin solution, stained with hematoxylin and eosin, and examined histopathologically under a light microscope.

The results for each of the 20 nanomaterials tested are summarized in Sects. 9.4.2–9.4.4.

9.4.2 Intratracheal Instillation Study of Nano-TiO₂

9.4.2.1 Background Information on TiO₂

Nano-TiO_2 is one of the most widely used nanomaterials in the world. TiO_2 is an excellent-white pigment that has been used in paint, printing ink, plastics, chemical fibers, paper manufacturing, and other white products as well as in almost everything that is colored.

Because TiO_2 is insoluble and inert, it traditionally has been considered to have low toxicity. However, the use of TiO_2 as small particles has prompted concerns about its effects on the lungs when TiO_2-containing dust is inhaled. This concern is common among poorly soluble and chemically inert particles in general. The physi-

cochemical properties of nano-TiO$_2$ differ from those of their fine-particle analogs and might alter their bioactivity. In particular, TiO$_2$ nanoparticles are more toxic than TiO$_2$ fine-particles [24]. Furthermore, nano-TiO$_2$ itself can be manufactured in various forms with differing physicochemical characteristics (e.g., crystallinity, shape, particle size, surface area, surface modification), thus leading to nanomaterials that have the same chemical formula but different pulmonary toxicities [25].

9.4.2.2 Materials and Methods

To assess the contribution of various physicochemical properties to the toxicity of TiO$_2$-containing nanomaterials, we selected seven types of nano-TiO$_2$ that represented differences in particle size, particle shape, surface coating (none or Al(OH)$_3$), and crystal structure (Table 9.1). The doses of nano-TiO$_2$ were set at 0 (vehicle: 2 mg/mL disodium hydrogen phosphate), 0.67, 2, and 6 mg/kg. The instilled volume was 1 mL/kg, except for FTL-100 (2 mL/kg) depending on the preparation concentration. For details regarding the nano-TiO$_2$ and preparation method used in the study, please refer to Chap. 7.

9.4.2.3 Results

All tested nano-TiO$_2$ were associated with acute pulmonary inflammation in rats on day 3 after instillation. In BALF examinations, total cell counts (Fig. 9.1 (vehicle control, 100%)), ratio of neutrophil, total protein content, concentrations of albumin, LDH, and ALP activity increased compared to the control group. Dose dependence was observed in almost all parameters for which pulmonary inflammatory changes were found. Relative lung weight increased after exposure to AMT-100, MT-150AW, TTO-S-3, TTO-S-3(Coated), P25, and FTL-100. For these nano-TiO$_2$, histopathologic examination revealed pulmonary inflammatory cell infiltration, hyperplasia of alveolar epithelial cells, and other pathologies (Fig. 9.2).

Pulmonary inflammation was moderate after exposure to MT-150AW, TTO-S-3, TTO-S-3(Coated), and P25 and mild with AMT-100 and FTL-100; little inflammatory change was observed after MP-100 instillation. For six of the seven tested nano-TiO$_2$, recovery from inflammation had occurred by day 28, when almost all parameters were comparable with those of corresponding controls. However, the pulmonary inflammatory changes induced by TTO-S-3(Coated) persisted on day 28. Specifically, histopathologic examination of TTO-S-3(Coated)-treated rat lungs on day 28 revealed inflammatory cell infiltration, alveolar epithelial cell hyperplasia, and degeneration and necrosis of alveolar macrophages. On day 91, these inflammatory features of TTO-S-3(Coated)-exposed lungs were greatly diminished but not entirely resolved (Fig. 9.2).

Table 9.1 Physicochemical characteristics of the seven tested forms of TiO_2

Material	Crystal structure	Shape[a]	Primary particle size[a] (nm)	Surface area[a] (m^2/g)	Surface coating[a]	Particle size[b] (nm)	
						Volume average diameter	Number average diameter
AMT-100	Anatase	Spherical	6	250–300	None	185 (161–198)	68.5 (60.6–82.6)
MT-150AW	Rutile	Spindle	Long axis: 28.8 Short axis: 7.6	100–120	None	58.5 (52.3–65.8)	28.7 (19.5–42.6)
TTO-S-3	Rutile	Spindle	Long axis: 50–100 Short axis: 10–20	102	None	61.9 (57.2–64.7)	45.8 (41.2–48.9)
TTO-S-3(Coated)	Rutile	Spindle	Long axis: 50–100 Short axis: 10–20	93	$Al(OH)_3$	241 (202–289)	125 (119–133)
P25	Rutile/ anatase (20/80)	Spherical	21	50 ± 15	None	99.2 (95.6–101)	73.8 (65.5–79.8)
MP-100	Rutile	Spherical	1000	6	None	531 (501–549)	289 (89.8–393)
FTL-100	Rutile	Needle	Long axis: 1680 Short axis: 130	12	None	Not determined[c]	Not determined[c]

[a]Data were obtained from the product catalog or manufacturer

[b]Average particle diameter was measured in the three administration formulations by means of dynamic light scattering (DLS) (Zetasizer Nano ZS, Malvern Instruments Ltd., Malvern, UK). Figures in parentheses are the smallest and largest values among the three concentrations. Intensity size distributions measured by DLS were converted into volume and number size distributions according to Mie theory

[c]Particle size was not calculated because DLS gives little effective information for needle-shaped particles with a large aspect ratio

9.4.2.4 Analysis of Correlation Between Physicochemical Characteristics of TiO_2 and Pulmonary Inflammatory Responses in Rats

To compare pulmonary inflammation quantitatively among the various nano-TiO_2, we analyzed BALF parameters at 2 mg/kg for all nanomaterials. We chose this dose because we were concerned that 6 mg/kg might cause saturation of effects during the acute phase.
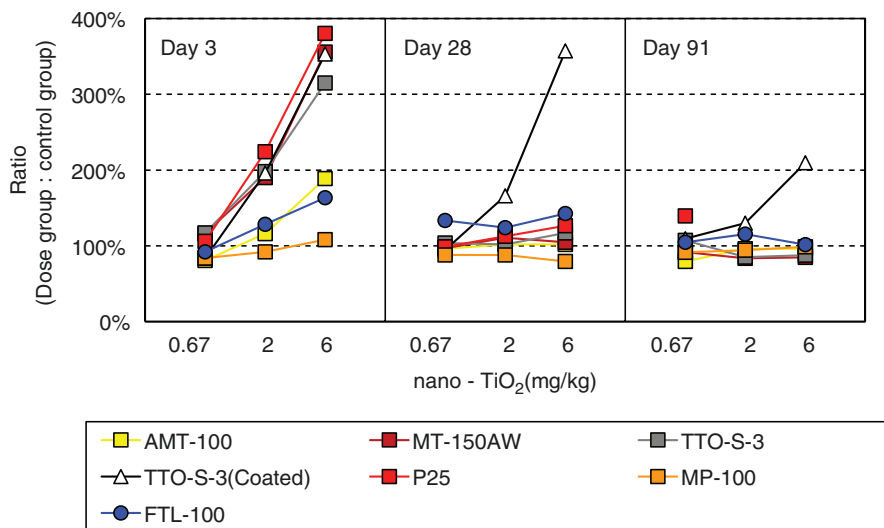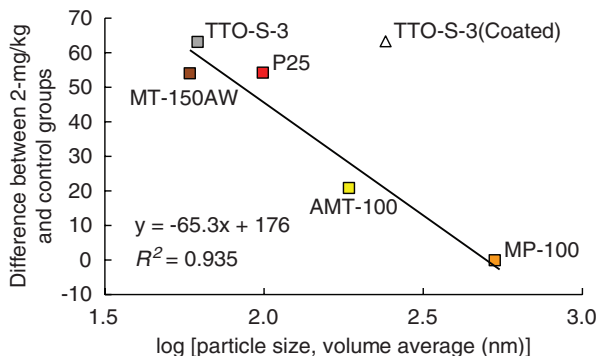
Fig. 9.1 Dose correlation and time course of total BALF cell count after intratracheal instillation of various forms of TiO$_2$. Data are presented as the average ratio of the value for the indicated dose group to that of the control group
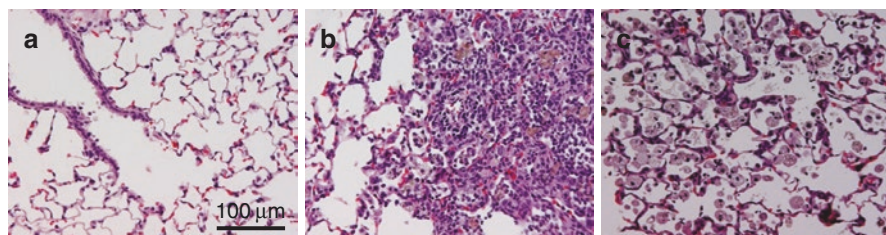
Fig. 9.2 Representative light micrographs of lung tissue from rats after intratracheal instillation of TiO$_2$ at 6 mg/kg. (**a**) Vehicle control on day 3 after instillation, (**b**) TTO-S-3(Coated) on day 3 after instillation, (**c**) TTO-S-3(Coated) on day 91 after instillation

Particle Size

We used DLS to measure the particle size (volume and number averages) in the administered solutions. To evaluate the contribution of particle size to the observed inflammatory response (ratio of neutrophil, total protein content, LDH), particle size in solution was expressed as a logarithm. The correlation between the volume average diameter and the ratio of neutrophil during the acute phase is shown in Fig. 9.3; note that FTL-100 was not plotted because its particle size could not be determined by using DLS. For all other TiO$_2$ except TTO-S-3(Coated), the volume average diameter and the ratio of neutrophil were significantly correlated ($P < 0.05$) during the acute phase and yielded high R^2 values: smaller nanoparticles were more toxic than larger ones. However, because recovery from pulmonary inflammation

Fig. 9.3 Correlation between particle size (nm) and the ratio of neutrophil in BALF on day 3 after intratracheal instillation of various forms of TiO_2. Data are presented as the average difference between the values for the 2-mg/kg and control groups. The solid line is the linear regression line derived from the five tested materials (i.e., excluding the data for TTO-S-3(Coated) and FTL-100). From Hashizume et al., with permission

was observed in the subacute to sub-chronic phase, the contribution of particle size to the inflammatory response during these phases could not be analyzed. Therefore, the particle size in the solution likely correlates with the acute pulmonary inflammatory response observed in the rats [23].

Shape

To evaluate its contribution to the inflammatory response, particle shape was expressed as an aspect ratio. Because aspect ratio and inflammatory response showed no clear correlation during the acute to sub-chronic phase, the contribution of the shape of nano-TiO_2 particles to pulmonary inflammation in rats is considered negligible [23].

Surface Coating

The plot of TTO-S-3(Coated) was well separated from the other TiO_2 (in Fig. 9.3). Furthermore, unlike with other nano-TiO_2, the pulmonary inflammatory response to TTO-S-3(Coated) persisted in the subacute and sub-chronic phases. Therefore, the $Al(OH)_3$ coating likely increases the inherent toxicity of TTO-S-3 [23].

Crystal Structure

To evaluate the contribution of the crystal structure to the inflammatory response to nano-TiO_2, we used the percentage of the material in rutile form (as determined by the manufacturer) as an index of crystallinity. For example, the percentage of

material in the rutile form for AMT-100 (for which TiO_2 was 100% anatase) was 0%, for MT-150AW was 100%, and for P25 was 20%. Consequently, the index of crystallinity showed no correlation with inflammatory response during the acute through sub-chronic phases. Therefore, the contribution of the index of crystallinity of nano-TiO_2 particles to acute through sub-chronic pulmonary inflammation in rats is negligible [23].

9.4.2.5 Equivalence Criteria for TiO_2

Using our results, we categorized the seven tested TiO_2 into two groups: a group containing TiO_2 with no surface coating (i.e., AMT-100, MT-150AW, TTO-S-3, P25, MP-100, and FTL-100) and a group comprising the surface-coated TiO_2 (i.e., TTO-S-3(Coated)). Our results indicated that the particle size of TiO_2 affects the pulmonary inflammation response. When instillation doses were normalized according to volume average particle size, the acute-phase inflammatory responses induced by the various nano-TiO_2 converged along the same sigmoidal dose–response curve ($R^2 = 0.957$) (Fig. 9.4). This result suggests that the acute pulmonary inflammatory response to non-coated TiO_2 is equivalent when they have the same particle size, regardless of any differences in crystallinity or shape: smaller TiO_2 particles induce more severe acute pulmonary inflammation than larger TiO_2 particles. Several previous studies have shown similar associations between particle size and pulmonary inflammation after intratracheal instillation of TiO_2 nanomaterials [26–28], but others report no correlation between the particle size and toxicity of TiO_2 [29]. Clearly, a robust understanding of the effect of TiO_2 particle size on acute pulmonary toxicity in rats has yet to be obtained.

Plot: y-axis "Ratio of neutrophil (%)" ranging from −10 to 110; x-axis "log [dose/particle size (mg/kg/nm)]" ranging from −3 to −0.5. Equation shown: $Y = 0.0937 + (67.6-0.0937) / [1 + 10^{[(-1.80-X) \times 4.16]}]$, $R^2 = 0.957$. Legend: AMT-100, MT-150AW, TTO-S-3, TTO-S-3(Coated), P25, MP-100.
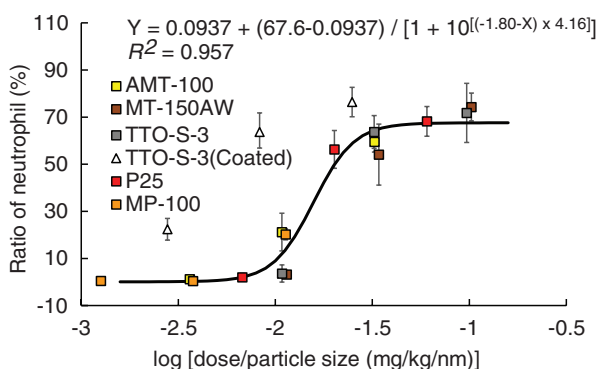
Fig. 9.4 Dose–response curves for the ratio of neutrophil in BALF on day 3 after intratracheal instillation of various forms of TiO_2. Data are from the 2-mg/kg group and are presented as average ±1 SD. The overlaid solid line is the sigmoidal dose–response curve derived from the five tested materials (i.e., excluding the data for TTO-S-3(Coated) and FTL-100). From Hashizume et al., with permission

In addition, our results showed that the surface coating can markedly affect the toxicity of nano-TiO$_2$. Several previous studies support our current findings regarding the effects of surface coating on the pulmonary toxicity of TiO$_2$ in rats [30–32]. Further studies are needed to determine the precise relationships between the surface treatment of TiO$_2$ particles and the pulmonary inflammatory response they induce.

Nanomaterial-induced pulmonary inflammation depends largely on the extent of deposition and clearance [3, 33]. In the METI project, the pulmonary clearance kinetics of TiO$_2$ in rats were examined by using the same seven test materials as we assessed in the present study; the pulmonary clearance rate constant of TTO-S-3(Coated) was much lower than that of the other six TiO$_2$ [34]. Therefore, delayed clearance from the lung may account for the persistent subacute pulmonary inflammation due to TTO-S-3(Coated), and further studies are required to elucidate the detailed toxicologic mechanism.

Our results allowed us to establish the following equivalence criteria regarding the relationship between the physicochemical characteristics of nano-TiO$_2$ and the pulmonary inflammatory response they induce: (1) particle size in solution is likely correlated with the severity of acute pulmonary inflammation (i.e., small size in solution = severe inflammatory response), (2) crystallinity and particle shape are unlikely to be correlated with pulmonary inflammatory responses, and (3) surface coating has the potential to alter the pulmonary inflammatory response relative to that for the uncoated counterpart.

9.4.3 Intratracheal Instillation Study of NiO

9.4.3.1 Background Information on NiO

NiO is an important industrial material. Because it is a vivid green, NiO is used as a coloring agent for glass, ceramics, and other products. Characteristics of nano-NiO include high catalytic activity, high surface energy, high magnetism, low melting point, high surface area, and low burning point [35, 36]. With the increased industrial applications of nano-NiO, occupational exposure of factory workers to nano-NiO is expected to increase as well.

NiO is well known as a toxic material. Due to its poor solubility in water and alkali, NiO is considered to show high biopersistence in lung [37], and nickel ions generated at accumulation sites may cause DNA damage [38, 39]. NiO-containing compounds are classified as carcinogenic substances (Group 1) according to the International Agency for Research on Cancer categories [40].

9.4.3.2 Materials and Methods

We selected four types of nano-NiO—representing two particle shapes and a range in particle size—to evaluate the contribution of their physicochemical properties to their toxicities (Table 9.2). Tested doses were 0 (vehicle: purified water), 0.67,

Table 9.2 Physicochemical characteristics of the four tested forms of NiO

Material	Shape	Primary particle size[a] (nm)	Surface area[b] (m²/g)	Converted spherical primary particle size based on specific surface area	Number-based agglomerate particle size[c] according to DLS (nm)
Ni(II) oxide nanopowder	Spherical	Could not be determined[d]	93	9.6	39
US3352	Spherical	20 ± 8	51	18	49
I small particle	Irregular	140 ± 67	6.6	140	1600
NovaWireNiO1	Wire	Length: 240 Diameter: 29	180	5.0	Not determined[e]

[a]Determined by scanning electron microscopy (SEM; model S4800, Hitachi High-Technologies Co., Tokyo, Japan) or transmission electron microscopy (TEM; model JEM-2010, JEOL, Tokyo, Japan) analysis of 500 particles for each material
[b]Determined by BET surface area analysis (GEMINI VII, Shimadzu Co., Kyoto, Japan) after drying
[c]Determined by using DLS (Zetasizer Nano-ZS; Malvern Instruments Ltd.)
[d]Particle size could not be calculated because the particles agglomerated once they were diluted and the suspension dried
[e]Particle size was not calculated because DLS measurement of NovaWireNiO1 was not reproducible

2, and 6 mg/kg. The instillation volume was 1 mL/kg, except for NovaWireNiO1 (1.3 mL/kg) depending on the preparation concentration. All other experimental details (e.g., strain, number, anesthesia of rats) were as described for the analysis of nano-TiO$_2$. For details regarding the nano-NiO selected and preparation method used in the current study, please refer to Chap. 7.

9.4.3.3 Results

Deterioration of clinical condition—including weight loss, anorexia, decreased spontaneous locomotion, abnormal respiratory sounds—occurred through day 28 in rats that received Ni(II) oxide nanopowder or NovaWireNiO1 by intratracheal instillation. In addition, 4 of the 30 rats that received NovaWireNiO1 at 6 mg/kg died on or before day 17. All four nano-NiO tested induced changes indicative of pulmonary inflammation on day 3. In BALF examinations, total cell counts (Fig. 9.5 (vehicle control = 100%)), ratio of neutrophil, total protein content, concentrations of albumin, LDH, and ALP activity increased compared to the control group. Dose dependence was observed in almost all parameters for which pulmonary inflammatory changes were found. Relative lung weights were increased after treatment with Ni(II) oxide nanopowder, US3352, and NovaWireNiO1. Histopathologic examination of rats that received these three nano-NiO materials revealed inflammatory cell infiltration, hyperplasia of alveolar epithelial cells, and other inflammatory changes. In contrast, I small particle induced almost no histopathologic inflammatory changes (Fig. 9.6).
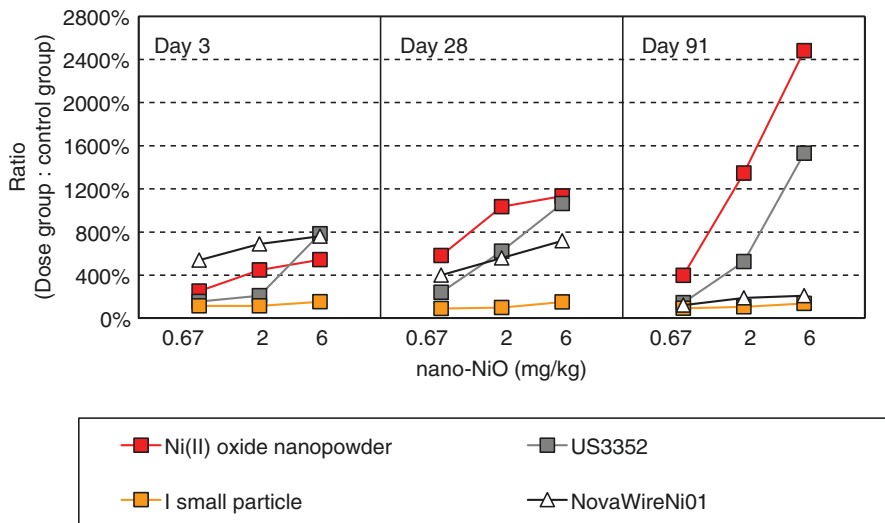
Fig. 9.5 Dose correlation and time course of total BALF cell count after intratracheal instillation of various forms of NiO. Data are presented as the average ratio of the value for the indicated dose group to that of the control group
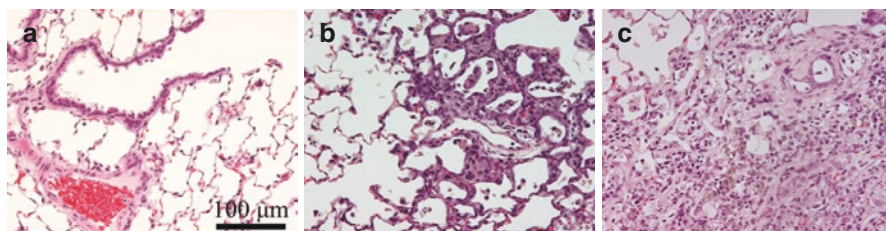
Fig. 9.6 Representative light micrographs of lung tissue from rats after intratracheal instillation of NiO at 6 mg/kg. (**a**) Vehicle control on day 3 after instillation, (**b**) Ni(II) oxide nanopowder on day 3 after instillation, (**c**) Ni(II) oxide nanopowder on day 91 after instillation

Ni(II) oxide nanopowder, US3352, and NovaWireNiO1 all induced severe pulmonary inflammation, whereas I small particle caused only mild inflammation. The toxic effects of NovaWireNiO1 tended to disappear by day 28, and nearly all parameters were comparable to those of corresponding controls by day 91. Almost all parameters after instillation of I small particle were comparable to those of corresponding controls from day 28 through day 91. In contrast, the pulmonary inflammatory changes due to Ni(II) oxide nanopowder and US3352 persisted on day 28, and the values for most parameters were even higher on day 28 than on day 3. Histopathologic examination of lung from rats treated with either Ni(II) oxide nanopowder or US3352 revealed inflammatory cell infiltration, hyperplasia of alveolar epithelial cells, and degeneration and necrosis of alveolar macrophages

on day 3; although many of these abnormalities decreased slightly over time, they were present continuously through day 91, and some of them even increased over time (Fig. 9.6).

9.4.3.4 Analysis of Correlation Between Physicochemical Characteristics of NiO and Pulmonary Inflammatory Responses in Rats

To compare pulmonary inflammation quantitatively among the various nano-NiO, we analyzed BALF parameters at 2 mg/kg for all nanomaterials. We chose this dose because we were concerned that 6 mg/kg might cause saturation of effects during the acute phase.

Particle Size

We used DLS to measure the particle size in the administered solutions. To evaluate the contribution of particle size to the observed inflammatory response (ratio of neutrophil, total protein content, LDH), particle size in solution was expressed as a logarithm.

The correlation between the volume average diameter and the ratio of neutrophil during the acute phase is shown in Fig. 9.7; note that NovaWireNiO1 was not plotted because its particle size could not be determined by using DLS. Ni(II) oxide nanopowder, US3352, and I small particle showed high correlation ($R^2 = 0.993$) between the number average diameter and the ratio of neutrophil during the acute phase: smaller nanoparticles were more toxic than larger ones. In addition, rats exposed to Ni(II) oxide nanopowder or US3352 showed mild recovery from pul-
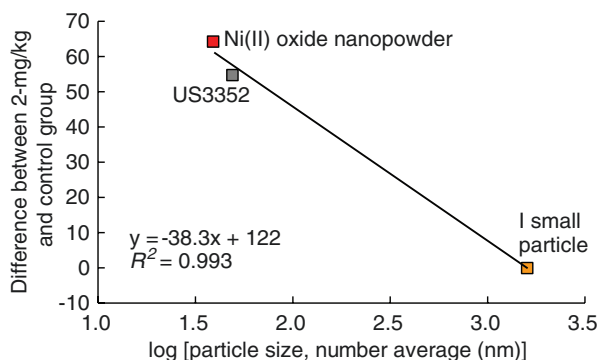
Fig. 9.7 Correlation between particle size (nm) and value of the ratio of neutrophil in BALF on day 3 after intratracheal instillation of various forms of NiO. Data are presented as the average of the difference between the values for the 2-mg/kg and control groups. The solid line is the linear regression line derived from the three tested materials (i.e., excluding the data for NovaWireNiO1)

monary inflammation during the subacute through sub-chronic phases. Although not as high as that during the acute phase, these nanomaterials continued to show high correlation between particle size and the pulmonary inflammatory response during the subacute ($R^2 = 0.814$) and sub-chronic ($R^2 = 0.893$) phases. Therefore, a NiO-containing nanomaterial's particle size in solution is likely to correlate with the pulmonary inflammatory response induced in rats after intratracheal instillation.

Shape

To evaluate its contribution to the inflammatory response, the particle shape of nano-NiO was expressed as an aspect ratio. However, aspect ratio and inflammatory response showed no correlation during the acute through sub-chronic phases. Therefore, the contribution of the shape of nano-NiO particles to acute to subchronic pulmonary inflammation in rats is considered negligible.

Solubility

To evaluate the contribution of the solubility of NiO to the inflammatory response, we used the dissolution rate coefficient in artificial lysosomal solution (see Chap. 10 or Ref. [41]) as a surrogate for solubility. NovaWireNiO1, which has high solubility and lung-clearance rate constants (see Chap. 10 or Ref. [41]), induced severe pulmonary inflammation during the acute phase but from which rats tended to recover during the subacute through sub-chronic phases. These findings suggest that early exclusion of NiO nanomaterials from the lung may contribute to the recovery from the inflammatory response. The remaining three NiO-containing nanomaterials showed no clear correlation between solubility or the lung clearance rate constant and pulmonary inflammatory response. Therefore, the solubility in the artificial lysosomal solution is unlikely to correlate with the persistence of pulmonary inflammatory response.

9.4.3.5 Equivalence Criteria of NiO

From our results, we categorized the four nano-NiO into two groups: one comprising an NiO with extremely high solubility in artificial lysosomal solution (NovaWireNiO1) and the other containing the remaining three nano-NiO compounds (Ni(II) oxide nanopowder, US3352, and I small particle). The dose–response curves including particle size for the ratio of neutrophil during the acute phase are shown in Fig. 9.8 (NovaWireNiO1 is not plotted). When instillation doses were normalized according to the number average particle size, the various NiO-induced inflammatory responses converged along the same sigmoidal dose–response curve ($R^2 = 0.9863$ [ratio of neutrophil], 0.8723 [total cell counts],
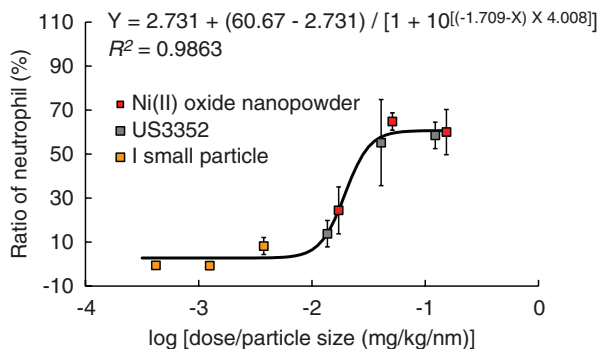
Fig. 9.8 Dose–response curves for the ratio of neutrophil in BALF on day 3 after intratracheal instillation of various forms of NiO. Data are from the 2-mg/kg group and are presented as average ±1 SD. Overlaid solid lines are the sigmoidal dose–response curves derived for three of the tested materials (excluding the data for NovaWireNiO1)

0.8902 [total protein], and 0.7987 [LDH]). These findings suggest that—excluding nano-NiO compounds highly soluble in artificial lysosomal solution—the intensity of the pulmonary inflammatory response is equivalent when the particle size is the same or, stated another way, smaller NiO particles induce more severe pulmonary inflammatory responses than larger NiO particles. Several previous studies have shown that the size or specific surface area of NiO particles plays an important role in their toxicity [37, 42, 43]. In addition, micron-sized NiO nanoparticle aggregates induced persistent pulmonary inflammation after intratracheal instillation, but NiO with a micron-sized diameter did not [44]. Furthermore, the dissolution rate coefficient in artificial lysosomes and the lung clearance rate constant were remarkably higher for NovaWireNiO1 than for the other three NiO materials (see Chap. 10 or Ref. [41]), suggesting that the solubility of NiO particles in lysosomes may contribute to the pulmonary inflammatory response and lung clearance in intratracheal administration studies of rats. For example, the solubility of nickel compounds contributes to their abilities to induce pulmonary toxicity or carcinogenicity, and highly soluble nickel compounds are severely toxic [45, 46]. Conversely, despite having low solubility, nickel compounds that continuously supply nickel ions at accumulation sites may contribute to carcinogenesis [38, 39].

Using our current results, we established the following equivalence criteria regarding the relationship between the physicochemical characteristics of nano-NiO compounds and the pulmonary inflammatory response after their intratracheal administration in rats: (1) particle size in solution likely is correlated with the magnitude of the pulmonary inflammatory response (i.e., small size in solution = severe inflammatory response), (2) particle shape is unlikely to be correlated with pulmonary inflammatory responses, and (3) the dissolution rate coefficient in lysosomes or the lung clearance rate constant may influence the persistence of the inflammatory response.

9.4.4 Intratracheal Instillation Study of SiO_2

9.4.4.1 Background Information on SiO_2

Silicon dioxide (SiO_2), one of the most abundant naturally occurring compounds, is used in many products in daily life. Silicon dioxide or substances composed of silicon dioxide are collectively referred to as silica. A typical example of industrially produced silica is silica gel. Silica takes various forms (i.e., shows crystal polymorphism) depending on conditions including pressure and temperature. As a result, silica compounds are roughly divided into crystalline silicas, such as quartz, and amorphous silicas, such as silica gel. Amorphous silica also includes SiO_2 present in uncalcified diatomaceous earth and organisms.

SiO_2 occurring naturally as crystalline silica is an important cause of occupational disease in the form of silicosis, especially in mining industry workers [47]; crystalline SiO_2 can also contribute to the development of tuberculosis, chronic bronchiolitis, chronic obstructive pulmonary disease, and lung cancer [48]. The International Agency for Research on Cancer has classified crystalline silica as a Group 1 compound—that is, carcinogenic to humans [49]. In contrast, silica in food additives, pigments, and health foods is noncrystalline (i.e., amorphous) and is classified into Group 3—not classifiable regarding carcinogenicity in humans [49].

9.4.4.2 Materials and Methods

We selected five types of crystalline silica (including one nano-sized crystalline silica) and four types of nano-amorphous silica for the evaluation of physicochemical properties. These materials could be classified into two groups according to their crystal structure: Min-U-Sil5 and SIO07PB (i.e., crystalline silicas) and a group of amorphous silica products (i.e., Sicastar). To obtain particles of smaller diameter, we centrifuged suspensions of Min-U-Sil5 to give Min-U-Sil5(Class). To obtain a broad range of particle sizes, we centrifuged suspensions of SIO07PB to yield SIO07PB(Class); ground it by ball milling to obtain SIO07PB(Gro); and alkalized it to give SIO07PB(100 nm). For the Sicastar group, we chose materials with two different particle sizes and two surface modifications ($Al(OH)_3$ and COOH) (Table 9.3).

Dose levels for the Min-U-Sil5 group were set at 0 (vehicle: purified water), 0.67, 2, and 6 mg/kg; doses for the SIO07PB and Sicastar materials were set at 0 (vehicle: purified water), 0.22, 0.67, and 2 mg/kg. For all compounds, the volume of instillation was 1 mL/kg. All other experimental details (e.g., strain, number, anesthesia of rats) were as described for the analysis of nano-TiO_2. For details regarding the nano-SiO_2 materials and preparation methods used in the current study, please refer to Chap. 7.

Table 9.3 Physicochemical characteristics of the nine tested forms of SiO_2

Material	Primary particle size[a] (nm)	Surface area[b] (m²/g)	Converted spherical primary particle size according to the specific surface area (nm)	Surface modification	Number-based agglomerate particle size according to DLS[c] (nm)
Min-U-Sil5	264	6.1	371.2	None	481
Min-U-Sil5(Class)	170	23.3	97.2	None	220
SIO07PB(Class)	218	18.8	120.4	None	222
SIO07PB(Gro)	251	33.8	67.0	None	231
SIO07PB(100 nm)	Could not be determined[d]	153.6	14.7	None	58.8
Sicastar	58.4	68.7	43.7	None	63.0
Sicastar(10 nm)	13.5	275.4	10.9	None	10.2
Sicastar-COOH	Could not be determined[d]	193.6	15.5	COOH	52.9
Sicastar-Al(OH)₃	59.8	75.3	39.8	Al(OH)₃	63.8

[a]Determined by SEM (model S4800, Hitachi High-Technologies Co.) or TEM (model JEM-2010, JEOL) analysis of 500 particles for each material
[b]Determined by BET surface area analysis (GEMINI VII, Shimadzu Co.) after drying
[c]Determined by using DLS (Zetasizer nano-ZS; Malvern Instruments Ltd.)
[d]Particle size could not be calculated because the particles agglomerated once they were diluted and the suspension dried

9.4.4.3 Results

After intratracheal instillation into rats, both crystalline silicas and nano-amorphous silicas induced acute pulmonary inflammation, although substance-specific differences were apparent. In BALF examinations, total cell counts, ratio of neutrophil, total protein content, albumin concentration, and LDH and ALP activities increased compared to the control group. The crystalline silicas SIO07PB(Class), SIO07PB(100 nm), and MIN-U-SIL5(Class) and amorphous silica Sicastar(10 nm) caused increases in relative lung weight. For these silica products, histopathologic examination revealed inflammatory cell infiltration in lung, hyperplasia of alveolar epithelial cells, and other signs of pulmonary inflammation (Figs. 9.9 and 9.10); in addition, SIO07PB(Class) led to degeneration and necrosis of alveolar macrophages. In contrast, SIO07PB(Gro) and Sicastar-COOH were associated with few inflammatory changes. All materials that caused pulmonary inflammation—particularly those associated with moderate to severe inflammatory changes—demonstrated dose dependence in almost all of the parameters assessed. As an example, the relative fold-changes in the total BALF cell count are shown in Fig. 9.11 (crystalline silicas) and Fig. 9.12 (amorphous silicas) (vehicle control = 100%).
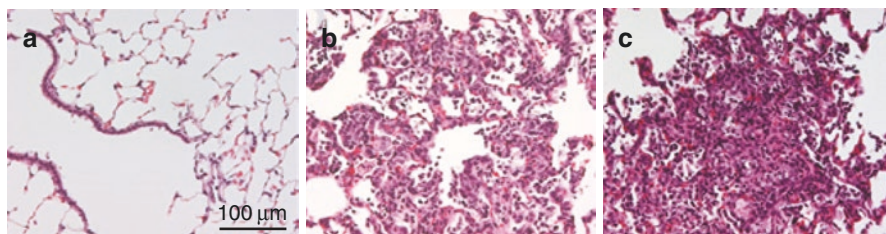
Fig. 9.9 Representative light micrographs of lung tissue from rats after intratracheal instillation of crystalline silica at 2 mg/kg. (**a**) Vehicle control on day 3 after instillation, (**b**) SIO07PB(Class) on day 3 after instillation, (**c**) SIO07PB(Class) on day 91 after instillation
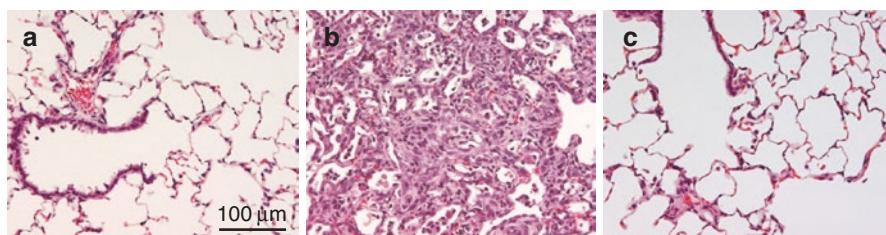
Fig. 9.10 Representative light micrographs of lung tissue from rats after intratracheal instillation of amorphous silica at 2 mg/kg. (**a**) Vehicle control on day 3 after instillation, (**b**) Sicastar(10 nm) on day 3 after instillation, (**c**) Sicastar(10 nm) on day 91 after instillation
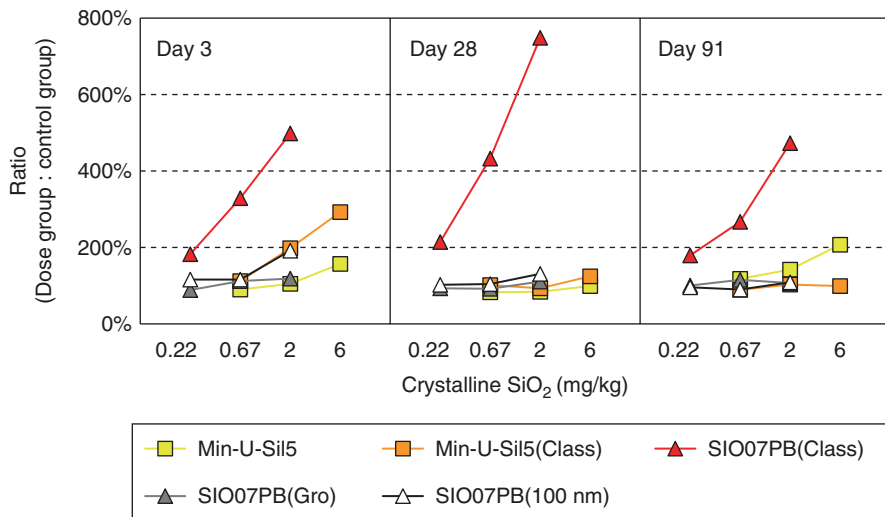
Fig. 9.11 Dose correlation and time course of total BALF cell count after intratracheal instillation of various forms of SiO_2 (crystalline). Data are presented as the average ratio between the value for the indicated dose group and that of the control group
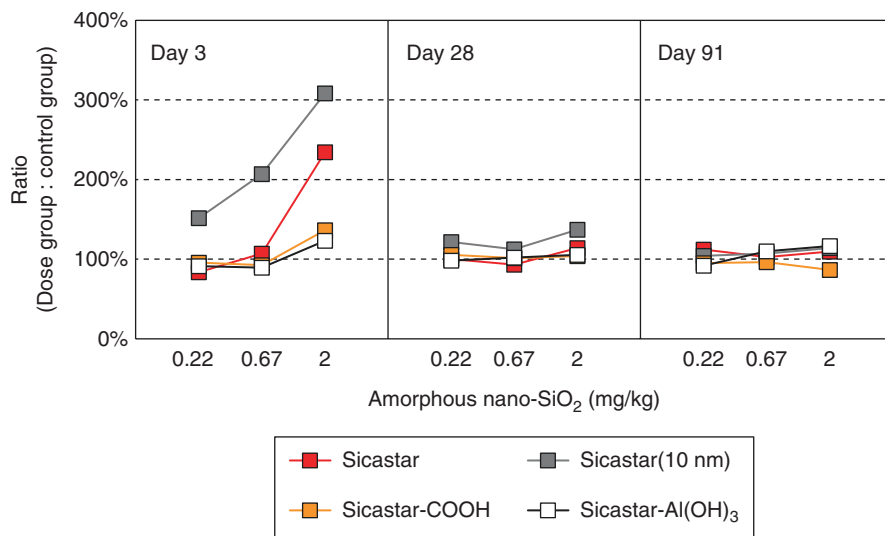
Fig. 9.12 Dose correlation and time course of total BALF cell count after intratracheal instillation of various forms of SiO₂ (amorphous). Data are presented as the average ratio between the value for the indicated dose group and that of the control group

The intensity of pulmonary inflammatory changes induced by crystalline silica was severe for SIO07PB(Class); moderate for Min-U-Sil5(Class), SIO07PB(100 nm), and Min-U-Sil5; and mild for SIO07PB(Gro). Amorphous silicas induced mild (Sicastar-COOH, Sicastar-Al(OH)₃) to moderate (Sicastar, Sicastar(10 nm)) pulmonary inflammation.

Although most of the SiO₂ caused acute pulmonary inflammatory changes, almost all of the evaluated parameters were comparable to corresponding controls by day 28. In sharp contrast to this pattern, the pulmonary inflammatory changes due to SIO07PB(Class) persisted on day 28, when most of the parameter values were even higher than on day 3. Histopathologic examination of SIO07PB(Class)-treated rats revealed maintenance of inflammatory cell infiltration in lung, hyperplasia of alveolar epithelial cells, and degeneration and necrosis of alveolar macrophages through day 91 (Fig. 9.9). In addition, pulmonary inflammatory changes due to Min-U-Sil5, which had subsided during the subacute period, manifested again on day 91 as pulmonary inflammatory cell infiltration and granulation tissue.

9.4.4.4 Analysis of Correlation Between Physicochemical Characteristics of SiO₂ and Pulmonary Inflammatory Responses in Rats

To compare pulmonary inflammation quantitatively among the various SiO₂, we analyzed BALF parameters at 2 mg/kg for all nanomaterials.
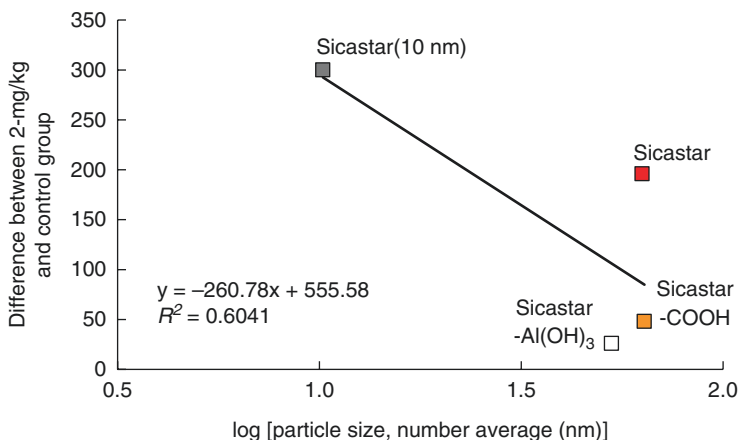
Particle Size

The particle size of SiO_2 nanomaterials in the administration solution was measured by using DLS. To evaluate its contribution to the inflammatory response, particle size in the solution was expressed as a logarithm. The correlation between the number average diameter and total BALF cell count during the acute phase is shown in Fig. 9.13 for crystalline silica and Fig. 9.14 for amorphous silica.
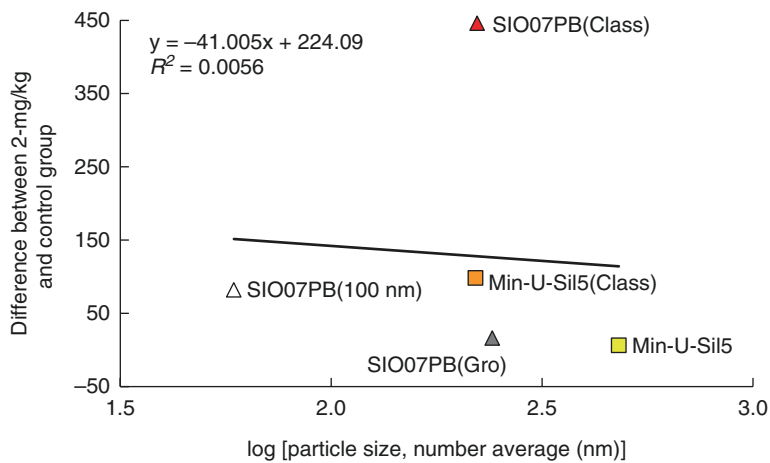
Fig. 9.13 Correlation between particle size (nm) and total BALF cell count on day 3 after intratracheal instillation of various forms of SiO_2 (crystalline). Data are presented as the average difference between the values for the 2-mg/kg and control groups. The solid line is the linear regression line derived from the five tested materials

Fig. 9.14 Correlation between particle size (nm) and total BALF cell count on day 3 after intratracheal instillation of various forms of SiO_2 (amorphous). Data are presented as the average difference between the values for the 2-mg/kg and control groups. The solid line is the linear regression line derived from the four tested materials

In the Min-U-Sil5 group of crystalline silicas, acute inflammation due to Min-U-Sil5(Class), which has a smaller particle size, was more severe than that from Min-U-Sil5. In the SIO07PB group, SIO07PB(Class) induced the most severe acute inflammation, whereas the inflammatory response to other SIO07PB derivatives was attenuated. SIO07PB(Gro) has almost the same particle size as SIO07PB(Class), but the surface area SIO07PB(Gro) is about twice that of SIO07PB(Class). In addition, the particle size of SIO07PB(100 nm) in the instillation solution was less than 25% of that of SIO07PB(Class). The contribution of particle size (and the related surface area) to nanotoxicity is well known [6, 50]. The Min-U-Sil5 group followed this tendency, but conflicting results were obtained for the SIO07PB group. However, comparison of SIO07PB(Gro) with SIO07PB(100 nm) showed that SIO07PB(100 nm), which had a smaller particle size, induced stronger acute inflammation. However, no clear correlation emerged when we comprehensively examined the five crystalline silicas, and any potential correlation was further obscured during the subacute through sub-chronic phases, when recovery from pulmonary inflammation was observed. Therefore, the effects of crystalline nano-SiO_2 on the pulmonary inflammatory response of rats is difficult to explain in terms of particle size involvement only.

In the Sicastar group of nano-amorphous silica, Sicastar(10 nm), which had a smaller particle size, induced more severe acute inflammation than Sicastar. In addition, Sicastar-$Al(OH)_3$ and Sicastar-COOH, which are similar in particle size to Sicastar, were less inflammatory not only than Sicastar(10 nm) but also than Sicastar. We consider that the surface modification of Sicastar-$Al(OH)_3$ and Sicastar-COOH may contribute to this effect. Comprehensive examination of the four amorphous silicas showed a modest correlation between particle size and severity of pulmonary inflammation. During the subacute through sub-chronic phases, this correlation was diminished further because recovery from pulmonary inflammation was observed. Therefore, particle size in solution is likely to correlate with the severity of the acute pulmonary inflammatory response to amorphous SiO_2-nanomaterials in rats: smaller nanoparticles were more toxic than larger ones.

Surface Modification

To evaluate the contribution of the surface modification of amorphous silica to the inflammatory response, we compared three types of Sicastar: that with no surface modification and those with surface modification by $Al(OH)_3$ or COOH. The acute inflammatory responses to the modified Sicastars both were attenuated relative to that from Sicastar. However, because recovery from pulmonary inflammation occurred during the subacute through sub-chronic phases, the contribution of surface modification to the inflammatory response during these phases could not be analyzed. Therefore, surface modification of amorphous SiO_2 nanomaterials is likely to correlate with the acute pulmonary inflammatory response observed in rats.

9.4.4.5 Equivalence Criteria of SiO$_2$

In the crystalline silica group, the correlation between particle size in the instillation solution and the acute inflammatory response differed between the Min-U-Sil5 group and SIO07PB group: the relevance was not as clear as for TiO$_2$ and NiO. However, as seen for the Min-U-Sil 5 group, the severity of the acute and sub-chronic pulmonary inflammatory responses differed according to particle size. Therefore, we inferred that the particle size of crystalline silica might contribute somewhat to the severity of inflammation and the phase of its development, but the details were unclear. In contrast, the pulmonary toxicity of quartz particles (crystalline silica) is related to their surface activity rather than to particle size or specific surface area [51]. In addition, hemolytic potential is considered to be a predictor of the hazards posed by nanomaterials [52], and surface silanol distribution has recently been reported to contribute to hemolytic activity [53]. We were unable to confirm whether the surface properties of crystalline silica contribute to their ability to induce pulmonary inflammation.

Among the amorphous silicas, particle size appears to contribute to the acute inflammatory response, as seen with TiO$_2$ and NiO. The dose–response curves including particle size for the total BALF cell counts during the acute phase are shown in Fig. 9.15. When instillation doses were normalized by number average particle size, the inflammatory responses induced by the different amorphous silicas tended to converge along the same sigmoidal dose–response curve ($R^2 = 0.7269$). Particle size and surface area of amorphous silicas are known important factors for lung toxicity [54]. In addition, surface modification nano-amorphous silica caused
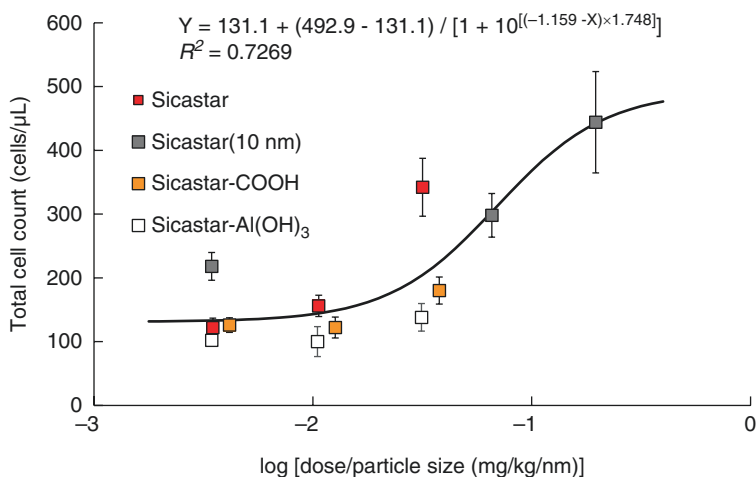
Fig. 9.15 Dose–response curves for total cell counts in BALF on day 3 after intratracheal instillation of various forms of SiO$_2$ (amorphous silica). Data are from the 2-mg/kg group and are presented as average ±1 SD. Overlaid solid line is the sigmoidal dose–response curve derived for the five tested materials

clear differences in acute inflammation but not in subacute inflammation. Surface modification (unmodified compared with amino- or carboxyl-modified) modulated cytotoxicity in in vitro studies of amorphous silica [55], and the authors suggested that surface modification of silica nanoparticles influences their interaction with bloodborne macromolecules [55]. In our study, the pulmonary inflammatory response to nanomaterials in the amorphous silica group was mild to moderate and did not persist during the subacute through sub-chronic phases. In general, the toxicity of amorphous silica is considered to be mild and transient [56].

Our results enable us to establish the following three equivalence criteria regarding the relationship between the physicochemical characteristics of nano-SiO_2 and the pulmonary inflammatory response after their intratracheal administration to rats: (1) the correlation between the particle size in solution of crystalline silicas and the severity of the acute pulmonary inflammatory response is unclear, (2) the particle size in solution of amorphous silicas likely is correlated with the severity of the acute pulmonary inflammatory response (i.e., small size in solution = severe inflammatory response), and (3) the surface modification of amorphous silica may influence the severity of the acute pulmonary inflammatory response.

9.4.5 Conclusion

Here we used intratracheal instillation to compare the effects of various physicochemical properties on the pulmonary toxicity of each of 20 nanomaterials representing three types (7 TiO_2, 4 NiO, and 9 SiO_2) in rats. As we showed in our current study, intratracheal administration studies are easily performed and are effective tools for comparing and evaluating the pulmonary toxicity of many materials. Particle size and surface properties are generally accepted as potentially important factors in the toxicity of nanomaterials. In agreement, our study results confirmed that particle size and surface properties of nanomaterials are equivalence criteria in regard to pulmonary toxicity. However, these equivalence criteria cannot necessarily be applied to some materials, such as crystalline silica. Therefore, the toxicity of nanomaterials still needs to be evaluated with sufficient caution.

We anticipate that our proposed equivalence criteria will facilitate the toxicity evaluation of nanomaterials. However, to sufficiently understand the correlation between these properties of nanomaterials and their ability to induce pulmonary toxicity, further accumulation of hazard assessment data is necessary. In addition, we surmise that our approach of using intratracheal administration studies will be an effective tool that further contributes to establishing additional equivalence criteria for nanomaterials.

References

1. The European Commission. Commission recommendation of 18 October 2011 on the definition of nanomaterial. Off. J. Eur. Union (2011/696/EU), 2011.
2. Hobson DW. Commercialization of nanotechnology. Interdiscip Rev Nanomed. 2009;1:189–202.
3. Braakhuis HM, Park MV, Gosens I, De Jong WH, Cassee FR. Physicochemical characteristics of nanomaterials that affect pulmonary inflammation. Part Fibre Toxicol. 2014;11:18.
4. Ferreira AJ, Cemlyn J, Robalo CC. Nanoparticles, nanotechnology and pulmonary nanotoxicology. Revista Portuguesa de Pneumologia (English Edition). 2013;19(1):28–37.
5. Driscoll KE, Costa DL, Hatch G, Henderson R, Oberdorster G, Salem H, Schlesinger RB. Intratracheal instillation as an exposure technique for the evaluation of respiratory tract toxicity: uses and limitations. Toxicol Sci. 2000;55:24–35.
6. Oberdorster G, Oberdorster E, Oberdorster J. Nanotoxicology: an emerging discipline evolving from studies of ultrafine particles. Environ Health Perspect. 2005;113:823–39.
7. Nakanishi J. Risk assessment of manufactured nanomaterials: "Approaches"—overview of approaches and results. Final report issued on Aug 17, 2011. NEDO project (P06041) "Research and development of nanoparticle characterisation methods", 2011.
8. NIOSH. Occupational exposure to titanium dioxide. Curr Intell Bull. 2011;63:1–119.
9. Donaldson K, Poland CA. Nanotoxicity: challenging the myth of nano-specific toxicity. Curr Opin Biotechnol. 2013;24:724–34.
10. WHO. Determination of airborne fibre number concentrations. A recommended method, by phase-contrast optical microscopy membrane filter method. Determination of airborne fibre number concentrations. A recommended method, by phase-contrast optical microscopy membrane filter method, 1997.
11. Donaldson K, Aitken R, Tran L, Stone V, Duffin R, Forrest G, Alexander A. Carbon nanotubes: a review of their properties in relation to pulmonary toxicology and workplace safety. Toxicol Sci. 2006;92:5–22.
12. Oberdorster G. Safety assessment for nanotechnology and nanomedicine: concepts of nanotoxicology. J Intern Med. 2010;267:89–105.
13. Peigney A, Laurent C, Flahaut R, Bacsa RR, Rousset A. Specific surface area of carbon nanotubes and bundles of carbon nanotubes. Carbon. 2001;39:507–14.
14. Veronesi B, de Haar C, Lee L, Oortgiesen M. The surface charge of visible particulate matter predicts biological activation in human bronchial epithelial cells. Toxicol Appl Pharmacol. 2002;178:144–54.
15. Oortgiesen M, Veronesi B, Eichenbaum G, Kiser PF, Simon SA. Residual oil fly ash and charged polymers activate epithelial cells and nociceptive sensory neurons. Am J Physiol Lung Cell Mol Physiol. 2000;278:L683–95.
16. Cho WS, Duffin R, Thielbeer F, Bradley M, Megson IL, Macnee W, Poland CA, Tran CL, Donaldson K. Zeta potential and solubility to toxic ions as mechanisms of lung inflammation caused by metal/metal oxide nanoparticles. Toxicol Sci. 2012;126:469–77.
17. Mura S, Hillaireau H, Nicolas J, Le Droumaguet B, Gueutin C, Zanna S, Tsapis N, Fattal E. Influence of surface charge on the potential toxicity of PLGA nanoparticles towards Calu-3 cells. Int J Nanomed. 2011;6:2591–605.
18. Greish K, Thiagarajan G, Herd H, Price R, Bauer H, Hubbard D, Burckle A, Sadekar S, Yu T, Anwar A, Ray A, Ghandehari H. Size and surface charge significantly influence the toxicity of silica and dendritic nanoparticles. Nanotoxicology. 2012;6:713–23.
19. Fubini B, Bolis V, Cavenago A, Volante M. Physicochemical properties of crystalline silica dusts and their possible implication in various biological responses. Scand J Work Environ Health. 1995;21(Suppl 2):9–14.
20. Gebel T, Foth H, Damm G, Freyberger A, Kramer PJ, Lilienblum W, Rohl C, Schupp T, Weiss C, Wollin KM, Hengstler JG. Manufactured nanomaterials: categorization and approaches to hazard assessment. Arch Toxicol. 2014;88:2191–211.

21. Baan RA. Carcinogenic hazards from inhaled carbon black, titanium dioxide, and talc not containing asbestos or asbestiform fibers: recent evaluations by an IARC Monographs Working Group. Inhal Toxicol. 2007;19(Suppl 1):213–28.
22. Morimoto Y, Izumi H, Yoshiura Y, Fujishima K, Yatera K, Yamamoto K. Usefulness of intratracheal instillation studies for estimating nanoparticle-induced pulmonary toxicity. Int J Mol Sci. 2016;17:165.
23. Hashizume N, Oshima Y, Nakai M, Kobayashi T, Sasaki T, Kawaguchi K, Honda K, Gamo M, Yamamoto K, Tsubokura Y, Ajimi S, Inoue Y, Imatanaka N. Categorization of nano-structured titanium dioxide according to physicochemical characteristics and pulmonary toxicity. Toxicol Rep. 2016;3:490–500.
24. Shi H, Magaye R, Castranova V, Zhao J. Titanium dioxide nanoparticles: a review of current toxicological data. Part Fibre Toxicol. 2013;10:15.
25. Wang J, Fan Y. Lung injury induced by TiO$_2$ nanoparticles depends on their structural features: size, shape, crystal phases, and surface coating. Int J Mol Sci. 2014;15:22258–78.
26. Oberdorster G, Ferin J, Gelein R, Soderholm SC, Finkelstein J. Role of the alveolar macrophage in lung injury: studies with ultrafine particles. Environ Health Perspect. 1992;97:193–9.
27. Renwick LC, Brown D, Clouter A, Donaldson K. Increased inflammation and altered macrophage chemotactic responses caused by two ultrafine particle types. Occup Environ Med. 2004;61:442–7.
28. Kobayashi N, Naya M, Endoh S, Maru J, Yamamoto K, Nakanishi J. Comparative pulmonary toxicity study of nano-TiO$_2$ particles of different sizes and agglomerations in rats: different short- and long-term post-instillation results. Toxicology. 2009;264:110–8.
29. Warheit DB, Webb TR, Sayes CM, Colvin VL, Reed KL. Pulmonary instillation studies with nanoscale TiO$_2$ rods and dots in rats: toxicity is not dependent upon particle size and surface area. Toxicol Sci. 2006;91:227–36.
30. Oberdorster G. Pulmonary effects of inhaled ultrafine particles. Int Arch Occup Environ Health. 2001;74:1–8.
31. Hohr D, Steinfartz Y, Schins RP, Knaapen AM, Martra G, Fubini B, Borm PJ. The surface area rather than the surface coating determines the acute inflammatory response after instillation of fine and ultrafine TiO$_2$ in the rat. Int J Hyg Environ Health. 2002;205:239–44.
32. Warheit DB, Brock WJ, Lee KP, Webb TR, Reed KL. Comparative pulmonary toxicity inhalation and instillation studies with different TiO$_2$ particle formulations: impact of surface treatments on particle toxicity. Toxicol Sci. 2005;88:514–24.
33. Oyabu T, Morimoto Y, Hirohashi M, Horie M, Kambara T, Woo Lee BW, Hashiba M, Mizuguchi Y, Myojo T, Kuroda E. Dose-dependent pulmonary response of well-dispersed titanium dioxide nanoparticles following intratracheal instillation. J Nanopart Res. 2013;15:1600–10.
34. Shinohara N, Oshima Y, Kobayashi T, Imatanaka N, Nakai M, Ichinose T, Sasaki T, Kawaguchi K, Zhang G, Gamo M. Pulmonary clearance kinetics and extrapulmonary translocation of seven titanium dioxide nano- and submicron materials following intratracheal administration in rats. Nanotoxicology. 2015;9:1050–8.
35. Horie M, Fukui H, Endoh S, Maru J, Miyauchi A, Shichiri M, Fujita K, Niki E, Hagihara Y, Yoshida Y, Morimoto Y, Iwahashi H. Comparison of acute oxidative stress on rat lung induced by nano and fine-scale, soluble and insoluble metal oxide particles: NiO and TiO$_2$. Inhal Toxicol. 2012;24:391–400.
36. Sager T, Wolfarth M, Keane M, Porter D, Castranova V, Holian A. Effects of nickel-oxide nanoparticle pre-exposure dispersion status on bioactivity in the mouse lung. Nanotoxicology. 2016;10:151–61.
37. Ogami A, Morimoto Y, Myojo T, Oyabu T, Murakami M, Todoroki M, Nishi K, Kadoya C, Yamamoto M, Tanaka I. Pathological features of different sizes of nickel oxide following intratracheal instillation in rats. Inhal Toxicol. 2009;21:812–8.
38. Sunderman FW Jr. Mechanisms of nickel carcinogenesis. Scand J Work Environ Health. 1989;15:1–12.

39. Dunnick JK, Elwell MR, Radovsky AE, Benson JM, Hahn FF, Nikula KJ, Barr EB, Hobbs CH. Comparative carcinogenic effects of nickel subsulfide, nickel oxide, or nickel sulfate hexahydrate chronic exposures in the lung. Cancer Res. 1995;55:5251–6.
40. IARC. Nickel and nickel compounds. IARC monographs on the evaluation of carcinogenic risks to humans. 2012;100C:169–218.
41. Shinohara N, Zhang G, Oshima Y, Kobayashi T, Imatanaka N, Nakai M, Sasaki T, Kawaguchi K, Gamo M. Kinetics and dissolution of intratracheally administered nickel oxide nanomaterials in rats. Part Fibre Toxicol. 2017;14:48.
42. Mizuguchi Y, Myojo T, Oyabu T, Hashiba M, Lee BW, Yamamoto M, Todoroki M, Nishi K, Kadoya C, Ogami A, Morimoto Y, Tanaka I, Shimada M, Uchida K, Endoh S, Nakanishi J. Comparison of dose-response relations between 4-week inhalation and intratracheal instillation of NiO nanoparticles using polimorphonuclear neutrophils in bronchoalveolar lavage fluid as a biomarker of pulmonary inflammation. Inhal Toxicol. 2013;25:29–36.
43. Zhang Q, Kusaka Y, Zhu X, Sato K, Mo Y, Kluz T, Donaldson K. Comparative toxicity of standard nickel and ultrafine nickel in lung after intratracheal instillation. J Occup Health. 2003;45:23–30.
44. Morimoto Y, Hirohashi M, Ogami A, Oyabu T, Myojo T, Hashiba M, Mizuguchi Y, Kambara T, Lee BW, Kuroda E, Tanaka I. Pulmonary toxicity following an intratracheal instillation of nickel oxide nanoparticle agglomerates. J Occup Health. 2011;53:293–5.
45. Benson JM, Chang IY, Cheng YS, Hahn FF, Kennedy CH, Barr EB, Maples KR, Snipes MB. Particle clearance and histopathology in lungs of F344/N rats and B6C3F1 mice inhaling nickel oxide or nickel sulfate. Fundam Appl Toxicol. 1995;28:232–44.
46. Kang GS, Gillespie PA, Gunnison A, Rengifo H, Koberstein J, Chen LC. Comparative pulmonary toxicity of inhaled nickel nanoparticles; role of deposited dose and solubility. Inhal Toxicol. 2011;23:95–103.
47. Thomas CR, Kelley TR. A brief review of silicosis in the United States. Environ Health Insights. 2010;4:21–6.
48. Rimal B, Greenberg AK, Rom WN. Basic pathogenetic mechanisms in silicosis: current understanding. Curr Opin Pulm Med. 2005;11:169–73.
49. IARC. IARC Working group on the evaluation of carcinogenic risks to humans: silica, some silicates, coal dust and para-aramid fibrils. Lyon, 15–22 October 1996. IARC Monogr Eval Carcinog Risks Hum. 1997;68:1–475.
50. Donaldson K, Stone V, Clouter A, Renwick L, MacNee W. Ultrafine particles. Occup Environ Med. 2001;58:194–9.
51. Warheit DB, Webb TR, Colvin VL, Reed KL, Sayes CM. Pulmonary bioassay studies with nanoscale and fine-quartz particles in rats: toxicity is not dependent upon particle size but on surface characteristics. Toxicol Sci. 2007;95:270–80.
52. Clouter A, Brown D, Hohr D, Borm P, Donaldson K. Inflammatory effects of respirable quartz collected in workplaces versus standard DQ12 quartz: particle surface correlates. Toxicol Sci. 2001;63:90–8.
53. Pavan C, Rabolli V, Tomatis M, Fubini B, Lison D. Why does the hemolytic activity of silica predict its pro-inflammatory activity? Part Fibre Toxicol. 2014;11:76.
54. Kaewamatawong T, Kawamura N, Okajima M, Sawada M, Morita T, Shimada A. Acute pulmonary toxicity caused by exposure to colloidal silica: particle size dependent pathological changes in mice. Toxicol Pathol. 2005;33:743–9.
55. Nabeshi H, Yoshikawa T, Arimori A, Yoshida T, Tochigi S, Hirai T, Akase T, Nagano K, Abe Y, Kamada H, Tsunoda S, Itoh N, Yoshioka Y, Tsutsumi Y. Effect of surface properties of silica nanoparticles on their cytotoxicity and cellular distribution in murine macrophages. Nanoscale Res Lett. 2011;6:93.
56. Fruijtier-Polloth C. The toxicological mode of action and the safety of synthetic amorphous silica-a nanostructured material. Toxicology. 2012;294:61–79.

Chapter 10
Toxicokinetics of Nano Materials After the Intratracheal Administration

Naohide Shinohara

Abstract Toxicokinetic data is important to evaluate the toxicity of nano materials because burden and toxicity for each organ can be different among particles even at same burden. Intratracheal administration has been proposed to use as screening method for the evaluation of inhalation toxicity to nano materials. In the manuscript, toxicokinetic test methods, deposition/clearance/distribution, and toxicokinetic models of nano materials after intratracheal administration mainly conducted in METI Project are described. By using XRF and ICP-MS, the deposition, clearance, and distribution were determined in the animal tests. Insoluble and poorly soluble nano particles detected in lung were 44–100% at 1–3 days after intratracheally administration, while poorly soluble coarse particle, which is likely to be trapped at bronchiole, detected in lung at 1–3 days after intratracheally administration were only 5–40%. Twenty-eight days after the intratracheal administration, the lung contained <1% (soluble NiO), 37–90% (poorly soluble NiO and Al(OH)$_3$-coated TiO$_2$), 40–62% (insoluble TiO$_2$ particles), 11–30% (amorphous SiO$_2$), and 21–63% (crystal SiO$_2$) of administered doses. Translocation from lung to extrapulmonary organs was quite low except for lymph nodes.

Keywords Animal test · ICP-MS · XRF · Deposition · Clearance · Distribution Compartment model

10.1 Introduction

There are growing concerns about the toxicity of nanomaterials owing to the lack of information on their potential risks in workers and the general population. Nanomaterials with the same chemical formula may exert different toxicities,

N. Shinohara (✉)
Research Institute of Science for Safety and Sustainability (RISS), National Institute of Advanced Industrial Science and Technology (AIST), Tsukuba, Ibaraki, Japan
e-mail: n-shinohara@aist.go.jp

depending on physicochemical characteristics such as size, shape, and crystalline structure.

It is important to know the toxicokinetics to evaluate the toxicity of nano materials and chemical compounds since even in the case of same dose, burden for each organ can be different among particles because translocation and accumulation could be different among particles. Considering the situation of manufacturing and usage of nano materials, inhalation exposure of labor, who treat nano materials, can be more likely to happen. Therefore, most toxicological studies of nano materials were targeted to the inhalation exposure.

For the evaluation of inhalation toxicity, inhalation exposure test and intratracheal administration test were conducted as in vivo test. In inhalation exposure test, test animals inhale aerosol of nano materials, which is closest method to real exposure. There are two methods; one is whole body exposure test, in which animals inhale aerosol at constant concentration in the cage, and another is nose-only exposure test, in which animals inhale aerosol through a mask in the holder.

For inhalation exposure test of chemical substances, following OECD test guidelines and guidance document have been published.

- TG403: Acute Inhalation Toxicity
- TG436: Acute Inhalation Toxicity—Acute Toxic Class Method
- TG412: Subacute Inhalation Toxicity: 28-Day Study
- TG413: Subchronic Inhalation Toxicity: 90-day Study
- GD39: Acute Inhalation Toxicity Testing

Although these test guidelines and guidance used to be not suitable for nano materials, revision to use for nano materials have been conducted recently.

In intratracheal administration test, animals are instilled or sprayed the suspension of nano materials directly into the trachea by using sonde. Comparing to the inhalation exposure test, intratracheal administration is much lower cost and less technical demand. However, nonspecific response could be induced early after administration because large amount of test substances is introduced into lung at one time. In addition, effect on the upper respiratory tract cannot be tested since test substances are directly administered into trachea.

Between 2011 and 2016 (5 years), Ministry of Economy, Trade and Industry of Japan (METI) launched a project on "Development of innovative methodology for safety assessment of industrial nanomaterials." In this project, seven kinds of TiO_2, four kinds of NiO, and nine kinds of SiO_2 were intratracheally administered into rats, and the toxicokinetics and lung inflammatory were evaluated. Hereinafter, this project is described as "METI project."

In this manuscript, test methods, deposition and distribution after intratracheal administration, and toxicokinetic models for nano materials after intratracheal administration mainly conducted in METI Project are described.

10.2 Test Methods

10.2.1 Animal Test

Animal species, sex, and age were selected depending on the object of test. In METI Project, F344/DuCrlCrlj rat (male, 12 weeks old), which have long-term survival rate, were used to be observed for up to 2 years. Suspensions of nano materials were appropriately prepared considering characterization and stability. To know the dose dependency, multiple dose group were set as well as vehicle control group. To avoid bolus effect and overload, which don't show toxicity of nano material but effect of administration itself, administer volume and dose have to be adequately set. Single administration is generally conducted, but multiple administration can be used for achieving high dose. Observation frequency and period is generally 3–5 times during 4–26 weeks after the administration. In METI project, five animals in each group were dissected 3, 28, and 91 days after the administration of nano materials. For one type of TiO_2 particle, five animals in each group were dissected 1, 3, 7, 28, 91, and 182 days after the administration.

In METI project, all animal was treated in accordance with the guidelines for animal experiments in our laboratory, which referred to the guidelines of the Ministry of the Environment, Ministry of Health, Labour and Welfare, Ministry of Agriculture, Forestry and Fisheries, and Ministry of Education, Culture, Sports, Science and Technology. The present experiment was approved by the Animal Care and Use Committee, Chemicals Evaluation and Research Institute, and by the Institutional Animal Care and Use Committee of the National Institute of Advanced Industrial Science and Technology.

10.2.2 Measurement of Distribution in Organ

Distribution in organ is measured to clarify in which part of organ exposed nanomaterial is likely to deposit and/or remain. The information is valuable for interpretation of results, extrapolation among different administration method, and estimation of toxicological mechanism. For the purpose, radioisotope analysis, fluorescent X-ray analysis (XRF), and microscope observation are used.

After administration of nanomaterial, which is labeled with a radioisotope or is synthesized with radioisotope, body distribution and tissue distribution can be measured with magnetic resonance imaging (MRI), positron-emission tomography (PET), gamma radiation detector, and scintillation technique. With these methods, distribution can be observed alive.

For the metal and metal oxide nano materials, XRF can be used to measure the distribution. When sectioned tissue is measured, it is necessary to check the subject

metal is not contained in glass slide since Ti and Ni sometimes contained in glass slide. In addition, cover glass often contains high concentration of Ti.

Optical microscope and transmission electron microscope (TEM) are often used for the observation in which part of tissue nanomaterial exist. Polarization microscope can be used for CNT observation in organ tissue. Dark-field microscope can be used for metal and metal oxide observation.

In METI project, Ti distribution in lung sectioned tissue of rat (3 μm of thickness) were measured with a high-performance energy-dispersive XRF microscopy with a rhodium target X-ray tube (XGT-7200; Horiba Int., Kyoto, Japan). The spectral intensity of the Ti-Kα line (4.511 keV) was acquired for the quantification of Ti in the selected rectangular areas of the samples. The analytical conditions of Ti were set as follows: beam size (spatial resolution), 100 μm; step size, 200 μm for lung sections from the control and TiO_2-treated rats; acquisition time, 60 s/point; excited voltage, 50 kV; excited current, 1 mA; full vacuum mode. The spectral intensity of Ti in a mesh (100 μm × 100 μm) was measured for each analytical point.

10.2.3   Analysis of Burden of Nano Materials in Organ

After dissection, each organ is weighed, cut into small pieces and homogenized, pretreated (acid-treatment, alkali-treatment, etc.), and analyzed.

10.2.3.1   Homogenization

Since most analysis of nano materials in organ is conducted for a part of organ, the concentration in a part of organ is necessary to be equivalent to the concentration in whole of organ. Therefore, organs are crushed to pieces and homogenate to decrease the sampling error. This operation is usually regarded as homogenize. Generally, a certain volume (twice to fourfold of organ weight) of ultrapure water or saline are added to organ sample, and homogenized using homogenizer. If biomarker (e.g., cell count and lactase dehydrogenase, etc.) will be measured after the halogenation, saline can be used, but ultrapure water is better to use for the contents analysis. Homogenizer include rotating rod with metal or resin blade to cut organs and high-speed shaking with glass or zirconia bead to grind organ. Before use of homogenizer, it is necessary to check not including and not dissolved the object nano material or metal in the homogenizer and tubes. For example, colored resin sometimes includes titanium oxide. As the other homogenizing method, crushing organ by shaking after vacuum-freeze drying and enzymatic degradation using ultrasonication were conducted.

In METI project, the lung, kidney, and spleen samples were homogenized with 2 mL of ultrapure water (Milli-Q Advantage A10 Ultrapure Water Purification System, Merck Millipore, Billerica, MA, USA), and the liver was homogenized with 10 mL of ultrapure water. An electric homogenizer (PT10-35 Kinematica AG, NS-50, and NS-52; Microtec Co. Ltd., Chiba, Japan) was used. The resulting homogenates were stored at −30 or −80 °C until analysis.

10.2.3.2   Pretreatment

Before the analysis, homogenate sample is sometimes pretreated appropriate for the analytical method to remove the coexisting material which interfere the analysis and to dissolve in the medium which can be introduced into the analytical instrument. Since organ tissue-derived organic carbon often interferes analysis, organic carbon is decomposed by acid-treating, ashing, enzymatic-treating, etc. at first. Then, the treated sample is dissolved in sorbent. Degradation and dissolution are sometimes simultaneously conducted. For the metal and metal oxide, homogenate samples are acidly treated in nitric acid at high temperature using microwave decomposition instrument or hot plate. Sulfuric acid or hydrogen peroxide is sometimes used to promote the decomposition of organic carbon, and hydrofluoric acid is used to promote the dissolution of metal in the acid solution. For fullerene C_{60} and some polymers, homogenate samples are shaken and sonicated in organic solvents such as toluene after enzymatic treatment. Centrifugation and/or filtration are used to separate subject substance such carbon nano tube (CNT) from coexisting materials after enzymatic treatment, acid treatment, or alkali treatment.

In METI project, the homogenate samples (0.1–1.0 g of organ tissue) with nitric acid (HNO_3: 68%; 0.5–1.0 mL), sulfuric acid (H_2SO_4: 98%; 0.1–0.2 mL), and hydrogen peroxide (H_2O_2: 35%; 0.1–0.2 mL) in PFA tube were heated to 180 or 220 °C for 20–40 min in microwave sample preparation instrument (Speedwave 4; Berghof, Germany) for TiO_2, NiO, and SiO_2 samples. For SiO_2 and some kinds of large TiO_2 particles, hydrofluoric acid (HF: 38%; 0.1–0.2 mL) was added to the solution after heating and kept for a night. After these treatments, the samples were diluted with ultrapure water to 5.0–100 mL to arrange the HNO_3 concentration of the sample solution in 5%.

10.2.3.3   Analysis

Various methods are used to analyze the nano materials. Inductively coupled plasma-mass spectroscopy (ICP-MS) and inductively coupled plasma-atomic emission spectrometry (ICP-AES) are often used to determine metals. Although ICP-MS has high sensitivity, it is required attention to the interfere by coexist materials such as Ar, O_2, and tissue-derived calcium. High-performance liquid chromatography (HPLC) with UV detector is used for the analysis of fullerene C_{60}. Combustion method with infrared spectroscopy (IR) or hydrogen flame ionization detector (FID), benzoperylene adsorption method with HPLC-fluorescence detector, and radioisotope analysis are used for the analysis of CNT.

In METI project, Ti and Ni contents in organ were determined by ICP-SFMS using a Finnigan ELEMENT II (Thermo Fisher Scientific Inc., Germany). For ICP-SFMS, RF power was 1250 W, cool gas flow rate was 16 L/min, auxiliary gas flow rate was 0.87 L/min, sample gas flow rate was 0.870–0.965 L/min, additional gas flow rate was 0.080–0.180 L/min, mass resolution (R) was 4000, and the measured mass number m/z was 48.9479 for Ti and 59.9308 for Ni. ^{49}Ti (mass: 48.9479) was analyzed because its spectrum could be separated from the spectra of $^{33}S^{16}O$

(mass: 48.9666), $^{31}P^{18}O$ (mass: 48.9729), and $^{32}S^{16}O^{1}H$ (mass: 48.9748). Si contents in organ were determined by ICP-AES using a ULTIMA2 (HORIBA Ltd., Japan). For ICP-AES, RF power was 1200 W, plasma gas flow rate was 14 L/min, auxiliary gas flow rate was 0.4 L/min, nebulizer gas flow rate was 0.8 L/min, sheath gas flow rate was 0.2 L/min, N_2 gas flow rate was 4 L/min, measured wave length was 251.611 nm.

10.3 Deposition, Clearance, and Distribution

10.3.1 Deposition

Inhaled particles are deposited on tracheobronchial (TB) and alveolar region. The deposition fraction, which depends on the particle size, can be estimated by using the Multiple-Path Particle Dosimetry (MPPD) model [1]. The deposition fraction on TB and alveolar region for particles with 100 nm of diameter 1.0 g/cm^3 of density are estimated to be 0.0936 and 0.200, respectively, by using MPPD model.

The lungs contained 55–89% of the administered insoluble TiO_2 dose 1–3 days after administration [2, 3] and 44–100% the administered poorly soluble NiO dose 3 days after administration [4]. Since particles deposited on bronchus and bronchiole can be removed by clearing by the rapid mucociliary clearance from the conduction airways within 1 day, the percentage showed the proportion of TiO_2 and NiO particles which reached to alveolar region in administered dose. For coarse NiO particles, which is likely to be trapped at bronchiole, only 5–40% of particles were detected in lung at 3 days after the intratracheal administration, indicating that most coarse particles cannot reach to alveolar region after intratracheal administration [4].

An example of TiO_2 distribution in rat lung after intratracheal administration of TiO_2 nano particles measured in METI project are shown in Fig. 10.1. Intratracheally administered TiO_2 was deposited more in the right caudal and accessory lobes located downstream of the administration direction of NP suspensions, and less deposited in the right middle lobes [5, 6]. Variations of TiO_2 content in sections of each lobe among rats, which were intratracheally administered TiO_2 nano particles, decrease using microsprayer comparing to using gavage needle, but pattern of pulmonary distribution in lung was not different among microsprayer and gavage needle [7]. Variations of TiO_2 content in sections of each lobe among rats, which were intratracheally administered TiO_2 nano particles, decrease depending on the frequency of intratracheal administration, but pattern of pulmonary distribution in lung was not different among different frequency of intratracheal administration [5]. In addition, pulmonary distribution was not different between inhalation exposure and intratracheal administration [8].

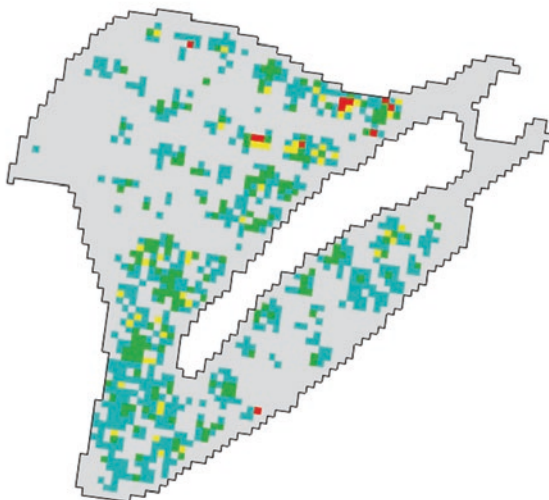ND (< DL)   ☐ DL—0.3 ng/mesh   ☐ 0.3—0.6 ng/mesh   ☐ 0.6—0.9 ng/mesh   ☐ >0.9 ng/mesh

Fig. 10.1 TiO$_2$ distribution in lung after intratracheal administration [8]

10.3.2 *Clearance from Lung*

Chemical substances, inhaled into alveolar region, are cleared from lung to blood or exhaled breath within a few minutes to hours. On the other hand, particles, inhaled and deposited on alveolar region, cannot be cleared immediately. Most of the particles, deposited on alveolar surface, are cleared both by the bronchial mucociliary escalator via the bronchi after macrophage phagocytosis/migration and translocation to the thoracic lymph nodes. However, some particles such as MWCNT cannot be cleared from lung for long duration even after the phagocytosis by macrophage [9].

In METI project, pulmonary clearance of seven types of TiO$_2$, four types of NiO, and nine types of SiO$_2$ was determined after intratracheal administration. For uncoated TiO$_2$ particles, the lungs contained 9.0–37% and 6.1–31% of the administered TiO$_2$ dose 91 days and 26 weeks after the administration, respectively, and the retained TiO$_2$ increased with dose [2, 3]. The dose dependency of clearance might be owing to the overload. On the other hand, for Al(OH)$_3$-coated TiO$_2$ particles, the lungs retained 28–61% of the TiO$_2$ administered, and the retained TiO$_2$ increased with dose 91 days after administration [2]. For poorly soluble NiO nano particles, the lungs contained 40–62% of the administered TiO$_2$ dose 91 days after the administration [2, 3]. For a certain type of NiO, which is moderately soluble in artificial lysosomal fluid, clearance was delayed in any doses [4]. For NiO particle with high solubility,

the lungs contained 22–33% and <1% of the administered dose 3 and 28 days after administration, respectively, because dissolved NiO were rapidly cleared into blood [4]. These slow clearances may be induced by persistent pulmonary inflammation because of their longer retention and continual release of Al or Ni ions in the lysosome. For amorphous and crystal SiO_2, the lungs contained 11–30% and 21–63% of the administered dose 28 days after administration, respectively [8].

10.3.3   Translocation to the Other Organs

Nano particle is likely to delay the phagocytosis and likely to transfer to interstitium and lymph nodes comparing to larger particles [10, 11]. Translocation to lymph nodes increase with dose of particle [2, 3, 12]. A certain MWCNT (MWNT7) can translocate to pleural area although much lower number of fibers needed to result in tumor formation [13].

   In METI project, the thoracic lymph nodes were increased with time (0.0088–0.30% at 3 days to 0.0057–11% at 91 days after administration of TiO_2 and NiO relative to the administered doses) and with dose (0.0057–2.2% for 0.375–0.75 mg/kg bw to 0.54–11% for 4.0–6.0 mg/kg bw at 91 days after administration) except for highly soluble NiO (Fig. 10.6 [2–4]). For SiO_2, a certain crystal SiO_2 translocated to lymph nodes without dose dependency (8.8–10% for 0.20–1.9 mg/kg bw at 91 days after administration) although translocation to lymph nodes increase with dose for some SiO_2. Translocation to liver were observed for TiO_2 (~0.11%), but was not observed for NiO (<1%) after the intratracheal administration [2–4]. TiO_2, NiO, and SiO_2 were not detected in spleen and brain after the intratracheal administration.

10.4   Toxicokinetic Models

10.4.1   Model of Pulmonary Clearance

Deposition on alveolar region and tracheal bronchus (TB) region and pulmonary clearance were mathematically modeled in ICRP model [14]. In the model, alveolar region was divided into three compartments, bronchiole was divided into three compartments, and bronchi was divided into three compartments. Stöber et al. [15] and Stöber [16] showed POCK (Physiology oriented compartment kinetic) model in which particles translocated among multiple compartments. The multiple compartments in alveolar region included alveolar surface, mobile macrophages, sequestrum, interstitium, and interstitial granuloma. The transfer rate coefficients in these models were estimated using physicochemical properties and in vitro test (Fig. 10.2). These compartments are too much to estimate the transfer coefficient by using animal test results. Therefore, simple compartment modes were used for fitting with in vivo test. For example, Kuempel et al. [17] described three-compartment model including two-compartment lung (Fig. 10.2). Gregoratto et al. [18]
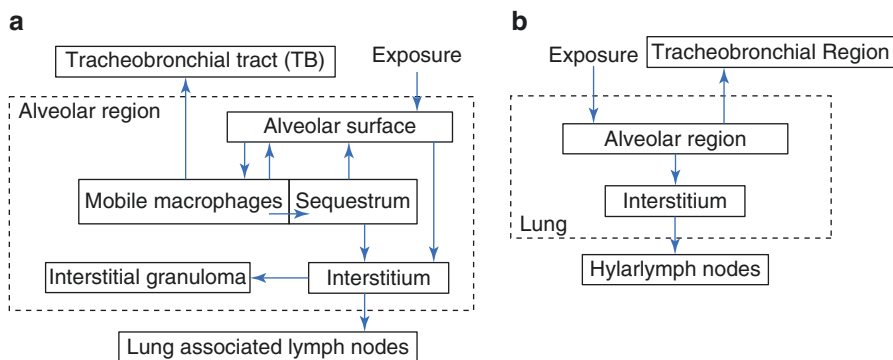
Fig. 10.2 Multicompartment models proposed in (**a**) Stöber [16] and (**b**) Kuemple et al. [17]

divided the lung into two compartments, one is transfer to trachea and bronchus, and the other is transfer to lymph nodes.

In METI project, two types of two-compartment models were fitted to the pulmonary burden measured in this project for one type of TiO_2 which were administered to rats and dissected 1, 3, 7, 28, 91, and 182 days after the administration. One two-compartment model was represented by a clearance from compartment 1 and reciprocal translocation between compartment 1 and 2 as shown in Eqs. (10.1) and (10.2), where k_{21} was the rate constant for translocation from compartment 1–2 (per day) (Fig. 10.3a).

$$dB_1 / dt = -k_1 B_1 - k_{12} B_1 + k_{21} B_2 \qquad (10.1)$$

$$dB_2 / dt = k_{12} B_1 - k_{21} B_2 \qquad (10.2)$$

The other two-compartment model was represented by a two-step clearance from compartment 1 and compartment 2 (Fig. 10.3b).

$$dB_1 / dt = -k_1 B_1 - k_{12} B_1 \qquad (10.3)$$

$$dB_2 / dt = k_{12} B_1 - k_2 B_2 \qquad (10.4)$$

The clearance/translocation rate constants, k, k_1, k_{12}, k_2, and k_{21} were estimated by curve fitting the decay curve to the TiO_2 burden measured in the lung using a least squares approach.

To compare the toxicokinetics of several nanomaterials, one-compartment model estimation was conducted because the lung burden was determined three times after intratracheal administration (Fig. 10.4).
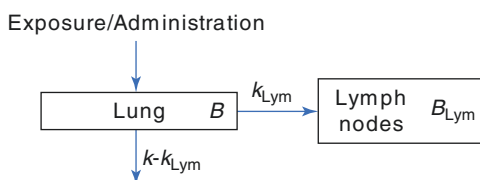
$$dB / dt = -kB \qquad (10.5)$$

$$dB_{Lym} / dt = k_{Lym} B \qquad (10.6)$$
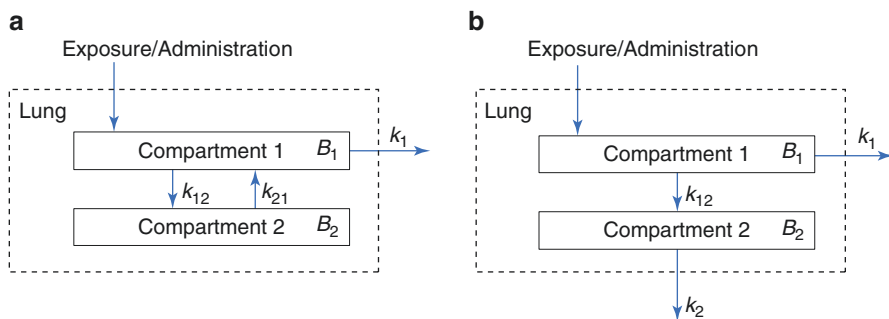
Fig. 10.3 Two-lung-compartment models proposed in METI project (**a**) in which nanoparticles are cleared from compartment 1 and translocate from compartments 2 to 1 and (**b**) in which nanoparticles are cleared from compartments 1 and 2 [3]

Fig. 10.4 One-lung-compartment models proposed in METI project [3]

10.4.2 Model of Pulmonary Clearance

In the METI project, fitting results did not differ significantly between 2 two-compartment models. The sum of square differences indicated that the estimated thoracic lymph node burdens were a much better fit to the measured burdens when TiO_2 translocation from compartment 1 to the thoracic lymph nodes was assumed, much rather than those where TiO_2 translocation from compartment 2 to the thoracic lymph nodes was assumed.

The results of one-compartment models for TiO_2, NiO, and SiO_2 are shown in Fig. 10.5. The pulmonary clearance rate constants, k_{Lung}, were higher at TiO_2 doses of 0.375–2.0 mg/kg bw (0.016–0.020/day) than TiO_2 doses of 3.0–6.0 mg/kg bw (0.0073–0.013/day) for the six uncoated TiO_2 particles [2]. The clearance rate constants for TiO_2 with $Al(OH)_3$ coating also decreased dose-dependently, and were lower than the other six TiO_2 nano and submicron particles, with values of 0.011, 0.0046, and 0.00018/day at doses of 0.67, 2.0, and 6.0 mg/kg bw, respectively [2].

The pulmonary NiO clearance rate coefficients, k_{Lung}, in animals treated with highly soluble NiO particles (0.15–0.16/day) were much higher than those in animals treated with the other types of NiO particles (<0.001–0.012/day) [4]. NiO which is highly soluble in lysosomal fluid was quickly transferred from alveolar region to blood and excreted to urine via kidney. The clearance rate coefficient of one type of NiO and $Al(OH)_3$-coated TiO_2 particles was quite similar for three doses and showed the overload effect, which may be explained by the toxicity of slightly dissolvable Ni or Al ions. The clearance rate coefficient of two types of NiO was quite slow and did not show the overload effect, which might be explained by the toxicity of moderately dissolvable Ni.
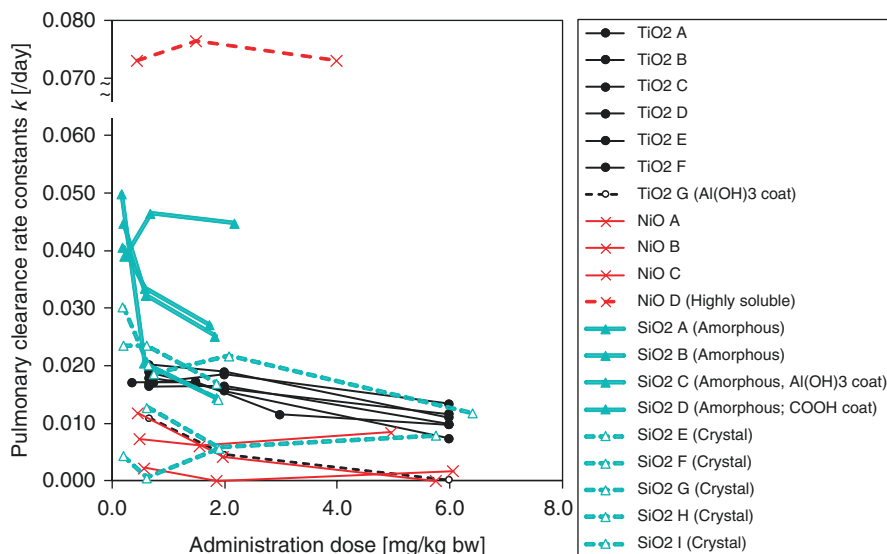
Fig. 10.5 Pulmonary clearance rate coefficients for TiO_2, NiO, and SiO_2 nano particles [2–4, 8]

The pulmonary SiO_2 clearance rate coefficients (0.00060–0.021/day) were higher for amorphous SiO_2 than for crystal SiO_2 (0.000023–0.0013/day) [8]. However, whether crystalline nature or size affected the clearance rates were not unclear because the amorphous SiO_2 particles were smaller than crystal particles. For SiO_2, surface modification with COOH group and $Al(OH)_3$ did not affect to pulmonary clearance (Fig. 10.6).

10.5   Comparison Between Inhalation Exposure and Intratracheal Administration

There were no significant differences on distribution of lung deposition between inhalation exposure and intratracheal administration for rat [8]. The alveolar deposition fraction for nano particle 100 nm in diameter after inhalation exposure was estimated to be approximately 20% by using MPPD model, while the fraction reach to alveolar after intratracheal administration of nano particles was between 44% and 100%.

The clearance rates from lung were similar for NiO and TiO_2 when the lung burdens were similar [19]. Lung burden of C_{60} nanoparticles after inhalation exposure can be well calculated by using the clearance rates obtained in the intratracheal administration test [20].

After both of intratracheal administration and inhalation exposure, translocation of nano materials to extrapulmonary organs was quite low and/or below detection limit except for lymph nodes. Unless miss selected solvent injured the alveolar epi-
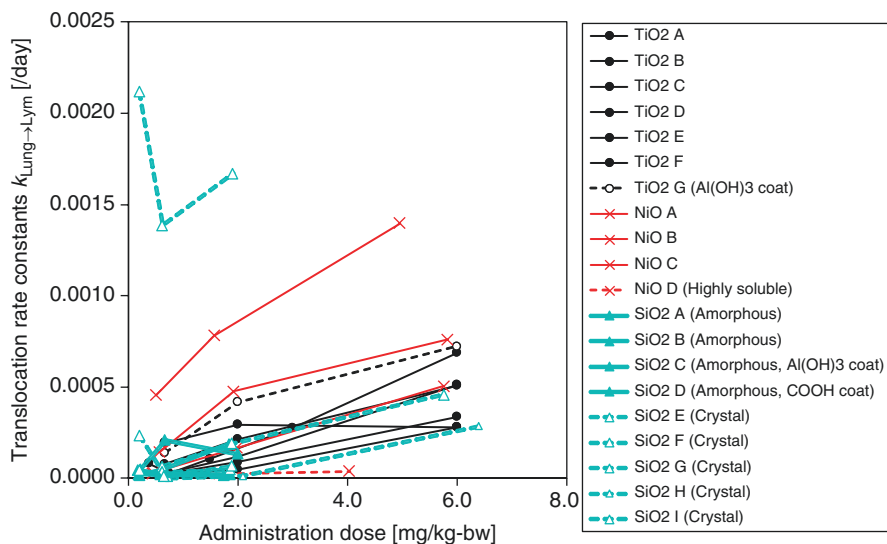
Fig. 10.6 Translocation rate coefficients from lung to lymph nodes for TiO_2, NiO, and SiO_2 nano particles [2–4, 8]

dermal cell, there might be difference on translocation to lymph nodes between inhalation exposure and intratracheal administration.

In the model, same models are used for both inhalation exposure and intratracheal administration of nano materials after lung deposition.

References

1. RIVM (National Institute for Public Health and the Environment, Netherlands). Multiple path particle dosimetry model (MPPD v.3.04): a model for human and rat airway particle dosimetry, Bilthoven, The Netherlands. RIVA report 650010030, 2017.
2. Shinohara N, Oshima Y, Kobayashi T, Imatanaka N, Nakai M, Ichinose T, Sasaki T, Kawaguchi K, Zhang G, Gamo M. Pulmonary clearance kinetics and extrapulmonary translocation of seven titanium dioxide nano and submicron materials following intratracheal administration in rats. Nanotoxicology. 2015;9(8):1050–8.
3. Shinohara N, Oshima Y, Kobayashi T, Imatanaka N, Nakai M, Ichinose T, Sasaki T, Zhang G, Fukui H, Gamo M. Dose-dependent clearance kinetics of intratracheally administered titanium dioxide nanoparticles in rat lung. Toxicology. 2014;325(5):1–11.
4. Shinohara N, Zhang G, Oshima Y, Kobayashi T, Imatanaka N, Nakai M, Sasaki T, Kawaguchi K, Gamo M. Kinetics and dissolution of intratracheally administered nickel oxide nanomaterials in rats. Part Fibre Toxicol. 2017;14(1):48.

5. Zhang G, Shinohara N, Kano H, Senoh H, Suzuki M, Sasaki T, Fukushima S, Gamo M. Quantitative evaluation of local pulmonary distribution of TiO$_2$ in rats following single or multiple intratracheal administrations of TiO$_2$ nanoparticles using X-ray fluorescence microscopy. J Appl Toxicol. 2016;36(10):1268–75.
6. Zhang G, Shinohara N, Kano H, Senoh H, Suzuki M, Sasaki T, Fukushima S, Gamo M. Quantitative evaluation of the pulmonary microdistribution of TiO$_2$ nanoparticles using XRF microscopy after intratracheal administration with a microsprayer in rats. J Appl Toxicol. 2015;35(6):623–30.
7. Zhang G, Shinohara N, Oshima Y, Kobayashi T, Imatanaka N, Kawaguchi K, Gamo M. Comparison of the local pulmonary distribution of nanoparticles administered intratracheally to rats via gavage needle or microsprayer delivery devices. J Appl Toxicol. 2017;37(4):502–7.
8. AIST (National Institute of Advanced Industrial Science and Technology). Final report of the program "Development of innovative methodology for safety assessment of industrial nanomaterials", supported by the Ministry of Economy, Trade and Industry (METI) of Japan, Tokyo, Japan, 2016.
9. Shinohara N, Nakazato T, Ohkawa K, Tamura M, Kobayashi N, Morimoto Y, Oyabu T, Myojo T, Shimada M, Yamamoto K, Tao H, Ema M, Naya M, Nakanishi J. Long-term retention of pristine multi-walled carbon nanotubes in rat lungs after intratracheal instillation. J Appl Toxicol. 2016;36(4):501–9.
10. Madl AK, Wilson DW, Segall HI, Pinkerton KE. Alteration in lung particle translocation, macrophage function, and microfilament arrangement in monocrotaline-treated rats. Toxicol Appl Pharmacol. 1998;153:28–38.
11. Oberdörster G, Ferin J, Lehnert BE. Correlation between particle size, in vivo particle persistence, and lung injury. Environ Health Perspect. 1994;102:173–9.
12. Ferin J, Oberdörster G, Penney DP. Pulmonary retention of ultrafine and fine particles in rats. Am J Respir Cell Mol Biol. 1992;6:535–42.
13. Kasai T, Umeda Y, Ohnishi M, Mine T, Kondo H, Takeuchi T, Matsumoto M, Fukushima S. Lung carcinogenicity of inhaled multi-walled carbon nanotube in rats. Part Fibre Toxicol. 2016;13:53.
14. ICRP. Human respiratory tract model for radiological protection. A report of a task group of the International Commission on Radiological Protection (ICRP publication 66). International Commission on Radiological Protection, Pergamon, Edinburgh, 1994.
15. Stöber W, et al. Compartmental modeling of the long-term retention of insoluble particles deposited in the alveolar region of the lung. Fundam Appl Toxicol. 1989;13:823–42.
16. Stöber W. Pock model simulations of pulmonary quartz dust retention data in extended inhalation exposures of rats. Inhal Toxicol. 1999;11:269–92.
17. Kuempel ED, et al. A biomathematical model of particle clearance and retention in the lungs of coal miners I. Model development. Regul Toxicol Pharmacol. 2001;34:69–87.
18. Gregoratto D, Bailey MR, Marsh JW. Modelling particle retention in the alveolar-interstitial region of the human lungs. J Radiol Prot. 2010;30:491–512.
19. Oyabu T, Myojo T, Lee B, Okada T, Izumi H, Yoshiura Y, Tomonaga T, Li Y, Kawai K, Shimada M, Kubo M, Yamamoto K, Sasaki T, Morimoto Y. Biopersistence of NiO and TiO$_2$ Nanoparticles Following Intratracheal Instillation and Inhalation. Int J Mol Sci. 2017;18:2557.
20. Shinohara N, Nakazato T, Tamura M, Endoh S, Fukui H, Morimoto Y, Myojo T, Shimada M, Yamamoto K, Tao H, Yoshida Y, Nakanishi J. Clearance kinetics of fullerene C$_{60}$ nanoparticles from rat lungs after intratracheal C$_{60}$ instillation and inhalation C$_{60}$ exposure. Toxicol Sci. 2010;118(2):564–73.

Chapter 11
In Vitro Alveolar Epithelial Models Toward the Prediction of Toxicity and Translocation of Nanoparticles: A Complementary Method for Mechanism Analyses in Humans

Kikuo Komori, Kokoro Iwasawa, Rie Ogasawara, Akira Suwabe, and Yasuyuki Sakai

Abstract Nanoparticles are promising materials in research and industrial fields because of their unique characteristics, their safety and toxicity are still being investigated. Although the safety and toxicity of nanomaterials are predicted by animal experiments, obtained results may be inconsistent with human outcomes due to the species difference. Recently, there has been an increasing interest in in vitro lung models, which allow control of experimental parameters and quantitative analyses, for the prediction of lung injuries and translocation into secondary organs of nanoparticles. In this section, we focus on developing in vitro alveolar models consisting of not only human-derived cell lines but also primary rat cells as complementary methods for intratracheal instillation in rats. We also coculture with macrophages to approach physiologically relevant alveolar environment. In addition, cytotoxicity and permeability tests of nanoparticles are presented to evaluate the in vitro alveolar coculture modles developed here. To further improve the physiological relevance of in vitro alveolar models, we discuss future issues.

Keywords In vitro lung model · Nanoparticles · Pulmonary cytotoxicity Pulmonary permeability · Alveolar type I and II cells · Alveolar macrophage

K. Komori · Y. Sakai (✉)
Department of Chemical System Engineering, The University of Tokyo, Tokyo, Japan

Institute of Industrial Science, The University of Tokyo, Tokyo, Japan
e-mail: sakaiyasu@chemsys.t.u-tokyo.ac.jp

K. Iwasawa
Institute of Industrial Science, The University of Tokyo, Tokyo, Japan

R. Ogasawara · A. Suwabe
Department of Laboratory Medicine, Iwate Medical University School of Medicine, Morioka, Japan

11.1   Introduction

Suspended particulate matters, which are one of the major sources of the air pollution, have been recognized to cause health injuries, such as direct damage to alveoli and secondary diseases of other organs through their pulmonary absorption. In the meantime, the development and application of nanomaterials, which possess novel properties and functions, have recently attracted great attention in the variety of fields, while their safety and toxicity to human bodies have also been evaluated considerably [1]. For instance, in the field of medicine, nanosized drug carriers [2, 3] for pulmonary administration have been developed and investigated to enhance their permeability into the bodies, compared to the route of drug administration through the small intestine. The safety/toxicity and drug effects of substances including nanomaterials and nanocarriers are basically predicted by their intratracheal instillation into rodents, such as rats. However, the obtained results don't often reflect human outcomes properly due to the species difference. In addition, detailed kinetic analyses are complicated due to the inherent complexity of the living system. Hence, alveolar epithelial cell-based in vitro model systems are required as complementary and alternative methods in animal experiments.

Alveoli, in which gas exchange takes place, are located at the most distal part of the respiratory tract and surrounded by a network of blood capillaries. The alveolar epithelial cell layer consists of alveolar type I and II cells. The type I cells, which are about 0.05–0.20 μm thick flat cells, provide approximately 95% of the alveolar wall and involved in the process of gas exchange between alveoli and blood. Meanwhile, the cuboidal type II cells are known as the progenitor of type I cells and occupy a small fraction of the alveolar wall. The type II cells also secrete pulmonary surfactants, which play a significant role in physiological homeostasis in the alveoli, such as the decrease in their surface tension of an air–liquid interface and prevention of alveolar collapse and pulmonary edema. Besides the alveolar type I and II cells, alveolar macrophages as one of the immune cells are seen in the alveolar lumen and also involved in physiological homeostasis, such as clearance of foreign substances including pathogens and repairing tissues after inflammation. In order to assess alveolar injury and transport into the human body against foreign substances including nanoparticles and nanofibers in vitro, at least coculture models consisting of alveolar epithelial cells and macrophages are needed.

Previously, cell lines have frequently been used for developing in vitro alveolar coculture models [4–6]. However, biologically relevant functions observed in the cell lines are decreased or lost partially. Therefore, primary cells are one of the potential cell sources to achieve in vitro alveolar coculture models, which mimic the in vivo situation. In the present section, we summarized procedures for developing in vitro alveolar epithelial models toward the prediction of pulmonary toxicity and permeability of nanoparticles using not only cell lines but also primary cells. It is known that a colloidal suspension of nanoparticles is frequently administered into

lungs in rodents for evaluating their lung injury and translocation to extrapulmonary organs in inhalation toxicity studies. Based on this, we therefore used primary cells isolated from rats to develop in vitro alveolar coculture models for the complementary method in animal experiments.
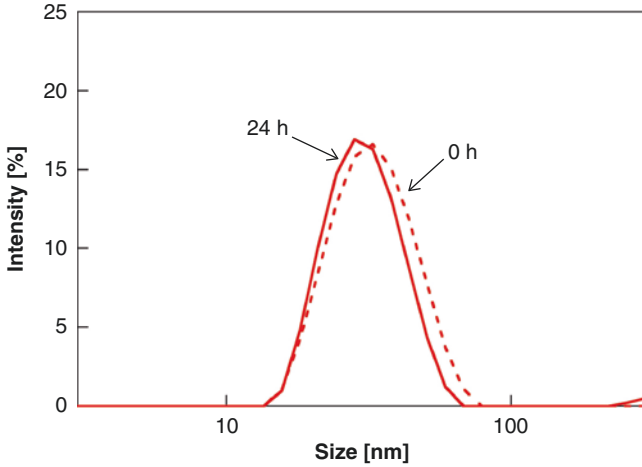
11.2 Nanoparticles

Today a numerous amount of nanomaterials, which possess novel physical, thermal, optical, and biological features, have been manufactured. Those features may depend on the chemical composition, crystal structure, size, and shape of nanomaterials. Nanoparticles as one subset of nanomaterials are contained in a variety of consumer products, such as drugs, dietary supplements, cosmetics, sunscreen, toiletry products, food packaging, clothing, sporting equipment, electronics, and batteries. To give an example, a lot of sunscreen include titanium dioxide (TiO_2) or zinc oxide (ZnO) nanoparticles to block ultraviolet rays. The permeated amount of TiO_2 and ZnO nanoparticles into normal skin is extremely low in general. However, TiO_2 nanoparticles are known to cause DNA and chromosomal damages and inflammation in mice fed TiO_2 nanoparticles for 5 days [7]. In addition, TiO_2, ZnO, and silica (SiO_2) nanoparticles have been reported to be toxic to human neural and lung cells in in vitro studies [8–11]. Therefore, SiO_2 and TiO_2 nanoparticles are helpful as a positive control for cell viability measurements (Table 11.1). Additionally, silica nanoparticles labeled with FITC or rhodamine (FITC-SiO_2NPs and Rho-SiO_2NPs) are useful for permeability measurements.

Cytotoxicity and pulmonary translocation of nanoparticles have been known to strongly depend on their surface characteristics, particle size, and chemical composition [1]. Among them, the size of nanoparticles is one of the key parameters. Nanoparticles often form aggregates in self-assembled manner with proteins in fetal bovine serum (FBS) and human serum via electrostatic and hydrophilic/hydrophobic interactions [12]. Not surprisingly, SiO_2 and TiO_2 nanoparticles used here formed their aggregates in a Dulbecco's modified Eagle medium (DMEM) containing 10% FBS. However, SiO_2 and TiO_2 nanoparticles maintained their size without any aggregation in DMEM containing no FBS even after 24 h (Fig. 11.1). The culture medium without FBS might therefore be employed in cytotoxicity tests and translocation studies.

Table 11.1 Particles used in this work

Nanoparticles	Product name	Diameter (nm)
TiO_2	P25	21
TiO_2	MP100	1000
SiO_2	MinU Silica	1600
FITC-labeled SiO_2	Sicastar GreenF	30
Rhodamine-labeled SiO_2	Sicaster RedF	10, 30, 100

Fig. 11.1 Size distribution by intensity of dynamic light scattering for 0.2 mg mL FITC-labeled SiO$_2$ nanoparticles (30 nm in diameter) immediately dispersed in DMEM without FBS and 24 h later
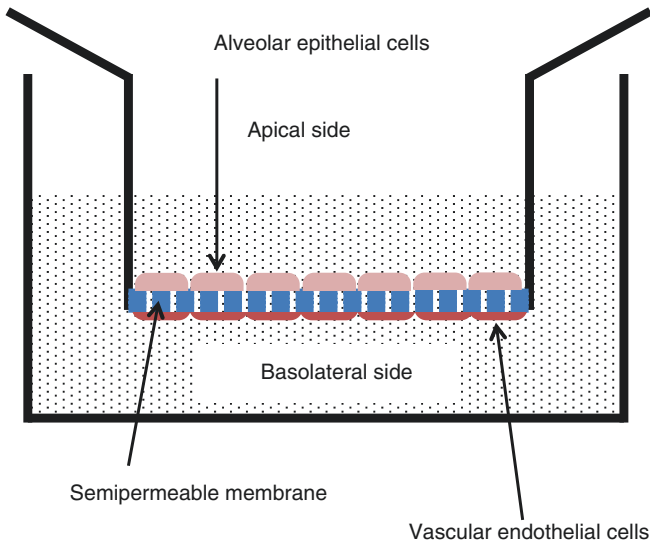
Fig. 11.2 Schematic illustration of the transwell insert culture system

11.3 Properties of In Vitro Alveolar Epithelial Models

To develop in vitro lung models, transwell inserts consisting of a semipermeable membrane are commonly utilized. The semipermeable membrane allows to separate across to apical and basolateral compartments (Fig. 11.2). As one of indexes of

the alveolar functions, the integrity of the blood–air barrier for alveolar epithelial cell layers cultured on the semipermeable membrane is determined from transepithelial electrical resistance (TEER), which is accepted as measuring their tight junction integrity and paracellular permeability. Here, we described the preparation and property of in vitro alveolar epithelial models using human alveolar epithelial cell lines and primary alveolar epithelial cells isolated from rats.

### 11.3.1 Human Alveolar Epithelial Cell Lines

Normal human alveolar epithelial cells are the optimal cell source for the in vitro lung model. Although primary human alveolar epithelial cells consisting of type I and II cells are commercially available, their extremely low proliferation rate causes the difficulty in obtaining a large amount of their cells in vitro inexpensively. The commercially available primary human alveolar epithelial cells are therefore unreasonable in the safety/toxicity testing and high-throughput screening. In the case of cell lines, a type I cell line has not yet been established in the present. In contrast, a human alveolar epithelial type II cell line A549 are already established [13] and serves as a potential model in the alveolar region [14], although its differentiation ability into the type I cell is lost. In order to mimic the situation in the human alveoli, we have used A549 cells and developed an in vitro human alveolar epithelial model cocultured with the human monocytic cell line THP-1, which is known to differentiate into a macrophage-like cell after stimulation of chemicals, such as phorbol 12-myristate 13-acetate (PMA) [15, 16].

A549 and THP-1 cells are basically cultured in DMEM and Roswell Park Memorial Institute medium (RPMI) 1640 containing 10% FBS and 1% antibiotics–antimycotic mixed solution (AA), respectively, in a 5% CO_2 incubator at 37 °C. A549 cells were seeded onto the semipermeable membrane at a cell density of 1.0×10^5 cells cm^{-2} and inoculated for at least 5 days to be formed monolayer. However, A549 cells are basically unable to form the strong blood–air barrier due to the type II-derived cells. Obviously, the TEER value was over one order of magnitude smaller than those of a cell layer consisting of Calu-3 or 16HBE14o-cells (~2000 Ω cm^2), which are known to possess high barrier properties because of airway and bronchial-derived epithelial cell lines, respectively [17] (Fig. 11.3). The macrophage-like cells (1.0×10^4 cells cm^{-2}), which are differentiated from THP-1 cells, were also added onto the apical side of the A549 monoculture system and further cultured for 24 h. However, the considerable improvement of the TEER value was not also obtained.

To improve the barrier properties, A549 cells were cocultured with human umbilical vein endothelial cells HUVECs, which were adhered on the lower surface of the transwell insert (A549/HUVEC system). Unfortunately, we didn't observe a nonlinear increase in the TEER value associated with the effect of coculture with HUVECs (Fig. 11.3). However, interestingly, the cuboidal shape of A549 cells was maintained and a rough A549 cell layer was formed on the semipermeable membrane at the monoculture system without HUVECs, whereas a flat and smooth layer of A549 cells was formed at the A549/HUVEC system (Fig. 11.4a, b). This
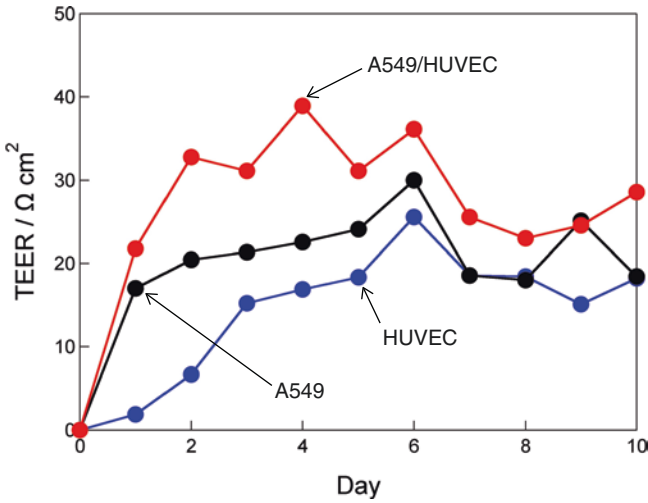
Fig. 11.3 Time course changes in the TEER values for A549, HUVEC, and A549/HUVEC culture systems
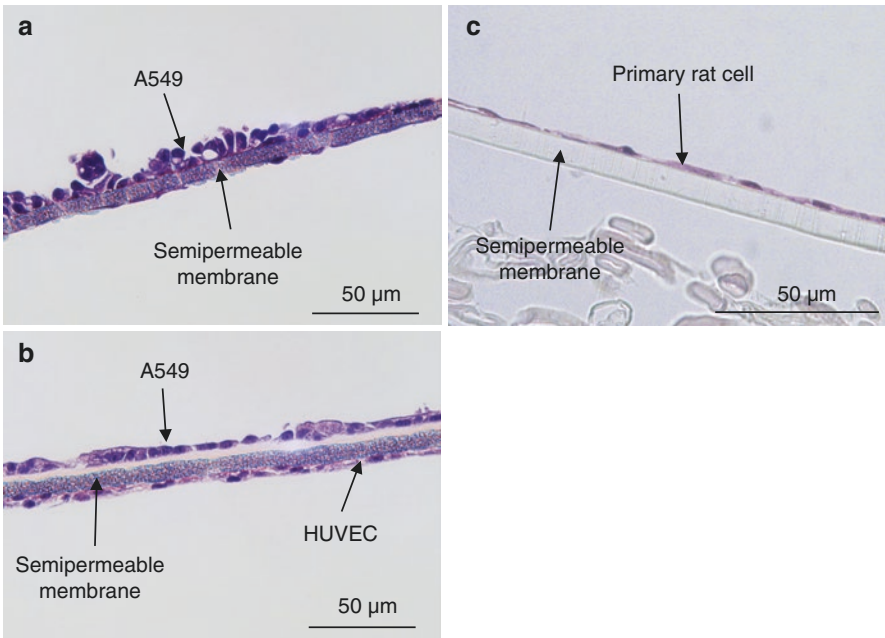
Fig. 11.4 Cross-section views of (**a**) A549, (**b**) A549/HUVEC, and (**c**) differentiated primary rat type I cell layers stained with hematoxylin and eosin

might indicate that extracellular matrixes secreted and accumulated from HUVECs contribute to increased stability of A549 cells.

11.3.2 Primary Rat Alveolar Epithelial Cells

Primary alveolar epithelial cells isolated from animals are also considered as a cell source for in vitro lung models. As described above, animal experiments have been performed in the safety and toxicity testing to chemicals including nanomaterials. Therefore, developing in vitro models of animal organs is significant as with those of human organs to verify correlation between in vitro results and in vivo outcomes obtained in animal testing.

An isolation method for alveolar epithelial type I cells from animals, such as rats, has been proposed previously, but the method has been much complicated. In contrast, high purified primary alveolar epithelial type II cells are easily collected on the basis of metrizamide density centrifugation [18]. Since the type II cells are also known to differentiate into type I cells [19], the isolation method for alveolar epithelial type II cells has been accepted. The isolation method for alveolar macrophages has also been reported. Briefly, the lung was washed with saline five times and then the bronchoalveolar lavage fluid (BALF) was recovered. After centrifugation, alveolar macrophages are collected from the recovered BALF. Note that in our investigation, the amount of alveolar epithelial type II cells and alveolar macrophages isolated from one rat was about $0.8–1.4 \times 10^7$ and $1.0–1.7 \times 10^6$ cells rat^{-1}, respectively. The isolated alveolar epithelial cells and alveolar macrophages were cultured in DMEM and RPMI 1640 containing 10% FBS and 1% antibiotics–antimycotic mixed solution (AA), respectively, in a 5% CO_2 incubator at 37 °C for 24 h after cell seeding. After 24 h or later, the amount of FBS in both DMEM and RPMI 1640-based culture medium was changed from 10% to 2% for cell culturing.

First, we show differentiation behavior of isolated type II cells. As shown in Fig. 11.5, cuboidal shape of the isolated type II cells was gradually changed to thin

100 µm
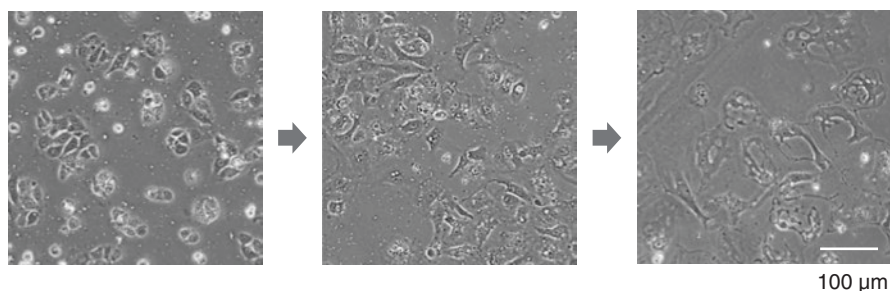
Fig. 11.5 Differentiation primary rat alveolar epithelial type II cells into the type I cells

Fig. 11.6 Time course change in the TEER values of primary rat alveolar epithelial type II cells
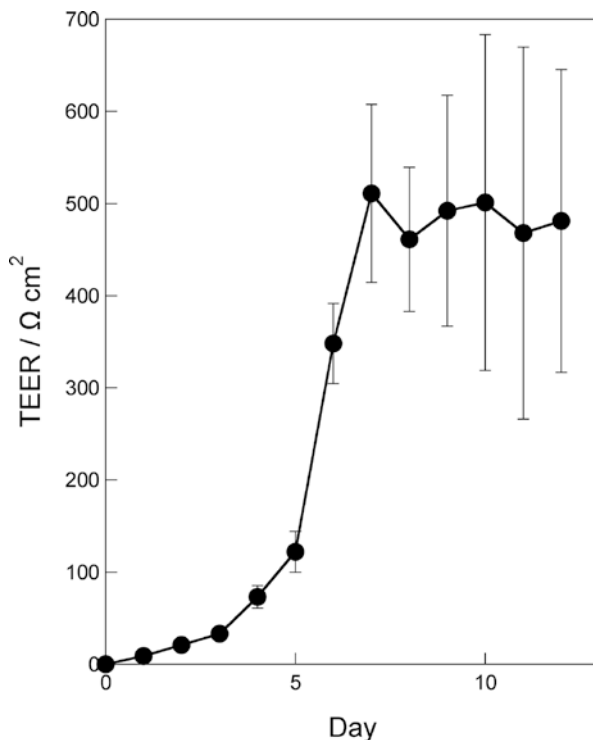

flat cells from 48 h after cell seeding. After 5 days of culture, a complete monolayer was obtained (Fig. 11.4c). The thickness of the obtained cell layer was ~3.0 μm and about a one-third or smaller of that of the A549 cell layer (~10 μm). During the formation of the monolayer, the TEER values significantly increased from day 4 and then leveled off after day 7 (Fig. 11.6). Subsequently, the TEER value was maintained at more than 300 Ω cm^2 for at least 5 days. This value was one order of magnitude larger than that for the A549 and A549/HUVEC systems due to the differentiation from type II cells into type I cells. The final cell density of differentiated type I cells was estimated to be 3.0–4.0 × 10^4 cells cm^{-2}.

Next, we describe the preparation of in vitro primary rat alveolar epithelial coculture models with primary rat alveolar macrophages (macrophage/type I system). The isolated primary rat alveolar macrophages were seeded onto the differentiated type I cell monolayer on day 6 and further cultured for 24 h. The final cell density of the primary rat alveolar macrophages was estimated to be 4.8 × 10^3 cells cm^{-2}. The obtained value was nearly equal to that in alveoli in vivo (3.0–6.0 × 10^3 cells cm^{-2}) [20].

11.4 Toxicity Tests of Nanoparticles

The cell viability is known to be influenced by SiO$_2$ and TiO$_2$ nanoparticles, as described above. Figure 11.7a–d shows the cell viability of A549 and primary rat alveolar epithelial type I cells after 24, 48, and 72 h of exposure to P25, MP100,

Fig. 11.7 Dependences of viability on the amount of P25, MP100, and silica nanoparticles for A549 (**a**, **c**) and primary rat alveolar epithelial type I cells (**b**, **d**) at the low-density (**a**, **b**) and high-density (**c**, **d**) culture systems, THP-1 derived macrophage-like cells (**e**), and primary rat alveolar macrophages (**f**)
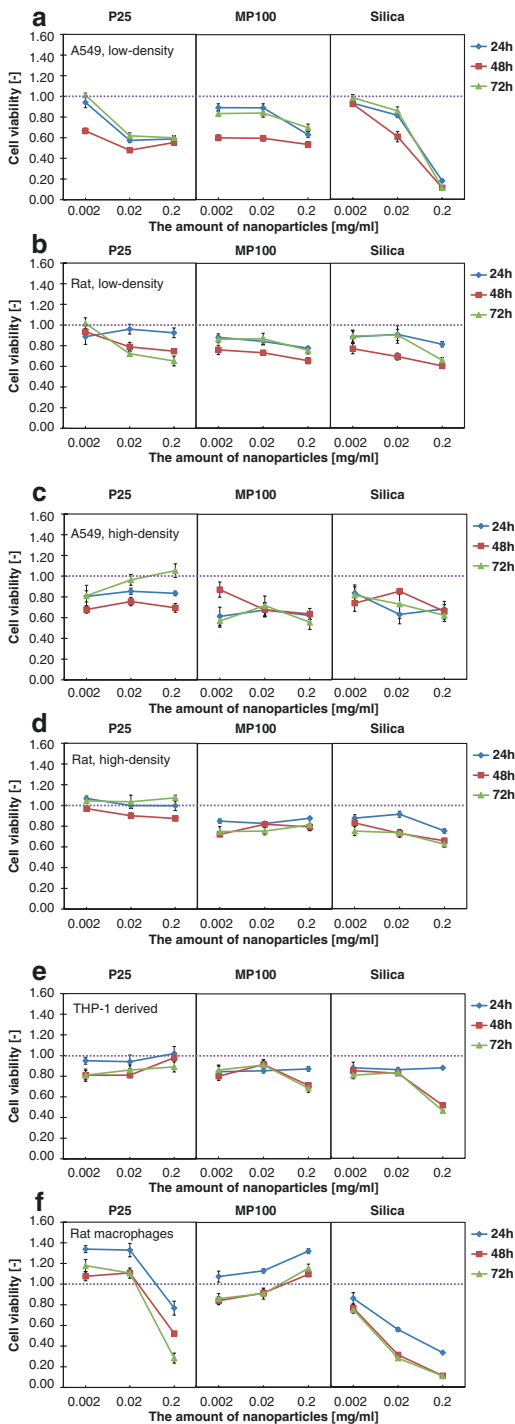
and MinU Silica (MUS). Here, low- and high-density culture systems were used. In the low-density culture system, the cell density was ~70% confluent. This value has generally been accepted in the cytotoxicity tests. In the high-density culture system, A549 and primary rat type I cells formed the complete monolayer. As the amount of the three nanoparticles increased, the cell viability at the low-density system for A549 cells clearly decreased (Fig. 11.7a), whereas that for primary rat type I cells slightly decreased (Fig. 11.7b). On the other hand, the cell viability for both A549 and primary rat type I cells at the high-density systems were not changed, as the amount of P25 and MP100 increased (Fig. 11.7c, d). Even after exposure to MUS, which is silica nanoparticles and known to strongly cause damage to cells, the cell viability for the both cells only slightly decreased. Notice that the cell viability for primary rat type I cells to silica nanoparticles at the low-density system was nearly equal to that at the high-density system, but that for A549 cells at the low-density system was much lower than that at the high-density system. From uptake of nanoparticles for the both cells by means of time course microscopic observation, apparently, primary rat type I cells firmly adhered on the culture dish and took up nanoparticles attached to only their cell surfaces through the endocytosis pathway. However, surprisingly, A549 cells not only took up nanoparticles attached onto their cell surfaces through the endocytosis pathway but also actively migrated and phagocytosed nanoparticles attached on the substrate surface, even though A549 cells are epithelial type II cell lines. The cytotoxicity of nanomaterials might be overestimated, when A549 cells at the low cell density are used for the toxicity tests. However, the low-density system for A549 cells would be useful as a high-sensitive detecting method of nanoparticles despite the lack of their physiologically relevant behaviors.

Similarly, Fig. 11.7e, f shows the cell viability of macrophage-like cells differentiated from THP-1 cells and isolated primary rat alveolar macrophages to the nanoparticles. As the amount of P25 and MUS increased, the cell viability of the rat macrophage significantly decreased, compared to that of the macrophage-like cells, probably due to the differences in functionality between primary cells and cell lines. As shown in Fig. 11.8, the rat macrophages were spherical shape and obviously different shapes from the macrophage-like cells. In addition, primary cells are widely believed to possess more biologically relevant functions than cell lines. A phagocytic capacity of the rat macrophages is likely higher than that of the macrophage-like cells. Indeed, the rat macrophages actively migrated and phagocytosed TiO_2 nanoparticles in comparison with the macrophage-like cells (Fig. 11.8). Thus, macrophages would be the essential element for predicting not only cytotoxicity tests but also translocation studies to nanoparticles properly.

11.5   Permeability Tests of Nanoparticles

Inhaled nanoparticles, the size of which is 10–100 nm in diameter, tend to be deposited in the alveoli region. Here, FITC-SiO$_2$NPs and Rho-SiO$_2$NPs 30 nm in diameter were used in the translocation study for THP-1/A549/HUVEC and macrophage/

Rat macrophages   THP-1-derived
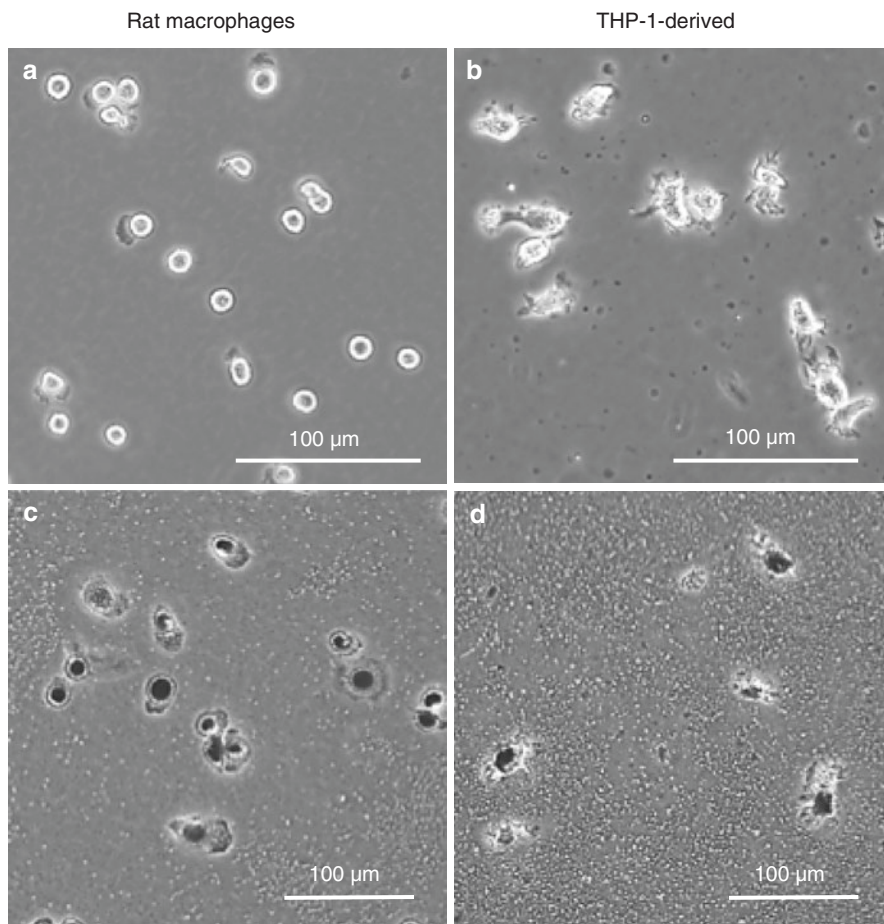
Fig. 11.8 Micrographs of primary rat alveolar macrophages (**a**, **c**) and THP-1 derived macrophage-like cells (**b**, **d**) with (**c**, **d**) and without (**a**, **b**) TiO$_2$ nanoparticles

type I systems, respectively. If cells are damaged by nanoparticles and detached from the insert surface, translocation ratio would not be determined appropriately. Based on the cell viability tests, the appropriate amount of nanoparticles, which is no influence to the cell viability, was determined to be about ≤ 0.02 mg mL^{-1} for FITC-SiO$_2$NPs and ≤ 0.2 mg mL^{-1} for Rho-SiO$_2$NPs. This difference might depend on the cell type and properties of fluorescent dyes on the surface of SiO$_2$NPs. The both nanoparticles used here were also still dispersed in DMEM without FBS even after 24 h. DMEM containing FITC-SiO$_2$NPs or Rho-SiO$_2$NPs was added into the apical side of THP-1/A549/HUVEC and macrophage/type I systems, respectively, and further incubated for 24 h. The amount of nanoparticles translocated from the apical to the basolateral side was apparently suppressed in comparison with the A549/HVEC and type I culture systems without macrophages (Fig. 11.9).
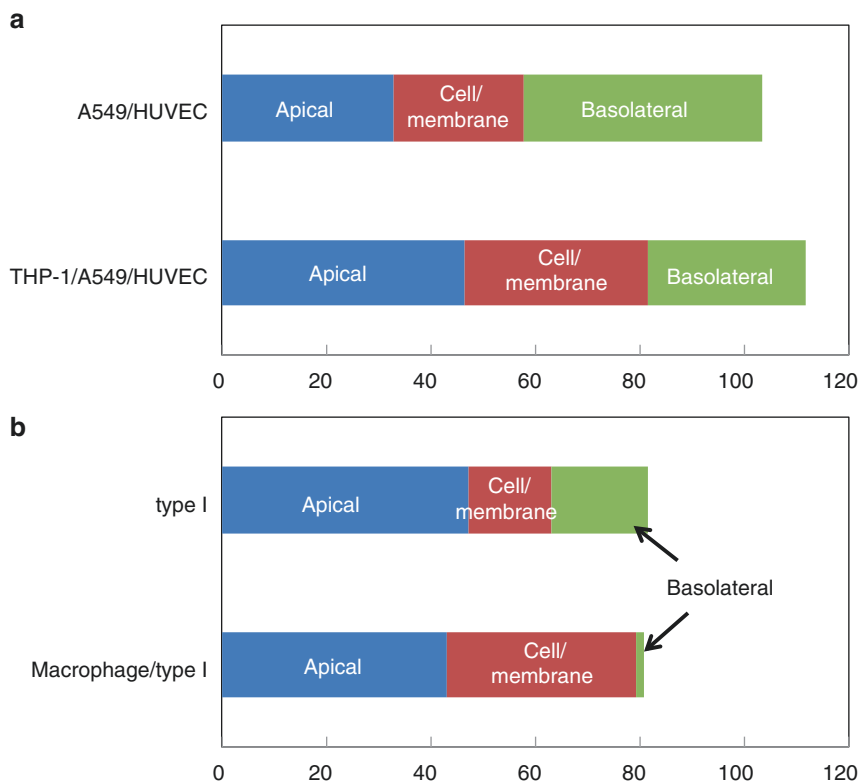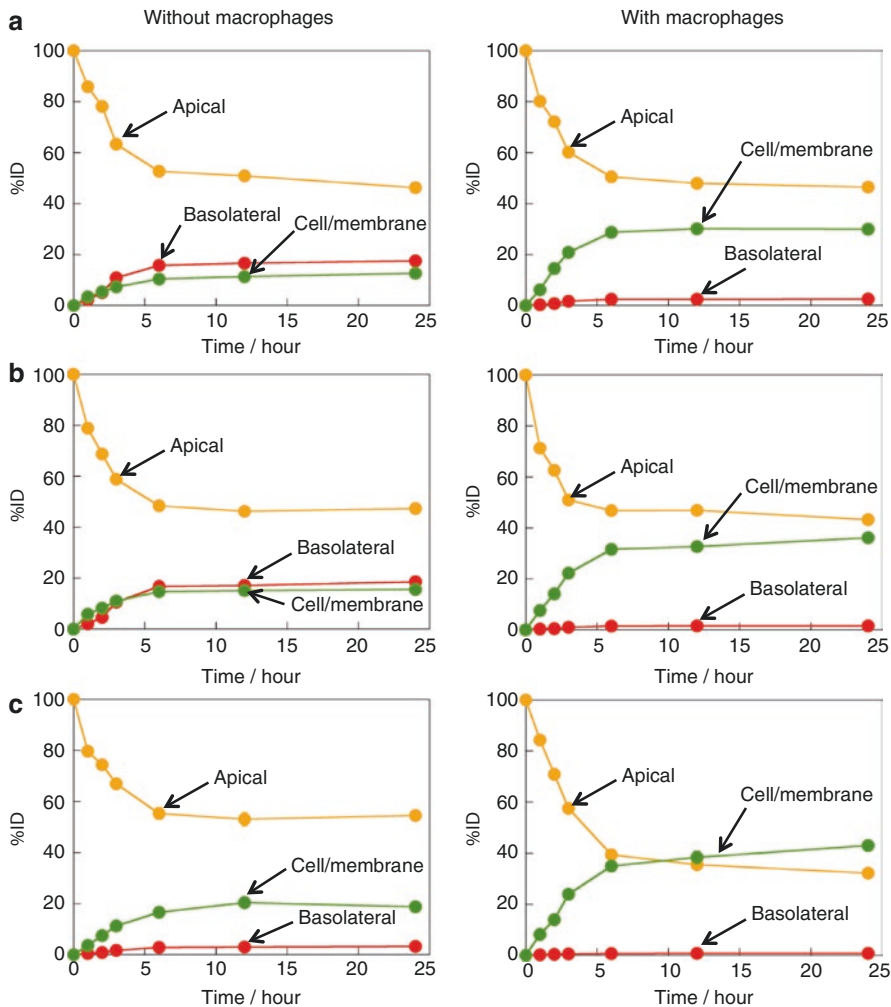
Fig. 11.9 Quantification of (**a**) FITC- and (**b**) rhodamine-labeled SiO_2 nanoparticle distribution in percentage at the apical, basolateral, and cell compartments at (**a**) A549/HUVEC and THP-1/A549/HUVEC culture systems and (**b**) rat type I and rat macrophage/type I culture systems

Nanoparticles were also accumulated in the cell layers and/or adsorbed at the surface of the semipermeable membrane. The increase in the amount of nanoparticles at the cell/membrane compartment is based on the fact that macrophages including differentiated macrophage-like cells phagocytosed the nanoparticles.

Compared with the THP-1/A549/HUVEC system, the macrophage/type I system may provide a physiologically relevant response of alveoli in vivo because of consisting of primary cells. The dependence of nanoparticle size on translocation characteristics was further examined at the macrophage/type I system. DMEM containing Rho-SiO_2NPs 10, 30, or 100 nm in diameters was added into the apical side of the macrophage/type I system and further incubated for 24 h. Transport of the nanoparticles 10 and 30 nm in diameter from the apical to basolateral side was clearly suppressed in comparison with the case of only type I cell culture system without the rat macrophages (~2.6%, Fig. 11.10). In contrast, the penetration of nanoparticles 100 nm in diameter was apparently disrupted by even only type I cell layer without macrophages. The alveolar epithelial tight junction

Fig. 11.10 Rate of rhodamine-labeled SiO_2 nanoparticle distribution in percentage at the apical, basolateral, and cell compartments at rat type I and rat macrophage/type I culture systems. The size of rhodamine-labeled SiO_2 nanoparticles used here was 10, 30, 100 nm in diameter (**a–c**, respectively)

might prevent the paracellular pathway of nanoparticles 100 nm in diameter or larger due to its narrow gap. In any case, the obtained value is still larger than that reported in animal experiments (<1.0%). This is likely due to the quite different environment between in vitro and in vivo. In addition, the present in vitro alveolar epithelial model is still far from completely mimicking the in vivo alveolar tissue. The improvement of in vitro alveolar epithelial models is absolutely necessary, as described later.

11.6   Future Remarks

In this work, we have been developing physiologically relevant in vitro alveolar epithelial models for cytotoxicity tests and translocation studies of nanoparticles. However, the present in vitro alveolar epithelial models are still quite different from the in vivo situation, as mentioned above. In order to overcome such problem, the in vitro alveolar epithelial models further have to fulfill the following at least four conditions, such as (1) applying an air-liquid interface culture (ALIC) method, (2) using human induced pluripotent stem cell (hiPSC)-derived type I and II cells, (3) reconstitution of the alveolar epithelial cell layer consisting of type I and type II cells, and (4) applying mechanical strain to semipermeable membranes. The details are as follows.

11.6.1   *Applying the ALIC Method*

The ALIC system has been widely used in the field of respiratory research [21–23]. The ALIC method enables cells to directly contact with air and gases at their apical side, while a culture medium is supplied to the cells from the basolateral side through the semipermeable membrane. The ALIC method has also been known to improve barrier function of in vitro pulmonary models, such as alveolar and bronchial epithelial cells [24]. Note that preliminary investigation of dispersibility and stability of nanoparticles in the atmosphere is imperative, when the ALIC technique is used for the prediction of transport from the apical to basolateral side and cytotoxicity of nanoparticles.

11.6.2   *Using hiPC-Derived Type I and II Cells*

Primary human cells would provide the best prospects for obtaining more meaningful information to human bodies in the cell-based assays and high-throughput screening. However, the use of the primary human cells has generally been limited due to the donor shortage, limited source materials, heterogeneity in cell type, and donor variability. To overcome this problem, hiPSCs are promising cell sources for the in vitro assays. However, it is required that a large amount of target cells differentiated from standardized hiPSCs is produced at low cost.

11.6.3   *Reconstitution of the Alveolar Epithelial Cell Layer Consisting of Type I and Type II Cells*

In our previous investigation, it was not easy to obtain the alveolar epithelial cell layer consisting of type I and II cells, the surface area ratio of which was 95:5, respectively, just by seeding and culturing primary rat alveolar epithelial type II

cells on the semipermeable membrane. The type II cells are known to usually reside at the corners of alveoli [25]. In addition, the differentiation from type II cells to type I cells is suppressed by culturing at the air-exposed apical surface [26]. Therefore, the surface morphology control and the ALIC method would be critical factors in controlling the surface area ratio of type I and II cells for the alveolar epithelial cell layer.

11.6.4   Applying Mechanical Strain to Semipermeable Membranes

The lungs expand and contract during normal breathing, so that alveolar epithelial cells are exposed to cyclic stretching. Mechanically applying the cyclic stretching to the alveolar epithelial cells in vitro is expected to improve their stability and physiological functions. In fact, Ingber and his coworkers have developed a lung on-a-chip with two parallel microchannels separated by a stretchable and semipermeable membrane, at the top and lower surfaces of which A549 and endothelial cells were cultured, respectively. They successfully reproduced the in vivo situation of the lung microenvironment by cyclic stretching of the membrane in addition to flowing air and culture medium at the apical and basolateral sides, respectively [27]. During cyclic stretching of the membrane, ideally, the alveolar epithelial cell layer should be covered with pulmonary surfactant secreted from type II cells.

11.7   Conclusion

We described the preparation and properties of in vitro alveolar epithelial models consisting of the human alveolar epithelial cell line A549 or primary rat alveolar epithelial cells. Coculture with macrophages improved the physiological performance of the in vitro alveolar epithelial models in cytotoxicity tests and translocation studies of nanoparticles. The present system would play a complementary role in the animal experiments, since the colloidal suspension of nanoparticles is frequently used to evaluate lung injury and translocation to extrapulmonary organs in rodents after its intratracheal instillation. However, the in vitro alveolar epithelial models developed here are not enough to achieve optimal in vivo performance yet. To improve the performance, the in vitro lung model consisting of human alveolar epithelial type I and II cells would be required for culturing under the ALIC with cyclic stretching condition. The improved in vitro alveolar epithelial models would be applied to accurately and kinetically understand and predict the potential toxic and alveolar permeability effects of various nanoparticles.

References

1. Nel A, Xia T, Mädler L, Li N. Toxic potential of materials at the nano level. Science. 2006;311:622–7.
2. De Jong WH, Borm PJA. Drug delivery and nanoparticles: applications and hazards. Int J Med. 2008;3:133–49.
3. Sung JC, Pulliam BL, Edwards DA. Nanoparticles for drug delivery to the lungs. Trends Biotechnol. 2007;25:563–70.
4. Klein CL, Wiench K, Wiemann M, Ma-Hock L, van Ravenzwaay B, Landsiedel R. Hazard identification of inhaled nanomaterials: making use of short-term inhalation studies. Arch Toxicol. 2012;86:1137–51.
5. Sayes CM, Reed KL, Warheit DB. Assessing toxicity of fine and nanoparticles: comparing in vitro measurements to in vivo pulmonary toxicity profiles. Toxicol Sci. 2007;97:163–80.
6. Yacobi NR, Phuleria HC, Demaio L, Liang CH, Peng CA, Sioutas C, Borok Z, Kim KJ, Crandall ED. Nanoparticle effects on rat alveolar epithelial cell monolayer barrier properties. Toxicol In Vitro. 2007;21:1373–81.
7. Trouiller B, Reliene R, Westbrook A, Solaimani P, Schiestl RH. Titanium dioxide nanoparticles induce DNA damage and genetic instability in vivo in mice. Cancer Res. 2009;69:8784–9.
8. Gurr JR, Wang ASS, Chen CH, Jan KY. Ultrafine titanium dioxide particles in the absence of photoactivation can induce oxidative damage to human bronchial epithelial cells. Toxicology. 2005;213:66–73.
9. Kim IS, Baek M, Choi SJ. Comparative cytotoxicity of Al2O3, CeO2, TiO2 and ZnO nanoparticles to human lung cells. J Nanosci Nanotechnol. 2010;10:3453–8.
10. Lai JCK, Lai MB, Jandhyam S, Dukhande VV, Bhushan A, Daniels CK, Leung SW. Exposure to titanium dioxide and other metallic oxide nanoparticles induces cytotoxicity on human neural cells and fibroblasts. Int J Nanomedicine. 2008;3:533–45.
11. Lin W, Huang YW, Zhou XD, Ma Y. In vitro toxicity of silica nanoparticles in human lung cancer cells. Toxicol Appl Pharmacol. 2006;217:252–9.
12. Mahmoudi M, Lynch I, Ejtehadi MR, Monopoli MP, Bombelli FB, Laurent S. Protein-nanoparticle interactions: opportunities and challenges. Chem Rev. 2011;111:5610–37.
13. Lieber M, Smith B, Szakal A, Nelson-Rees W, Todaro G. A continuous tumor-cell line from a human lung carcinoma with properties of type II alveolar epithelial cells. Int J Cancer. 1976;17:62–70.
14. Foster KA, Oster CG, Mayer MM, Avery ML, Audus KL. Characterization of the A549 cell line as a type II pulmonary epithelial cell model for drug metabolism. Exp Cell Res. 1998;243:359–66.
15. Daigneault M, Preston JA, Marriott HM, Whyte KB, Dockrell DH. The identification of markers of macrophage differentiation in PMA-stimulated THP-1 cells and monocyte-derived macrophages. PLoS One. 2010;5:e8668.
16. Fleit HB, Kobasiuk CD. The human monocyte-like cell line THP-1 expresses FcγRI and FcγRII. J Leukoc Biol. 1991;49:556–65.
17. Braakhuis HM, Kloet SK, Kezic S, Kuper F, Park MVDZ, Bellmann S, van der Zande M, Gac SL, Krystek P, Peters RB, Rietjents IMCM, Bouwmeester H. Progress and future of in vitro models to study translocation of nanoparticles. Arch Toxicol. 2015;89:1469–95.
18. Dobbs LG, Mason RJ. Pulmonary alveolar type II cells isolated from rats. J Clin Invest. 1979;63:378–87.
19. Sakagami M. In vivo, in vitro and ex vivo models to assess pulmonary absorption and disposition of inhaled therapeutics for systemic delivery. Adv Drug Deliv Rev. 2006;58:1030–60.
20. Wallace WAH, Gillooly M, Lamb D. Intra-alveolar macrophage numbers in current smokers and non-smokers: a morphometric study of tissue sections. Thorax. 1992;47:437–40.
21. Iwasawa K, Tanaka G, Aoyama T, Chowdhury MM, Komori K, Tanaka-Kagawa T, Jinno H, Sakai Y. Prediction of phthalate permeation through pulmonary alveoli using a cultured A549 cell-based in vitro alveolus model and a numerical simulation. AATEX. 2013;18:19–31.

22. Komori K, Murai K, Miyajima S, Fujii T, Mohri S, Ono Y, Sakai Y. Deveopment of an in vitro batch-type closed gas exposure device with an alveolar epithelial cell line, A549, for toxicity evaluations of gaseous compounds. Anal Sci. 2008;24:957–62.
23. Whitcutt MJ, Adler KB, Wu R. A biphasic chamber system for maintaining polarity of differentiation of cultured respiratory tract epithelial cells. In Vitro Cell Dev Biol. 1988;24:420–8.
24. Sakai Y, Tomita K, Suzuki M, Ono Y, Sakoda A. Development of a toxicity evaluation system for gaseous compounds using air-liquid interface culture of a human bronchial epithelial cell line. Calu-3 AATEX. 2005;11:59–67.
25. Weibel ER. Morphometry of the human lung: the state of the art after two decades. Bull Eur Physiopathol Respir. 1979;15:999–1013.
26. Dobbs LG, Pian MS, Magrio M, Dumars S, Allen L. Maintenance of the differentiated type II cell phenotype by culture with an apical air surface. Am J Physiol. 1997;273:L347–54.
27. Huh D, Matthews BD, Mammoto A, Montoya-Zavala H, Hsin Y, Ingber DE. Reconstituting organ-level lung functions on a chip. Science. 2010;328:1662–8.